Durham University

Durham E-Theses

The interpretation of the spectrum of energetic cosmic rays

Margaret C. Bell

How to cite:

Bell, Margaret C. (1974) The interpretation of the spectrum of energetic cosmic rays. Doctoral thesis, Durham University.

Use policy

The full-text may be used and/or reproduced, and given to third parties in any format or medium, without prior permission or charge, for personal research or study, educational, or not-for-profit purposes provided that:

- a full bibliographic reference is made to the original source
- a https://etheses.durham.ac.uk/id/eprint/10506/ is made to the metadata record in Durham E-Theses
- the full-text is not changed in any way

The full-text must not be sold in any format or medium without the formal permission of the copyright holders.

Please consult the full Durham E-Theses policy for further details.

Academic Support Office, The Palatine Centre, Durham University, Stockton Road, Durham, DH1 3LE
e-mail: e-theses.admin@durham.ac.uk Tel: +44 0191 334 6107
https://etheses.durham.ac.uk

The interpretation of the spectrum of energetic cosmic rays

A thesis submitted to the University of Durham

for the Degree of Doctor of Philosophy

by

Margaret C. Bell, B.Sc.

April 1974

DURHAM UNIVERSITY
SCIENCE
3 AUG 1974
SECTION
LIBRARY

To my parents

ABSTRACT

One of the most prominent and well established features in the primary energy spectrum of cosmic rays observed at the Earth is the change of slope occurring at several 10^{15} eV. A comprehensive survey of experimental EAS data is used to establish the integral size spectrum for electrons and muons at sea level and for electrons at mountain altitudes.

A model for the diffusion of protons in the Galaxy is developed based on experimental observations of the structure of hydrogen in the interstellar medium and of the magnetic field strengths and their orientations in galactic space. A numerical treatment of the diffusion problem is adopted. A prediction is made of the primary cosmic ray proton energy spectrum at the top of the atmosphere.

A survey of the data on cosmic ray primaries with energies below $\sim 10^{11}$ eV obtained by balloon and satellite experiments, was used to establish the relative abundances of all cosmic rays. By assuming that the cosmic ray composition remains the same at EAS energies the primary spectrum representing diffusion of cosmic rays with mixed composition is derived.

Comparison of the theory with experiment was made by converting the integral primary energy spectrum representing diffusion to the integral size spectrum by using results of EAS simulations through the atmosphere. Excellent agreement of theory with experiment is obtained provided that the primary cosmic radiation is protonic.

The problems encountered with ensuring isotropy of cosmic rays at the Earth are dealt with in great detail and are shown to create little problem over the part of the spectrum considered provided the solar system lies in the centre of the spiral arm.

Finally, a model is proposed as an alternative to that of diffusion which provides a qualitative but adequate explanation for the origin of the 'knee'.

PREFACE

The work presented in this thesis was carried out while the author was a research student under the supervision of Professor A. W. Wolfendale at the Physics Department of the University of Durham, between 15th September, 1970 and 1st October, 1973.

The calculations carried out by the author represent a numerical treatment of the problem of diffusion of cosmic rays. The diffusion model has been based on experimental observations which have been published by other physicists. A complete data survey has been performed by the author who has, herself, interpreted and processed the experimental data in order to develop these calculations.

J. Köta, on leave from the University of Budapest, Hungary, has spent the period December 1972 - December 1973 at the University of Durham performing calculations (independent of the author) based on an analytical solution of the problem of diffusion of cosmic rays. Differences appearing between this work and that of the author are due to the approximations made by Mr. Köta in order to obtain soluble integrals in his analytical treatment.

The results of the author's preliminary calculations were presented at the third European Symposium on cosmic rays held in Paris. An interim report was presented at the 13th International Conference on cosmic rays held at Denver 1973 and a full report has been published in the Journal of Physics A: Math., Nucl. Gen., Vol. 7, No. 3, 420 (1974).

Chapter 1 Introduction

1.1 History of cosmic radiation

The discovery of cosmic rays over 55 years ago activated man's resources to obtain an understanding of what they are, their physical properties and where they are coming from. Answers to such questions might lead us to a better understanding of the characteristics of the solar system, of the Galaxy or even the Universe.

The very first observation of the penetrating radiation was made by physicists such as C.T.R. Wilson, Elster and Geitel who showed that despite careful precautions to prevent known radiations from reaching the samples of air in their ionisation chambers, a significant residual conductivity remained. Because a reduction in the conductivity resulted by shielding the chambers with lead it was proved that the residual conductivity was due to radiation from outside the chamber. At first it was believed that the conductivity could be due to radioactive materials in the Earth. It was left to Hess (1912) to transport his apparatus to great altitudes in a balloon. He found that the ionisation in his chambers decreased with height above sea level up to 700 meters above which the ionisation increased. It was realised that the decrease in ionisation was due to a decrease in the contribution from the Earth's radioactivity whilst the increase was obviously due to radiation coming from out of space.

Initially, the penetrating radiation was believed to be gamma rays but Bothe and Kolhörster (1929) interpreted the variation of cosmic ray intensity with geomagnetic latitude, discovered earlier by Clay (1928), to be a consequence of the cosmic rays being charged. Later, Johnson and Street (1933) discovered that the cosmic ray intensity coming from the east was less than that coming from the west, proving that the majority of cosmic rays are positively charged.

DURHAM UNIVERSITY
SCIENCE
3 AUG 1974
SECTION
LIBRARY

In their journey from "outer space" to the Earth the particles will be affected by the media through which they travel (both by way of interaction and deflexion in the galactic magnetic field) and therefore, studies of the charged primaries (or their secondary particles arriving at sea level) give little information about the primary sources. For this reason only observations of neutral primaries i.e. gamma rays and possibly neutrons will give direct information on the origins of the primary cosmic rays.

There are two main reasons for interest in the primary cosmic rays, the first is to learn about the nuclear physics of the interactions of cosmic ray particles from studies on the secondaries and the second is the astrophysical significance of the particles, e.g. the interpretation of the shape of the energy spectrum and the mass composition.

Concerning the form of the primary spectrum, in the energy range 10^{10} - 10^{14} eV it has been demonstrated that stacks of emulsions flown to the top of the atmosphere can provide quite good information. For energies beyond $\sim 10^{14}$eV, however, the emulsion technique is defeated by low primary intensity and we are left with only indirect ways of establishing the spectrum, i.e. by examining the "extensive air showers" of secondary particles.

If cosmic rays are produced by sources in the Galaxy then typical candidates include stars, novae, supernovae, the galactic centre and pulsars. Because most cosmic rays are of energy $\sim 10^{9}$eV nucleon^{-1} non exploding stars are ruled out because insufficient energy is available. However, explosions occurring in novae and, say, in the galactic nucleus, liberate $\sim 10^{46}$ ergs and thus contribute appreciably to the cosmic ray flux. Supernovae explosions occurring approximately once every 30 years liberating $\sim 10^{52}$ ergs are, in the writer's view, the most likely sources

of cosmic rays of most energies. This view comes from the fact that synchrotron emission from supernovae indicates the presence of magnetic fields $\sim 10^{-3}$ gauss which are responsible for accelerating electrons and presumably nuclear components. As pointed out by Ginzburg and Syrovatskii(197 there is no definite proof that supernovae are sources of cosmic rays but they do seem very likely. On their model energies at least as high as 10^{17}eV could be reached.

Prior to the discovery of pulsars, there was difficulty in producing cosmic rays above 10^{17}eV and these particles had to come from the metagalaxy. Pulsars, however, are now known to be supernova remnants supporting fields $\sim 10^{12}$ Gauss over typical dimensions of $\sim 10^{6}$cm. Although the exact accelerating mechanisms operating in pulsars are not understood, it appears that they could accelerate cosmic rays to $\sim 3\ 10^{20}$eV nucleon^{-1} (Gunn and Ostriker, 1969 ; Gold, 1969).

A summary of the energy spectrum for cosmic rays observed at the Earth (above the atmosphere) is shown in figure 1.1. It can be seen to exhibit three basic characteristics: the region below ~ 2 GeV (the solar modulated part of the spectrum) the intermediate energy region around the "knee" occurring at $\sim 10^{16}$eV and the rather controversial "ankle" at $\sim 10^{18}$eV. A brief summary of the astrophysical significances of these three regions will be given.

1.2 Spectral region below ~ 2 GeV

A plasma, in the form of a gusty wind is blown out at a variable rate from the Sun. It supports a magnetic field which is predominantly radial due to the outward motion of the plasma but turbulence develops "knots" in the field structure. The bulk of cosmic rays have a momentum of a few GeV/c and their Larmor radii are small compared with the scale

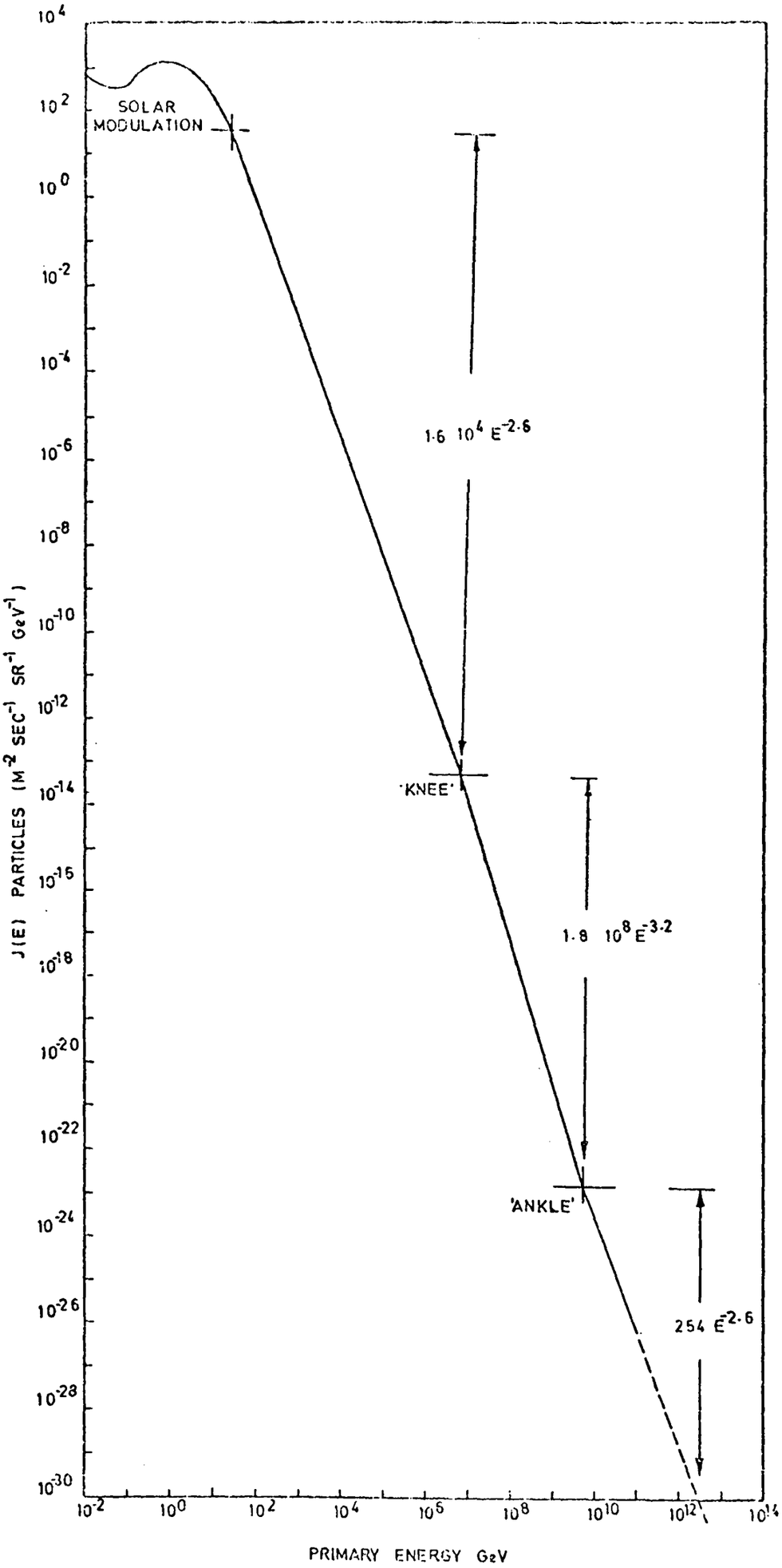

Figure 1-1 The differential energy spectrum of cosmic rays as observed above the Earth's atmosphere.

size of the system. We therefore have the necessary conditions for isotropic diffusion in the reference frame of the moving gas, whilst the outward convection supports solar particles to the Earth and continually impedes the arrival of galactic cosmic rays, causing modulation.

Cosmic rays with energies $\lesssim$2 GeV arriving at the Earth are not in general coming from the Sun but solar effects modulate the flux of particles from more distant parts of the Galaxy. Furthermore, their distributions are distorted by the Earth's magnetic field and by magnetic and electrical disturbances occurring in its immediate vicinity. These phenomena have no appreciable effect on primaries of intermediate and EAS energies.

1.3 Intermediate energy region $\sim 10^{10}$ - $\sim 10^{17}$ eV

The energy density and the isotropy of primary cosmic rays cannot be accounted for on the basis of a galactic origin theory without the existence of a trapping mechanism, generally believed to be a magnetic field, preventing the escape of particles to regions of low stellar density. For the trapping mechanism to be effective in this energy range, magnetic fields of a few μgauss coherent over a few parsecs must exist within the spiral arms. Cosmic rays would then be expected to come from regions more distant than the Sun but probably still within our local spiral arm and their motion from the source to the Earth would be of a diffusive nature. In fact, retention of particles by these fields is expected to break down ultimately when the energy is so high that particles can no longer be effectively trapped. This will occur when the radius of curvature of particles is the same order as the dimensions of the scattering elements. Therefore, an upper limit to the energy spectrum is forseen depending on the magnetic field strengths and sizes of the magnetic

clouds and degree of order in their orientation. Leakage from the magnetic fields depends on the magnetic rigidity and not the total energy of a particle; thus it is different for heavy nuclei and protons and it is conceivable on this account that most energetic primaries may be heavy. The characteristic known as the "knee" observed at $\sim 10^{16}$ eV would on this theory represent the gradual breakdown of the retention of the cosmic ray particles in the spiral arm as the energy considered increases.

If the particles obtained their energy by a gradual process of acceleration along their path from the source to the Earth then the "knee" could be a consequence of the accelerating mechanism. A simple explanation of the "knee" which could result is that the rate at which a particle is accelerated decreases with energy. In a situation such as this the most energetic particles will be those that have the longest lifetimes within the Galaxy. Since heavy nuclei may be expected to be shorter lived than protons because of the greater probability of suffering a collision with interstellar atoms then the spectrum would become more protonic with increasing energy.

Some physicists believe that the cosmic rays of this energy range are of extragalactic origin, e.g. according to Hillas (1967), if extragalactic sources of cosmic rays in an evolving Universe were more active in the past then the interaction of protons with the black body radiation would produce a greater energy loss with lower threshold energies in the past and this could produce the observed steepening near 10^{16} eV.

1.4 Ultra high energy region $\geq 10^{17}$ eV

Although galactic cosmic rays of energy between 10^{17} and 10^{19} eV can be trapped in the Galaxy by large scale magnetic fields of strength ~ 3 μgauss coherent over dimensions ≥ 1 kpc, they are unlikely to arrive at the Earth isotropically. Above $\sim 10^{19}$ eV the trapping is negligible and

very great anisotropies should appear. In fact, cosmic rays $\gtrsim 10^{17}$eV are found to arrive at the Earth isotropically which suggests that some, at least, must be of a metagalactic origin and this is particularly true above $\sim 10^{19}$eV. Possible sources here are radio galaxies and quasars.

The shape of the energy spectrum at the ultra high energy region ($\gtrsim 10^{18}$eV) is rather controversial. The "ankle" first discovered by Linsley in (1963) "disappeared" at the time of the Hobart conference see Hillas (1971a) and has "reappeared" at the recent Denver conference Krasilnikov (1973). The situation is thus unclear.

Some remarks of relevance to the extragalactic origin for the very energetic cosmic rays are:

(i) If the 2.7°K black body radiation first detected by Penzias and Wilson (1965) is Universal in origin and cosmic rays pervade the whole Universe then their resulting interaction would produce a cut off in the cosmic ray spectrum at about 6 10^{19}eV (Griesen, 1966, Zatsepin and Kuzmin, 1966 and others).

(ii) A number of workers have suggested that the "ankle" at $\sim 10^{18}$eV is due to the transition from galactic to extragalactic particles.

(iii) Berezinsky and Zatsepin (1969), Berezinsky and Zatsepin (1971) have proposed that neutrinos are responsible for the cosmic ray energy spectrum beyond 10^{19}eV. These neutrinos may be secondaries of the interactions of protons with microwave photons that pervade the metagalaxy.

The problem with respect to an interpretation of the cosmic ray energy spectrum is highly complicated and therefore it is necessary to concentrate on a selected area for a detailed study. The possibility of explaining the well established and prominent feature occurring at an energy of $\sim 10^{16}$eV in terms of diffusion of cosmic rays in the spiral arm of the Galaxy has been chosen as the subject for study in this thesis.

Chapter 2 Cosmic Ray properties:

The integral primary energy spectrum above 10^{14}eV

2.1 Introduction

Below an energy of 10^{14}eV the primary cosmic ray energy spectrum is observed directly by satellite and balloon experiments. Many research groups, e.g. Baradzei et al (1964), Yanovlev (1969) and Grigorov et al (1971) have studied this energy region for a number of years and the energy spectrum and to a lesser extent the mass composition of primary cosmic rays have been measured up to about 10^{14}eV. There is currently a controversy about the primary mass above an energy $\sim 3\ 10^{13}$eV but this will be dealt with in more detail in the next chapter.

Because the intensity of cosmic rays falls off very rapidly with energy it is quite impossible to observe cosmic rays with energy $>10^{14}$eV directly for reasons of rate. For example, at 10^{16}eV only one cosmic ray would fall on one square meter per year per steradian. Experimenters make use of the Earth's atmosphere with which cosmic rays interact causing a rapid build up of the number of particles to a maximum followed by a slower fall off, a phenomenon known as an extensive air shower (EAS). The total number of particles at a particular level in a shower can be estimated by sampling the density of particles at a number of positions across the shower front. The total number of particles reflects the primary energy of the cosmic ray thus providing an indirect method of establishing the primary energy spectrum.

In this chapter a discussion of a simplified model for an EAS developing in the atmosphere will be followed by a brief summary of actual parameters used to simulate showers by Monte Carlo techniques. The application of these model calculations to determine the size spectrum and subsequently the primary energy spectrum will be outlined, together

with a measure of their success. The effect the fluctuations in the electron size for a cosmic ray of specific primary energy will have on smearing out any features in the energy spectrum will be calculated.

A survey of EAS data will be used to establish the integral size spectrum of electrons at both mountain altitudes and at sea level over a size range of $10^5 < N_e < 10^8$ and $10^5 < N_e < 10^9$ electrons respectively, and of muons at sea level in the size range $5.10^3 < N_\mu < 3.10^5$ muons. The observed change of slope $\Delta\gamma$, the sharpness and the position of the "knee" N_K, and the absolute intensity of the two electron spectra obtained will be discussed. The muon spectrum observed experimentally will be compared with that of electrons. Some indication of the shape of the primary cosmic ray energy spectrum beyond $\sim 10^{17}$eV will be made. Finally, the degree of isotropy of primary cosmic rays observed at the Earth will be dealt with briefly.

2.2 Some general remarks on EAS modelling

The earliest work on the development of EAS in the atmosphere was of a purely theoretical nature, e.g. Fermi (1951) considered a simple development of the pion component whilst Nishimura and Kamata (1958) developed a theory for the electron-photon cascade. Details of the physics of nuclear interactions obtained from cosmic ray experiments using emulsion techniques Rozental (1952) marked the beginning of the phenomenological models, e.g. Ueda and Ogita (1957), who based their model on a 1-D solution of diffusion equations. Since the late 1950's particle accelerators, (such as those at Brookhaven, Batavia Serpukov and CERN) have been used to establish the physics of nuclear interactions up to energies $\sim 2\ 10^{12}$eV. These energies are still many orders of magnitude lower than those involved in the early interactions in an

EAS. Extrapolation of the nuclear physics data to much higher energies has been the only available means of establishing working hypotheses for shower modelling. Cocconi et al (1961) showed empirically that secondary pions from proton-light nucleus collisions are produced with an energy distribution in the laboratory system given by

$$S(E,E_o) = \tfrac{1}{2}\left[\frac{n(E_o)}{T}\exp\left(\frac{-E}{T}\right) + \frac{n(E_o)}{G}\exp\left(\frac{-E}{G}\right)\right]$$

where $n(E_o)$ is the multiplicity of pions produced, E_o the transferred energy, G and T are the average energy of pions in the backward and forward cones respectively, and the distribution in transverse momentum p_t of the produced pions is given by

$$f(p_t) = \frac{p_t}{p_o 2}\exp - \left(\frac{p_t}{p_o}\right)$$

where $2p_o$ is the mean transverse momentum, independent of energy. These results led to the development of the CKP model which was first developed by Hillas (1966), Lal (1967), Suschenko and Fomin (1968), de Beer (1966, 1968a, 1968b, 1968c, 1969) and Adcock et al (1968, 1969). This model has since been developed by Hillas et al (1971a, 1971b) and Marsden D. J. et al (1971) at Leeds and by Dixon et al (1973) at Durham. By using computers these authors carried out detailed 3-D simulations of EAS with results that agree very favourably with experimental data. Other shower models include the ideas of isobars first presented by Pal and Peters (1964), e.g. Cowsik (1966), McCusker (1969) and Goorevich (1971). Bradt and Rappaport (1968) made a 3-D Monte Carlo simulation based on a selection of two centre and isobar models. Grieder (1969, 1971) developed a refined model which considers single as well as double fireballs, which are assumed to

decay into pions and nucleon-antinucleon pairs and are chiefly responsible for particle production at high collision energies.

An understanding of shower development in the atmosphere is essential in order to make a successful analysis of EAS data, and therefore in the next section, a brief outline of the basic details of a CKP type model will be given

2.3 Simple type of shower model

The common features of models are as follows. The primary proton interacts with an interaction length $\lambda_n \sim 80$ gm cm^{-2}. The high energy nucleon loses a fraction ~ 0.5 of its energy in the first as well as in successive interactions. At high energies it is usual to assume equality of the number of pions produced in the various charged states i.e. $n_+ = n_- = n_o$. The energy distributions for the pions determined empirically by Cocconi et al (1961), abbreviated CKP, at accelerator energies are often assumed to hold at EAS energies. The mean transverse momentum $\langle p_t \rangle$ for the produced pions is rather controversial but is typically set equal to 400 MeV/c. The total number of pions n_s produced in the nucleon interaction depends on the energy of the interaction E_o, and can be written as $n_s = K E_o^{\alpha}$ with E_o in GeV. K and α are constants determined experimentally. Sometimes n_s is taken to have a logarithmic dependence on the energy but more commonly α is set equal to 0.25.

Subsequent pion interactions are assumed to differ in that they are catastrophic with an interaction length $\lambda_\pi \sim 120$ gm cm^{-2}. The multiplicity of particles produced in a pion interaction has the same type of energy dependence as above but with a different value of the constant K.

The products of the nucleon and pion interactions travel along the shower axis, and only when a pion decays is its angle of divergence from the axis considered. π^os however, decay at once and the resultant photons move almost along the π^o direction. These photons cause a build up of an electron-photon cascade which is often taken to obey the approximation A treatment of the Nishimura (1967) electron shower theory. The muons, the decay products of the pions, are considered to be inactive particles and their decay probability in the atmosphere is calculated in a standard fashion.

2.4 Results of Model Calculations of EAS

It is unnecessary here to go into all the details of the results of Monte Carlo shower simulations, only the details relevant to this work will, therefore, be discussed.

2.4.1 The derivation of the number of particles in a given shower

An array detects only a small fraction of the total number of particles in a shower. It is necessary to locate the core of the shower and then fit a function, known as the lateral distribution or structure function f(r), to the number of particles per unit area as a function of distance from the shower axis. The fit is often made many meters away from air shower axis, and therefore extrapolation of f(r) into the core region is necessary. Integrating the lateral distribution over all values of r defines the size of the shower. This is critically dependent on the structure function assumed, the core location criterion and the goodness of the fit in the region determined experimentally. Too steep a lateral distribution function causes an overestimate in the size of the shower and vice versa for too flat a distribution.

The most popular form for f(r) fitted to experimental data is that defined by Nishimura and Kamata (1950, 1951, 1952, 1958, 1967) which is dependent on s, the age of the shower. Young showers have lateral distributions steeper than older showers. However, the structure function fitted to the data varies from experiment to experiment, often they are assumed independent of shower age, e.g. a simple power law or exponential.

Subsequently there is no way of standardising the method of analysis used to obtain the size spectrum from the data measured by EAS arrays. In fact, even if this were possible, there are other problems to overcome. These include problems with EAS arrays built with different geometries having different acceptance biasses, the use of different types of detectors, e.g. Geiger-Muller counters, scintillation counters, Cerenkov detectors which all measure particles with different threshold energies and screening of detectors with wooden huts for example, also has an effect on the threshold energy of the particles to be detected.

The size assigned to a particular shower suffers considerable deviation depending on the model used in the shower analysis and whether or not allowance is made for the threshold energy of the particles detected. For this reason, it is believed incorrect to compare the intensity at a particular size defined by one experiment with the intensity observed at the same size in another experiment. Instead, since it is believed that the sizes derived in an individual experiment are absolute in themselves, some normalisation of the data is necessary in order to compare the spectra. This is achieved by dividing the data into two groups, spectra measured at sea level and those measured at mountain altitudes, then two straight lines at an angle of $\mathrm{Tan}^{-1}\ 0.5$ are chosen arbitrarily and their

"best fit" to a set of data is found by normalising at positions remote from the "knee".

2.4.2 The relationship between the total number of particles recorded at sea level and mountain altitudes to the proton primary energy

Obtaining the energy spectrum from air shower data is rendered difficult by the lack of precise knowledge of the nucleonic cascade which governs the development of the shower. The average parameters involved in high energy nuclear interactions are not well known and fluctuations add to the complexity. Monte Carlo calculations have shown that the effects of these uncertainties are minimised if showers are observed near the average depth of maximum development, which occurs lower in the atmosphere as the energy of the initiating particle increases.

Most theoretical models predict an almost linear relationship between the primary energy and the shower size at maximum amounting to $2\ 10^9$ eV/ particle (e.g. Bradt and Rappaport, 1968). At any one observation level in the atmosphere however, this is true for only a small energy range, e.g. at Mount Chacaltaya primaries of energy $\sim 2.10^{15}$ - $\sim 2.10^{17}$ eV are at maximum development. For model I de Beer et al (1966) defined the $N_e - E_o$ relationship for cosmic ray primary protons arriving vertically at sea level, in two ways. The first

$$E_o = 9.5\ 10^{13} \left(\frac{N_e}{10^4}\right)^{0.91} \text{ eV} \qquad 2.1$$

represents the mean electron size for showers initiated by cosmic ray primaries with fixed primary energy and the second

$$E_o = 5.6\ 10^{13} \left(\frac{N_e}{10^4}\right)^{0.93} \text{ eV} \qquad 2.2$$

represents the mean primary energies for showers of fixed size. The $N_\mu - E_o$ relationship for vertical showers at sea level has been defined accurately by de Beer et al (1969) only for muons with an energy threshold of 1 GeV using model II. The relationship is defined by

$$E_o = 1.8\ 10^{15} \left(\frac{\bar{N}_\mu (>1\ \text{GeV})}{10^4} \right)^{1.13} \text{eV} \qquad 2.3$$

In figure 2.1 is plotted the total number of muons above 1 and 10 GeV as a function of primary energy resulting from the various models developed by Hillas (1971), at a zenith angle 14^o. It can be seen that agreement with the results of the Łódz group, Giler et al (1969), is quite good, subject to the lack of precise details of their calculations: also with de Beer et al, whilst the results of Grieder (1969, 1971) are low, perhaps due to consideration of N-N interactions only. The calculations of Rathgeber (1969) give a very low slope for N_μ vs E_o at very high energies and therefore the primary energy is considerably overestimated.

On the whole, this graph supports the statement that extreme caution must be taken when establishing energy spectra from size spectra.

The recent work of Dixon et al (1973, 1973a) has produced N_e-E_o and N_μ-E_o curves for particular experiments performed at particular atmospheric depths as a function of the energy threshold of the electrons and muons detected at the observation level. Only those relationships to be used in this thesis will be presented here. It is believed that the energy threshold for electrons detected by Geiger Muller tubes and plastic scintillators is a few eV and $\geq$2 MeV respectively, but due to shielding of apparatus by wooden huts for example, the energy thresholds could be higher. For this reason it was necessary to establish the N_e-E_o curves for energy thresholds up to 10 MeV. By using the one dimensional development of air showers according to approximation B, the N_e-E_o curve for a zero energy threshold was calculated by Dixon et al (1973) at the atmospheric depths 530 gm cm^{-2}, Mount Chacaltaya and at 1030 gm cm^{-2}, Moscow State University air shower array. As a result of a one dimensional treatment according to approximation A plus results from the numerical

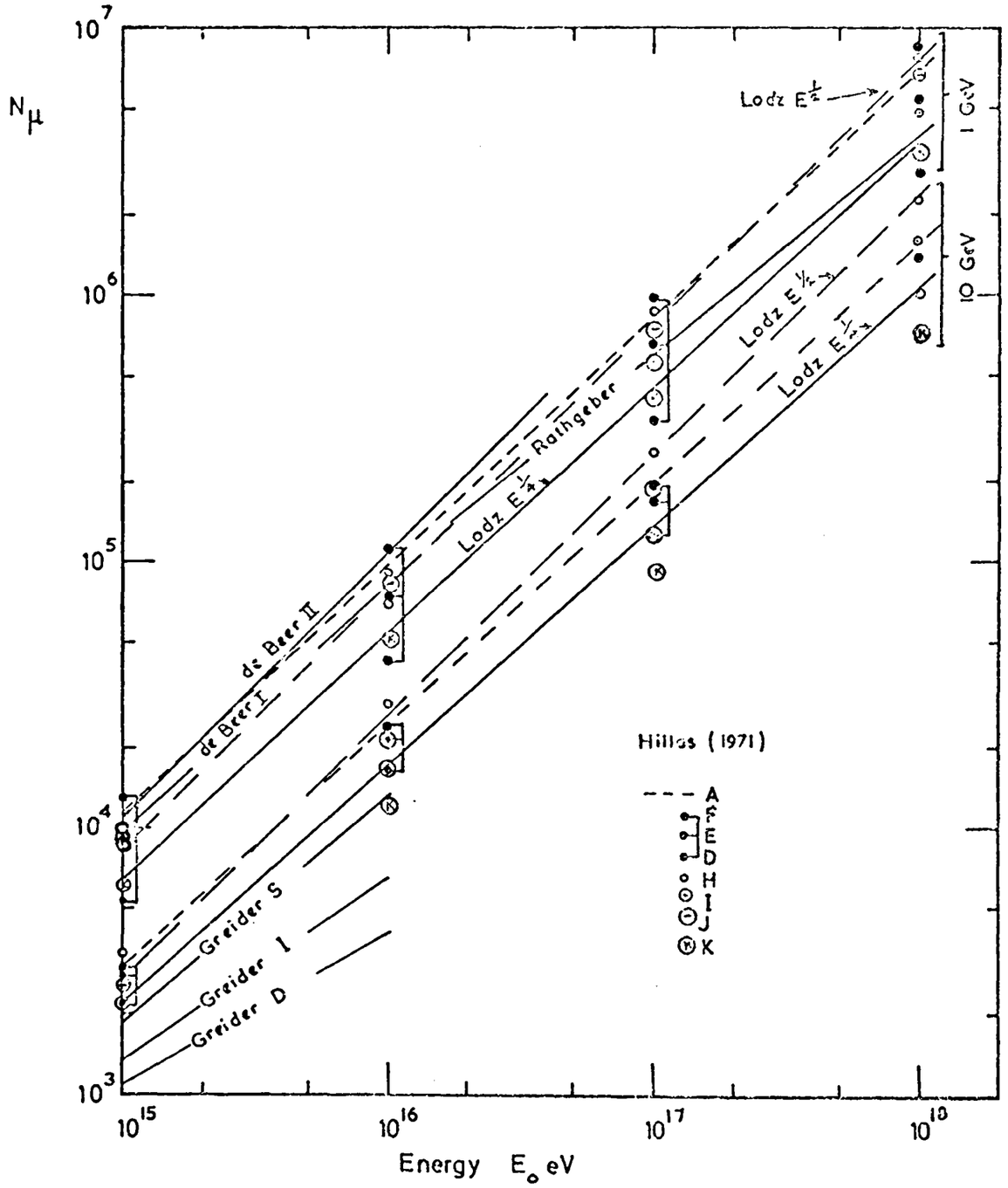

Figure 2-1 The number of muons above various threshold energies in proton showers at 14° for models A-K Hillas (1971) compared with those for vertical showers of de Beer et al (1966), Rathgeber (1969), Grieder (1970, 1971) and Giler et al (1969) marked Lodz.

treatment by Messel and Crawford (1969) of the shower when the energy of the secondary particles falls below approximately 56 GeV, the N_e-E_o curves for electron thresholds of >1 MeV and >10 MeV were established for the atmospheric depths 530 gm cm^{-2} and 1030 gm cm^{-2}. In the case of muons a 2-D treatment yields the N_μ-E_o curve for a muon threshold energy of 10 GeV at sea level. All these size-energy curves are shown in figure 2.2 and are for primary protons developing into showers that arrive vertically at the observation point.

2.4.3 The relationship between the total number of particles recorded at sea level and mountain altitudes to the primary energy of a cosmic ray with atomic mass A>1

When the incoming energy of E_o is carried by a nucleus with atomic mass A(>1) then the model calculations of de Beer et al (1966) assumed that as a first approximation the shower produced is the result of the superposition of A showers each with an energy E_o/A. The dependence on E_o of N_e and N_μ (equations 2.1, 2.2 and 2.3) are such that for heavy primaries N_e will be reduced and N_μ will be increased.

Most of the simulations of heavy primary particle initiated showers have been made on the basis of "superposition" although there is little published evidence in support of the validity of this assumption. There is, however, information on how a heavy nucleus fragments when it collides with an air nucleus, obtained from cosmic ray emulsion experiments. Bradt and Rappaport (1968) considered a fragmentation model which was also adopted by Theilheim and Beiersdorf (1970), in which each nucleus of energy E_o and atomic weight A caused 30-50% of the mass to be detached in interactions in the form of alpha particles each of energy $\frac{4\,E_o}{A}$; no pions are produced. In the subsequent generation each alpha particle fragments into four nucleons of equal energy which then produce pions.

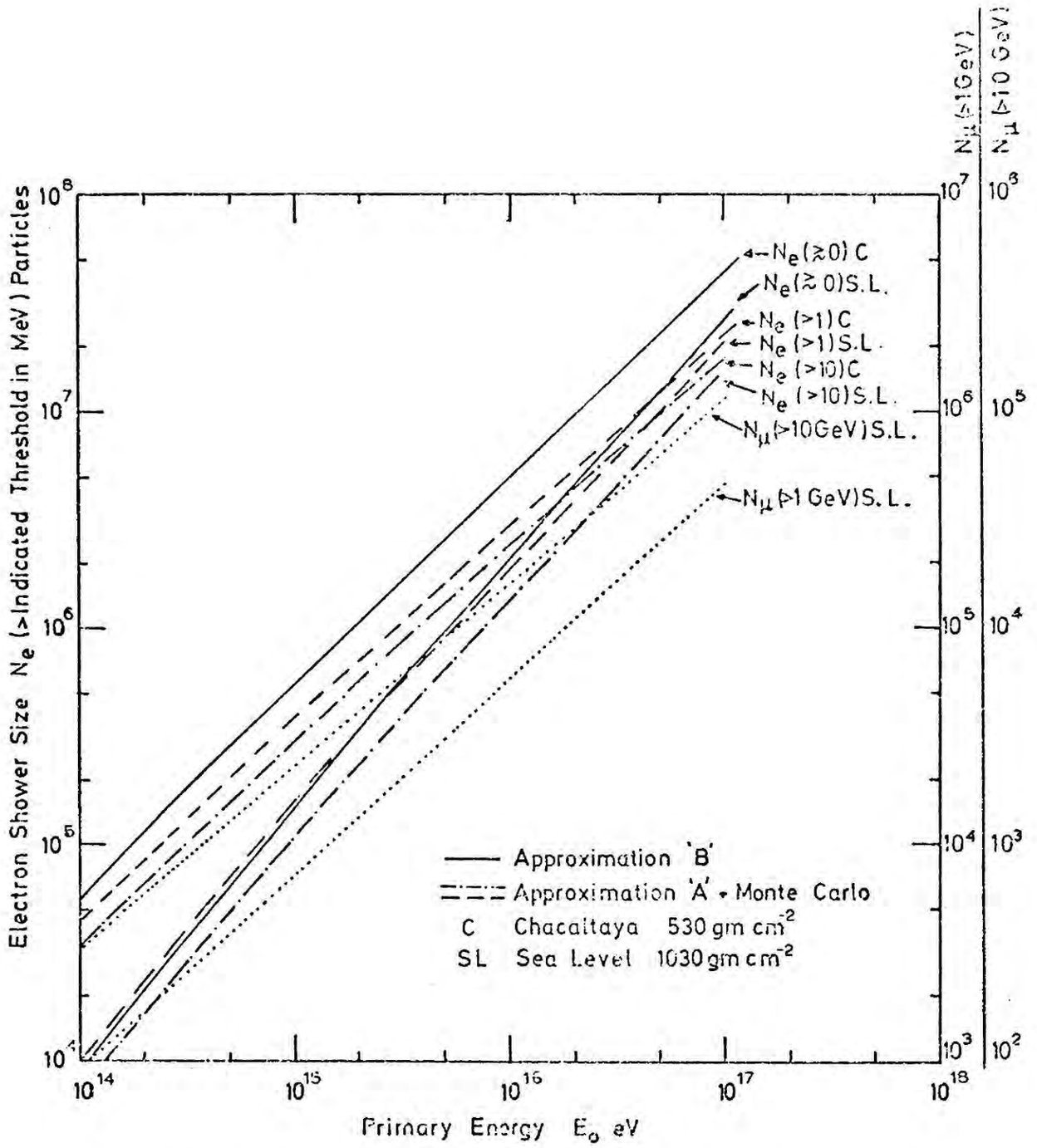

Figure 2-2 E_o-N_e and E_o-N_μ relationship for vertical showers initiated by primary cosmic ray protons as defined by the shower simulations of Dixon et al (1973). The threshold energy of the secondary particles detected at the observation level i.e. at mountain altitudes (C) and at sea level (SL) is indicated in brackets. The unit of threshold energy is MeV unless otherwise stated.

The residual heavy nucleus continues to fragment producing alpha particles until eventually only nucleons remain. A more complicated model for the break up of the primary heavy nucleus used by Dixon et al (1973a) is shown in figure 2.3. Here the depth of maximum development of the electron cascade for showers initiated by particles of different energy and atomic weight are shown. The broken and chained lines are obtained for primary particles of atomic weight 20 and 56 respectively using the model for fragmentation shown in the inset (Dixon et al 1973a). The depths of maximum development at primary energies around 10^{17}eV derived from superposition model are indicated by ←[10] (Dixon et al, 1973a) and (10) (Fomin and Khristiansen, 1970). The effect of this new model is to modify the shower development curves such that, on average, showers reach their maximum of development higher up in the atmosphere. This means that the showers arriving at the observation point are more mature.

The size-energy curves for cosmic rays of mixed composition are dependent on the variation of the mean atomic weight as a function of energy. At this stage the latter is not available and therefore the N_e-E_o and N_μ-E_o curves for converting the primary energy spectrum for mixed composition with galactic modulation obtained by the diffusion model to the size spectrum will be derived later using the results of the model calculations of Bradt et al (1968), de Beer et al (1966) and Dixon et al (1973, 1973a) discussed in this section.

2.4.4 The effect of fluctuations in the electron size expected at sea level

Because of the effects of fluctuations in shower development in the atmosphere, primary cosmic rays of energy E_o develop into showers such that there is a distribution of shower sizes at a particular depth in the atmosphere. Obviously the shape of the distribution predicted by

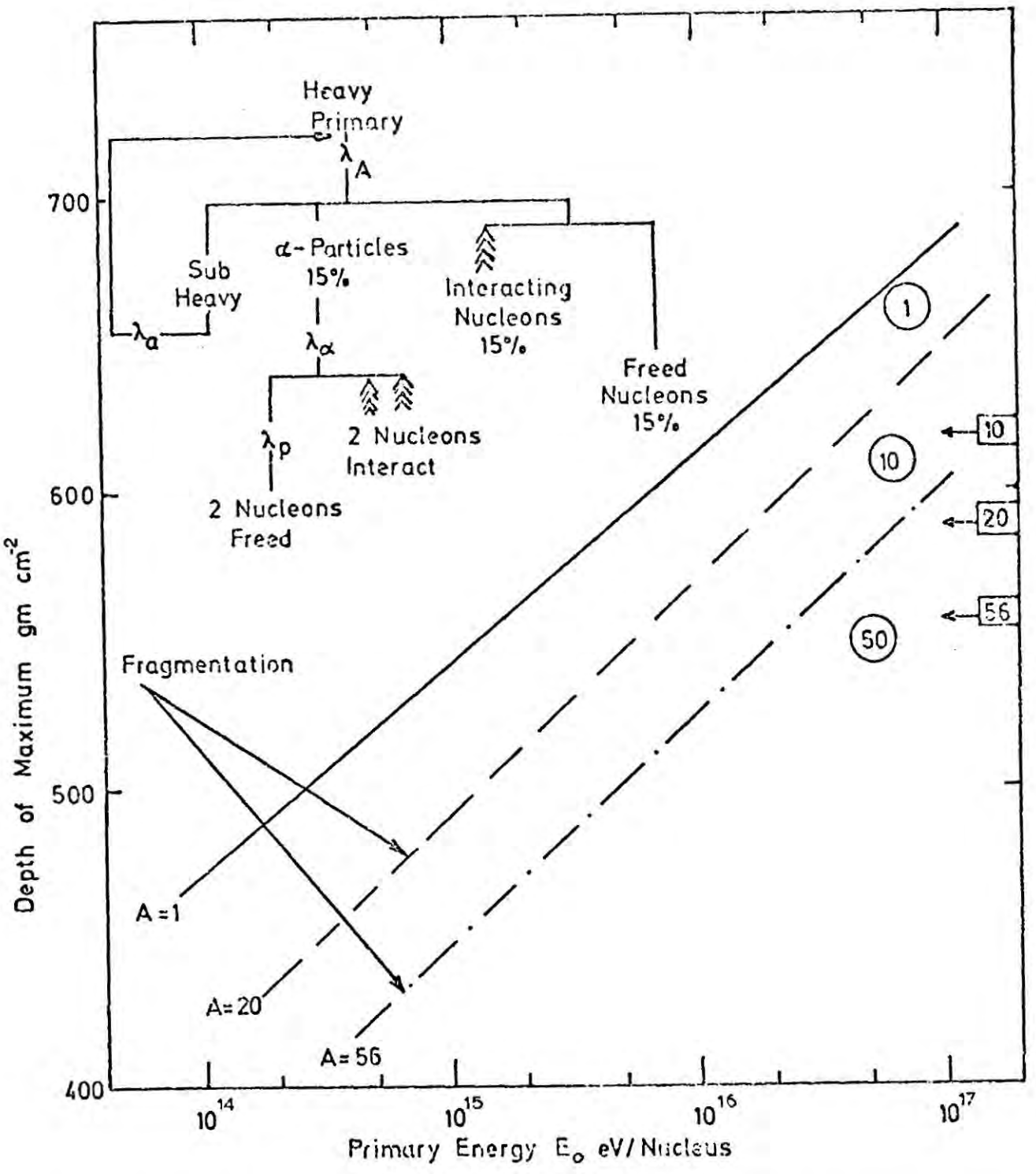

Figure 2-3 The depth of maximum development of the electron cascade for showers initiated by particles of different energy and atomic weight. The inset shows the model of the break up of a primary heavy nucleus used by Dixon et al (1973a).

any particular shower model is different, but for the present discussion, the model calculations of de Beer et at (1966, 1968a, 1968b, 1968c, 1969) and Adcock et al (1968, 1969) were considered. Table 2.1 gives the basic parameters assumed by these authors. In fact, they give particular attention to large zenith angle showers in order to throw light on the gross features of EAS.

The electron shower size distribution at sea level for a particle of energy $\sim 4\ 10^5$ GeV predicted by model II (see table 2.1 for details) is well approximated by the sum of two Gamma functions with $\frac{\sigma}{\bar{N}_e}$ ratios of 0.55 and 0.37 respectively. The calculation performed to establish the effect fluctuations have on smoothing the size spectrum in the region of the "knee" is dealt with in detail in appendix (i).

It is found that even if the fluctuations are as high as a factor of two in size for all cosmic rays of all energies arriving at the Earth at all zenith angles, there is no significant smoothing in the size spectrum in the region of the knee. Consequently, fluctuations can be ignored.

2.5 Extensive Air Shower Data

2.5.1 Integral size spectrum for secondary cosmic ray electrons

The integral size spectrum has been measured over the range 10^4 - 10^8 electrons at mountain altitudes by Chudakov et al (1960), Clark et al (1963), Bradt et al (1965), Amineva et al (1969), Hlavac et al (1969), Aseikin et al (1971), Antonov et al (1971) (aircraft) and Yoshii (1972) and over the range 10^5 - 10^8 electrons at sea level by Khristiansen (1964), Vernov et al (1967), and Khristiansen et al (1972). Because these experiments are performed at different altitudes and different experimental and shower analyses have been used, the data were treated in the way outlined in section 2.4.1 The experimental data considered

Table 2.1: Summary of the parameters used in the three air shower models developed by de Beer et al (1966)

Model		I	II	III
Type of Model		nucleon-air-nucleus		
Momentum Distribution		CKP: $f(p_t) = \frac{p_t}{p_o}^2 \exp - (\frac{p_t}{p_o})$		
Mean Transverse Momentum p_t GeV/c		$2\,p_t = 0.4$ independent of energy		
Multiplicity of secondary particles produced in nucleon interactions		In general $n_s = 2.7 \times 2^{\frac{1}{4}} (KE_o)^{\frac{1}{4}}$ where K is the inelasticity coefficient		
		$n_s = 2.7\ E_o^{\frac{1}{4}}$	$n_s = 2.3\ E_o^{\frac{1}{4}}$	$n_s = 3.2 (KE_o)^{\frac{1}{4}}$ up to $E_o = 2\ 10^{12}$ eV; $n_s = 0.57 (KE_o)^{\frac{1}{2}}$ at higher energies
$n_+ : n_- : n_o$		1 : 1 : 1		
Mean free path ($gm\ cm^{-2}$)	nucleon λ_n	80		
	pion λ_π	120		
Inelasticity coefficient	K_n	0.5		
	K_π	1.0		
Multiplicity of pions for pion interactions		$n_s = 3.2\ E_o^{\frac{1}{4}}$	$n_s = 2.7\ E_o^{\frac{1}{4}}$	$n_s = 3.2\ E_o^{\frac{1}{4}}$
Pion energy distribution in the laboratory system		CKP: $S(E,E_o) = \frac{1}{2}(\underbrace{\frac{n(E_o)}{T}\exp-(\frac{E}{T})}_{\text{Forward Cone}} - \underbrace{\frac{n(E_o)}{G}\exp-(\frac{E}{G})}_{\text{Backward Cone}})$		
Comments		a) Varied the inelasticity parameter b) Normal statistical fluctuations in the depth in the atmosphere of the interactions c) Model I gave a good fit to the experimental observations		

to give the most accurate estimate of the integral size spectrum at mountain altitudes and at sea level only are shown in figures 2.4 and 2.5 respectively. After collection of the data in this way, a straight line was fitted to the data lying beyond the "knee" by a weighted least squares method.

Comparing the size spectrum at mountain altitudes with that at sea level three striking characteristics are noticeable. These are:-

	Mountain altitudes	Sea level
a) Position of the "knee"	$1.3\ 10^6$	$7.4\ 10^5$
b) Change of slope	0.70	0.54
c) Absolute intensity	∿20xJ(N<kink)	J(N<kink)

The "knee" is considered to be sharp in both cases perhaps a little less sharp at mountain altitudes than at sea level.

The change in position of the "knee" is caused by showers of different energies reaching their maximum of development at different depths in the atmosphere. Also the size plotted here is not necessarily that at maximum development and depends on the experimental and shower analysis techniques used. When the intensity is matched below 10^6 particles the size spectrum at mountain altitudes crosses over that at sea level at a point where their showers reach a maximum midway between the two altitudes and have the same size at both depths. The change of slope at mountain altitudes is, therefore, observed to be steeper than that at sea level. This is due to the fact that at mountain altitudes a 10^6 particle shower could be either a mature shower or one that would develop into a 10^7 or 10^8 particle shower at near sea level. This causes a false increase in the number of showers with $N_{e_{max}} = 10^6$ particles at mountain altitudes at the expense of showers with $N_{e_{max}} > 10^6$ particles, and consequently a steepening of the slope.

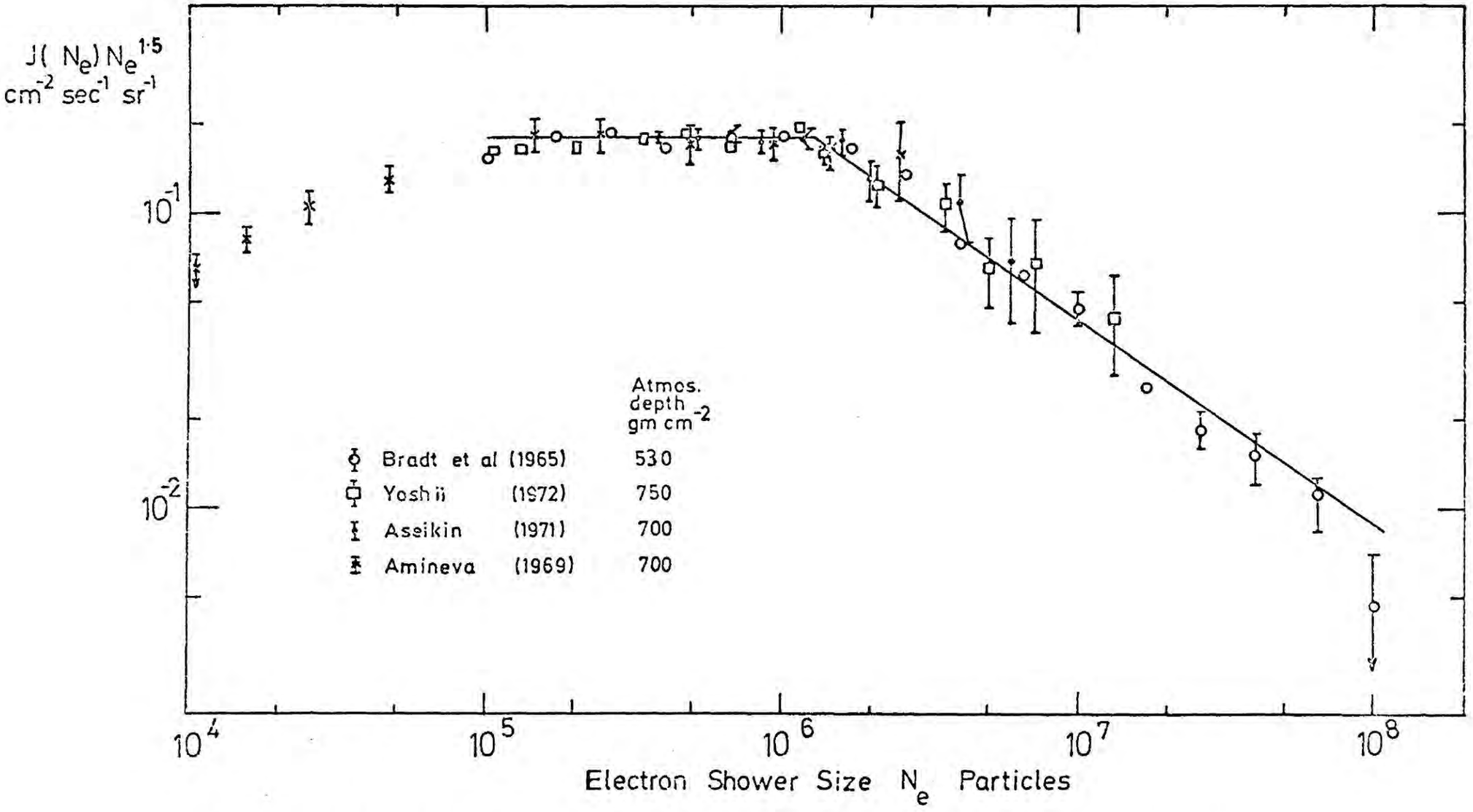

Figure 2-4 Integral size spectrum of EAS at mountain altitudes. A least squares fit to the data beyond 10^6 particles gives the change of slope $\Delta\gamma = 0.70$.

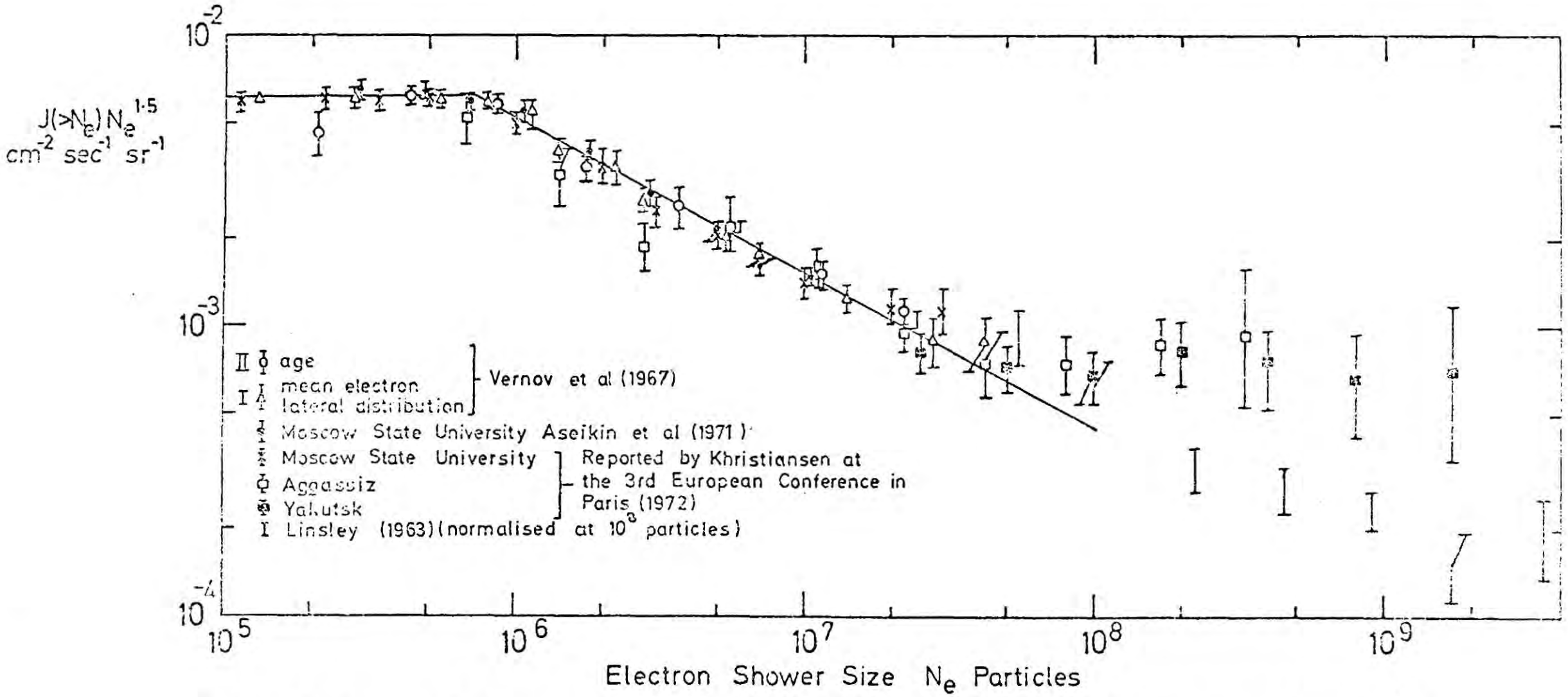

Figure 2-5 Integral size spectrum of EAS at sea level. A least squares fit to the data beyond 10^6 particles (excluding the Paris and Linsley data) gives the change of slope $\Delta\gamma = 0.54$.

In considering the spectrum for showers at their maximum of development then the experimental data suggests that only one in approximately twenty showers reach sea level compared with mountain altitudes. The spectrum for size at maximum development would be expected to have a change of slope $\Delta\gamma$ to be the same at all altitudes.

Finally a comment on the sharpness of the integral size spectrum. If the spectra observed in different experiments were compared by taking the derived shower size as absolute, no abrupt change in slope would be observed because the "knee" occurs at slightly different size in each experiment. However, for reasons stated previously, the normalised spectrum is assumed to be the correct one. The sharp "knee" reflects a discontinuity in the differential size spectrum as indicated in figure 2.6. This possibility is not inconsistent with experiment.

2.5.2 The 'f' factor

The survey of experimental data on the integral electron size spectrum suggests that the transitional region is rather short, i.e. there is a sharp change of slope. The degree of sharpness can be represented by the quantity f* as follows. Draw the best lines through the data points well away from the transition region, let these intersect at a size N_K and spectral intensity $J_K(>N_K)$. Now a "smooth" curve is drawn through the experimental points and the spectral intensity at N_K:$J(>N_K)$ is determined.

Then $f_i^* = \frac{J(>N_K)}{J_K(>N_K)}$ and similarly the factor for differential intensities can be defined as

$$f_d^* = \frac{J(N_K)}{J_K(N_K)}$$

Inspection of figures 2.4 and 2.5 suggest that $f_i^* = 1.00 \pm 0.06$ and $f_i^* = 0.96 \pm 0.04$ for the mountain altitude and sea level data respectively.

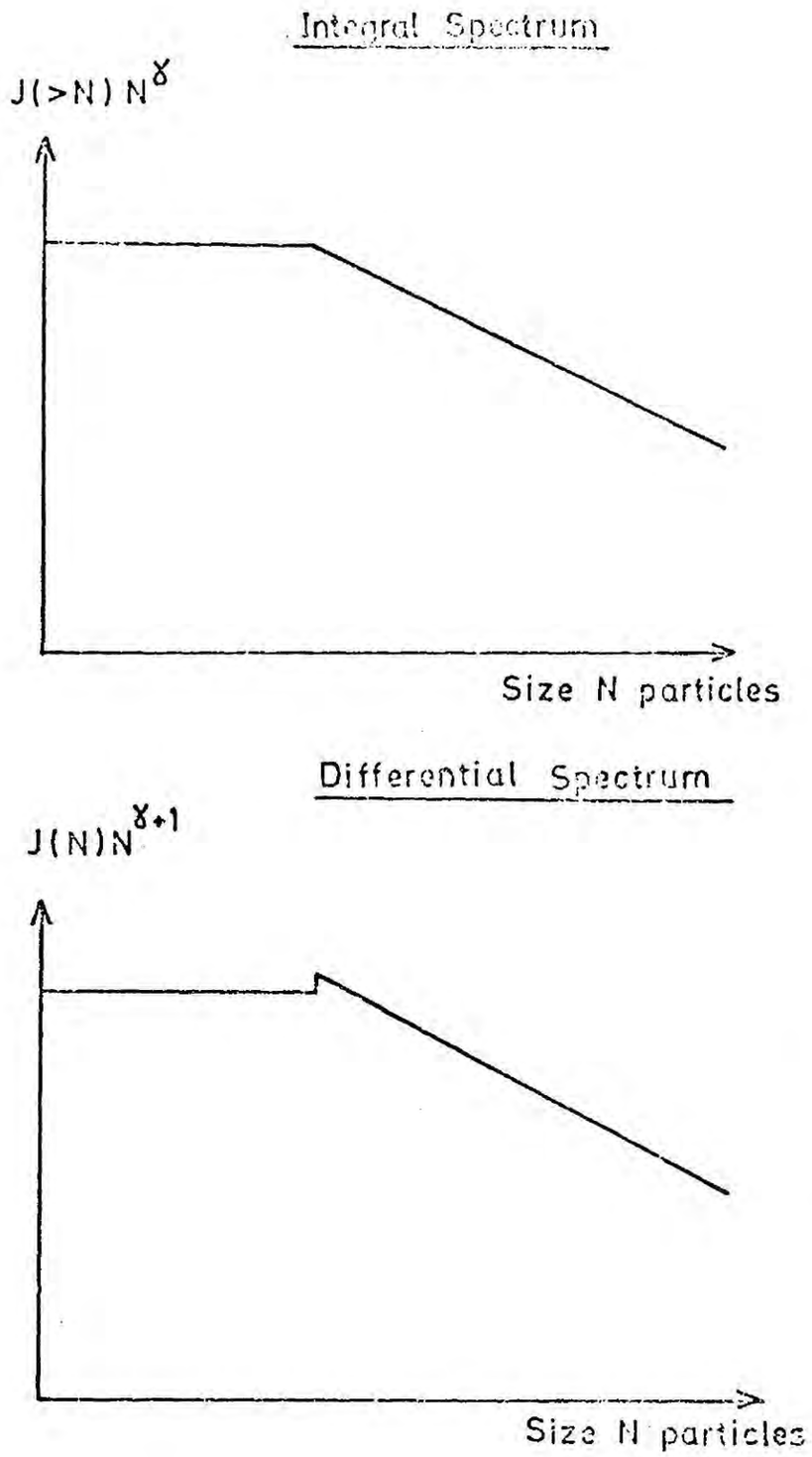

Figure 2-6 The consequence of a sharp "knee" in an integral size spectrum.

This implies that within experimental error $f_d^* = 1.0 \pm 0.1$ at both mountain altitudes and sea level.

Ultimately, we will be involved with energy spectra in both the differential and integral form, we therefore define $f_i = \frac{J(>E_K)}{J_K(>E_K)}$ and $f_d = \frac{J(E_K)}{J_K(E_K)}$ in a similar manner as for the size spectra above.

2.5.3 The muon size spectrum

In an EAS the mean number of muons is less than the number of electrons and because muons are relatively inactive particles the fluctuations in muon size at sea level are smaller. For this reason the muon size is a better quantity for measuring the primary cosmic ray energy. The muon size spectrum reported by Khristiansen at the 3rd European Symposium on cosmic rays in Paris (1972) is believed to be the most up to date and the best estimate of the muon integral size spectrum and is plotted in figure 2.7. The details of the EAS array and shower analysis will be dealt with in section 2.5.5. The change of slope $\Delta\gamma = 0.75$ occurs at $\sim 2\ 10^4$ particles with a value of $f_i = 0.96 \pm 0.04$ or $f_d \sim 1.0 \pm 0.1$, as expected the muon spectrum has a change of slope similar to that for electrons at sea level. The data implies that the number of electrons in an EAS is approximately two orders of magnitude greater than the number of muons. The muon spectrum has a transition region which is extremely short and exhibits similar characteristics to those of the electron spectrum.

2.5.4 Best estimate of the integral electron size spectrum at mountain altitudes and at sea level and muon spectrum at sea level

It is believed that the early work performed by Bradt et al (1965) and Amineva et al (1969) at mountain altitudes and the revised data presented at 3rd European Symposium on Cosmic Rays in Paris in September 1972 by Khristiansen for EAS at sea level are the most accurate. These spectra

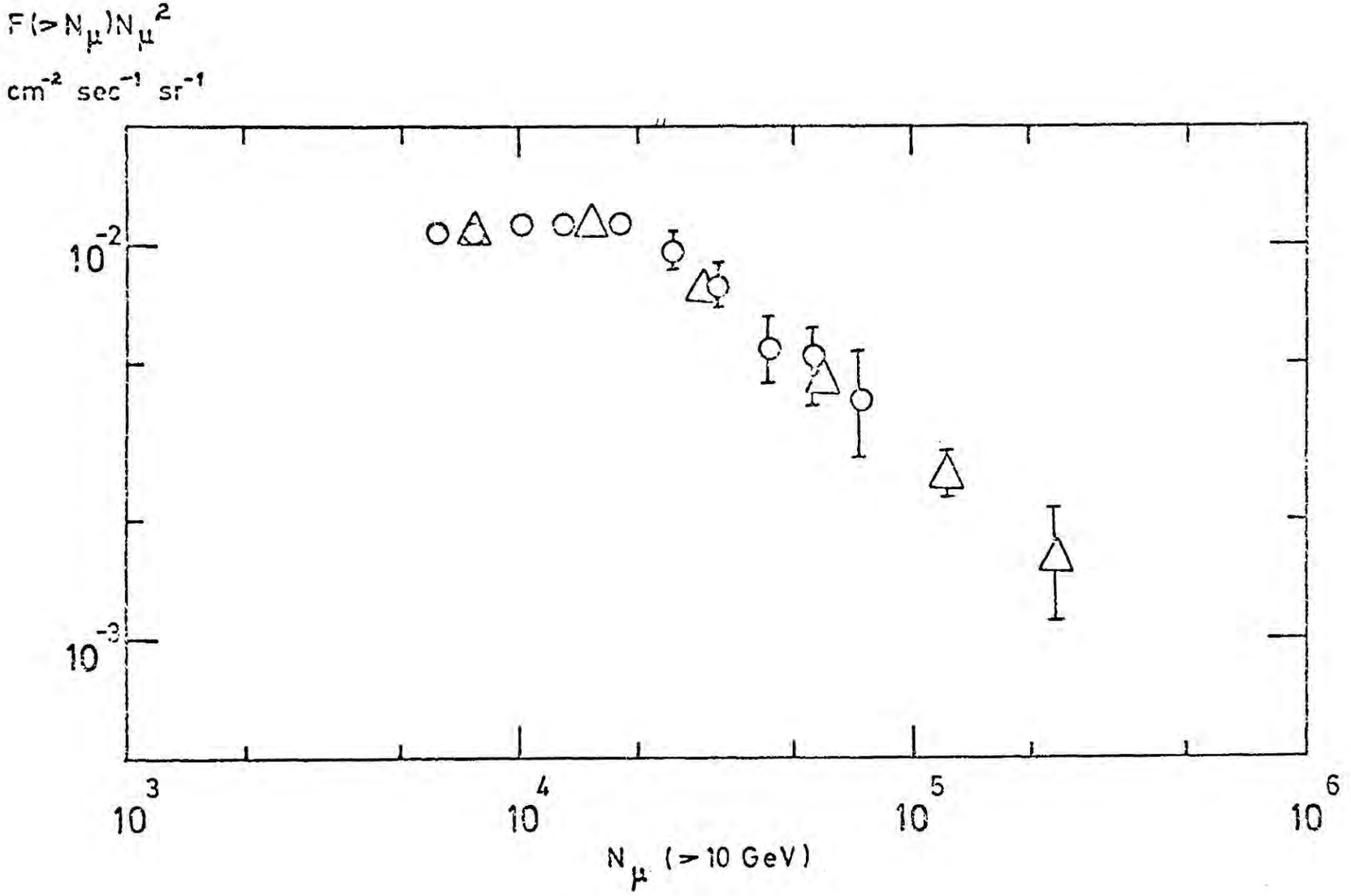

Figure 2-7 The integral muon size spectrum at sea level as measured experimentally at Tien Shan o and Moscow State University Δ, see Khristiansen et al (1972).

will be used to make comparisons with the diffusion model to be developed in a later chapter. The details of the arrays and the method of data analysis for these two particular experiments are now discussed.

2.5.5 The EAS array positioned at sea level used by Moscow State University

The reader is referred to Nikolskii (1963), Fomin and Khristiansen (1964), Dedenko (1964), Danilova, Denisov and Nikolskii (1964), Nikolskii (1965), Vernov et al (1967), Efimov, Krasil'nikov and Nikolskii (1968), Vernov, Khrenov and Khristiansen (1969), Nikolskii (1969), Vernov et al (1969), Aseikin et al (1971) and also Khristiansen et al (1972) for the full details of the design, analysis and results of the series of experiments carried out by this group in the last ten years. Only a brief discussion of the air shower array and the method of analysis will be given here. The array consists of 6000 hodoscoped counters of various areas (330 cm^2, 100 cm^2 and 18 cm^2) placed in groups on the plane of observation, i.e. at 1030 gm cm^{-2} atmospheric depth. The groups cover an area of a circle with radius 200 metres drawn from the centre unit. These counters determine the shower axis, the lateral distribution of electrons and the total number of electrons. Because the counters are Geigers then effectively all electrons falling on the counters are detected and therefore the energy threshold for electrons is expected to be very low ($\to 0$).

The system to determine the flux, N_μ, of μ-mesons with energy >10 GeV consists of 2000 Geiger counters each included in the hodoscope and situated at a depth of 40 m.w.e. underground.

Due to the lack of knowledge of the exact behaviour of both the experimental and theoretical (Nishimura and Kamata 1958) electron lateral distribution function at the shower periphery a systematic error of 10% in N_e is possible. N_μ is found from $N_\mu = \frac{\rho_\mu}{f_\mu(r)}$ where ρ_μ is the density

of muon flux measured underground, $f_\mu(r)$ is the lateral distribution of muons and r is the distance from the shower axis to the detector of muons in the plane perpendicular to the shower axis, therefore r depends on θ and ϕ. A systematic error in N_μ due to the inaccurate knowledge of $f_\mu(r)$ at the periphery can be as large as 20%.

In figure 2.5 the experimental data on the electron size spectrum at sea level obtained by the MSU group is presented in two ways. The first, open triangles, is found under the assumption that the lateral distribution of electrons in each individual shower coincides with their averaged lateral distribution whilst the open circles are found by assuming each shower has an individual lateral distribution function of the Nishimura-Kamata type. Before normalisation, there was a difference in the absolute value of the spectra I and II which is completely explained in the difference in behaviour at the periphery of the shower between the averaged function and the function by Nishimura and Kamata corresponding to the average value s. The real spectrum over N_e probably lies between these two and to obtain it the accurate behaviour of the lateral distribution of electrons must be known. Normalisation of the data removes this uncertainty. Another systematic error possible in the N_e-spectrum is connected with the possible dependence of the electron lateral distribution function f(r) upon the total number of particles N_e. Detailed calculations indicate that if f(r) does depend on N_e the effect would be equivalent to a change $\Delta\gamma \lesssim 0.03$. At the 3rd European symposium on cosmic rays Khristiansen reported their most recent electron size spectrum which is shown by crosses in the same figure.

The muon spectrum, $N_\mu(E_\mu > 10$ GeV), was initially obtained in two ways, the first corresponded to a direct measurement of the N_μ spectrum whilst

the second required the N_e- spectrum from which the N_μ-spectrum was obtained with the use of the empirical dependence of $\bar{N}_\mu$ on N_e at fixed N_e. The data indicate that the change in the shape of the N_μ-spectrum is similar to the change of the N_e-spectrum.

2.5.6 Extensive Air Shower Array positioned at mountain altitudes. The Bolivian Air Shower Joint Experiment

The air shower array built at Mount Chacaltaya (530 gm cm^{-2}, 5200 m.a.s.l.) early in the 1960's consisted of detectors made up of a disk of plastic scintillating material 105 cm in diameter and 10 cm thick. Advantage was taken of the possibility at a given station of observing showers that have developed through various definite thicknesses of atmosphere as determined by the inclinations of their axes. The arrival times of the particles defined the shower direction. The detectors probably measure the density of shower particles with an energy threshold of $\sim$1 MeV.

Showers were selected from the processed data using criteria which ensured that the detection probability was close to 100%. Having divided the accepted showers into sub groups, according to zenith angle, it was possible to construct the integral size spectrum for each group taking into account the projected effective areas for different sizes, the solid angle included in each zenith angle interval, and the total observation time. Each size spectrum spans a narrow interval of atmospheric depth and effectively describes the integral intensity of showers of size greater than N particles at a fixed atmospheric depth x i.e. $J(N,x)_{x=}$ constant.

The integral size spectrum for near vertical showers is shown in figure 2.4 based on some 3820 events. The characteristic change in

slope is from -1.4 near 10^5 particles to -2.3 near 10^7 particles giving a value for $\Delta\gamma=0.9$. This change of slope not only reflects a change in the primary energy exponent in this region but indicates that for small showers $\sim 10^5$ particles the average depth of development lies above the level of observation while showers of size $\sim 10^7$ particles or more reach their average maximum development below the level of observation. In this respect the intensity of the smaller showers is artificially enhanced at the expense of the larger showers.

By making a cut at the same integral intensity the function $N(J,x)_J$, J=constant can be derived from $J(N,x)_{x=\text{constant}}$ of the Mount Chacaltaya data, thus establishing the longitudinal development curves (Clark et al, 1963, Bradt et al, 1965) from which the size at maximum development can be estimated. In this way a plot of the intensity versus the estimated size at the maximum of development (for the size range 10^6-10^8 particles) can be obtained without resorting to a particular model of shower development. The resulting spectrum is plotted in figure 2.8 and a power law with exponent $\gamma=-2.3$ is the best fit beyond $\sim 10^6$ particles. The two experimental points plotted at $5.2\ 10^5$ and $1.55\ 10^6$ particles are much in error due to the method of analysis. There are no complete development curves available for showers with sizes less than $5.2\ 10^5$ particles and therefore because the levelling off expected at low shower sizes is not defined the actual position of the "knee" cannot be located. However, it can be assumed to occur just below 10^6 particles, to be compatible with other data (as will be explained, the exact position of the "knee" is unimportant).

2.5.7 Integral size spectrum beyond 10^7 particles

Linsley (1963) detected EAS with sizes $\geq 5\ 10^7$ particles with an

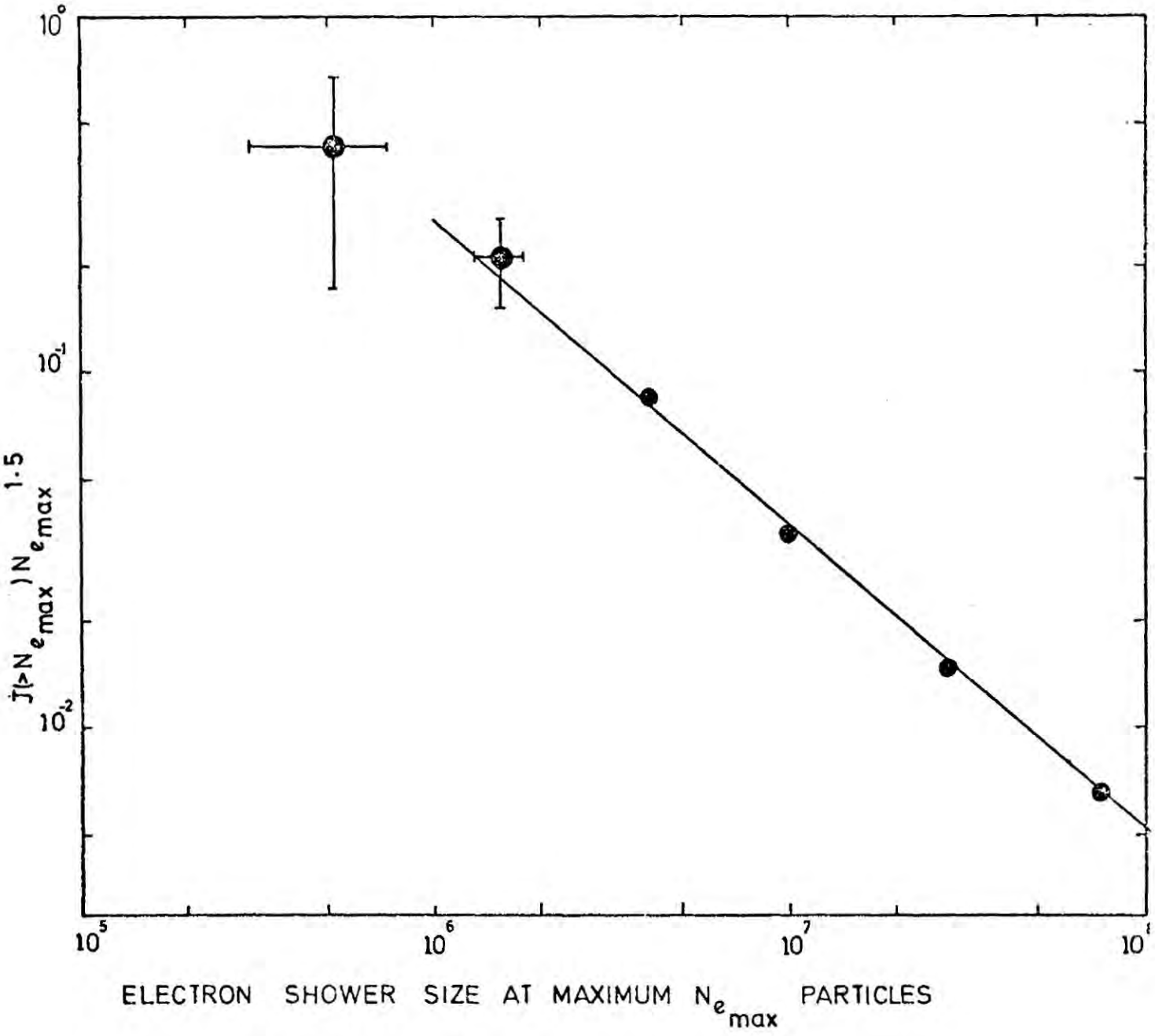

Figure 2-8 The integral intensity as a function of shower size at the maximum of development measured experimentally by Bradt et al (1965).

array extending over a total area of 8 km^2 and consisting of 20 scintillation counters each of area 3.3m^2. All types of secondary particles (with ∿zero threshold energy) are detected and counted at an atmospheric depth of 820 gm cm^2. The integral size spectrum obtained experimentally is shown in figure 2.5 where it is normalised to the summary size spectrum at 10^8 particles. All showers were assumed to be at maximum development and conversion to the energy spectrum was made using $E_o=2.10^9 N_e$. The energy spectrum has a slope of 2 up to 10^{18}eV and a slope of 1.6 beyond thus giving rise to the "ankle".

More recently experiments have been performed at the Haverah Park array at Leeds and at the Pilliga forest array, Sydney, Australia. The array at Haverah Park extends over a total area of 11 km^2 and is located near sea level, Tennent (1967). All muons and a percentage of the electrons in a shower are "counted" by water Cerenkov detectors. The experimental data, Andrews et al (1971), has been analysed in terms of the parameter ρ_{500} found to be relatively model insensitive (Hillas 1971, 1971a, 1971b). With this new parameter it is unnecessary to calculate the size N_e of the shower because ρ_{500} is directly related to the primary energy of particle. The primary energy spectrum in the energy range $3\ 10^{17} \lesssim E_o \lesssim 10^{19}$eV was found to be

$$J(>E_o) = (4.5\pm0.2)\ 10^{-10} \left(\frac{E_o}{10^{17}}\right)^{-2\cdot24\pm0.04} \quad m^{-2}\ sec^{-1}\ sr^{-1}$$

with no evidence for any change of slope. Furthermore, Andrews et al (1971) gave conclusive evidence that the "ankle" observed by Linsley (1963) was due to an instrumental bias.

The EAS at Sydney Australia is situated at sea level and extends over an area of 40 km^2. It consists of a number of dual detectors (called stations) arranged in a square grid. The 400m grid measures

small showers in detail whilst the larger 1600m grid was designed to detect showers with an energy $\sim 10^{19}$eV. Each station has two tanks of area $6m^2$, 50m apart containing liquid scintillator viewed by two 7" photomultipliers. The detectors are buried beneath the earth so all electrons are absorbed leaving only the muons to be detected. Analysis of the shower data was based on the calculations of McCusker (1963) and Goorevich (1971). These authors presented the muon size spectrum in the differential form, see Bell et al (1971), and no attempt was made to derive the energy spectrum because they believed their model calculations were unreliable. There is no evidence of any flattening in the integral size spectrum as observed by Linsley.

The preliminary results of the new EAS array at Yakutsk presented by Khristiansen et al (1972) are plotted in figure 2.5 where no normalization was necessary. The "ankle" was found to be a prominent feature in the size spectrum occurring at a size of approximately 10^8 particles. At the Paris conference (1972) where this work was reported, a great deal of discussion led to the conclusion that this feature was caused by the combined effect of poor shower analysis techniques and an instrumental biassing effect.

In conclusion, the experimental data is consistent with an energy spectrum with only one feature, i.e. the "knee" at approximately 10^{16}eV, in the opinion of most cosmic ray scientists the energy spectrum has a constant slope beyond 10^{16}eV up to the maximum cosmic ray energy observed, i.e. $\sim 10^{20}$eV.

2.5.8 The measured anisotropy of cosmic rays

A summary of all the available data on the anisotropy of cosmic rays has recently been made by Dickinson and Osborne (1973). These authors conclude that there is no evidence for a significant anisotropy

at any energy. The upper limit (one standard deviation) to the anisotropy from their summary is given in figure 2.9. Observations are consistent with an anisotropy $\delta \lesssim 10^{-2}$. A significant anisotropy in the cosmic ray flux, observed at the Earth, would provide a very important key to understanding the origin of cosmic rays by reflecting the whereabouts in space of the cosmic ray source. The absence of any anisotropy however, suggests that the sources of cosmic rays are uniformly distributed in the galaxy or are extragalactic. If this were the case and the motion of the cosmic rays from the source to the Earth is unhindered by interstellar matter, then the "knee" would be a consequence of the source itself. Perhaps there is a break-down in the mechanism confining the cosmic rays to the source and preventing some cosmic rays from being accelerated to higher energies. Alternatively, there may be "cut offs" in the region of $E \approx 10^{15}$eV in the nuclear physics of the interactions that are responsible for cosmic ray production.

The more attractive theory for explaining the "knee" is one of diffusion of cosmic rays within the interstellar matter lying between the source and the Earth. Such a theory demands cosmic ray production at all sources to be the same.

Naturally in developing the theory of diffusion the observed lack of anisotropy must be preserved, the extent to which it is preserved in the diffusion model considered will be dealt with in detail in a later chapter.

2.6 Conclusions

There is quite an appreciable lack of consistency obtained in the N_e-E_o and N_μ-E_o curves as defined by different model simulations for pure proton primaries. What is more, even though changes that occur in air shower

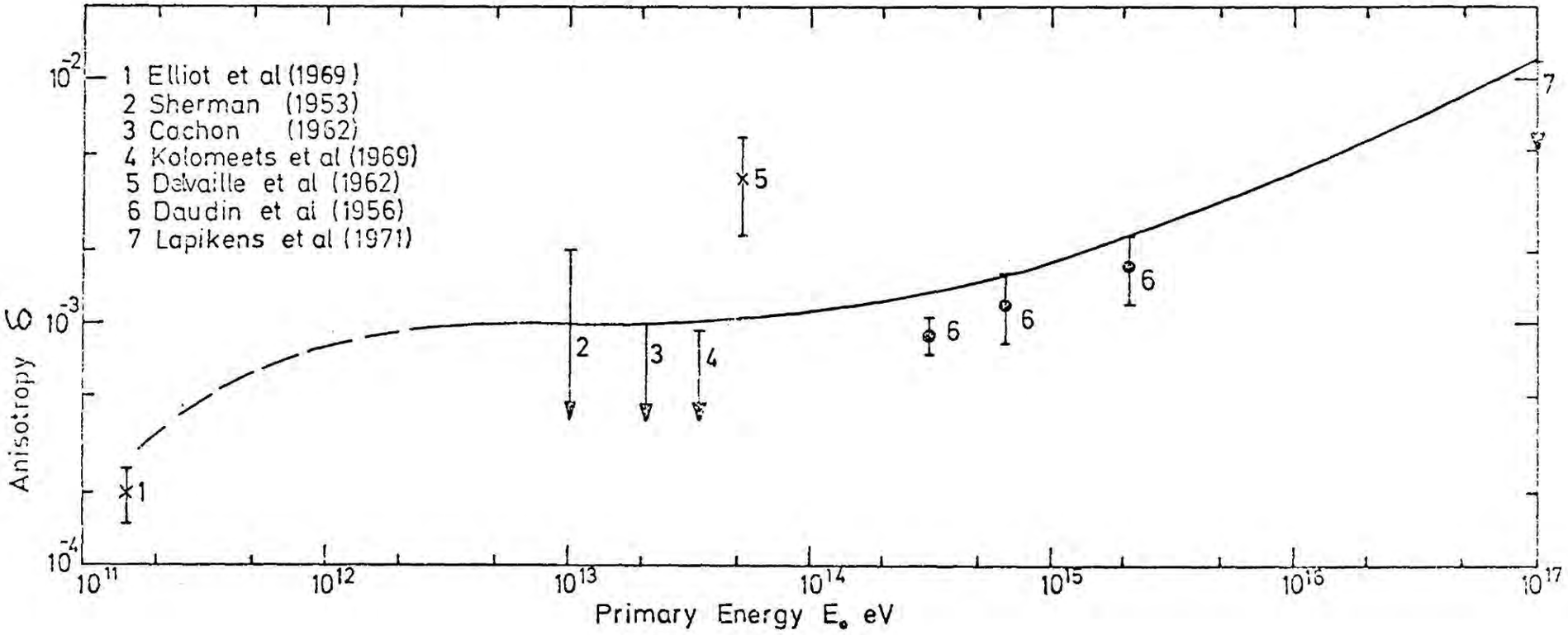

Figure 2-9 Experimental measurements of cosmic ray anisotropy.

development due to the primary cosmic rays having an atomic weight A>1 can be investigated by Monte Carlo simulations either by superposition or fragmentation most EAS arrays are insensitive to mass and therefore not knowing the mass of the particle producing the shower, it cannot be accurately assigned a primary energy. Integral size spectra are already extremely model dependent and their conversion to primary energy spectra will only introduce additional errors. In order to maintain the uncertainties to a minimum then, we deal with the experimental data in the form of integral size spectra. The energy spectra for pure protons and for mixed composition with galactic modulation defined at the top of the atmosphere will be derived on the basis of the theory of diffusion of cosmic rays in the interstellar medium and then converted to the size spectrum to compare with the experimental data. The following factors must be taken into account:

(a) the particular depth in the atmosphere at which the experiment was performed

(b) The energy threshold of the particles detected, and

(c) the mean atomic mass of the cosmic ray particle predicted by the model.

This will be ultimately achieved by using the results of the model calculations available from Dixon et al (1973a),but in addition, the sensitivity of deriving the energy spectrum from the size spectrum will be illustrated by considering the N_e-E_o curves of Bradt et al (1968) and de Beer et al (1966).

Table 2.2 gives the comparison of the characteristics of the best estimates of the integral size spectra for cosmic rays. f_i^* and f_d^* are defined in section 2.5.2 whilst $\Delta\gamma$ represents the change of slope at the "knee" which occurs at a size N_K particles. N_T represents the

Table 2.2 Comparison of the "best" size spectra defined experimentally

Type of size spectrum	Altitude	Reference	f_i^*	f_d^*	$\Delta\gamma$	N_K	N_T	$\log_{10} \frac{N_T}{N_K}$
Electrons	Mountain	Amineva et al (1969) and Bradt et al (1965)	1.00 ±0.06	∿1.0 ±0.1	0.70	$1.3\ 10^6$	$\gtrsim 10^8$	>1.89
Electrons	Sea level	Khristiansen et al (1972)	0.96 ±0.04	∿1.0 ±0.1	0.54	$7.4\ 10^5$	$\sim 10^8$ debateable	$\gtrsim$2.13
Muons	Sea level	Khristiansen et al (1972)	0.96 ±0.04	∿1.0 ±0.1	0.75	$2\ 10^4$	$\gtrsim 3\ 10^5$	$\gtrsim$1.18

size at which $\Delta\gamma$ equalling a constant alters and takes on a different value. The parameter $\log_{10}(N_T/N_K)$ therefore gives a measure of the range of size for which $\Delta\gamma$ is constant, i.e. for $\log_{10}(N_T/N_K) = n$ means that $\Delta\gamma$ is constant over n orders of magnitude in particle size.

The characteristics of the integral size spectra for electrons and muons measured experimentally at sea level and the electron size spectrum at mountain altitudes reflect the characteristics of the differential cosmic ray energy spectrum. Therefore, we can develop a set of parameters which can serve as a guide to establish the correct spectral features when considering cosmic ray diffusion. If the shower size bears an approximate linear relationship with energy then $f_d \sim 1.0 \pm 0.1$ and $\Delta\gamma \sim 0.6$. Because the value of N_K changes with atmospheric depth and is dependent on shower modelling it is rather difficult to predict, accurately, the position of the "knee" in the energy spectrum. It probably lies between $3\ 10^{15}$ eV and 10^{16} eV. This parameter, in fact, is not too critical because the spectrum can suffer a shift to a higher or lower energy as a result of any of the following:

(a) because the threshold energy of the particles detected is a very uncertain parameter this could effect the shower size by the order of a factor of two

(b) incorrect fitting of a structure function to experimental data which defines only the outer edges of shower: the size assigned to the shower would be overestimated if too steep a distribution is fitted and the opposite is true if it is too flat

(c) uncertainties in the nuclear physics of very high ($\geq 10^{12}$ eV) energy interactions lead to incorrect relationships between the size of showers at the level of observation and the primary cosmic ray energy.

The parameter $\log_{10}(N_T/N_K)$ is therefore more informative. Such values (shown in table 2.2) point towards the need for a corresponding value of $\log_{10}(E_T/E_K)$ in the energy spectrum defined by cosmic ray diffusion to be large. In other words, the change of slope of $\sim$0.6 should be constant over as large an energy range as possible.

Chapter 3

Cosmic Ray Properties: Chemical composition

3.1 Introduction

Although some EAS arrays, eg Pilliga Forest (Sydney, Australia) where only muons are detected, are in principle sensitive to primary mass the methods of analysis and uncertainties in the high energy nuclear physics make it impossible to ascertain the actual mass of the primary cosmic ray from the measurement of its secondary radiation. At best, EAS data tend to give only a mean mass for all cosmic rays as a function of primary energy.

To determine the relative cosmic ray abundances of individual elements direct observations of the primaries are necessary. Production of the secondary radiation reaches a maximum at ∿20 km above sea level and only beyond a height of 50 km does the intensity level off corresponding to the rate of individual primary nuclei. The necessity to be near the top of the atmosphere to observe the primary radiation directly, presents not only technical problems for experimental design and transport of the apparatus but limits the measurable energy of the cosmic rays to $\lesssim 10^{12}$ eV/nucleon. This is because the flux of cosmic rays falls off very rapidly with increasing energy and only below this energy is it sufficiently high to give a significant count rate.

After a brief discussion of the cosmic ray detectors and the vehicles used for their transportation to the necessary high levels, the problems associated with albedo and fragmentation in the atmosphere will be dealt with. The energy spectra for protons, helium atoms, Li + Be + B, C + O(+N) and heavier elements observed experimentally will be discussed with respect to solar modulation. A review of the data on the chemical composition of primary cosmic rays will be presented and the "best estimate" for the ratio

of protons to alphas will be calcuated.

The recent results of Balasubrahmanyan and Ormes (1972,1973) which suggest an energy dependence of (i) the ratio of 'secondary' particles (produced by interaction of C + O and Fe with the interstellar medium) to the 'primary' (in source) particles and (ii) the ratio of C + O to Fe, will be presented.

3.2 Balloon and Satellite experiments

Detectors typically weigh ∿5000 lbs and basically consist of three components, a charge measuring module, a device to measure the particle trajectory to eliminate background and a device to measure total energy. The early detectors were flown to heights of 25-40 km (equivalent to an atmospheric depth of 20-3 gm cm^{-2}) above sea level by balloons. The time of flight is short, typically of the order of half a day, and therefore limited statistics often make the results unreliable, particularly for the rare heavy elements (Fe, Co, Ni etc.)

The invention of the rocket and satellite increased the scope for the experimentalist but they are very expensive vehicles compared with the balloon. Much greater heights above sea level are reached, the pay load has been marginally increased and the duration of the flight has been improved by two orders of magnitude. However, the more recent balloon borne detectors with a geometric factor of 2700 sr cm^2 (eg Ormes and Balasubrahmanyan 1969) and an exposure time of 10 hours have been equivalent to one year's data from a typical satellite charge composition experiment.

3.3 Albedo and Fragmentation

When carrying out experiments near the top of the atmosphere it is very important to take into account the following processes: (a) absorption, (b) splash and geomagnetic albedo, (c) fragmentation.

Absorption of primary radiation at high altitudes is usually considered negligible but the effect of albedo and fragmentation is to modify the primary cosmic ray intensity. Splash albedo occurs when a particle interacts in the denser atmosphere below the detectors, and a backward moving secondary particle of the interaction enters the counting device and is interpreted as a primary particle. The effect can be reduced to some extent by inserting absorbers below the detector but poor design could increase the effect. Geomagnetic albedo is the result of cosmic ray secondaries being trapped in the Earth's magnetic field. The lack of knowledge of the nature of the field prevents accurate corrections to the counting rate to compensate for the increase in flux.

Fragmentation of heavy nuclei is extremely important, particularly when the relative abundances are to be determined. A heavy nucleus splits up into a number of light nuclei which are indistinguishable from the primary flux. The interaction length for a heavy element such as Fe is only 14 gm cm^{-2} and therefore this process is important close to the top of the atmosphere. Fragmentation of primary radiation causes underestimation of the abundance of heavy elements: eg.Fe, Ni, Co and an overestimation of the light nuclei eg.Li, Be, B. It is even possible that the latter could be completely absent in the true primary radiation.

The problems presented by albedo and fragmentation become less important as the top of the atmosphere is reached, therefore satellite data is probably more reliable than balloon data in this respect.

3.4 Energy spectrum of cosmic ray primaries of varying mass composition

3.4.1 Solar modulation

The differential energy spectrum of various primary nuclei is shown in figure 3-1 (see table 3-1 for details).

Table 3-1 The key for figure 3-1

Protons	Helium	Reference *	Year expt. performed
		Ormes (1965)	1963-1965
		Waddington (1965)	1963
		Freier (1967)	1964
		Anand (1968c)	1963
		Pinkau (1969)	1967
		Cartwright (1971)	1967-1970
		Garcia Munoz (1971)	1967-1970
		Ryan (1972)	1970
		Smith (1972)	1970
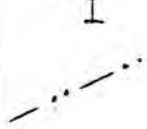		Gloeckler (1967)	Spectrum compiled from data observed near solar minimum 1965
(Li+Be+B)	(C+O+N)		
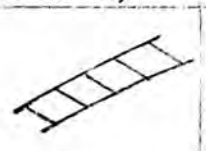		Garcia Munoz (1971)	1967-1970
		Ormes (1971)	1970
V.H.		Freier (1967)	1964
Fe only		Balasubrahmanyan (1972)	1969

* For convenience 'et al' or a second author is omitted from the references listed in this table.

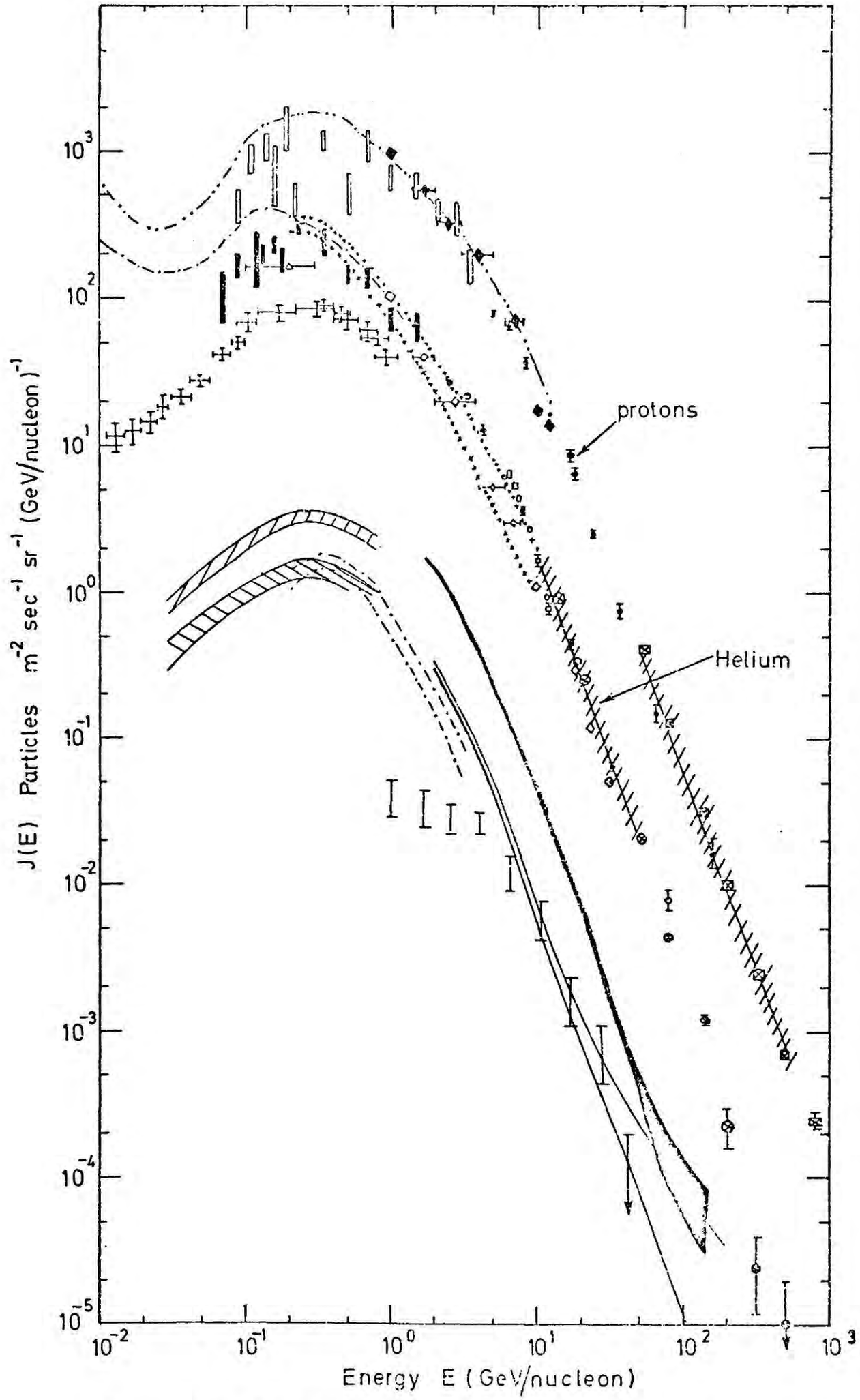

Figure 3-1 The differential energy spectrum for protons, alpha particles, Li+Be+B, C+O+N and heavies. For the key to this figure see table 3-1 opposite this page.

Below an energy of ∿2 GeV/nucleon the effects of solar modulation are easily observed by the deviation of the cosmic ray intensity from the power law which is true for energies above 2 GeV/nucleon very little is understood about the mechanisms involved in the solar modulation and therefore it is impossible to compute the compensating factor and thus the true primary cosmic ray spectrum at these lower energies. The solar cycle has an eleven year period and the effect on cosmic rays is through the associated interplanetary magnetic field. At solar minimum there is an increase in the observed intensity of low energy particles at the Earth. The last solar minimum occurred in 1965.

Superimposed on the solar modulation cycle are two other cycles which cause an additional variation in the cosmic ray intensity. The first has a period of one day having a maximum cosmic ray intensity at noon. This is because the Earth rotates in an anisotropic cosmic ray flux due to the fact that the solar field is not constant in space as the Earth rotates. The second has a 27 day recurrence period which is associated with the rotation of the Sun itself.

In addition to these periodic variations, there are randomly occurring solar flares and magnetic storms which also cause fluctuations in the cosmic ray intensity. A solar flare is a sudden outburst from the surface of the Sun. Flares are responsible for a sudden increase in the number of cosmic rays of energies up to several GeV with an energy spectrum steeper than the 'normal' spectrum. Magnetic storms cause the horizontal component of the Earth's magnetic field to suddenly increase. After a period of an hour or so the field rapidly decreases to a value below the normal level. 'Normality' is reached after a few days. There is an inverse correlation between cosmic ray flux and magnetic storms which do exhibit a 27 day

periodicity and are therefore associated with the Sun.

Thus, below an energy of ∿2 GeV/nucleon the primary flux is distorted by localised and changing magnetic fields, the cosmic ray intensity constantly changes depending on the time of day, year or decade.

A comparison of the helium spectrum of Freier (1967) and Waddington (1965), observed during a period of minimum solar activity, with that of Garcia-Munoz (1971), observed near solar maximum, illustrates the severity of solar modulation. However, it is apparent that, except for the proton to alpha ratio, the relative abundances of cosmic ray primaries observed at a particular time do not change over the entire energy range of 10 MeV/nucleon to 1000 GeV/nucleon within experimental error. In other words, all elements except protons are affected equally by solar modulation. This is particularly evident from figure 3-2. Plotted there are the abundance of all elements(with $Z \lesssim 28$)relative to carbon as measured experimentally in various experiments performed at different times of the solar cycle. Table 3-2 gives the relevant information concerning the experiments considered in figure 3-2. Within experimental error, the data are in good agreement. Because the experiment performed by Cartwright et al (1971) (a) was repeated giving results at two different times with respect to the solar cycle, (b) had a long exposure time, 12 months for IMP 4 and 7 months for IMP 5, and (c) was carried out at satellite altitudes and therefore the data presumably is less contaminated by background due to albedo and fragmentation in the atmosphere, the relative abundance of elements with $Z \geq 2$ averaged over the two exposures IMP 4 and IMP 5 were considered to best represent the data. This was believed to be particularly true for the heavy elements $Z \gtrsim 15$ because at an energy of 100-300 MeV/nucleon the count rate for heavies is about a thousand times higher than at 10 GeV, and therefore must be more accurate.

Table 3-2 Details of the experiments performed to measure the abundance of cosmic rays relative to carbon

	Reference	Time experiment performed	Vehicle	Residual Atmosphere gm cm^{-2}	Geometric Factor cm^2 sr	Duration of the flight hrs.	Threshold
□	Cartwright et al (1971)	May 1967 - May 1968	IMP 4	-	-	∿9000	100-300 MeV/n
□□		June 1969 - Dec 1970	IMP 5	-	-	∿5000	
1	Smith et al (1972)	Sept 1970	Balloon	4.8	643 ± 8	6	4.5 GV/c
2		May 1971		5.9		13	4.0 GV/c
3	Webber et al (1971)	July 1970	Balloon Telescope B	2.3	230	36	250-850 MeV/n
4							>850 MeV/n
5	Lezniak et al (1969)	Early 1968	Pioneer 8	-	-	∿2400	>1.1 GeV/n
6	Juliusson et al (1972)	Sept 1971	Balloon	4.8	820	29.5	1.6 GeV/n
7	Shapiro et al (1971)	May 1969	Balloon	-	660	-	4.5 GV/c
8	Ormes et al (1971)	November 1970	Balloon	6.0	300	16	<2 GeV/n
9	Ryan et al (1972)						

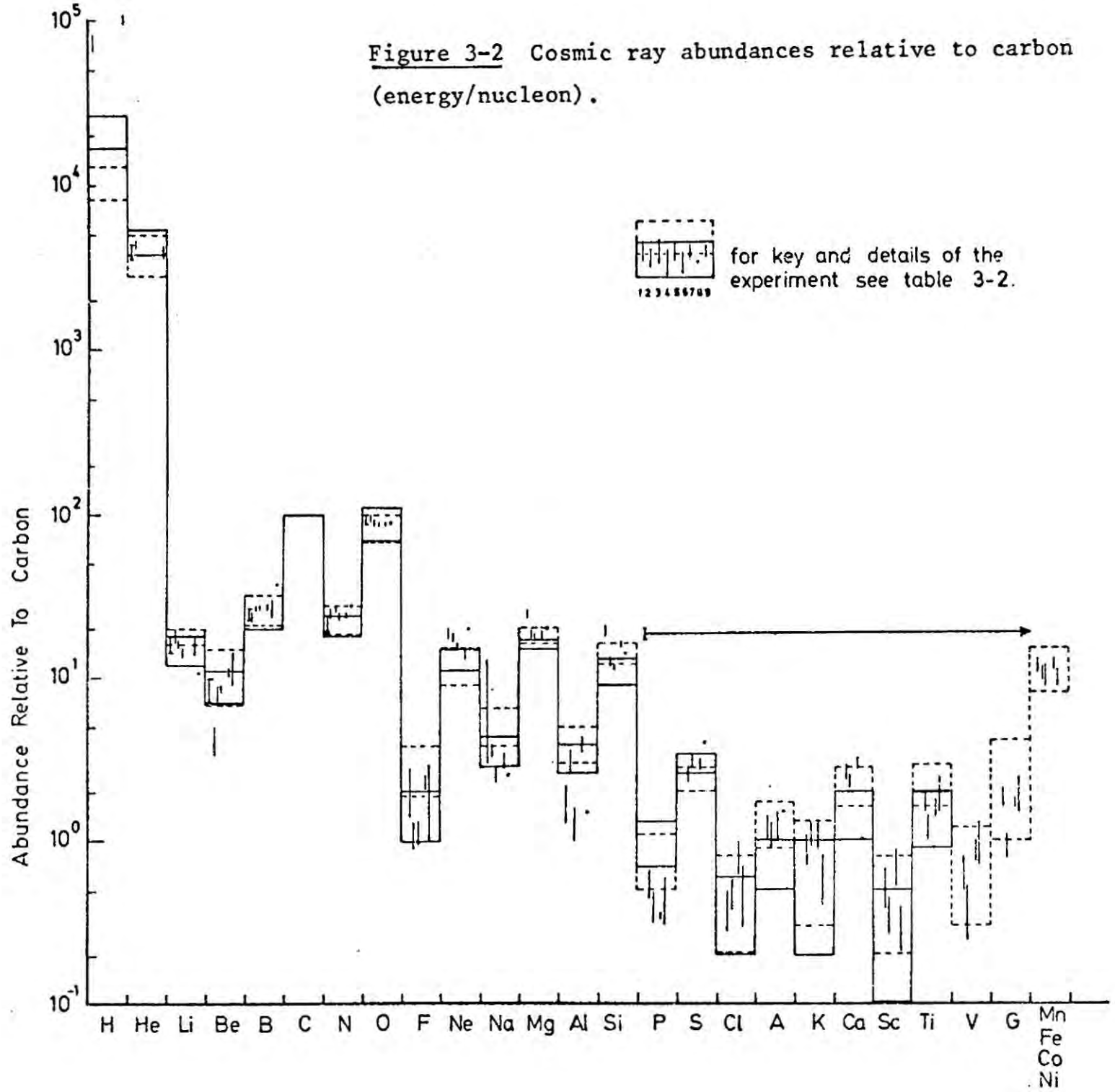

Figure 3-2 Cosmic ray abundances relative to carbon (energy/nucleon).

3.4.2 Proton to Alpha ratio

The proton spectrum is distorted to a much greater extent than that for charged primaries below an energy of 300 MeV/nucleon. This fact is supported by the drastic reduction in intensity of primary protons as observed by Waddington (1965), Gloeckler (1967) and Cartwright et al (1971) see figure 3-1. Cartwright et al gives the proton to alpha ratio observed at 100-300 MeV/nucleon during a period of maximum solar activity as $p/\alpha=4$. To obtain a p/α ratio which can be assumed true at energies of 10^{14}-10^{17} eV a survey was made of the proton and helium spectrum beyond an energy of 5 GeV/nucleon i.e. where solar modulation has no effect on the primary radiation. Table 3-3 summarises the experimental results along with details relevant to each experiment. The measurements cover both the period of minimum as well as maximum solar activity. The p/α ratio has been calculated at an energy of 100 GeV/nucleon and the best estimate for p/α was found to be 18. A recent paper by Balasubrahmanyan and Ormes (1973) finds a value of $p/\alpha = 23\pm1$, consistent with previous estimates.

The spectral index for the proton and helium differential energy spectrum, also listed in table 3-3, agree within experimental error and have a mean value of 2.69 and 2.67 respectively. There is no indication for the p/α ratio being energy dependent beyond 5 GeV/nucleon. This conclusion is supported by Balasubrahmanyan and Ormes (1973).

3.4.3 Energy dependence of the relative abundance of primary cosmic radiation

The abundance of L nuclei, Li, Be and B, relative to the M nuclei, C + O (+N), as observed by Garcia-Munoz (1971) is plotted as a function of energy/nucleon in figure 3-3. These data, along with those listed in table

Table 3-3 Summary of the details of the experiments (along with their results) carried out to define the proton and helium spectra beyond an energy of 5 GeV/nucleon.

Reference *	Year Experiment Performed	Vehicle	gm cm^{-2} Residual Atmosphere	Duration of flight hours	p/α (@100 GeV per nucleon)	γ_p †	γ_α †
Anand (1968c)	1963	Balloon	10.2	6.63	20	2.64	2.66
Pinkau (1969)	1967	Balloon	11.4 5.7	8 14.3	20	2.75±0.04	2.76±0.07
Ryan (1971)	Nov 1970	Balloon	6.0	16	26	-	-
Ryan (1972)					11	2.75±0.03	2.77±0.05
Smith (1972)	Sept 1970	Balloon	4.8	-	12	2.63±0.08	2.47±0.03
Best estimate (mean)	-	-	-	-	18	2.69	2.67
Balasubrahmanyan (1973)	April 1969	Balloon	7.0	30	23	2.75±0.03	2.77±0.05

† γ_p and γ_α are the exponents of the proton and helium differential energy spectrum respectively

* For convenience 'et al' ar a second author is omitted from the references listed in this table

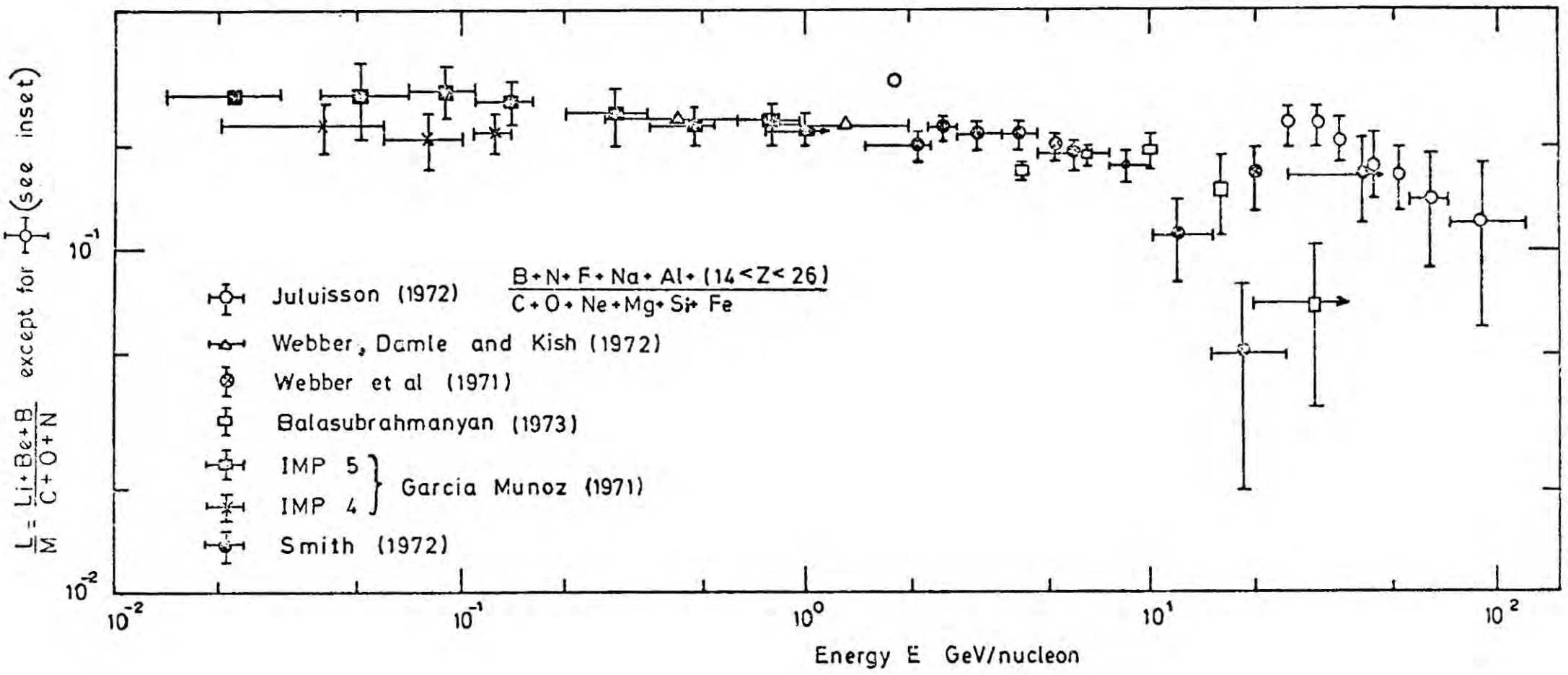

Figure 3-3 The abundance of light to medium nuclei as a function of energy.

3-4 indicate that within experimental error the L/M ratio is constant up to at least an energy of 1.5 GeV/nucleon. However, Balasubrahmanyan and Ormes (1973) reported recently that beyond an energy of 2 GeV/nucleon the exponents of the energy spectra of L nuclei are steeper than those of C + O by an amount $\Delta\gamma = 0.14 \pm 0.07$. This value compares reasonably with $\Delta\gamma = 0.31 \pm 0.01$ as measured by Smith (1972). Similar spectral changes have been suggested by Webber et al (1971) and Webber, Damle and Kish (1972) as shown in figure 3-3. As mentioned earlier, the L nuclei are probably produced as secondaries when the M nuclei interact with matter. Therefore, this observed change of slope can be explained in terms of an energy dependent breakdown of the trapping of these nuclei in the source regions or in interstellar space because the fragmentation parameters are considered to be energy independent at these high energies.

Balasubrahmanyan and Ormes (1973) show that the group of elements $15<Z<24$ having spectral index of 2.36 ± 0.12 is steeper than the Fe group with $\gamma = 2.12 \pm 0.13$ by an amount similar to that for the L with respect to M nuclei. Elements with $15<Z<24$ arise as secondaries from the collisions of Fe nuclei with interstellar matter and therefore a propagation argument as above explains this change of slope. The slope of the spectrum of the secondaries from Fe is slightly flatter than the L nuclei but this can perhaps be explained in terms of experimental inadequacies.

A more striking feature observed by Balasubrahmanyan was the spectrum of the M group being flatter by an amount $\Delta\gamma = 0.52 \pm 0.15$ compared with the Fe group. This sharp and drastic change cannot easily be explained in terms of a propagation effect but most probably reflects the acceleration mechanism of the particles, perhaps there are two types of sources or even Z

Table 3-4 The L/M ratio measured at various energies

Reference	Year	Energy MeV/nucleon	L/M
Balasubrahmanyan et al	(1966)	∿400	0.28±0.08
von Rosenvinge et al	(1969)	∿400	0.26±0.02
Lezniak et al	(1969)	∿400	0.25±0.02
Reames and Fichtel	(1966)	40-90	0.19±0.07
Garcia Munoz and Simpson	(1969)	30-100	0.22±0.04
Comstock et al	(1969)	100	0.26±0.03
Hagge et al	(1967)	100	0.30±0.06
Balasubrahmanyan et al	(1966)	100	0.29±0.07
Fan et al	(1967)	<200	0.23±0.04
Garcia Munoz and Simpson	(1969)	120	0.22±0.03
O'Dell et al	(1961)	≥1500	0.25±0.04
Durgaprasad et al	(1970)	≥1000	0.24±0.06
von Rosenvinge et al	(1969)	≥1500	0.25±0.02

dependent forces on the particles.

Juliusson et al (1972) who defines secondaries as B+N+F+Na+Al+ (15-25) and primaries as C+O+Ne+Si + Mg+Fe makes comparison with the data of Balasubrahmanyan and Ormes (1973) difficult. This ratio of elements has been plotted in figure 3-3 along with the data of the ratio L to M. The very sudden and steeper change of slope $\Delta\gamma\sim0.6$ occurring at an energy of $\sim$20 GeV/nucleon could be artificially overestimated because his results are based on integral measurements and the points plotted are not statistically independent. At low energies the ratio is dominated by (B+N) and (C+O) which contribute approximately 75% to the numerator and denominator respectively. Half the nitrogen and a fraction of the other nuclei are primary so the spectral exponent should approach that for (C+O) at higher energies as the number of secondaries decrease. Basically, this ratio groups together nuclei of different spectral indices and so the composition of the ratio is energy dependent particularly due to Fe and its secondaries. In conclusion, the work of Juliusson is not inconsistent with Balasubrahmanyan and Ormes.

3.5 Conclusion

Before the more recent data of Juliusson (1972), Smith (1972) and Balasubrahmanyan and Ormes (1972, 1973) it was generally accepted that, within experimental error, the relative abundances of all cosmic ray primaries beyond an energy $\sim$2 GeV/nucleon are independent of energy. In a conservative model, the chemical composition of cosmic ray primaries in the energy region of 10^{14} - 10^{17} eV would thus be defined by the best estimate of $p/\alpha=18$ along with the abundances of individual elements with $Z\geq2$ relative to carbon as measured by Cartwright et al (1971) (see table 3-5). The cosmic ray abundance of protons and the groups of elements L, M, MH, H and VH relative

Table 3-5 Relative abundances of cosmic ray primaries

Element	Z	A	Cartwright et al: Abundance relative to carbon	Cartwright et al: Abundance relative to helium	Balasubrahmanyan and Ormes: Abundance relative to helium
Energy			100-300 MeV/n	100-300 MeV/n	4 GeV/n
Hydrogen	1	1	$7.2\ 10^4$	$7.2\ 10^4$	$2.9\ 10^5$
Helium	2	4	$4\ 10^3$	$4\ 10^3$	$1.25\ 10^4$
Lithium	3	7	16.5		
Berylium	4	9	9.5	52	64
Boron	5	11	26	Light nuclei	
Carbon	6	12	100		
Nitrogen	7	14	23	210	248
Oxygen	8	16	87.5	Medium nuclei	
Flourine	9	19	2.15		
Neon	10	20	13		
Sodium	11	23	4.3		
Magnesium	12	24	17	52	70
Aluminium	13	27	3.55	Medium-Heavy	
Silicon	14	28	12		
Phosphorus	15	31	0.9		
Sulphur	16	32	2.2		
Chlorine	17	35	0.44		
Argon	18	40	1.0		
Potassium	19	39	0.7	10	12
Calcium	20	40	1.75	Heavy	
Scandium	21	45	0.4		
Titanium	22	48	1.9		
Vanadium	23	51	0.8		
Chromium	24	52	2.2		
Manganese	25	57	10	12	9
Iron				Very Heavy	
Cobalt					
Nickel					
$P/_\alpha$				18	23

to helium defined at $\sim$4 GeV/nucleon by Balasubrahmanyan and Ormes (1972) are compared with those calculated from the data of Cartwright et al (1971) in table 3-5. They are seen to be in reasonable agreement.

Because the energy dependence of the L to M nuclei is only slight and the L nuclei are rare compared with protons, alphas and M nuclei, this energy dependence has negligible effect in the present work. However, the difference in slope of $\Delta\gamma\sim0.5$ between M and Fe nuclei found by Balasubrahmanyan and Ormes (1972) is dramatic and if substantiated by later work it will have an effect at high energies. The spectrum of Fe extrapolated with this 'new' slope crosses over that for protons at an energy of $\sim2\ 10^{13}$ eV/nucleus and therefore even before EAS shower energies are reached Fe would be the dominant element. In view of experimental results on fluctuations in EAS (see Appendix i) this is believed not to be the case and what evidence there is at EAS energies (at least below $\sim10^{16}$eV) suggests mainly proton primaries.

The consequences of the energy dependence described above with respect to diffusion will be dealt with in Chapter 7.

Chapter 4 Diffusion in an idealised medium

4.1 Introduction

This chapter will be devoted to developing the basic laws of diffusion as applied to the problem of the motion of cosmic rays in an interstellar medium. The basic parameters for a model for the diffusion of protons in an idealised medium will be discussed in an attempt to explain the shape of the energy spectrum in the region of several 10^{15} eV.

4.2 Basic Theory of Diffusion

4.2.1 Simple laws of diffusion and their application to cosmic rays

Diffusion is a process which is responsible for causing an equalization of concentration within a single phase. Consider a volume inside which there are sources of cosmic rays, these are discrete regions of high cosmic ray concentration. The sources are embedded in a medium, the interstellar matter, which has low cosmic ray concentration (relative to the source regions) thus building up a concentration gradient. The laws of diffusion connect the rate of flow of the diffusing particles with the concentration gradient which is responsible for this flow. Diffusion is a process which continues until a state of total equilibrium exists between the cosmic ray density and the density of matter. Because there are at least two materials involved there are, in general, more than one diffusion equation expressing the fact that the rate of flow of one material (cosmic rays) is in the opposite direction to the other (the interstellar matter particles). However, the motion of the interstellar matter is extremely slow compared with that of cosmic rays, therefore it can be assumed static.

Defining the diffusion flow or current J of the cosmic rays inside a volume (which besides interstellar matter contains stellar bodies as well) as the number of cosmic rays passing perpendicularly through a

reference surface of unit area during unit time. The dimension of J is the number of particles / unit area / second. In cgs. the units are particles cm^{-2} sec^{-1}.

Fick's first law of diffusion, independent of the system of co-ordinates, is given by the vector notation

$$\bar{J} = -D \nabla n \qquad 4.1$$

where D is the coefficient of diffusion of cosmic rays assumed constant for a particular cosmic ray energy, with units cm^2 sec^{-1}. n is the 'concentration' or the number of cosmic rays per cubic centimeter. Equation 4-1 states that the vector J of the diffusion current is in the opposite direction to the particle concentration gradient ∇n, being proportional to its absolute value. The surface of the reference is always chosen perpendicular to the direction of this vector.

A determination of the diffusion coefficient by means of equation 4.1 necessitates an arrangement where both J and ∇n are measurable. A constant concentration gradient implies the establishment of the steady state, i.e. when there is no change of concentration of particles with time.

Consider the situation when the cosmic ray sources are lying inside the Galaxy in an inactive state and suddenly they are switched on and emit cosmic rays. We observe a change in concentration of cosmic rays with time caused by diffusion in the interstellar medium, a determination of the latter gives us another link with the diffusion current which is a measure of the diffusion coefficient.

For example, consider diffusion in the x direction only, the increase in the number of cosmic rays within a volume element bounded by two parallel planes of unit area situated at x and $x+dx$ is

$$J_x - J_{x+dx} = D \left[\left(\frac{\partial n}{\partial x}\right)_{x+dx} - \left(\frac{\partial n}{\partial x}\right)_{x} \right]$$

$$= D \left(\frac{\partial^2 n}{\partial x^2}\right)_{x} dx + \ldots\ldots$$

Dividing by the volume $\Delta V = dx.1\ cm^2$ of the element leads to the definition of the increase of the number of particles with time, in the limit as $dx \to o$

$$\frac{\partial n}{\partial t} = D \frac{\partial^2 n}{\partial x^2}$$

which is Fick's second law of diffusion derived on the assumption that D is a constant which is true for a cosmic ray of a particular energy. The corresponding vector equation is

$$\frac{\partial n}{\partial t} = D \ \nabla.\nabla n$$

Conservation of matter demands that

$$\frac{\partial n}{\partial t} + \frac{\partial J}{\partial x} = q \qquad 4.2$$

where q is the source matter density.

At the present moment in time a condition of steady state exists in our region of the Galaxy such that the cosmic ray density is ~ 1 eV cm^{-3}. This means that the term $\frac{\partial n}{\partial t} = o$ and equation 4.2 reduces to

$$q = - D \ \nabla.\nabla n$$

For a cosmic ray particle diffusing out of a spiral arm of width 2a considering a one dimensional treatment only, the solution of the diffusion equation

$$q = - D \frac{\partial^2 n}{\partial x^2} \qquad 4.3$$

yields $n = q \frac{(a^2 - x^2)}{2D}$ 4.4

and n is the number of cosmic ray particles per cubic centimetre.

There exists in the spiral arm a distribution of sources $q(x)$, from equation 4.3 then for a particular cosmic ray path of length L

$$\int_0^L q(x)\ dx = -\ D\ \frac{\partial n}{\partial x} = J \qquad 4.5$$

The streaming current or particle flux is equal to the line integral of the source matter density.

4.2.2 Mean displacement of a diffusing particle - Pandom motion or Brownian movement

If the motion of a particle from its starting point $x=0$, $t=0$ is at random then the distance it may have moved away from $x=o$ in time t can be anything from zero to very great values. Consider a single particle undergoing consecutive displacements $\lambda_1, \lambda_2, \lambda_3 \ldots \lambda_i$ in either the $+x$ or $-x$ directions, all displacements being of the same absolute magnitude $|\lambda_1| = |\lambda_2| = \ldots = |\lambda_i| = \lambda$, but completely independent and at random. Then, the mean square displacement is small compared with the square of the sum of the absolute amounts of the single displacements i.e.

$$\overline{\Delta x^2} << (\Sigma_{i=1}^{n} |\lambda_i|)^2,$$

provided n is large. It follows that

$$\overline{\Delta x^2} = \overline{(\Sigma_{i=1}^{n} \lambda_i)^2} = \overline{\Sigma_{i=1}^{n} \lambda_i^2} = n\lambda^2 \qquad 4.6$$

because the sum of the dot products $\lambda_i \cdot \lambda_k$ vanishes when taking averages because they are independent of each other and there is equal probability of their being a positive or negative displacement i.e. $\Sigma_{i \neq k}\ \lambda_i \cdot \lambda_k = 0$.

Given that t is the time necessary for a displacement whose average square is $\overline{\Delta x^2}$, and if τ is the time necessary for one single displacement ℓ, then $n\tau = t$ or $n = \frac{t}{\tau}$ and it follows that

$$\overline{\Delta x^2} = \frac{t\lambda^2}{\tau} \qquad 4.7$$

The actual total displacement x after n single displacements ℓ may have a value between 0 and $\pm n\ell$. The probability for a displacement $x=\nu\lambda$ is $P(x) = P(\nu\lambda)$ can be calculated by using standard methods of the theory of probabilities. Assuming that the number of displacements is large compared with unity and ν and n are either both even or both odd (this ensures that we deal with integer numbers only) then if n is the total number of displacements, a positive displacement $x=\nu\lambda$ must be the resultant of $\frac{n+\nu}{2}$ positive and $\frac{n-\nu}{2}$ negative displacement. The probability of a single positive displacement is equal to a negative one namely $\frac{1}{2}$. The probability of $\frac{n+\nu}{2}$ positive and $\frac{n-\nu}{2}$ negative displacements, in a <u>definite</u> given order, is $(\frac{1}{2})^n$. However, in the particular instance of Brownian movement, the resultant displacement is obtained by $\frac{n+\nu}{2}$ positive and $\frac{n-\nu}{2}$ negative displacements irrespective of the order in which they were carried out. The above probability is modified by the number of distinguishable arrangements of $\frac{n+\nu}{2}$ positive and $\frac{n-\nu}{2}$ negative displacements giving

$$\frac{n!}{(\frac{n+\nu}{2})\,!\,(\frac{n-\nu}{2})\,!}$$

consequently

$$p(\nu\lambda) = \frac{n!}{(\frac{n+\nu}{2})\,!\,(\frac{n-\nu}{2})\,!}\,(\tfrac{1}{2})^n \qquad 4.8$$

If n and ν are large numbers and $\nu\lambda=x$ then by using Stirling's formula, 4.8 reduces to

$$P(\nu\lambda) \approx \sqrt{\frac{2\tau}{\pi t}} \exp \left(-\frac{x^2\tau}{2\lambda^2 t}\right)$$

ν is assumed to be even therefore 4.8 can be assumed to represent the probability of a displacement $x=\nu\lambda$ and $x = (\nu+2)\lambda$. Therefore, the probability between x and $x+dx$ will be

$$P(x)dx = P(\nu\lambda) \frac{dx}{2\lambda}$$

giving

$$P(x)dx = \frac{1}{2\sqrt{\pi Dt}} \exp\left(-\frac{x^2}{4Dt}\right) dx \qquad 4.9$$

where D is the diffusion coefficient equal to $\frac{\lambda^2}{2\tau}$. Equation 4.9 represents one dimensional diffusion. Since the mean square displacement is defined by

$$\overline{\Delta x^2} = \int_{-\infty}^{\infty} x^2 P(x)\, dx$$

then for one dimensional diffusion

$$\overline{\Delta x^2} = 2Dt$$

which is identical to equation 4.7 knowing $D = \frac{\lambda^2}{2\tau}$. In 2-D diffusion the mean square displacement $\overline{\Delta r^2}$ in a plane is computed in a similar way to give

$$\overline{\Delta r^2} = 4Dt \qquad 4.10$$

For the case of 3-D diffusion $\overline{\Delta r^2} = 6Dt$.

4.3 Development of the basic model for cosmic ray diffusion in the Galaxy

4.3.1 Cosmic Ray production at the Source

Cosmic rays are assumed to be produced at all sources with an energy spectrum given by

$$J_p(E)\, dE = A_p E^{-\gamma_p} dE \qquad 4.11$$

such that $\gamma_p \sim 2.5$ and constant for all energies.

4.3.2 Cosmic ray source distribution

A numerical treatment of diffusion involves tracing a particle from its source through an interactive medium to the Earth. Because the Earth is, relative to the spiral arm and the source positions, a specific point in space it is impossible to trace the particle from its origin to the Earth. Experimental observations at the Earth show that primary cosmic rays entering the atmosphere are positively charged. It is convenient, then, to assume that the cosmic rays are negatively charged particles leaving the Earth and to trace them back through an interactive medium to their points of origin.

Consider cosmic rays "arriving" at the Earth having traversed a unique path of length L. The source of cosmic rays can be at any point along the track. Given that q represents the source matter density, then for a particular distribution of sources $q(x)$, the streaming current is obtained from equation 4.5

$$J = \int_0^L q(x)\, dx$$

For the diffusion model considered here, it is assumed that a uniform distribution of sources exists throughout the spiral arm, each source emitting cosmic rays randomly with time. We have therefore $q(x)=Q$ as a constant giving

$$J = Q \int_0^L dx = QL$$

therefore $J \alpha L$

and the particle flux is proportional to the length of the track L. Given that the cosmic ray particles travel with the speed of light c the particle flux is proportional to the time t taken to travel a certain path L

$$J \alpha t \qquad 4.12$$

4.3.3 Model of the spiral arm in the vicinity of the Earth

In the first approximation, the spiral arm is considered to be an infinitely long cylinder of diameter 2a=600 pc. In dealing with 2 dimensional diffusion only the cross section along the length of the spiral arm is taken. The Earth lies at C (see figure 4.1) midway between the edges of the rectangle defined by straight lines $x=-a$ and $x=+a$. The interactive medium is represented by circular clouds of hydrogen of constant size R_o pc spaced uniformly, such that the distance apart is ℓpc.

4.3.4 Distribution of angle of scatter of a cosmic ray particle by a magnetic field cloud

Figure 4.2a represents a circular cloud of hydrogen with a magnetic field of strength H_o μgauss, coherent over its total area $A=\pi R_o^2$. The field is directed out of the paper. A positively charged cosmic ray of energy EeV, momentum (p) eV/c entering the cloud at X moves in a circle such that the Larmor radius r pc of the particle is given by

$$E = pc = 300\, H_o r$$

When considering clouds with a constant magnetic field. The energy of the cosmic ray is directly proportional to its Larmor radius.

The total angle through which the cosmic ray is deflected is $\phi^o = 180^o + \beta$. From the trigonometrical properties of the circle

$$\frac{\text{Sin}\,(90-\theta-\frac{\beta}{2})}{r} = \frac{\text{Sin}\,(90+\frac{\beta}{2})}{R_o}$$

therefore $$\text{Tan}\,\frac{\beta}{2} = \frac{R_o\text{Cos}\theta - r}{R_o\text{Sin}\theta}$$

and $$\text{Tan}\,\frac{\phi}{2} = \frac{R_o\text{Sin}\theta}{r - R_o\text{Cos}\theta} \qquad 4\text{-}13$$

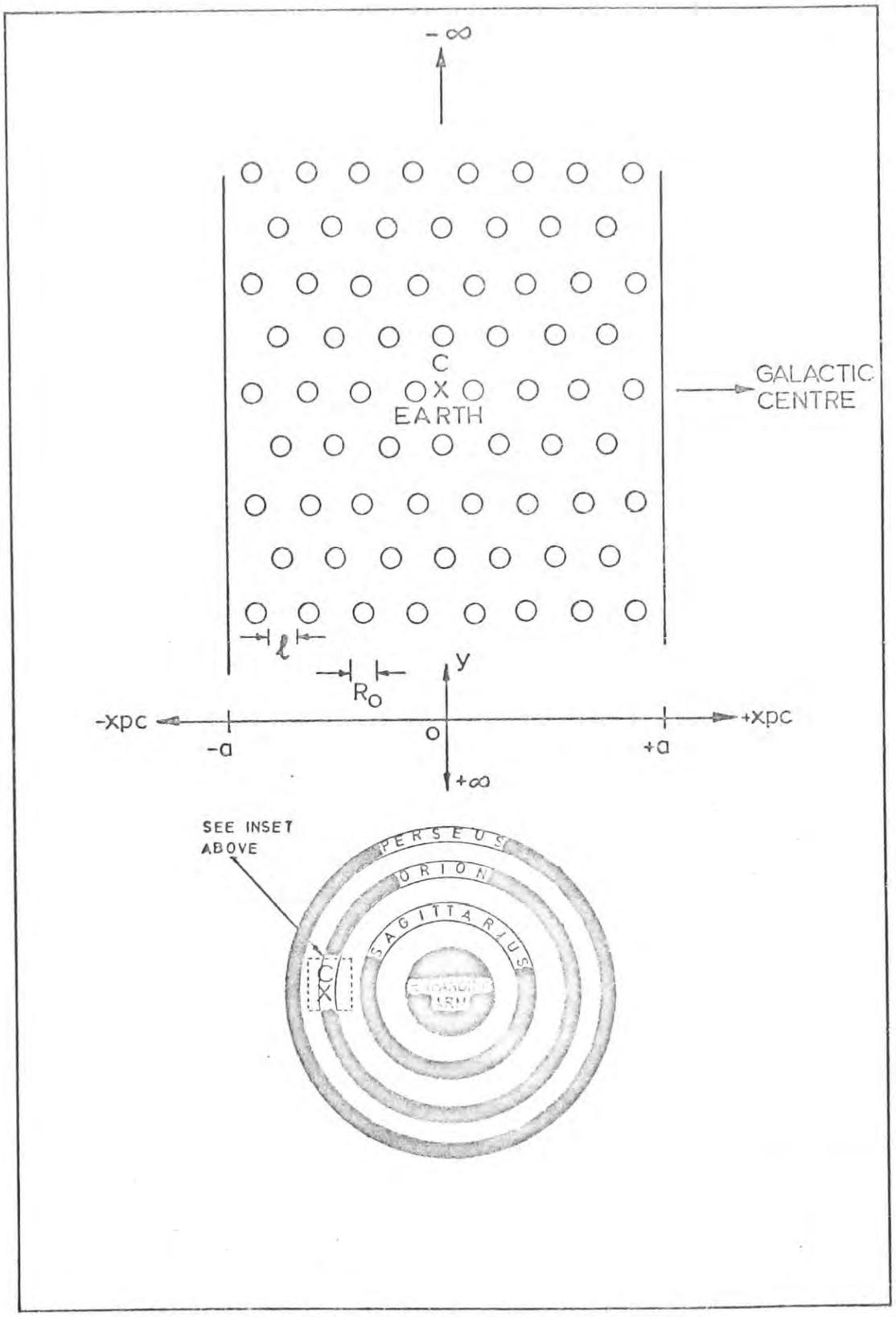

Figure 4-1 A schematic representation of the "spiral" arm in the vicinity of the Earth (C) - not to scale.

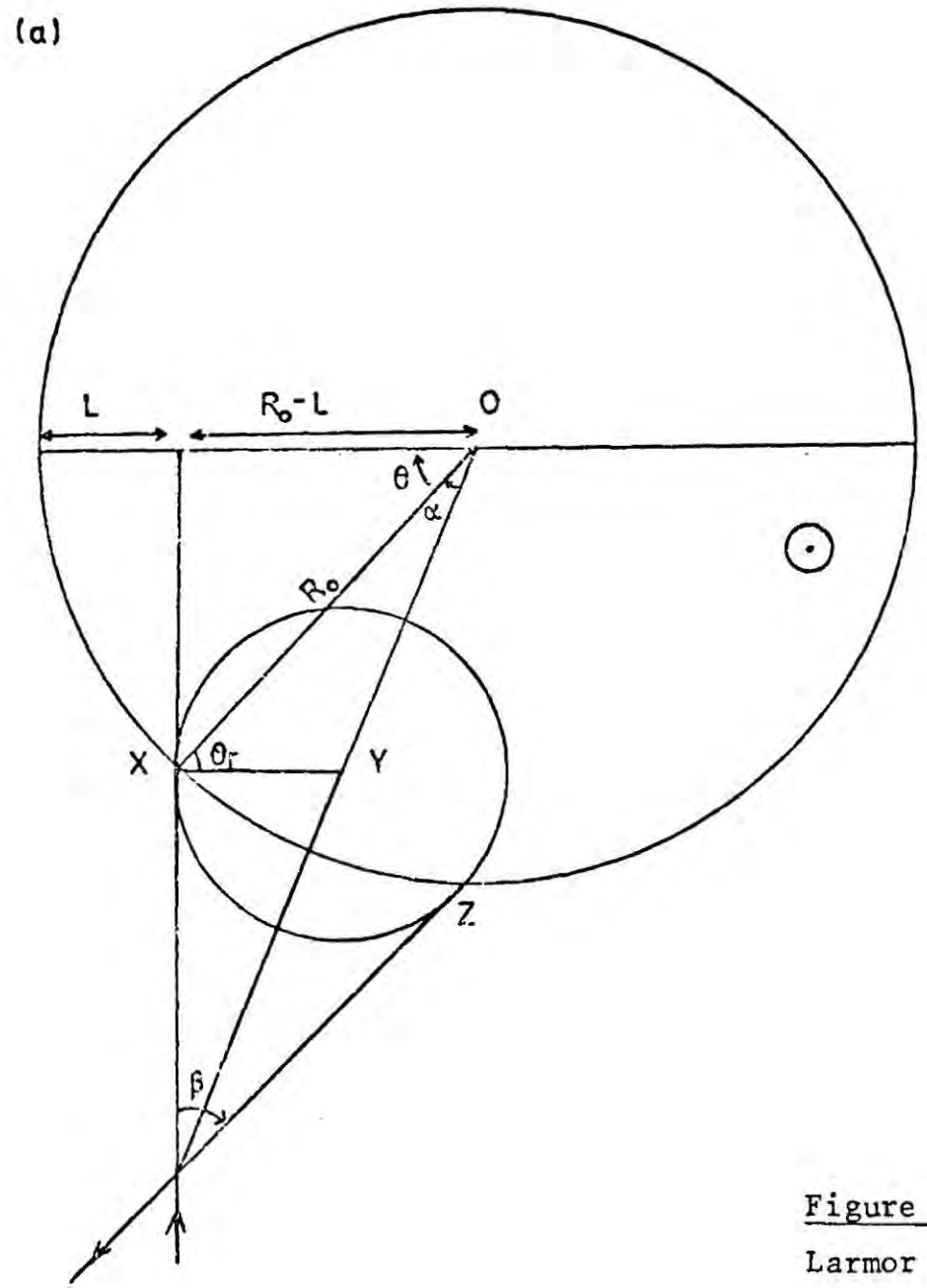

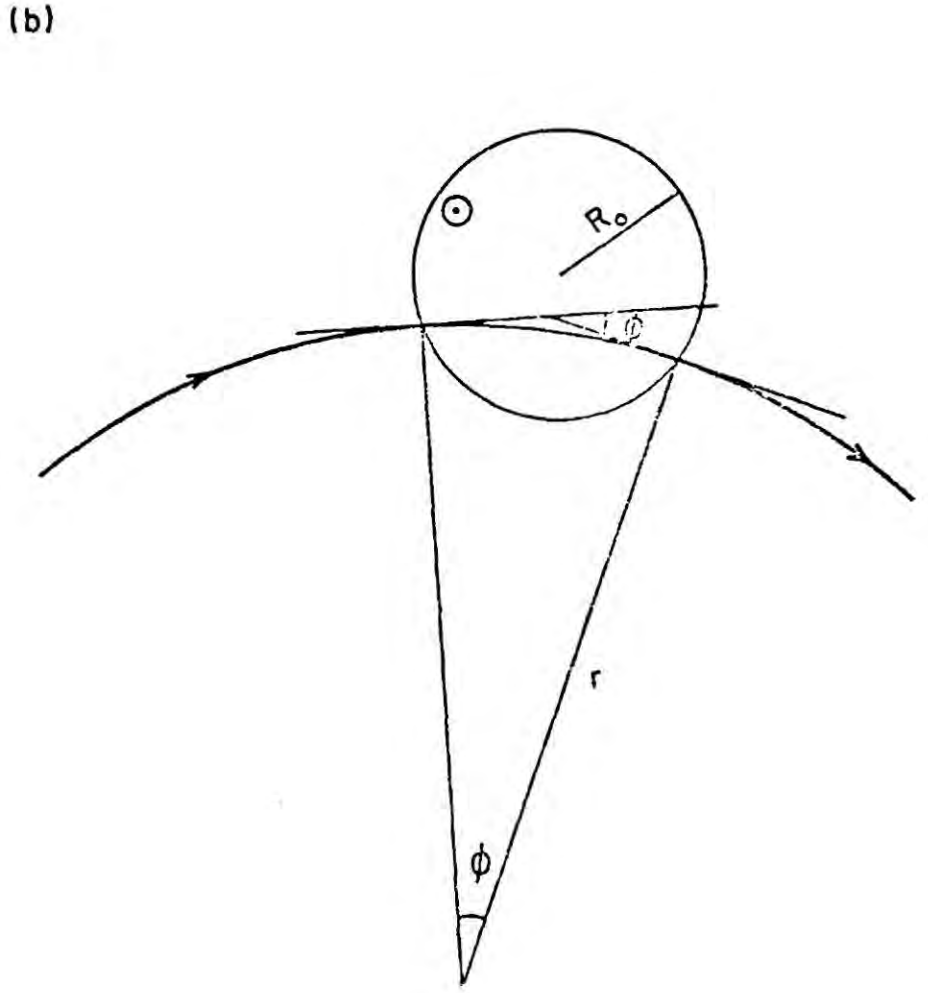

Figure 4-2 The deflection of a positively charged cosmic ray (with Larmor radius r) by a circular cloud with radius R_o, magnetic field strength H_o directed out of the plane of the paper, for the two physical conditions defined by (a) $r<R_o$ and (b) $r>R_o$.

$$\text{Since } \text{Cos}\theta = \frac{R_o - L}{R_o} \; ; \quad \text{Sin}\theta = \frac{1}{R_o} \sqrt{L(2R_o - L)}$$

the angle of deflection is

$$\phi^o = 2 \, \text{Tan}^{-1} \left(\frac{\sqrt{L(2R_o - L)}}{r - (R_o - L)} \right)$$

The angle ϕ^o through which the particle is deflected is dependent on the impact parameter $I=(R_o-L)$ and the size of the cloud with respect to the Larmor radius of the particle r pc moving in a cloud of magnetic field strength H_o μgauss. Now $f(\phi)d\phi$, the probability of a cosmic ray particle being deflected through an angle ϕ and $\phi+d\phi$ as a function of energy $E\alpha\frac{r}{R_o}$ was established by computer in the following way. Assume $\frac{r}{R_o} = k$ and $L = cR_o$ then

$$\phi^o = \left(2 \, \text{Tan}^{-1} \left(\frac{1-c-k}{\sqrt{c(2-c)}}\right) \right) + 180$$

For a particular value of $\frac{r}{R_o}$, ϕ^o was calculated for one thousand values of c ranging from c=0 to c=2 (i.e. for all possible impact parameters thereby establishing $f(\phi)d\phi$. The procedure was repeated for values of $\frac{r}{R_o}$ = 20, 10, 8, 5, 2, 1, 0.33, 0.5, 0.8, 0.1, 0.01, 0.001 and 0.0001. The results are tabulated in table 4.1. The general trend of $f(\phi)$ with changing $\frac{r}{R_o}$ is illustrated in figure 4.3 where the distribution of the angle of scatter is plotted as a function of $\frac{r}{R_o}$. High energy cosmic rays ($r>>R_o$) are affected very little by a magnetic field cloud with a result that they are deflected through very small angles and traverse relatively straight paths over long distances. As the cosmic ray energy decreases, but has not reached the critical energy defined by $r=R_o$, small angles become less probable with respect to a cut off angle which is dependent on the relative curvature of the track with respect to that of the cloud. At the critical energy the probability distribution is

Table 4.1 Distribution of angle of scatter of particle, Larmor radius r, by cloud of radius R_o as a function of $\frac{r}{R_o}$. (Normalise $f(\phi)$ by $\times 10^{-3}$.)

ϕ^o ↓ / $\frac{r}{R_o}$ →	0.0001	0.001	0.01	0.10	0.33	0.50	0.80	1.0	2.0	5.0	8.0	10	20
1-10	2	2	2	3	4	5	7	1	19	103	286	511	1000
11-20	6	6	6	7	10	12	18	8	58	408	714	489	
21-30	10	10	10	11	16	21	30	23	96	489			
31-40	13	13	13	16	23	29	40	50	142				
41-50	16	16	17	20	28	35	50	62	201				
51-60	20	21	21	24	34	42	59	71	473				
61-70	24	23	24	27	38	46	64	79	11				
71-80	26	27	27	31	41	51	69	85					
81-90	30	29	29	34	45	54	72	86					
91-100	32	32	33	36	47	55	72	87					
101-110	35	35	35	39	49	57	71	84					
111-120	37	37	37	41	50	56	68	79					
121-130	38	39	39	42	49	54	63	72					
131-140	41	40	41	43	50	53	58	61					
141-150	41	42	42	44	48	50	51	50					
151-160	43	42	43	45	46	47	43	37					
161-170	43	43	43	44	45	44	36	23					
171-180	44	44	43	43	42	39	29	7					
181-190	43	44	44	43	40	36	24						
191-200	43	43	43	42	38	33	18						
201-210	43	42	43	41	34	28	14						
211-220	42	42	41	39	32	25	10						
221-230	40	40	40	37	29	22	9						
231-240	39	39	38	35	26	19	6						
241-250	36	37	37	33	23	17	5						
251-260	35	34	34	30	21	14	3						
261-270	32	32	32	28	19	12	3						
271-280	30	30	29	25	16	10	2						
281-290	26	26	26	23	14	9	2						
291-300	24	24	23	19	12	7	1						
301-310	20	20	20	17	10	6	1						
311-320	16	16	16	14	8	5	1						
321-330	13	13	13	11	6	3	1						
331-340	10	10	9	7	4	3	0						
341-350	6	6	6	5	3	1	0						
351-360	1	1	1	1	0	0	0						

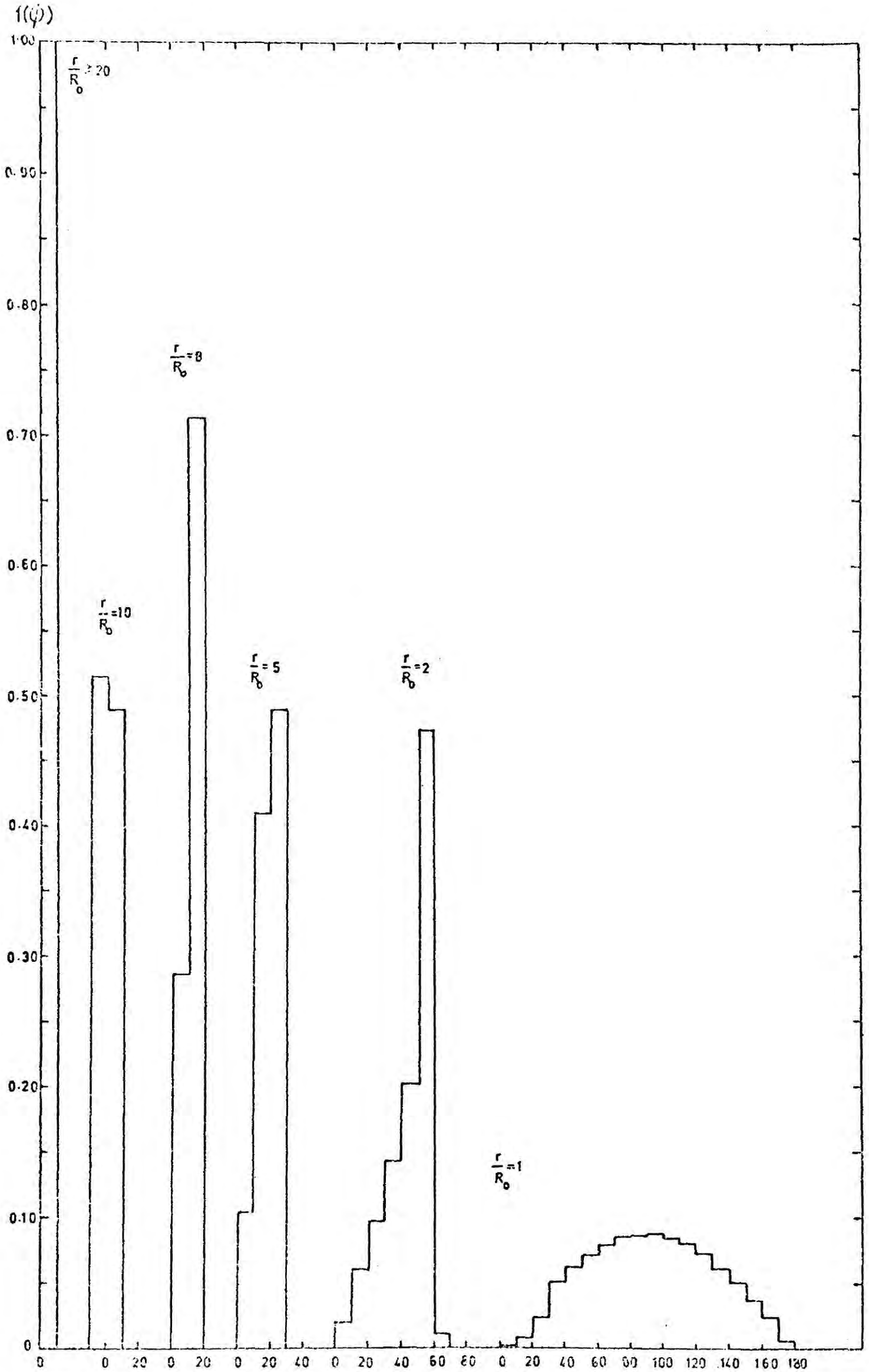
f(ψ)
1·00
0·90
0·80
0·70
0·60
0·50
0·40
0·30
0·20
0·10
0
r/R0 = 20
r/R0 = 8
r/R0 = 10
r/R0 = 5
r/R0 = 2
r/R0 = 1
0 0 20 0 20 0 20 40 0 20 40 60 80 0 20 40 60 80 100 120 140 160 180
ANGLE OF DEFLECTION ∅°

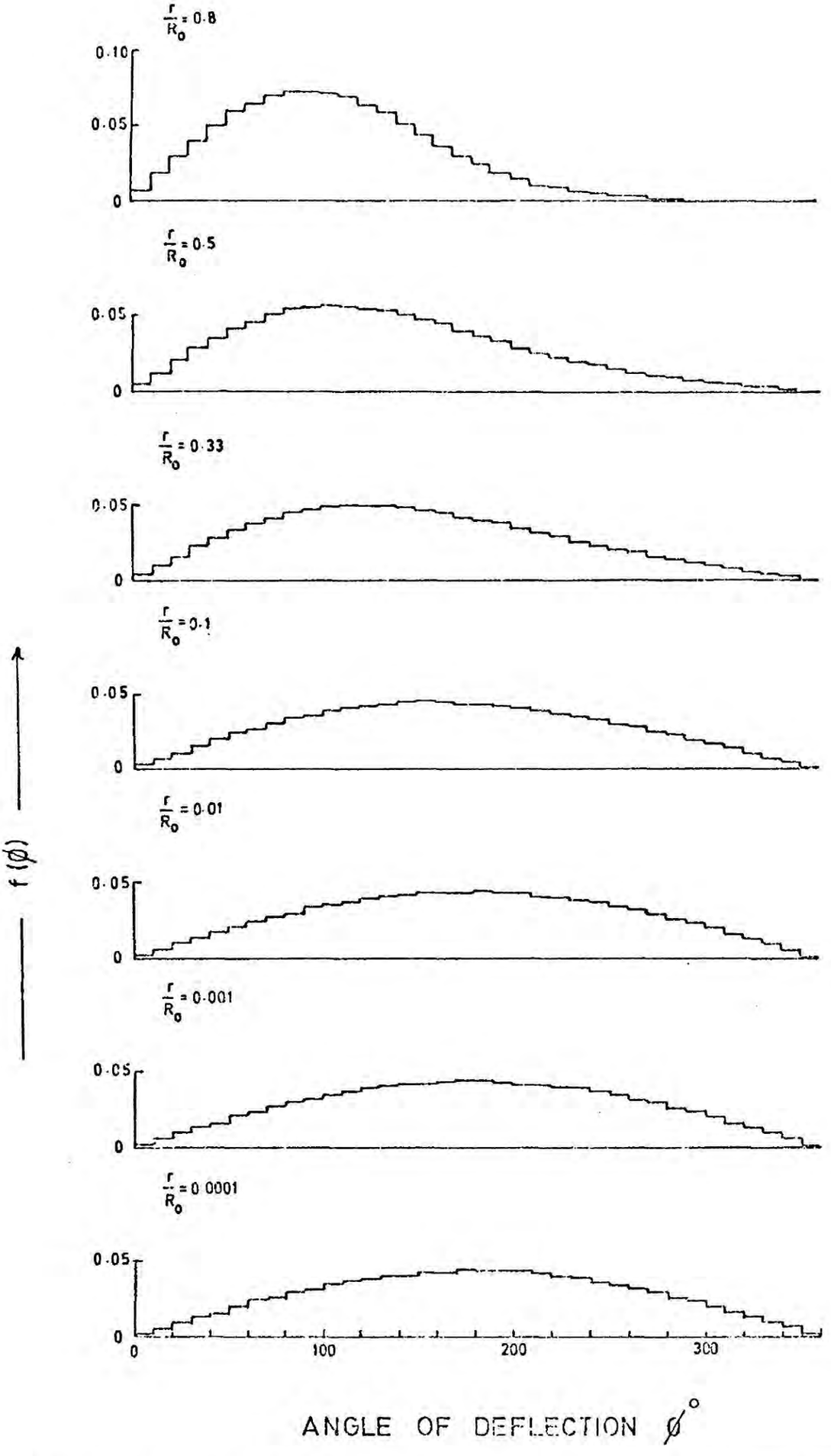

Figure 4-3 (above and left) The distribution of the angle of scatter suffered by a cosmic ray particle with Larmor radius r when it passes across a circular cloud radius R_o and magnetic field strength H_o.

symmetrical about 90^{o} with a total range of deflection of 180^{o}. Just below this critical energy the distribution is no longer symmetrical but increases to a maximum relatively quickly and has a very long tail at large angles. As the energy decreases the peak of the distribution shifts to higher values of the angle and the long tail becomes less pronounced. Finally for very low energy particles $r<<R_o$ the probability distribution tends to a constant shape which is symmetric about 180^{o}.

4.4 Diffusion of cosmic ray protons in an idealised medium

4.4.1 Diffusion of "low energy" cosmic ray protons

The condition $r<<R_o$ defines a "low energy" cosmic ray. The angle of scatter for "low energy" cosmic rays is energy independent because when $r<<R_o$ equation 4.13 reduces to

$$\phi^{o} = 2(\pi-\theta) = 2(\pi - \cos^{-1}(\frac{R_o-L}{R_o})) \qquad 4.14$$

which is dependent on the impact parameter $I = R_o-L$ and the cloud size only. Since by definition

$$f(\phi)d\phi = f(I)dI$$

$$f(\phi) = f(I)\left|\frac{dI}{d\phi}\right|$$

From equation 4 - 14

$$f(\phi) = f(I)\left[\frac{2}{\sqrt{R_o^{2}-I^{2}}}\right]^{-1}$$

Because all impact parameters between 0 and $2R_o$ are equally probable the distribution f(I) is a constant. Normalisation demands

$$f(I) = \frac{1}{2R_o}$$

$$\text{Giving } f(\phi) = \frac{\sqrt{R_o^{2}-I^{2}}}{4R_o} = \frac{\sqrt{L(2R_o-L)}}{4R_o} = \frac{\text{Sin }\theta}{4}$$

$$f(\phi) = \frac{1}{4}\text{Sin}(\pi-\frac{\phi}{2}) = \frac{1}{4}\text{Sin}\frac{\phi}{2}$$

$f(\phi)$ is defined only by the impact parameter I for a constant cloud size R_o, it is independent of r and hence energy, provided $r \ll R_o$. An analysis of the results of the computer calculations, first three columns of Table 4.1 show that $f(\phi)$ is the same within statistical error for all values of $\frac{r}{R_o} \lesssim 0.01$. $f(\phi)$ as defined by the computer is shown by the histogram in figure 4.4 for the case when $\frac{r}{R_o} = 0.0001$. It can be seen that $f(\phi) = \frac{1}{4} \sin \frac{\phi}{2}$ is in excellent agreement after normalisation.

All cosmic rays travel with the speed of light c, and therefore for a particular geometry of a uniform medium (constant a, ℓ, R_o and H_o with equal probability of there being a positive as negative magnetic field direction) all "low energy" particles ($\frac{r}{R_o} \lesssim 0.01$) have the same probability of being deflected through ϕ and $\phi+d\phi$ and $-\phi$ and $-(\phi+d\phi)$ at each scattering centre. This means that the mean time taken for such a particle to escape from the spiral is constant ($=t_o$) provided that the cosmic rays were produced by a uniform source distribution and the Earth lies at the centre of the spiral arm.

Equation 4-10defines the mean square distance moved by a particle in any direction given that the particle is confined to move in two dimensions. We are dealing here, with the motion of a particle along one particular direction. Therefore, since $\overline{\Delta r^2} = 4Dt$, and by definition $\overline{\Delta r^2} = \overline{\Delta x^2} + \overline{\Delta y^2}$ then $\overline{\Delta x^2} = 2Dt$. However, simple diffusion theory of the Brownian type motion outlined in §4.2 is not strictly applicable to the case of cosmic ray diffusion which we are dealing with here. $\overline{\Delta x^2} = 2Dt$ is valid only for the case when an isotropic distribution of angle of scatter is considered or the case when the diffusing material is confined to a region of space which is sufficiently large to allow particles to suffer a large number of interactions thus ensuring randomisation of particle direction. The cosmic

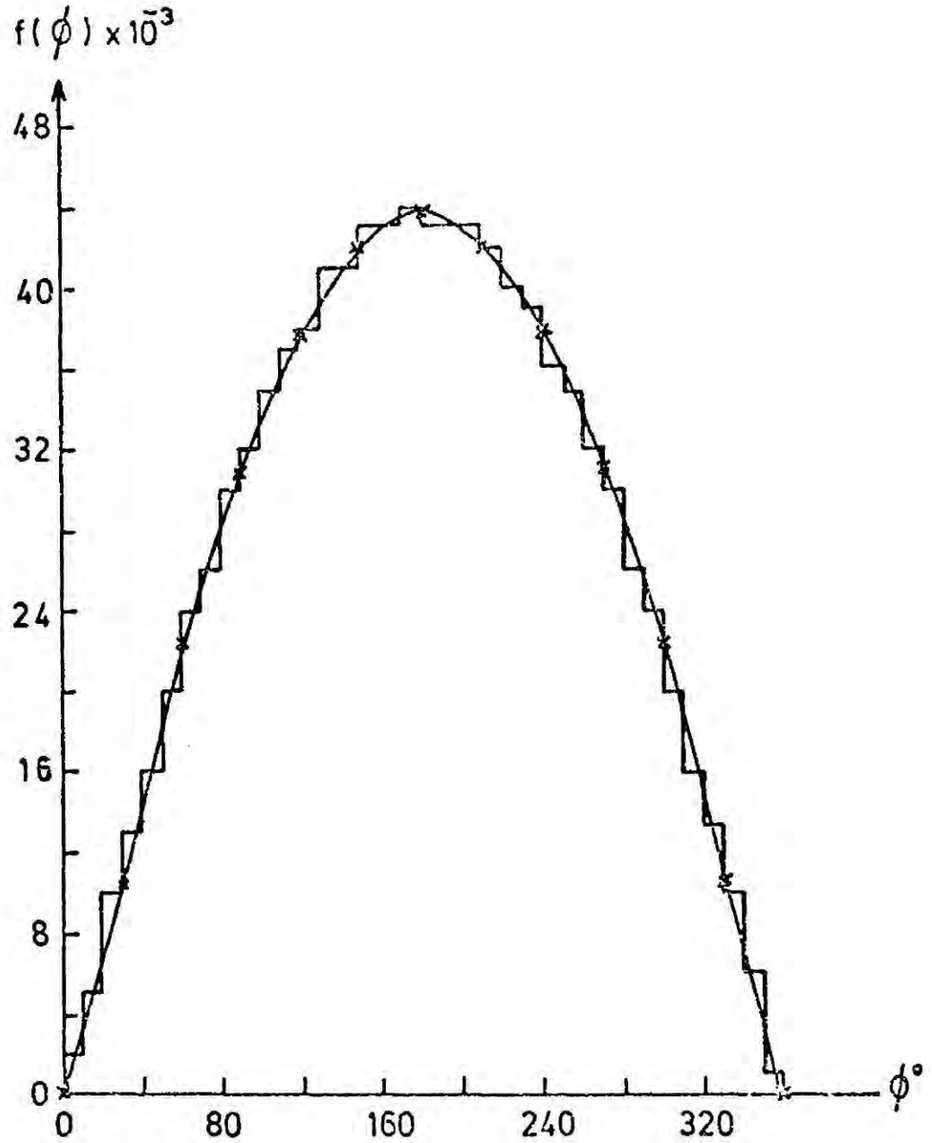

Figure 4-4 The distribution of the angle of scatter for a cosmic ray with Larmor radius r traversing a circular cloud with radius $R_o = 10^4 r$ and magnetic field H_o as calculated by the computer (histogram) compared with the theoretical curve defined by $f(\phi)d\phi = \frac{K}{4} \text{Sin} \frac{\phi}{2}$ with K as a normalisation factor.

rays, however, do not suffer deflections according to an isotropic distribution nor are they confined to move within a volume that is large compared with the distances traversed by the particles, instead they are allowed to escape from that volume, the spiral arm, and once lost never return to the diffusing medium. For this reason, true diffusion breaks down and $\overline{\Delta x^2}=2Dt$ becomes only a first order approximation. However, if the lack of confinement was taken into account then $\overline{\Delta x^2}=2fDt$ where f would be some fraction. This has little affect on the following arguments.

When $r<<R_o$, the mean time taken for all cosmic rays to leave the spiral arm is constant = t_o and the total distance moved through in a particular direction i.e. $\overline{\Delta x^2}=a^2$, the square of the half width of the spiral arm, is a constant, the diffusion coefficient becomes

$$D = \frac{\overline{\Delta x^2}}{2ft} = \frac{a^2}{2ft_o} = D_o$$

If the distribution of the angle of scatter was isotropic as is the case for Brownian motion then $D=\frac{\lambda c}{4}$. There is no real physical meaning attached to λ, the mean free path if the scattering is not isotropic. It can, however, be thought of in terms of an elapse time T during which time a particle travelling at a speed of v cm/sec moves a distance λpc necessary for it to forget its original direction, i.e. until it becomes isotropised. Obviously, if the distribution is isotropic then the particle almost immediately forgets its direction and then λ can be set identically equal to the step length ℓpc.

For the case of cosmic rays, we can to a first order approximation assume for $r<<R_o$ the distribution $f(\phi)$ is isotropic and therefore

$$D_o = \frac{\ell c}{4} \qquad 4.15$$

As the cosmic ray energy increases the particles have to travel

further and further before they forget their original direction, therefore λ_{pc} increases and the step length ℓ_{pc} can no longer be identified with λ.

Recent work by Kóta (1973) outlined in appendix (ii) defines the diffusion coefficient for low energy cosmic rays by the following expression

$$D = \frac{\lambda c}{4} = \frac{\ell c(1+\langle\cos\phi\rangle)}{4(1-\langle\cos\phi\rangle)}$$

since $\langle\cos\phi\rangle = \int_0^{2\pi} f(\phi)\cos\phi\, d\phi$

then for $r \ll R_o$

$$\langle\cos\phi\rangle = \int_0^{2\pi} \frac{1}{4}\sin\frac{\phi}{2}\cos\phi\, d\phi = \frac{-1}{3}$$

$$\text{and } D_o = \frac{\ell c}{8}$$

This result implies that the mean free path λ is 5pc rather than 10pc assumed in the more simple treatment above. The fact that $f(\phi)$ was considered to be isotropic instead of $f(\phi) = \frac{1}{4}\sin\phi$ is responsible for the increase of factor of 2 in the mean free path.

4.4.2 Diffusion of "high energy" cosmic ray protons

When $r \gg R_o$ a cosmic ray is said to have a "high energy". This condition applied to equation 4.13 implies that $\text{Tan}\,\phi/2$ is always very small giving a very small value for ϕ. As illustrated by figure 4.2b when $r \gg R_o$ $\phi \sim \frac{2R_o}{r}$. Consider as before uniformaly distributed circular clouds with constant radius R_o and magnetic field H_o, such that the field is directed positive and negative with equal probability. Assume that a high energy cosmic ray particle suffers consecutive collisions such that $|\phi_1| = |\phi_2| = |\phi_3| = \ldots = |\phi_i| = \phi$ and ϕ is small. The particle is expected to lose its sense of direction after n collisions, provided n is large, then the mean square

deviation of the angle will be $\overline{\phi^2} \propto n\phi^2 = n(\frac{2R_o}{r})^2$. If the distances travelled between collisions are such that $|\ell_1|=|\ell_2|=|\ell_3|= ..=|\ell_i|=\ell$ the total distance travelled after n collisions of this kind is $\lambda=n\ell$. If the scattering length, λ is taken as the distance over which $\overline{\phi^2}\sim 1$ then $\lambda=n\ell\sim (\frac{r}{2R_o})^2\ell$. At this stage we are considering random motion of an imaginary particle making steps of λ between collisions. In fact there are n collisions of step length ℓ pc that make up the imaginary step length of λ.

For a random walk in two dimensions we have

$$D = \frac{\lambda c}{4} = \left(\frac{r}{R_o}\right)^2 \frac{\ell c}{16}$$

since $D_o = \frac{\ell c}{4}$ (equation 4.15)

$$D = (\frac{r}{R_o})^2 \frac{D_o}{4}$$

Now $E_o = 300\ H_o R_o$ and $E = 300\ H_o r$

so it follows that

$$D \propto (\frac{E}{E_o})^2 D_o$$

Since $\overline{\Delta x^2} = 2D_o t_o = 2Dt$ where t_o is the time taken by a "low energy" cosmic ray particle to escape from the spiral arm and t is that time taken by a particle of energy E such that $r>>R_o$ takes to escape, it follows that

$$t \propto (\frac{E_o}{E})^2 t_o$$

Because the differential energy spectrum of cosmic rays at the source is defined by equation 4.11 the effect of the diffusion of particles between magnetic field clouds has on the energy spectrum is

for $r<<R_o$ $\quad J(E)\ dE = A\ E^{-\gamma}\ dE$

and for $r>>R_o$ $\quad J(E)\ dE = A'\ E^{-(\gamma+2)}\ dE$

$E_o = 300\ H_o R_o$ is the critical value of the particles energy at which its radius of curvature is comparable in order of magnitude with the size of the scattering magnetic cloud, the condition $\frac{r}{R_o} = \frac{E}{E_o} = 1$ defines the position of the "knee", the point where, in the above case, γ changes by 2.

So far the cases of free diffusion and adiabatic motion have been discussed and these represent the two extreme cases for the possible types of motion of charged particles in given magnetic fields. The fact that diffusion does cause a change of slope in the energy spectrum is encouraging but the magnitude of the change of slope $\Delta\gamma = 2$ does not compare at all favourably with the experimentally observed change of slope $\Delta\gamma \sim 0.6$. However this difference is not too important because only those energies remote from the knee have been considered. We turn now to the problem of diffusion of cosmic rays with energies in the region of the knee in an attempt to establish the detailed shape over some two orders of magnitude in energy.

4.4.3 Diffusion of cosmic ray protons in the region of the "knee"

The confinement time t seconds for cosmic rays of energies $E \sim 300\ H_o R_o$ was calculated by a numerical method involving Monte Carlo techniques using an IBM 360 computer. The model adopted for the interstellar medium and the dimensions of the spiral arm are as defined above and illustrated in figure 4.1. The probability distributions for the angle of scatter of a cosmic ray as a function of its energy are defined by figure 4.3

A particle of energy E(i.e. a particle whose Larmor radius in field H_o is r) "leaves" the Earth C, midway between the edges of the spiral arm, at an angle ϕ_o^o. Because cosmic rays are known to arrive at the Earth in a purely isotropic manner a value of ϕ_o is set at random to a value between 0^o and 360^o. For convenience 0^o is defined as the direction +y which gives $\phi_o^o = 90^o$ as the galactic centre direction.

The particle is stepped through a constant distance ℓ=10 pc in this initial direction thus moving a distance x_o=10 $\sin\phi_c$ pc in a direction +x if $180^o > \phi_o > 0^o$ and in the -x direction if $360^o > \phi_o > 180^o$. After the first step the cosmic ray suffers a collision with a cloud such that the angle of scatter is defined by the distribution $f(\phi)$ (figure 4.3) corresponding to its value of $\frac{r}{R_o}$.

The selection of ϕ according to the distribution $f(\phi)$ is achieved by generating two random numbers. The first between ϕ^o_{min} and ϕ^o_{max} which are respectively the maximum and minimum possible values of the angle of scatter for a particle of that particular energy. The second random number is used to generate a value of $f(\phi)$ between $f(\phi)=0$ and $f(\phi)=f(\phi)_{max}$, the maximum of the probability distribution. If the randomly generated value $f(\phi)$ lies on or beneath the curve defined at ϕ then the value of ϕ is accepted. Because magnetic fields are equally positive and negative a random number is generated between 0 and 1 if the random number is less than 0.5 then ϕ is set equal to $-\phi$ otherwise it remains positive. As the particle travels a distance 10 pc in the new direction it progresses x_1=10 $\sin(\phi_o \pm \phi_1)$ pc in the $\pm$x direction. The particle then makes consecutive interactions causing a deflection of $\phi_2, \phi_3, \phi_4 \ldots \phi_i$ each occurring after a step of 10 pc. In this manner the particle diffuses away from the Earth until it finally escapes from the spiral arm. This occurs when the condition

$$\left(\sum_{k=0}^{n} 10 \sin \sum_{i=0}^{k} \phi_i \right) \geq |300|$$

is fulfilled and the particle can escape through either edge of the spiral arm. It never returns to the interactive medium.

The total number of steps taken by the particle to escape from the arm

defines the total distance L pc travelled. Knowing the particle travels at the speed of light the escape time of the particle t secs is defined. For a particular value of $\frac{r}{R_o}$, 2400 trajectories are traced by the computer and the mean time of escape from the spiral arm $\bar{t}$ along with its statistical error are calculated. Randomly selected values for ϕ_o ensures an isotropic distribution of cosmic rays "leaving" the Earth.

The entire procedure outlined above is repeated 13 times for different values of $\frac{r}{R_o}$ i.e. deflecting the particle according to a different $f(\phi)$ at each scattering centre, thus establishing the mean time of escape from the spiral arm as a function of energy $\propto \frac{r}{R_o}$.

The results of the calculations are tabulated in table 4.2 and plotted in figure 4.5. The mean time of escape is directly proportional to the particle flux of cosmic rays from the source to the Earth (equation 4.12). Given that the production spectrum of primary cosmic ray protons at the source is a power law with constant spectral index over all energies, the shape of the curve defined by the mean time of escape of a primary proton from the spiral arm as a function of energy directly reflects the change in energy spectrum of the primary protons observed at the Earth caused by the diffusion process.

$$\text{i.e. } \bar{t}\ (E) \propto \frac{1}{D(E)} \propto \frac{1}{\lambda(E)}$$

if $J_p(E)$ represents the energy spectrum at the source the energy spectrum at the Earth is

$$J(E) = J_p(E)\ \bar{t}(E)$$

Sections 4.4.1 and 4.4.2 dealt with the diffusion of cosmic rays with "low" and "high" energies. The dotted lines in figure 4.5 indicate the results of this treatment fitted to the results of the Monte Carlo calcula-

Table 4.2

Mean times of escape from the spiral arm for particles "leaving" the Earth a) isotropically, b) in a direction along the spiral arm $\phi_o = 0^o$ and c) in the direction of the galactic centre. Mean values are based on 2400 particle trajectories and the errors represent one standard deviation.

$\frac{r}{R_o}$	(a) $\bar{t}$ seconds	(b) $\bar{t}_o$ seconds	(c) $\bar{t}_{90}$ seconds
≥ 20	$(7.12\pm0.36)\times10^{10}$	$(1.16\pm0.07)\times10^{11}$	$(3.46\pm0.15)\times10^{10}$
10	$(7.34\pm0.54)\times10^{10}$	$(8.51\pm0.72)\times10^{10}$	$(5.68\pm0.44)\times10^{10}$
8	$(7.66\pm0.36)\times10^{10}$	$(8.63\pm0.47)\times10^{10}$	$(6.43\pm0.42)\times10^{10}$
5	$(1.05\pm0.05)\times10^{11}$	$(1.14\pm0.08)\times10^{11}$	$(9.88\pm0.66)\times10^{10}$
2	$(3.63\pm0.35)\times10^{11}$	$(3.69\pm0.19)\times10^{11}$	$(3.57\pm0.34)\times10^{11}$
1	$(1.82\pm0.16)\times10^{12}$	$(1.83\pm0.14)\times10^{12}$	$(1.81\pm0.18)\times10^{12}$
0.8	$(2.37\pm0.22)\times10^{12}$	$(2.45\pm0.17)\times10^{12}$	$(2.40\pm0.14)\times10^{12}$
0.5	$(3.11\pm0.20)\times10^{12}$	$(3.15\pm0.26)\times10^{12}$	$(3.13\pm0.28)\times10^{12}$
0.33	$(3.37\pm0.28)\times10^{12}$	$(3.37\pm0.20)\times10^{12}$	$(3.44\pm0.31)\times10^{12}$
0.1	$(3.54\pm0.23)\times10^{12}$	$(3.69\pm0.47)\times10^{12}$	$(3.62\pm0.20)\times10^{12}$
0.01	$(3.73\pm0.35)\times10^{12}$	$(3.72\pm0.24)\times10^{12}$	$(3.67\pm0.23)\times10^{12}$
0.001	$(3.59\pm0.33)\times10^{12}$	$(3.64\pm0.24)\times10^{12}$	$(3.65\pm0.32)\times10^{12}$
≤ 0.0001	$(3.62\pm0.25)\times10^{12}$	$(3.72\pm0.26)\times10^{12}$	$(3.63\pm0.30)\times10^{12}$

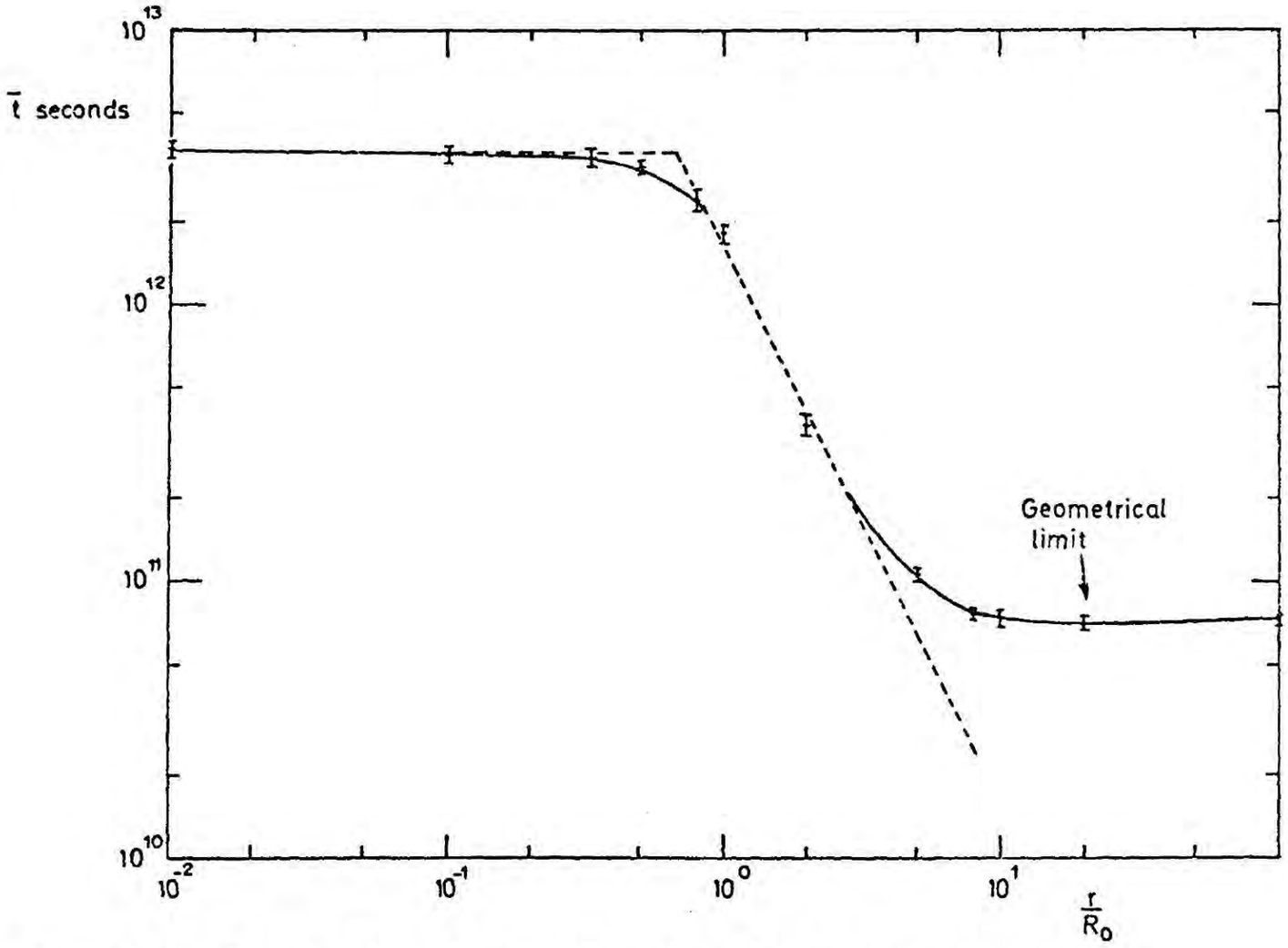

Figure 4-5 The mean time of escape from the spiral arm as a function of $\frac{r}{R_o}$ for particles "leaving" the Earth isotropically.

tions. The position of the "knee" is defined in this case by $\frac{r}{R_o} = 0.68$ occurring at an energy $E_K = 300\ H_o R_o$ which is dependent on the cloud size and the magnetic field.

Above $\frac{r}{R_o} = 3$ there is a characteristic flattening of the curve which is due to the fact that the particles escape from the spiral arm and re-entrance is not considered. We refer to this flattening as the geometrical limit. The value of $\bar{t}$ at $\frac{r}{R_o} = 100$ is $\bar{t}\ (100) = 7\ 10^{10}$ seconds which is the quickest possible time of escape of particles "leaving" the Earth isotropically, from the spiral arm. The ratio $G = \frac{\bar{t}(\lesssim 0.01)}{\bar{t}(100)}$ depends on the assumed step length ℓ between interactions. In the present calculation ℓ is constant and numerically set equal to 10 pc. As ℓ increases G decreases. If instead we assume say an exponential distribution of ℓ with a mean of 10 pc then G would decrease. This can be understood by considering "low energy" cosmic rays. If the step interval is constant then the particle is forced into a circular type of motion and consequently makes little progress in a direction to escape from the spiral arm and $\bar{t}_c\ (\lesssim 0.01)$ is high. However, with an exponential distribution of ℓ, the particle can make large as well as small steps. This irregular motion helps to prevent the particle from "going round in circles" thus ensuring that some progress is made in a direction of escape from the spiral arm. Therefore, $\bar{t}_c\ (\lesssim 0.01)$, for constant step length, is greater than $\bar{t}_e\ (\lesssim 0.01)$, for an exponential distribution for step length, since $\bar{t}_c\ (100) = t_e\ (100)$ then $G_c > G_e$. The greater the value of G the greater the range of E (or $\frac{r}{R_o}$) over which diffusion is a valid process

4.4.4 The 'f' factor for diffusion of cosmic ray protons

For the simple model of diffusion of cosmic protons in an idealised medium the factor 'f' is found to be 0.75.

4.4.5 Mean free path and diffusion coefficient for cosmic ray protons "arriving" at the Earth isotropically.

For 2-D diffusion $\overline{\Delta x^2} \sim 2Dt$ and $D \sim \frac{\lambda c}{4}$ and therefore $\lambda \sim \frac{1.8\ 10^{13}}{t}$ pc. In figure 4.6 the mean free path and the corresponding diffusion coefficient is plotted as a function of $\frac{r}{R_o}$ for both the simple theoretical treatment (dotted line) and for the results of the Monte Carlo calculation (solid line with error bars). The solid line represents the diffusion of protons in an uniform medium with clouds of constant size R_o and magnetic field H_o.

For 'low energy' cosmic rays the mean free path as obtained from the computer calculations is 5 pc whilst the theoretical model suggests a value of 10 pc. (Therefore the two models are normalised in figure at $\frac{r}{R_o} = 10^{-2}$, λ=5pc). The result from the Monte Carlo calculations is consistent with a non isotropic distribution of angle of scatter for low energy cosmic rays as discussed in section 4.4.1 in agreement with Kóta (1973).

4.5 Essential tests on the model

It is important to make selected tests on the model to ensure the validity of its basic assumptions.

4.5.1 Uniformity of the source distribution with respect to the isotropy of cosmic ray protons "leaving" the Earth

It is necessary to have a uniform source distribution to satisfy the condition $J \propto t$, equation 4.12, and yet we demand isotropy of the cosmic ray flux at the Earth. To establish whether these conditions were achieved in the model we assume that cosmic rays leave the Earth isotropically and calculate the degree of uniformity of the source distribution using the model parameters. This was done in the following way.

For a particular value of $\frac{r}{R_o}$ the position of the particle after 100 steps was calculated using the following formulae

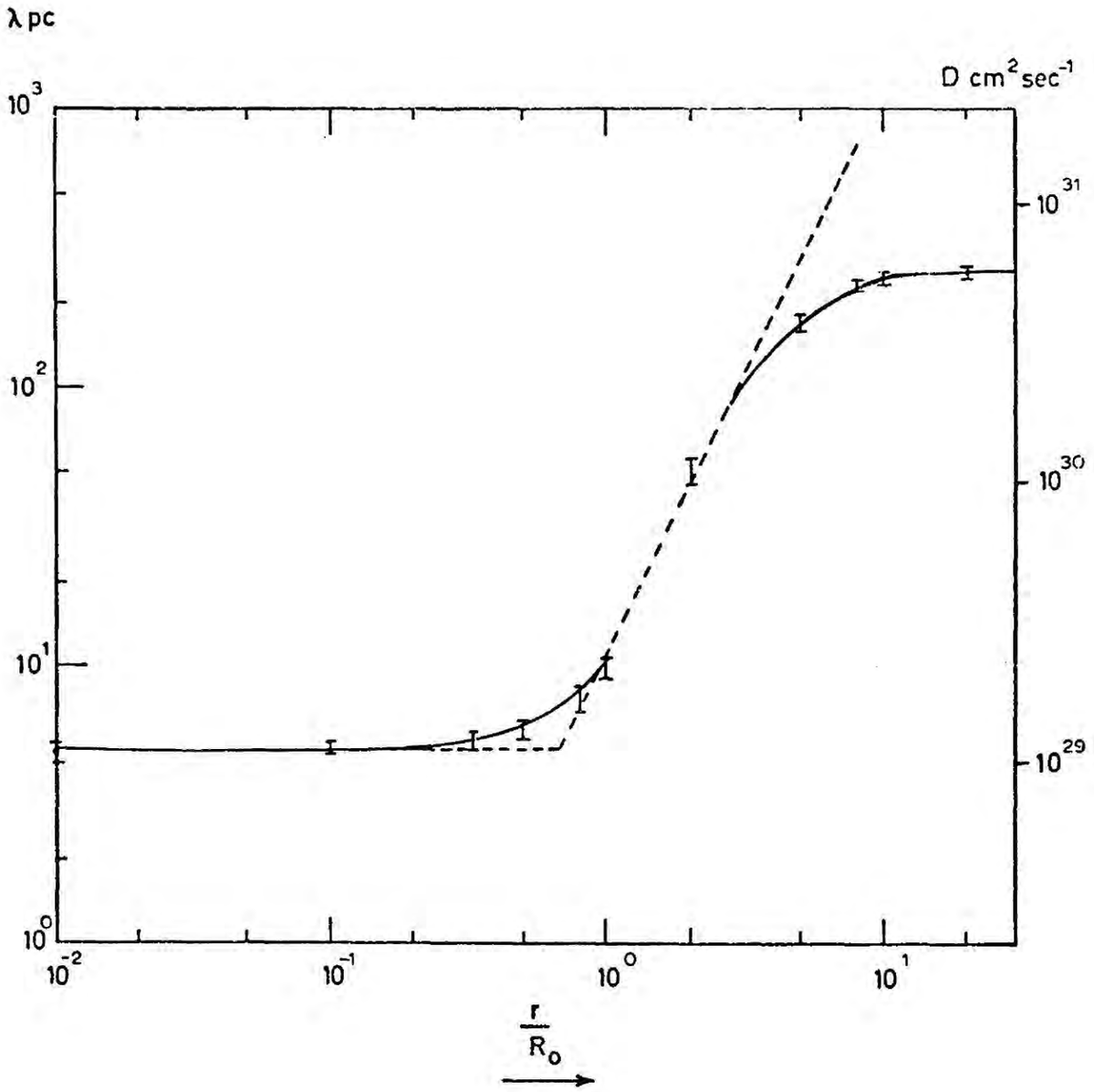

Figure 4-6 The mean free path λpc and the diffusion coefficient D cm^2 sec^{-1} as a function of $\frac{r}{R_o}$ for cosmic rays "leaving" the Earth isotropically.

$$\alpha = \mathrm{Tan}^{-1} \left(\frac{Y}{X}\right)$$

$$\text{where } Y = \sum_{k=0}^{100} y_k \text{ and } y_k = 10 \cos \left(\sum_{i=0}^{k} \phi_i\right) \text{ pc}$$

$$X = \sum_{k=0}^{100} x_k \text{ and } x_k = 10 \cos \left(\sum_{i=0}^{k} \phi_i\right) \text{ pc}$$

The angle α was calculated for 2400 trajectories and the process repeated for values of $\frac{r}{R_o}$ = 10, 5, 2, 1, 0.5, 0.1, 0.01 and 0.001. The distribution $f(\alpha)$ was established and the χ^2 was calculated for the expected distribution $f_e(\alpha) = \frac{N_E}{18}$ where N_E is the number of particles out of N_T=2400 that make 100 steps and still remain inside the spiral arm. The results are plotted in figure 4.7. The χ^2 calculated as a function of $\frac{r}{R_o}$ is tabulated along with the confidence levels in table 4.3.

In conclusion for values of $\frac{r}{R} \lesssim 2$($E \sim 10^{16}$ eV if H_o=3μG, R_o=2pc) the diffusion model is consistent with a uniform source distribution as well as isotropic flux of cosmic rays at the Earth. However, for values of $\frac{r}{R_o} > 2$ the inherent distribution of sources is not consistent with uniformity. In order to maintain isotropy of the cosmic ray flux at the Earth it is necessary to assume that sources where cosmic rays with $\frac{r}{R_o} > 2$ are most probably coming from are weaker than those sources in the region of the "sky" where these cosmic rays are less likely to come from, if a uniform source distribution is to be retained. The anisotropy observed can be explained because cosmic rays with values of $\frac{r}{R_o} > 2$ only suffer small angles of deflection at each scattering centre. The particles effectively make one dimensional walks in the direction defined by the initial angle ϕ_o with which it leaves the Earth. Because the adopted model for diffusion considers a cross section along the length of the spiral arm and particles can leave only by way of its

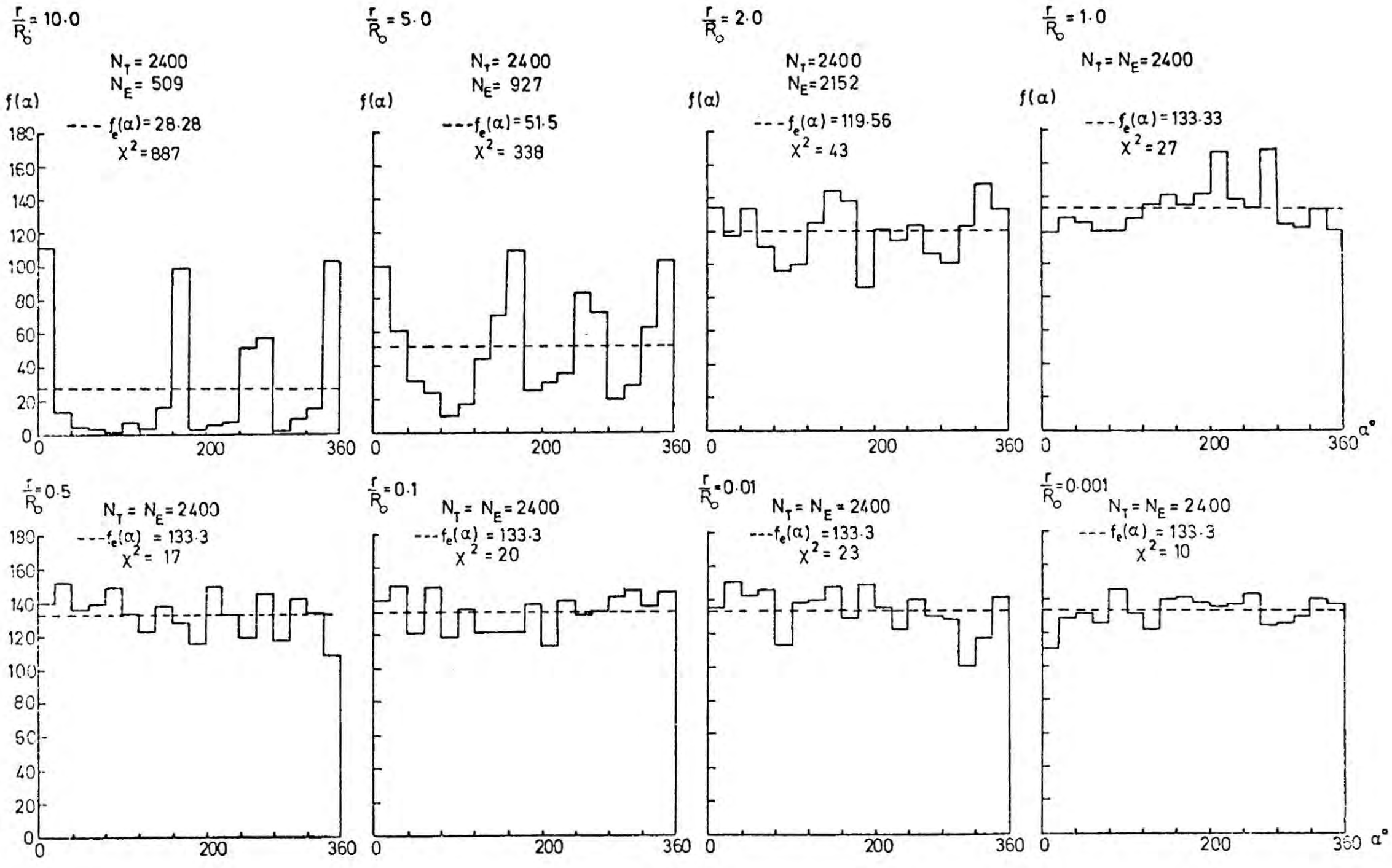

Figure 4-7 The distribution of cosmic ray sources.

Table 4.3

The χ^2 probability of there being an isotropic source distribution as a function of $\frac{r}{R_o}$ for the considered diffusion model.

$\frac{r}{R_o}$	χ^2	C.L. %
10	887	0
5	338	0
2	43	0.12
1	27	5
0.5	17	50
0.1	20	30
0.01	23	18
0.001	10	95

edges those particles emitted initially along the length of the spiral arm have to travel great distances before escaping whilst those particles emitted elsewhere escape more quickly often before making 100 steps. As the energy of the particle increases so the more peaked to 0^{o} becomes the distribution $f(\phi)$, consequently more and more particles escape in less than 100 steps resulting in an increase in the anisotropy. In the next section a numerical value for the anisotropy will be estimated and hence an estimate of how much weaker the sources in directions $\sim 10^{o} \pm 10^{o}$, $\sim 170 \pm 10^{o}$, $\sim 260 \pm 20^{o}$ and 350 ± 10^{o} have to be to ensure isotropy of both the cosmic ray flux at the Earth and isotropic distribution of sources.

Finally, if the number of trajectories traced by the computer was increased beyond 2400 the source distributions would be better defined and for $\frac{r}{R_o} \lesssim 2$ they would be isotropic with a much higher confidence level. However, since this Monte Carlo type calculation takes a great deal of CPU time in the computer it was totally impractical to increase the statistics beyond 2400 when calculating the mean time of escape of a particle from the spiral arm as a function of energy. Table 4.3 therefore, represents the accuracy of the present calculations.

4.5.2 Degree of anisotropy achieved in the model calculations

As pointed out in chapter 2 cosmic rays are observed to be virtually isotropic at the Earth. In the model under test we demanded that cosmic rays "leave" the Earth in an isotropic manner. However, as suggested in the previous section, the degree of anisotropy is not only dependent on the energy of the cosmic ray particle but also on the geometry of the spiral arm adopted in the model.

A general feel for the degree of anisotropy can be obtained by establishing the variation of the mean time of escape of the particle from the spiral

arm $\bar{t}_{\phi_o}$ as a function of the angle ϕ_o at which the particle "leaves" the Earth. (The mean time of escape reflects the intensity of cosmic rays reaching the Earth, if there is a significant change of $\bar{t}_{\phi_o}$ with ϕ_o then significant lack of isotropy results).

Because of limited CPU time on the computer $\bar{t}_{\phi_o}$ as a function of ϕ_o was only calculated for a representative set of $\frac{r}{R_o}$ values namely 10, 5, 2, 1 and 0.01 and only 1200 trajectories were traced in each case. It must be realised that the actual diffusion model has an accuracy $\sim \sqrt{2}$ better than that suggested by the results tabulated in table 4.4 and plotted in figure 4.8 where the $\bar{t}_{\phi_o}$ is plotted as a function of ϕ_o.

Because within statistical error $\bar{t}_{\phi_o}$ is constant for all values of ϕ_o for cosmic rays with energy such that $\frac{r}{R_o} \lesssim 5$ all cosmic rays of these energies are considered to be isotropic. However, for $\frac{r}{R_o} \gtrsim 5$ anisotropy becomes increasingly significant with increasing values of $\frac{r}{R_o}$ and some measure of this will be made.

It is possible to define anisotropy in two ways. In general $\delta = \frac{J_{max}-J_{min}}{J_{max}+J_{min}}$, however since it is usual for the cosmic ray flux to be at its maximum and minimum in opposite directions the above equation reduces to $\delta^* = \frac{J_{\text{in one direction}}-J_{\text{in opposite direction}}}{J_{\text{in one direction}}+J_{\text{in opposite direction}}}$ which is dependent on the choice of direction.

J represents the flux of cosmic rays which is proportional to the mean escape time of cosmic rays from the spiral arm. These two definitions of anisotropy will be dealt with in turn.

a) Anisotropy δ

If we define N_o^* as the maximum cosmic ray flux coming down the length of the spiral arm to the Earth and N the particle density averaged over every direction then

Table 4.4

The mean time of escape of particles of different energy leaving the spiral arm as a function of the angle at which it "leaves" the Earth. (Statistics 1200, error represents one standard deviation).

$\frac{r}{R_o}$ → / ϕ_o ↓	10	5	2	1	0.01
	t_{ϕ_o} x 10^{10} secs	x 10^{10} secs	x 10^{11} secs	x 10^{12} secs	x 10^{12} secs
45	7.3±0.5	10.8±0.5	3.7±0.2	1.74±0.09	3.7±0.2
90	5.7±0.4	10.2±0.5	3.7±0.2	1.8±0.1	3.7±0.2
135	6.9±0.2	10.2±0.5	3.7±0.2	1.8±0.1	3.8±0.3
180	8.5±0.5	11.2±0.6	3.7±0.2	1.8±0.2	3.7±0.2
225	7.2±0.3	10.5±0.8	3.5±0.2	1.7±0.1	3.6±0.3
270	5.8±0.4	9.7±0.8	3.5±0.2	1.7±0.2	3.7±0.2
315	7.1±0.3	10.5±0.7	3.6±0.2	1.8±0.1	3.7±0.2
0 and 360	8.6±0.3	11.3±0.3	3.6±0.1	1.8±0.1	3.9±0.4

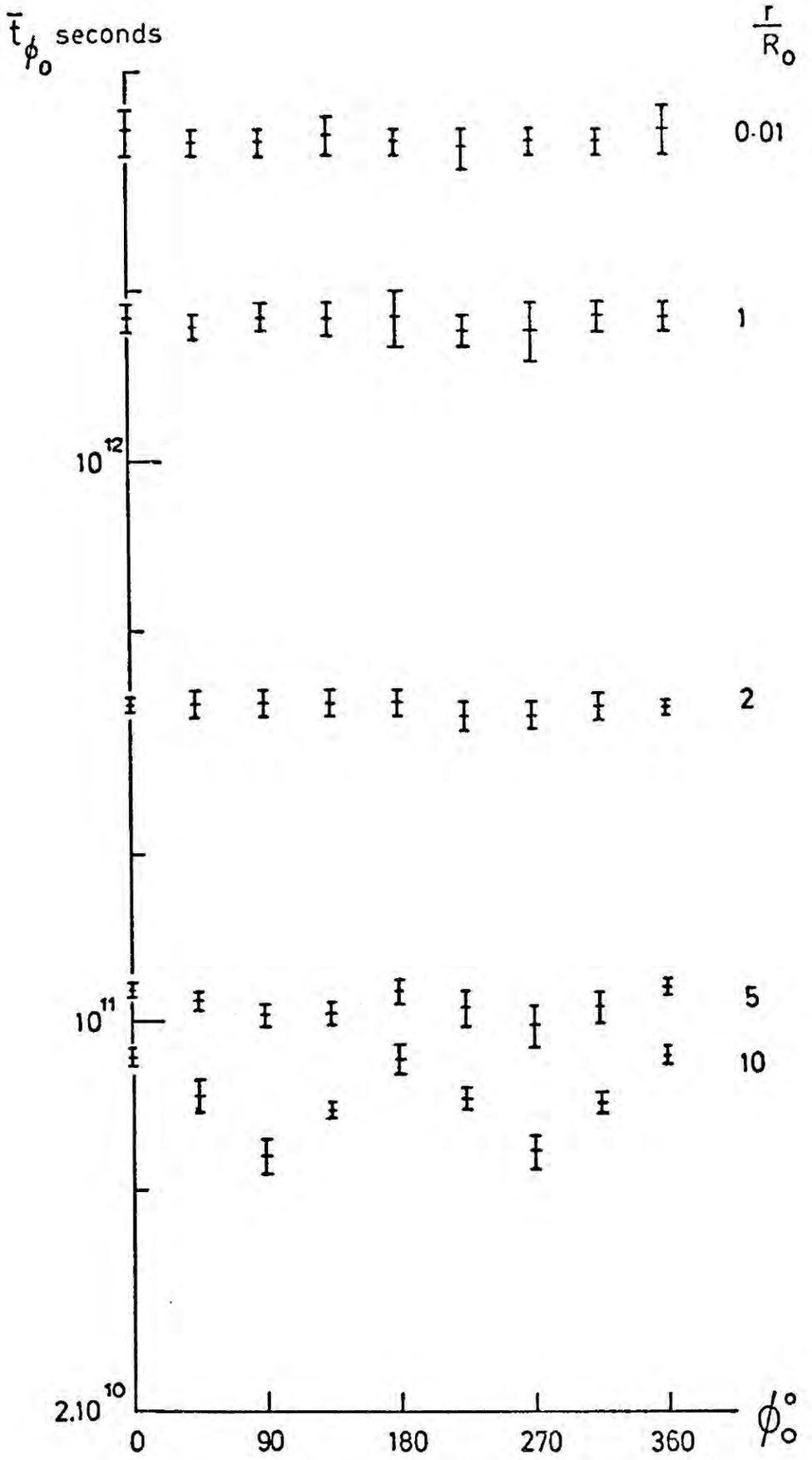

Figure 4-8 The mean time of escape of a particle from the spiral arm as a function of the angle ϕ_o with which it "leaves" the Earth for different values of $\frac{r}{R_o}$

$$J_{max} = N_o^* \propto N(x=o)$$

$$J_{min} = N_{90}^* \propto N(x+\lambda) = N + \lambda \frac{\partial N}{\partial x} + \frac{\lambda^2}{2} \frac{\partial^2 N}{\partial x^2}$$

Then at the centre only i.e. $\frac{\partial N}{\partial x} = 0$

$$\delta = -\frac{\lambda^2}{4N} \frac{\partial^2 N}{\partial x^2}$$

The theory of diffusion gives $N \propto a^2 - x^2$, see equation 4.4, where a is the half width of the spiral arm, and so

$$\delta = \frac{\lambda^2}{2a^2} \qquad 4.16$$

For $\frac{r}{R_o} << 1$ since λ and a are 5 pc and 300 pc respectively, $\delta = 1.4\ 10^{-4}$. The computer was used to measure the anisotropy δ as a function of $\frac{r}{R_o}$ for the diffusion model according to the definition above. The particle was restricted to start its journey in a direction along the spiral arm i.e. the value ϕ_o was set initially to zero. This model is then consistent with all particles arriving at the Earth from along the length of the spiral arm. The mean time of escape $\bar{t}_o$ was calculated as a function of $\frac{r}{R_o}$. 2400 particle trajectories were traced. The procedure was repeated to calculate the mean time of escape $\bar{t}_{90}$ as a function of energy i.e. starting the particle at an angle $\phi_o = 90^o$ which is consistent with all cosmic rays arriving at the Earth from the direction of the galactic centre.

In figure 4.9 the mean times of escape $\bar{t}_o$ and $\bar{t}_{90}$ are plotted as a function of the ratio $\frac{r}{R_o}$. The numerical values appear in table 4.2. Within experimental error the times agree for values of $\frac{r}{R_o} \leq 2$, but beyond $\frac{r}{R_o} = 2$ the times of escape deviate. This marks the point where isotropy of cosmic rays breaks down. The anisotropy for the computer model is calculated as a function of $\frac{r}{R_o}$ along with its error, $\alpha\delta$ defined by the equation

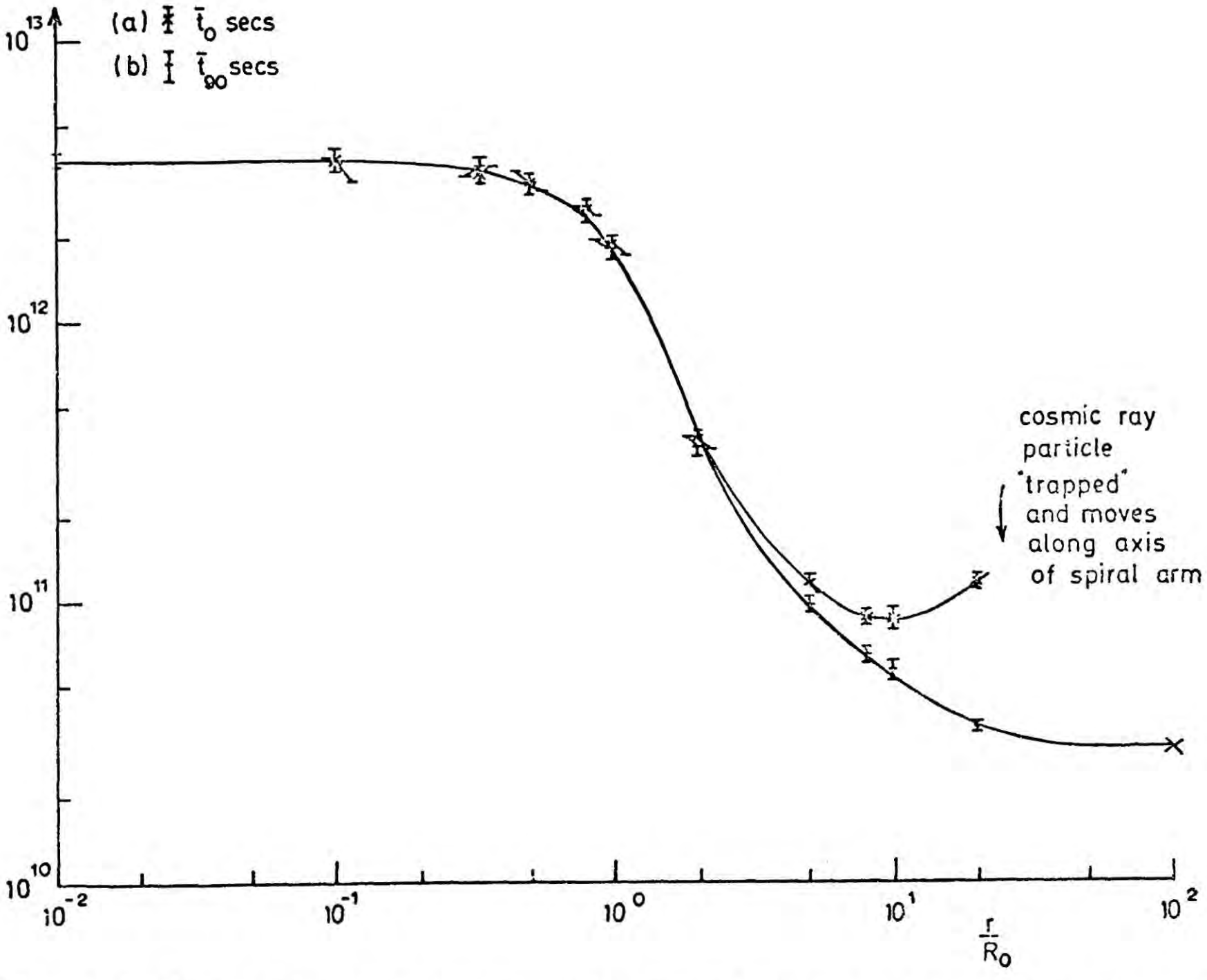

Figure 4-9 The mean time of escape of a particle from the spiral arm as a function of $\frac{r}{R_o}$ for particles"leaving" the Earth in the direction (a) along the length of the spiral arm and (b) of the galactic centre.

$$\alpha\delta = \frac{4}{(J_o+J_{90})^4}\left[(\alpha J_o)^2 (J_{90})^2 + (\alpha J_{90})^2 J_o^2 \right]$$

where $J_o\alpha\bar{t}_o$, $J_{90}\alpha\bar{t}_{90}$, $\alpha J_o = \frac{\sigma_{J_o}}{\sqrt{2400}}$ and $\alpha J_{90} = \frac{\sigma_{J_{90}}}{\sqrt{2400}}$. The results of the calculations are tabulated in table 4.5 and plotted as open circles in figure 4.10. The calculated values of δ for $\frac{r}{R_o} \lesssim 1.0$ are somewhat scattered two anisotropies for $\frac{r}{R_o} = 0.01$ and 0.33 being negative. These facts can be explained in terms of statistical deviations in the quantity $J_o - J_{90}$. Obviously, as the number of trajectories traced by the computer approaches infinity the anisotropy will approach the theoretical value given by 4.16 and plotted as a function of $\frac{r}{R_o}$ in figure 4.10 as a solid line.

The degree of isotropy achieved by the model is not inconsistent with experimental observations for all values of $\frac{r}{R_o} \lesssim 2$ (for $R_o \sim 2$pc and $H_o \sim 3\mu$G, E $\sim 10^{16}$eV) Below this value cosmic rays arriving at the Earth, given a uniform source distribution all of equal strength, are totally isotropic. Anisotropy increases with increasing energy of the cosmic ray. As explained in the previous section this problem can be overcome by assuming that some sources are stronger emitters than others. It is estimated that total isotropy is achieved for all cosmic rays provided that the sources in the directions $\sim 10^\circ \pm 10^\circ$, $170^\circ \pm 10^\circ$, $260^\circ \pm 20^\circ$ and $350 \pm 10^\circ$ are $\sim$100 times weaker emitters of cosmic rays, with energies such that $\frac{r}{R_o} \gtrsim 2$, than sources in the other regions of the "sky". But such a physical situation is rather unlikely.

The one dimensional type behaviour of particles of high energy described in the previous section is illustrated in figure 4.9 where the curve for $\bar{t}_o$ curls up for large values of $\frac{r}{R_o}$. $\bar{t}_{90}$ flattens off at $3\ 10^{10}$ seconds which is consistent with a high energy particle travelling the distance

Table 4.5

The expected anisotropy as a function of $\frac{r}{R_o}$

$\frac{r}{R_o}$	δ
≥ 20	$(5.405 \pm 0.003) \times 10^{-1}$
10	$(2.09 \pm 0.01) \times 10^{-1}$
8	$(1.461 \pm 0.008) \times 10^{-1}$
5	$(7.14 \pm 0.07) \times 10^{-2}$
2	$(1.7 \pm 0.1) \times 10^{-2}$
1	$(5 \pm 1) \times 10^{-3}$
0.8	$(1.03 \pm 0.09) \times 10^{-2}$
0.5	$(3 \pm 1) \times 10^{-3}$
0.33	$(-1.0 \pm 0.6) \times 10^{-3}$
0.1	$(1.0 \pm 0.1) \times 10^{-2}$
0.01	$(6.8 \pm 0.9) \times 10^{-3}$
0.001	$(-1 \pm 1) \times 10^{-3}$
≤ 0.0001	$(1.2 \pm 0.1) \times 10^{-3}$

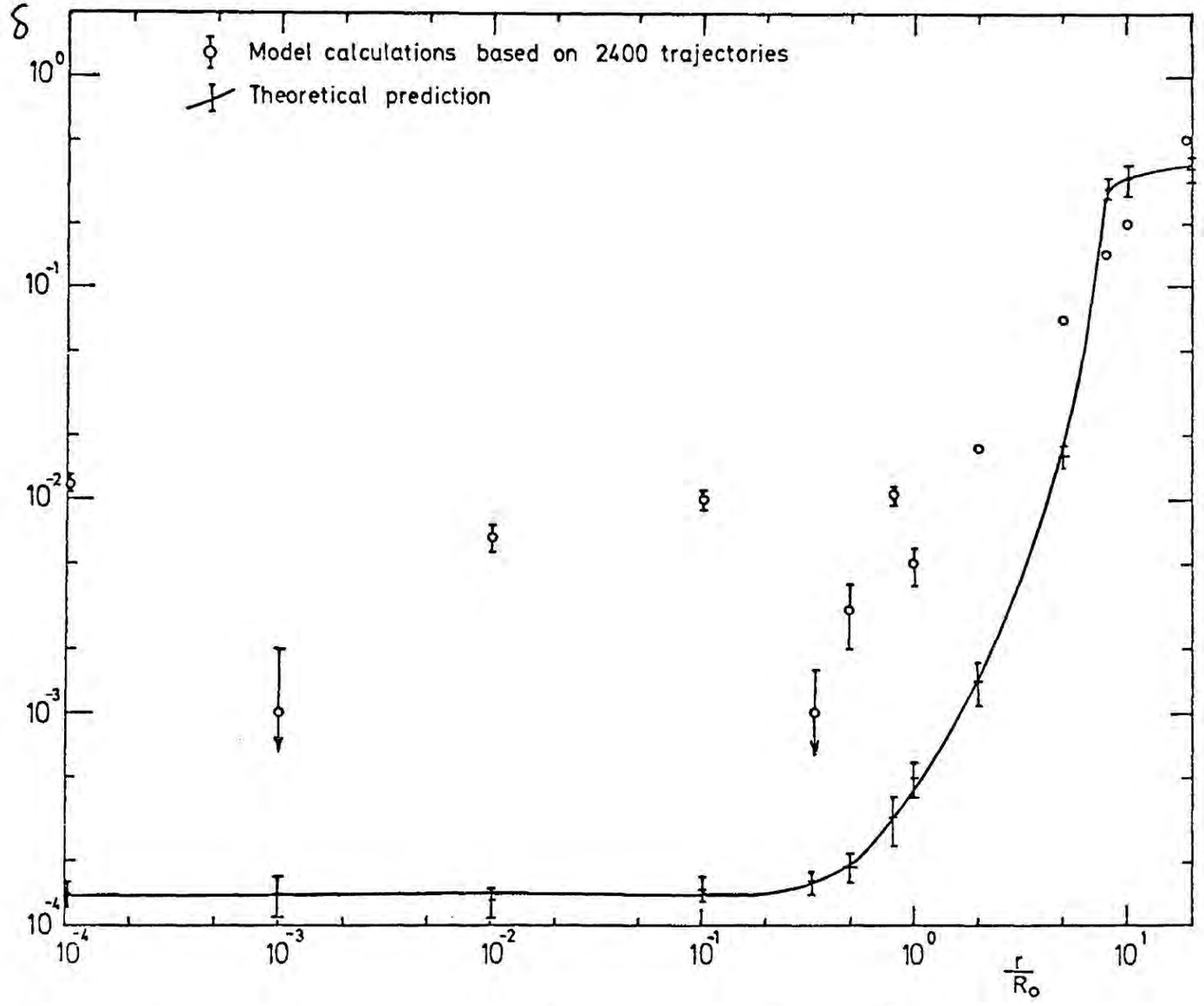

Figure 4-10 The anisotropy of cosmic rays as a function of $\frac{r}{R_o}$.

300 pc out of the spiral arm at the speed of light. However, $\bar{t}_o$ for high energies theoretically approaches infinity equivalent to a particle being trapped along the length of the spiral arm.

b) Anisotropy δ^*

Defining J_{ϕ_o} as the flux of cosmic rays entering the Earth from the direction ϕ_o^o (and $J_{\phi_o} \propto \bar{t}_{\phi_o}$, is the mean time of escape of a particle "leaving" the Earth at an angle ϕ_o) then J_{90} is the flux from the positive x direction (from the galactic centre) and J_{270} is the flux from the negative x direction (from the galactic anticentre). If N is the particle density averaged over every direction then at one mean free path away from the Earth along the $+x$ and $-x$ direction we have

$$J_{90} = N(x+\lambda) = N + \lambda \frac{\partial N}{\partial x} + \frac{\lambda^2}{2} \frac{\partial^2 N}{\partial x^2}$$

$$J_{270} = N(x-\lambda) = N - \lambda \frac{\partial N}{\partial x} + \frac{\lambda^2}{2} \frac{\partial^2 N}{\partial x^2}$$

and $\delta^* = \frac{\lambda}{N} \frac{\partial N}{\partial x} = \frac{-2x\lambda}{(a^2-x^2)}$

For the diffusion model developed here the anisotropy δ^* is obviously zero because the Earth lies at the centre of the spiral arm and the geometry of the spiral arm is symmetrical about the position of the Earth (i.e. the quantity of diffusing matter and the number of sources in a direction ϕ^o and $(\phi+180)^o$ are the same). Within the statistical errors of the Monte Carlo calculation δ^* is consistent with zero when calculated from the results plotted in figure 4.8.

In conclusion, for the anisotropy to be consistent with the experimentally observed value of $\delta \lesssim 10^{-2}$ then the Earth must lie at or close to the centre of the spiral arm.

4.6 Conclusion

We have shown that the basic laws of diffusion can be successfully applied to the diffusion of cosmic rays in the interstellar medium. The model for the medium involved a uniform distribution of clouds of constant size and magnetic field the direction of which is perpendicular to the plane in which diffusion occurs, being directed out of and into the plane with equal probability.

Only a 2-D treatment was possible because the Monte Carlo calculation is CPU bound. It is believed, however, that a 3-D treatment would yield very little overall change in the shape of the curve defining the mean time of escape of function of energy. It is thought that perhaps only a shift of the entire curve in the vertical direction would result. This of course is irrelevant in this treatment.

For 2-D diffusion, as a result of the computer calculations (figure 5.4) a change of slope $\Delta\gamma=2$ is achieved and there is a smearing in the region of the "knee" over an energy range of approximately a decade. The 'f' factor is 0.75. None of these properties compare favourably with experiment and therefore this simple model for diffusion in a uniform medium is totally unsatisfactory. A more realistic picture of the Galaxy is essential. It is important to establish the distribution of $H_o R_o$ before any progress can be made.

The geometry of the spiral arm causes the serious flattening in the mean free path as diffusion breaks down for large values of $\frac{r}{R_o}$. For this reason the part of the curve beyond $\frac{r}{R_o} \simeq 2$ must be ignored. As a result of making this assumption we automatically have a model consistent with total isotropy of the cosmic ray flux at the Earth as well as a uniform source distribution, provided that the Earth is at or very close to the

centre of the spiral arm. The last statement is not inconsistent with some observations on the relative position of the solar system with respect to the Orion arm. (See discussion in section 9.2).

Some experiments, however, claim that the solar system is nearer the edge on the galactic centre side of the spiral arm. Serious problems connected with the isotropy conditions observed at the Earth would result if this were true. On the other hand, evidence for a definite "ring" of hydrogen gas surrounding the solar system has been reported by Hughes and Routledge (1972) the kinematics of which has been dealt with by Lindblad et al (1972). This "ring" of hydrogen could act as a reflecting surface that would help to randomise the directions of cosmic rays. This point will be taken up again in Chapter 9.

Chapter 5 Experimental observations of the interstellar matter

5.1 Introduction

The diffusion model explained in detail in Chapter 4 does not represent the true physical state of our Galaxy. Before a more realistic model for diffusion of cosmic rays in the Galaxy can be made, the characteristic properties of the interstellar medium must be established. Our main sources of information are continuous and line spectra in both the radio and optical regions of the electro-magnetic spectrum.

Neutral hydrogen is the most abundant constituent of the interstellar gas and at radio wavelengths we obtain a 21 cm emission profile which gives information about the cloud structure. Its disadvantage is the limited angular resolution. However, 21 cm absorption against strong radio sources provides good angular and velocity resolution measurements of the inter-cloud medium. Both continuous and line spectra are emitted at radio wavelengths by ionised hydrogen (H_{II}) regions and the 18 cm lines are absorbed and emitted by OH molecules.

Optical continuum carries information on extinction, reddening, polarization, scattering and reflection - all by solid particles. Optical line spectra (along with a weak optical continuum) are emitted by H_{II} regions known as diffuse emission nebulae. Optical absorption lines are produced by various interstellar atoms and molecules and are observed in spectra of early type stars. From such measurements the distribution and motion of interstellar matter and the chemical composition and physical state of the interstellar gas can be estimated.

5.2 Neutral hydrogen -21 cm emission

5.2.1 Galactic rotation model

A high percentage of interstellar matter is in one form of neutral

hydrogen. The ground state of the hydrogen atom is split into two levels, the upper and lower sublevel correspond to the proton and the electron having their spins aligned antiparallel and parallel, respectively. The transition between the sublevels corresponds to a frequency of 1420.406 mc/sec equivalent to a wavelength of 21.105 cm in the radio region of the electromagnetic spectrum.

Excitation of electrons into the higher energy sublevel is caused by collisions of hydrogen atoms moving, within a cloud of typical temperature 80-100^{o}K, at speeds with a Maxwellian distribution. De-excitation to the lower energy sublevel is possible by collision with another hydrogen atom or by emitting a photon of wavelength λ=21 cm. This transition is strongly forbidden because transitions between two hyperfine levels must involve a change of orbital quantum number L. However, we are concerned here with transitions between hyperfine structure components occurring because of magnetic dipole radiation and the selection rule only applies to the case of electric dipole radiation. Also, since lifetime is inversely proportional to frequency cubed the radiative transition will occur only once every 3.5 10^{14} seconds equivalent to 10^{7} years (Shklovsky 1956).

De-excitation by collision is therefore much more frequent than by emission of a quanta but eventually equilibrium is established with 3 atoms in the upper state for each atom in the lower state. Although the 21 cm emission is rare we observe a strong emission feature in the radio spectrum because the telescope samples an enormous quantity of neutral hydrogen along the line of sight. The intensity of the radiation is proportional to the total number of hydrogen atoms along the line of sight and the range of frequencies detected in each direction is a measure of the Doppler shift due to galactic rotation.

In order to interpret the complex line profiles obtained by 21 cm galactic surveys it is necessary to build up a model of the dynamics of our spiralling Galaxy. This problem was investigated by Oort, Kwee, Muller and Westerhaut (1954) and by van de Hulst, Muller and Oort (1954). They establish a general formula for radial velocity v_r of a feature at a distance r from the galactic centre as $v_r = r_o\,(\omega(r) - \omega_o(r_o))\sin \ell$ 5.1 where $\omega(r) = \theta(r)/r$ is the angular velocity of rotation at a distance r from the galactic centre and $\theta(r)$ is the linear rotation velocity perpendicular to radius r. $\omega_o(r_o) = \theta_o(r_o)/r_o$ is the angular velocity of rotation of the Local Standard of Rest (L.S.R.) and $\theta_o(r_o)$ is the linear rotation velocity of the L.S.R. perpendicular to radius r_o which is radius of the L.S.R.. ℓ is the galactic longitude of the feature with respect to the L.S.R.

Observations of v_r yield $\omega(r)$ but the value of r to be associated with a given value of $\omega(r)$ is in general not known. Kwee, Muller and Westerhaut (1954) derived the maximum radial velocity, hence the maximum value for $\omega(r)$, at a variety of galactic longitudes between 0^o and 90^o and 270^o and 360^o and constructed the rotation curve $\omega(r)$ or $\theta(r)$ as a function of r for $r \lesssim r_o$ shown in figure 5.1. He assumed $r_o = 8.2$ kpc and $\theta_o(r_o) = 216$ km sec^{-1} and explains the points falling beneath the curve in terms of the lack of hydrogen at the point at which the radial velocity is a maximum (i.e. at $r_{min} = r_o \sin \ell$) giving an underestimate of the true $\theta(r)$ observable in the presence of hydrogen. The places where the observed points coincide with the smooth curve indicate the positions of the spiral arms giving reliable points for fitting the curve. This work was repeated by Rougoor and Oort (1960) see also Schmidt and Blaauw (1965). Since there is no maximum radial velocities in the directions

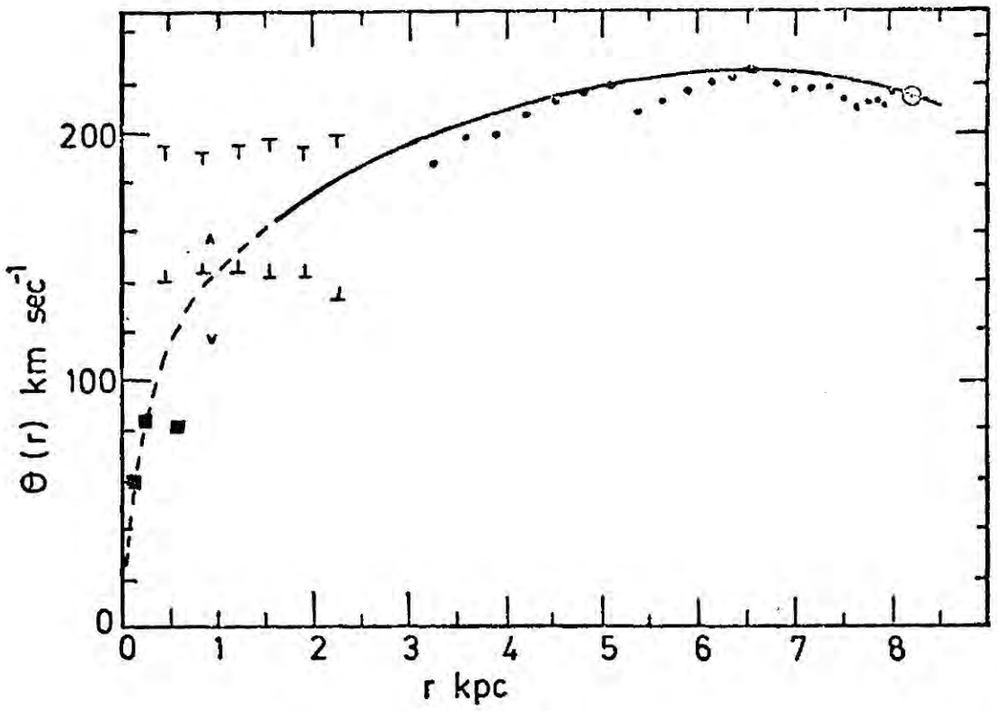

Figure 5-1 The rotation curve i.e. the circular velocity as a function of the distance from the galactic centre. • represent $\theta(r)$ for $\ell > 327^{\circ}.5$; $\overset{\top}{\perp}$ represent the limits of $\theta(r)$ for $\ell > 327^{\circ}.5$ and ▪ and $\overset{\wedge}{\vee}$ refer to the observations on the other side of the galactic centre. $\theta_o(r_o)$ is indicated by ⊙

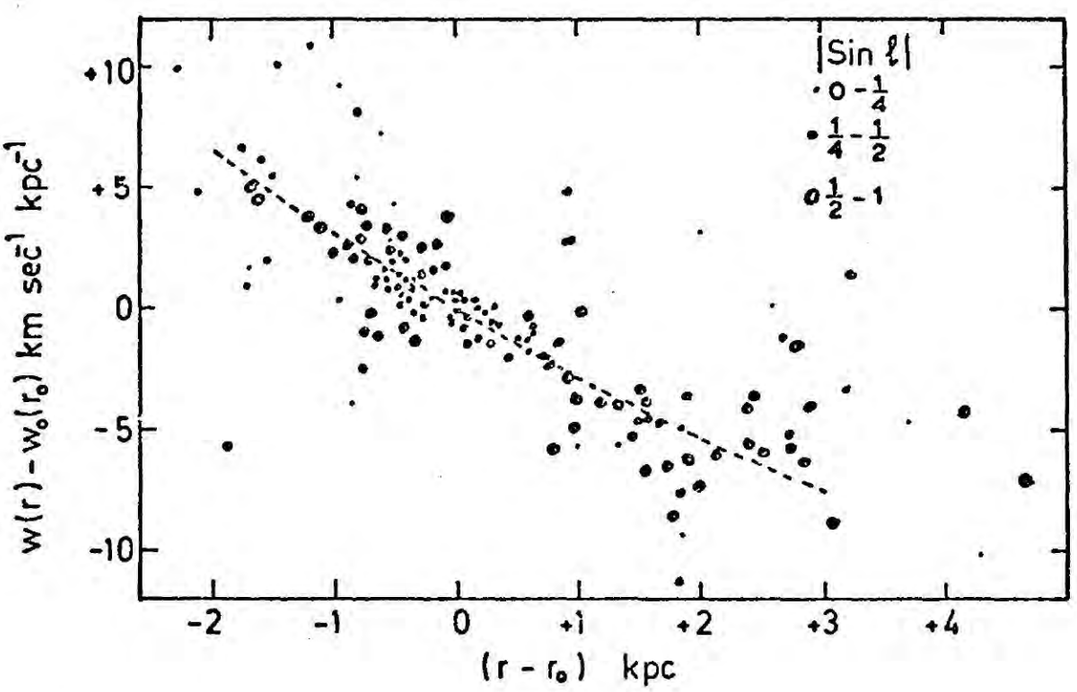

Figure 5-2 The angular velocity $\omega(r)$ as a function of distance r from the centre of the Galaxy.

$90^{o} \leq \ell \leq 270^{o}$ it is impossible to obtain $\omega(r)$ or $\theta(r)$ from 21 cm observations for $r > r_o$. In fact $\omega(r)$ can be estimated from equation 5.1 but there is no way of obtaining the r associated with the value of $\omega(r)$. Therefore for $r > r_o$, we rely on optical observations of the Cepheid variables which were made by Kraft and Schmidt (1963). The distance d pc to the Cepheid from the L.S.R. was estimated from observations of period luminosity and period colour relations. The law of cosines was used to estimate r; then by observing v_r and using equation 5.1 a plot was made of $\omega(r)$ versus r over a range $8 < r < 14$ kpc (see figure 5.2) where r_o = 10 kpc and θ_o = 250 km sec^{-1}. By combining the optical and radio results Contopolous and Strömgren (1965) derived the rotation curve $\theta(r)$ based on the most recent values for $\theta_o(r_o)$ (= 250 km sec^{-1}) and r_o (=10 kpc). This curve is plotted in Figure 5.3.

5.2.2 Method of analysis of the 21 cm emission data

A survey of the 21 cm emission data obtained in various experiments carried out over the past twenty years has been made. The data are in general presented in the form of contour maps of brightness temperature or hydrogen density, diagrams of velocity versus galactic latitude or longitude and emission profiles which are often analysed into Gaussian components with the aid of a computer. Other parameters measured in these experiments include spin temperature, optical depth, number of emitting atoms in the line of sight and the velocity dispersion which describes random and thermal motions of the clouds. Appendix (iii) develops the theory essential for a full understanding of the measurable parameters. All the data reveal patchiness in the structure of the hydrogen in the Galaxy but as all experiments are carried out using different techniques they have very different angular resolutions and therefore the scale of the hydrogen substructure differs considerably.

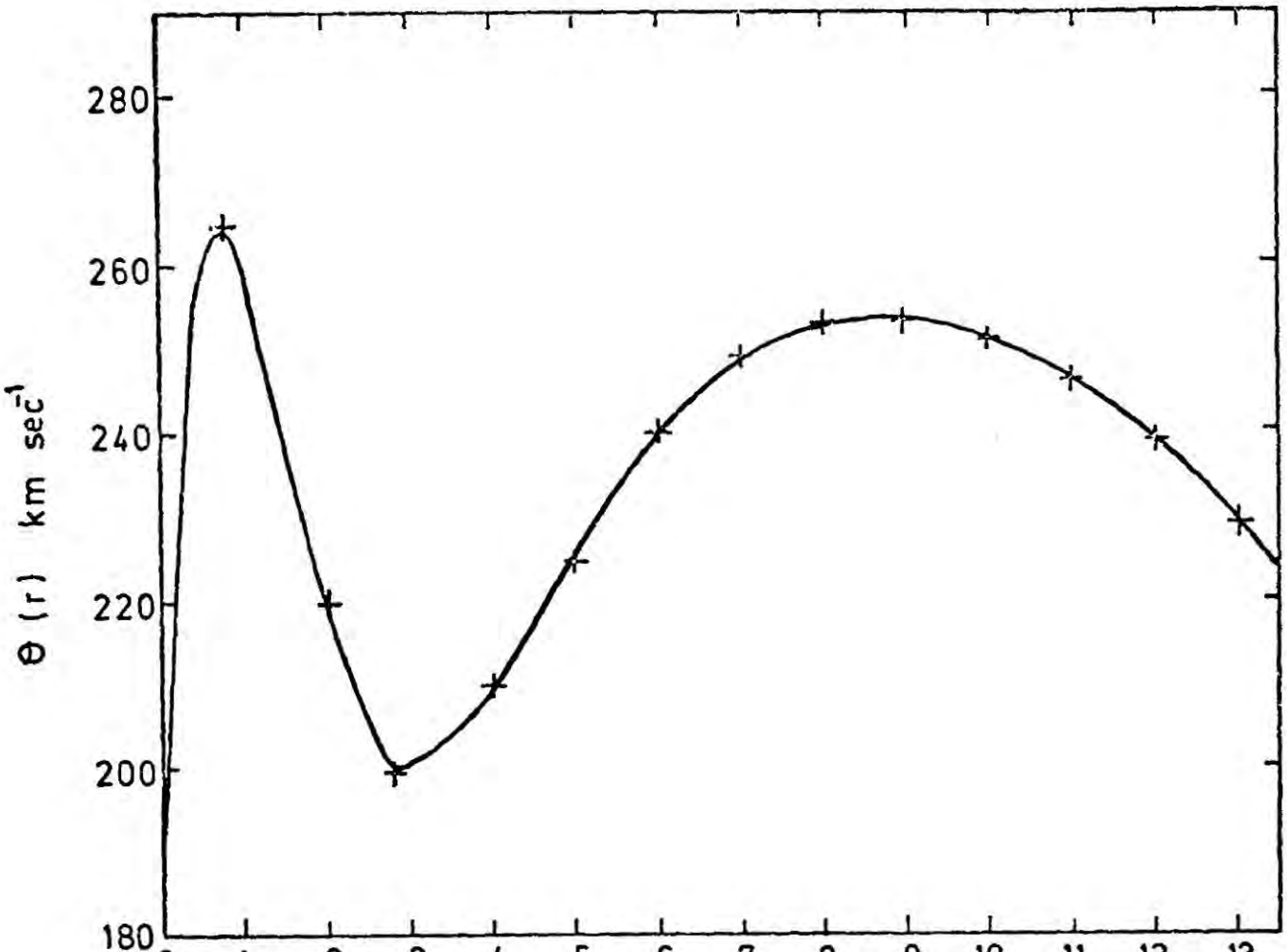

Figure 5-3. The rotation curve based on the most recent values for $\theta_o(r_o)$ and r_o (The rotation velocities for $r<r_o$ were obtained from radio observations and values for $r>r_o$ were derived from optical observations - see Contopolous and Strömgrem 1965).

A successful comparison of the data was possible by firstly establishing the volume of galactic space under observation and then making an estimate of the "size" of the irregularities in the hydrogen (loosely termed "clouds"). The distance d pc to the hydrogen under observation from the L.S.R. was estimated by using equation 5.1, figure 5.3 and the law of cosines. The spacial extent of the "clouds" was determined by assuming the "cloud" to be circular with radius R_o pc. If the "cloud" subtends a solid angle $\Delta b^o \times \Delta \ell^o$ (where Δb and $\Delta \ell$ are the angular range in galactic latitude and longitude respectively) from the L.S.R. then by definition (see figure 5.4) at ℓ^o, b^o and distance d pc away there is a cloud of radius $R_o = \frac{d}{180}\sqrt{\Delta \ell \ \Delta b}$ pc.

Figure 5.5 gives the range in galactic longitude and latitude observed in the 21 cm emission experiments listed in the key. The size(R_o pc) and the position (d pc) of the "clouds" with respect to the L.S.R. calculated in the above way are tabulated in table 5.1. The structures in the hydrogen observed in these experiments are termed "large scale" in the sense that they are arm and interarm features. It must be stressed that the above treatment is only approximate because (a) the galactic rotation model is applicable to hydrogen very close to the galactic plane and we deal with values of b different from zero and (b) the velocity v_r assumed in the analysis is not necessarily the true radial velocity, due solely to galactic rotation, but most probably involves a component due to random or thermal motion of the hydrogen which has caused dispersion of the cloud to the position of observation. However, this treatment has proved successful in separating the "large scale" data from the "small scale" data which are summarised as above in figure 5.6 and table 5.2.

It is important to develop a general picture of the Galaxy and to make estimates of the mean parameters e.g. typical cloud sizes, densities,

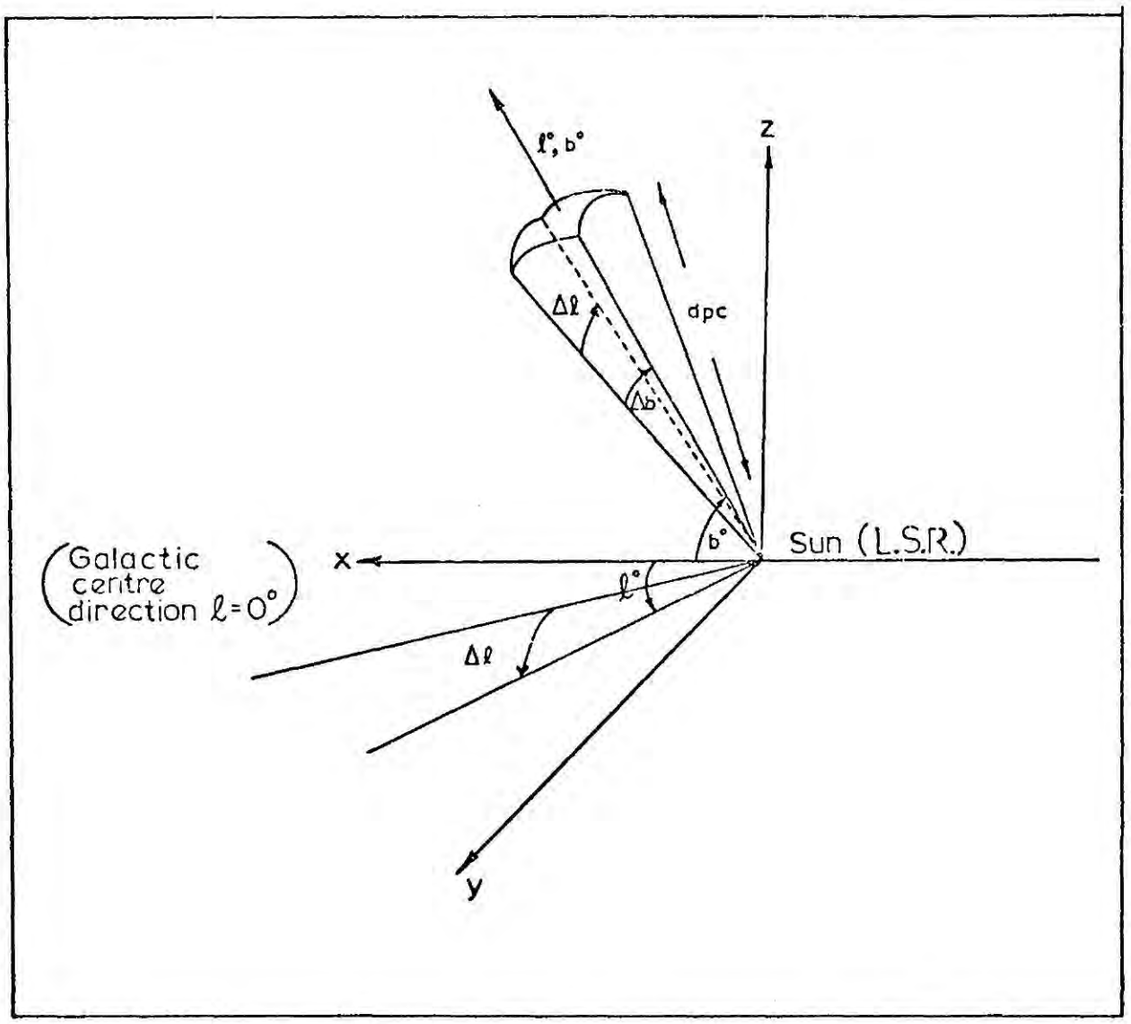

Figure 5-4 For a cloud subtending a solid angle $\Delta b^{o} \times \Delta \ell^{o}$ from the L.S.R. then by definition at ℓ^{o}, b^{o} and distance d pc away there is a cloud with radius $R_{o} = \frac{d}{180} \sqrt{\Delta \ell \times \Delta b}$ pc.

Table 5.1: Regions of the sky surveyed on a large scale by observing the neutral hydrogen 21 cm emission. (The numbers in the first column correspond to those circled in figure 5.5. Typical large scale features observed are indicated in the last column by the following abbreviations, A-arm, I.A.-inter arm, L-mainly local hydrogen).

	Reference (year)	ℓ°	b°	distance from L.S.R. d kpc	Usual sampling interval	Features observed and scale of irregularities $R_\odot$ pc
1	Helfer et al (1955)	82.2 122.2	-24_+26 -29_+41	≲7 ≲7	b,2°.5,5° b,2°.5,5°	A and I.A. very large gas clouds beyond the Perseus Arm
2	Bolton et al (1958)	326-360	-7_+9	13-20	ℓ,b,2°	A and I.A., L, ∿1kpc
3	Burke et al (1958)	349-252	±20	∿10	ℓ,10°;b,25°	A and I.A., L.
4	Braes (1963)	355-5	±5	≲7	ℓ,10°;b*	A and I.A., L.
5	Höglund (1963)	155-200	-16_+14	16-6	ℓ,5°; b,25°	Orion Arm. I.A., ∿1kpc
6	Burke et al (1963a)	11-50	-0.8_+2	23-17	ℓ,5°;b,12′	A and I.A., 40-400 pc
7	Burke et al (1963b)	333-2	±2	10	ℓ,2°;b,1°	galactic nucleus observes 3 kpc expanding arm whose depth is∿350 pc.
8	Butler Burton (1966)	43-56	±4.5	7-8	ℓ,b,0.5°	A. 45 pc
9	van Kuilenburg (1972)	30-290	-15_-40 +15_+70	-	8,2°.5	high velocity
10	Wannier et al (1972)	252-322	+10_+30	12-15	ℓ,b,2°	A. 200-1500 pc

* continuous

Key

1 Helfer et al (1955)
2 Bolton et al (1958)
3 Burke et al (1958)
4 Braes (1963)
5 Höglund (1963)
6 Burke et al (1963a)
7 Burke et al (1963b)
8 Butler Burton (1966)
9 van Kuilenburg (1972)
10 Wannier et al (1972)

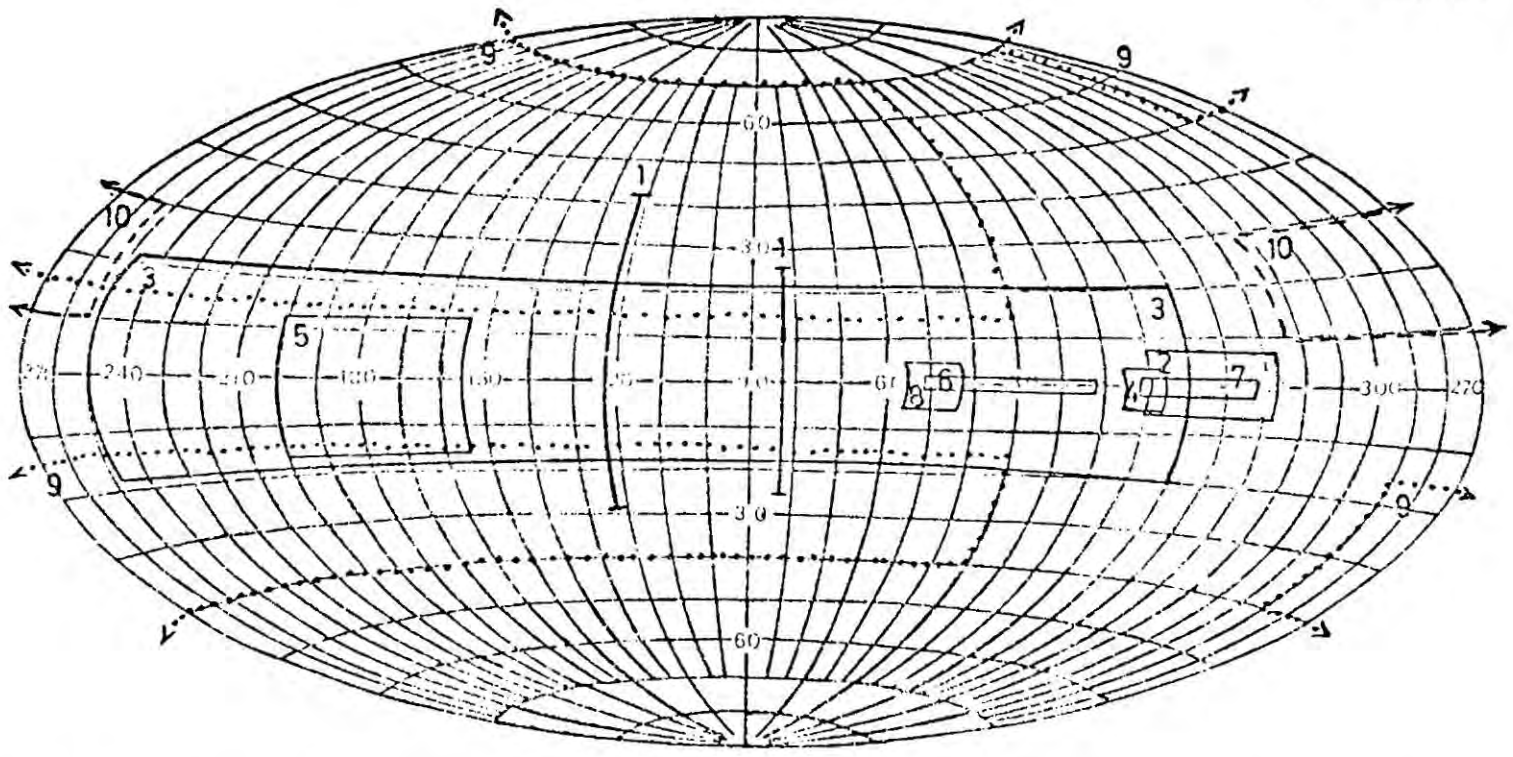

Figure 5-5 The regions of the sky surveyed on a large scale by observing the neutral hydrogen 21 cm emission. The details of the experiments are given in Table 5-1.

Key

1 Heeschen (1955)
2 Menon (1958)
3 Kaftan-Kassim (1961)
4 Davis (1962)
5 Dieter (1964)
6 Dieter (1965)
7 Makarova (1965)
8 Raimond (1966)
9 Takakubo and van Woerden (1966)
10 Heiles (1967)
11 Lindblad (1967)
12 Takakubo (1967)
13 Riegel and Jennings (1969)
14 Ames and Heiles (1970)
15 Gordon (1970)
16 Weaver and Williams (1970)
17 da Rocha Vieira (1971)
18 Knapp and Verschuur (1972)

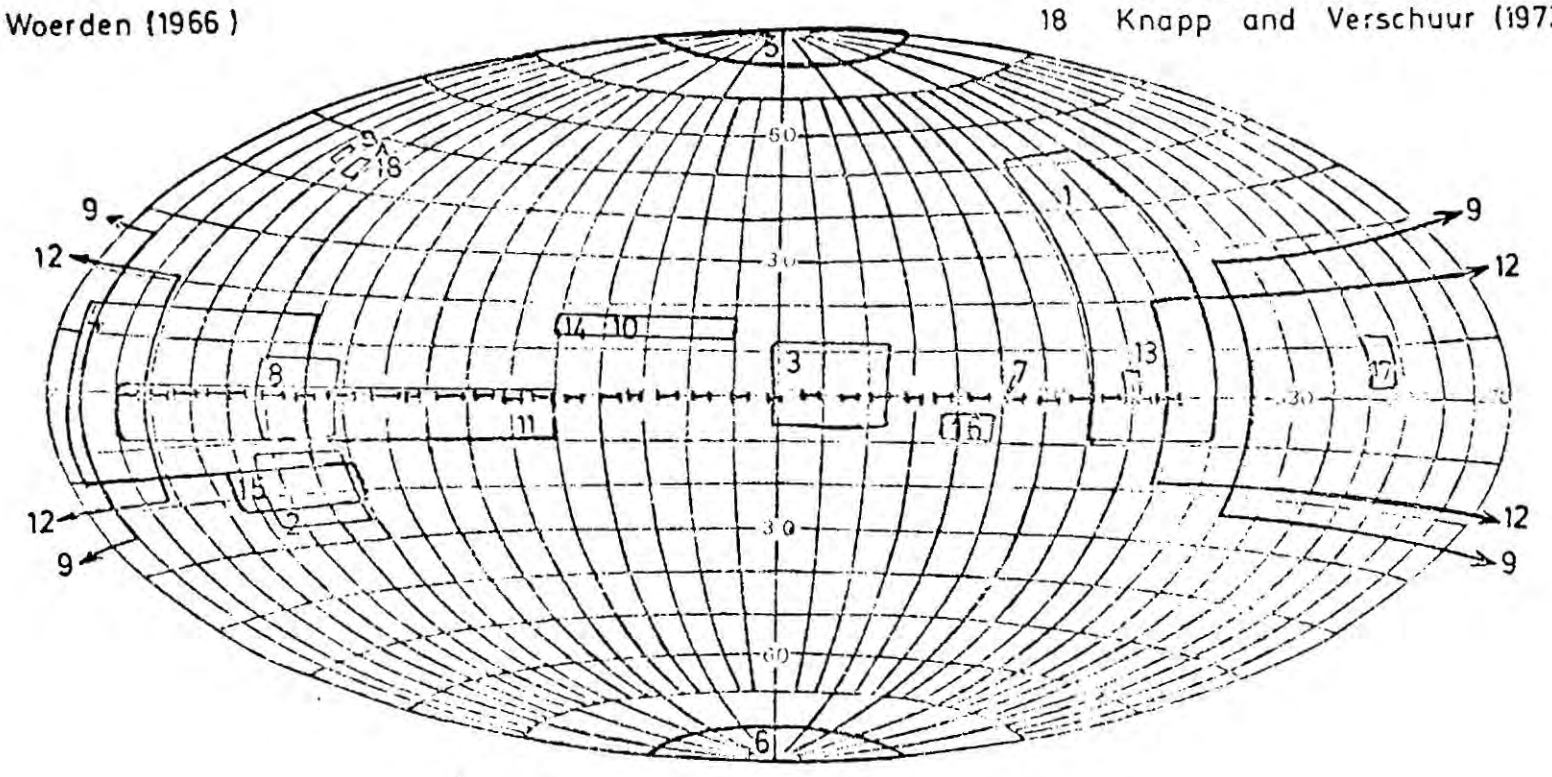

Figure 5-6 The regions of the sky surveyed on a small scale by observing the neutral hydrogen 21 cm emission. The details of the experiments are given in Table 5-2.

Table 5.2: Regions of the sky surveyed on a small scale by observing the neutral hydrogen 21 cm emission. (The numbers in the first column correspond to those circled in figure 5.6. Typical small scale features observed are indicated in the last column).

	Reference	Year	ℓ°	b°	distance from L.S.R. d pc	usual sampling interval (when known)	Features observed, cloud sizes $R_\odot$pc calculated as indicated in the text
1	Heeschen	(1955)	350-19	-9_+51	∿1800	ℓ,5°;b,2.5°	"hot" and "cold" clouds situated in the Sagittarius arm
2	Menon	(1958)	192-216	-26_-11	∿500	ℓ,b,3°	Orion region, ring of hydrogen expanding at a velocity of 10 km sec^{-1}. Inner radius of ring 38 pc, outer radius 67 pc.
3	Kaftan-Kassim	(1961)	67-92	-9_+11	1500	ℓ,b,2°	Observing hydrogen in the Orion arm in the region of Cygnus. 26 pc feature at ℓ=48°, b=0°.
4	Davis	(1962)	200-265	±15	8800	ℓ,b,5°	4 - 300 pc clouds
5	Dieter	(1964)	0-360	>+80	100	ℓ,b,1°	north galactic pole. $R_\odot$∿5pc
6	Dieter	(1965)	0-360	<-80	100	ℓ,b,1°	south galactic pole. $R_\odot$∿5pc
7	Makarova	(1965)	0-240	along galactic equator	local out to edge of Galaxy	ℓ,10°	Observed∿200 neutral hydrogen profiles - average cloud $R_\odot$=7.5pc
8	Raimond	(1966)	192.3-212.3	-9.5_+8.5	-	ℓ,b,0.5°,1°	11 concentrations, discrete character, two associated with Mon II, $R_\odot$=13 & 29 pc - 2 clouds associated with Mon I, $R_\odot$∿55pc
9	Takakubo and van Woerden	(1966)	260-340	-24_+26	∿400	ℓ,10°;b,5°	Emission profiles separated into Gaussian Components using a computer
10	Heiles	(1967)	100-140	+13_+17	310-500	-	Distribution of cloud sizes (range $R_\odot$ = 1→36 pc) inside 2 parallel sheets
11	Lindblad	(1967)	140-250	-9_+1	-	-	Perseus and Orion arms; interarms; observes a local expanding arm
12	Takakubo	(1967)	243-2	-19_+21	∿400	ℓ,10°;b,5°	Emission profiles separated into Gaussian components using a computer.

Table 5.2 continued

	Reference	Year	ℓ^{o}	b^{o}	distance from L.S.R. d pc	usual sampling interval (when known)	Features observed, cloud sizes R_{o} pc calculated as indicated in the text
13	Riegel & Jennings	(1969)	9.5-11.0	-1_+5	<1 kpc	-	cold gas cloud
14	Ames & Heiles	(1970)	100-140	+13_+17	$\gtrsim$200	-	2 parallel sheets, 10 pc thick
15	Gordon	(1970)	193-224	-15_-22	~500	b,6' & 1^{o}	Orion region - detailed analysis of hydrogen associated with Orion Nebula. Hydrogen extends over R_{o}~20 pc
16	Weaver & Williams	(1970)	44-54	-4_-10	750	-	Looked through local gas to more distant features. Observed hydrogen in a narrow distance range at a fixed distance from Sun
17	da Rocha Vieira	(1971)	302-310	+2_+12	1500-700	ℓ,b,0.5^{o}	3 elongated features parallel to the galactic plane at heights ~200 pc above plane. Nos. small clouds negative velocity. One cloud positive velocity.
18	Knapp & Verschuur	(1972)	220.6-227.8 233.6-237.0	42.9-45.3 44.5-46.5	20 23	ℓ,0.2^{o};b,0.2^{o}	Cloud A size 400 pc Cloud B size 300 pc Small scale study of these two clouds

fields etc. Ultimately the distribution of $H_o R_o$ where H_o is the magnetic field strength of a cloud of radius R_o pc will be established with some measure of how characteristic a cloud distribution in one region of the Galaxy is with respect to hydrogen in another part of the Galaxy.

5.2.3 The large scale hydrogen structure in the Galaxy

Bolton et al (1958) observed material outside the Sun's radius on the opposite side of the Galaxy. The arm structures observed are highly inclined and vary in distance from the plane. The hydrogen over almost the entire longitude range has a high negative velocity indicating pronounced outward motion of the arms as observed by the Leiden group.

Braes (1963) found that except for slight non-circular motion mainly in the centre parts of the Galaxy, the hypothesis of circular motion is not too much in error. He also observed a nearby cloud of hydrogen receding from the Sun at a velocity $\sim$6 km sec^{-1}.

Burke et al (1963a) revealed the presence of a very complex hydrogen distribution inside a spiral arm $\sim$11 kpc from the galactic centre (equivalent to a radial velocity of -30 km sec^{-1}). The substructure was of angular size 0.2^o-2^o equivalent to $\sim$40-400 pc in physical size. The hydrogen appeared to be divided into two components (a) dense hydrogen concentrations, associated features fluctuating widely in density and exhibiting small (5-11 km sec^{-1}) internal velocity dispersion on a small scale, with larger deviations from strictly circular orbits on a large scale and (b) a thin substrate of gas with rather smooth distribution exhibiting circular motion with small scale random motions of at least 20 km sec^{-1}.

Butler Burton (1966) analysed emission profiles in terms of Gaussian components. He observed fragments of the spiral structure of the Galaxy

including the Sagittarius spiral arm which is seen in cross section with another stream of hydrogen with a systematically higher velocity than itself. Irregularities observed were of angular extent $\frac{1}{2}^{o}$-1^{o} equivalent to a size of ∿45 pc.

Helfer et al (1955) and Höglund (1963) oberved hydrogen in the spiral arm in which the solar system is located i.e. the Orion arm and the inter-arm features that are well known to exist in the solar neighbourhood.

Searches for high velocity hydrogen gas have been made by Smith (1963), Oort (1963), Prata (1964), Dieter (1965, 1972), Cugnon (1968), Kerr (1969), Hindman and Kerr (1970), Garzoli (1970), da Rocha Vieira (1971), van Kuilenburg (1972) and Wannier et al (1972).

A near galactic plane survey ($b \lesssim \pm 5^{o}$) by Hindmann and Kerr (1970) shows hydrogen extending to velocities of +150 km sec^{-1} in the same galactic longitude range as the survey by Wannier et al (1972). Kerr (1969) identified the presence of a spiral arm at a distance of 18 kpc from the galactic centre with the absence of a section of the arm between galactic longitudes of 270^{o} and 280^{o}. An analysis of the data presented by Wannier et al (1972) using the galactic rotation model aforementioned confirms the presence of the spiral arm some 18-20 kpc from the galactic centre. An enhancement of the hydrogen emission at v∿+153 km sec^{-1} at latitudes $<+12^{o}$ and between longitude $268^{o}<\ell<280^{o}$ is interpreted as an extension of the 18 kpc spiral arm bending upwards at the point where Kerr (1969) sees no hydrogen. Wannier et al (1972) also observed a high z extension of a 50 kpc spiral arm rising to a height of 13 kpc above the galactic plane. (The application of the galactic rotation model to this distance from the galactic centre may not be correct). In the region of Centaurus da Rocha Vieira (1971) observed two continuous features that run exactly above the two arm

features observed in the plane by Garzoli (1970) whilst Oort (1963) found in the eastern galactic hemisphere some arms showing extensions at considerable distances from the plane.

Dieter (1964, 1965, 1972) analysed the hydrogen of the north and south galactic pole by fitting Gaussian functions to the velocity profiles using computer techniques. In the north galactic pole high negative velocity hydrogen with velocities ranging from -20_-55 km sec^{-1} with σ_v=8 km sec^{-1} was observed to have no correlation with the low velocity hydrogen with velocities almost zero with respect to the local standard of rest and σ_v=4 km sec^{-1}. These high velocity clouds are contributing quite a significant amount of hydrogen to the galactic plane as they are seen to be condensing from the halo.

If it is assumed that the mean distance to this hydrogen is 100 pc, a typical size for one of the major condensations is $\sim 5^{o}$ which is equivalent to a radius of 3.5 pc, an hydrogen density of 10 atoms cm^{-3} and a typical mass of 30 $M_{\odot}$. In the southern polar cap ($b<-80^{o}$) the distribution of velocity of the components shows the same marked assymetry as observed in the north but the details of the distribution differ in several respects. In the south the median velocity is -10 km sec^{-1} whilst in the north it is -15 km sec^{-1} a difference attributable to the absence of the group of a large number of components with velocities between -25 and -55 km sec^{-1} in the south. Several components having velocities $v<-60$ km sec^{-1} in the south have no counterpart in the north.

The histogram for N_H, the number of atoms along the line of sight is different in shape in the two regions but the median values are not very different ($N_H=10^{20}$ atoms cm^{-2} in the south galactic pole and $N_H=8\ 10^{19}$ atoms cm^{-2} in the north galactic pole). The amount of material in the two regions is the same.

Da Rocha Vieira (1971) observed a high positive velocity cloud with $v=+57$ km sec^{-1} at $\ell=306.5^{o}$ where according to the galactic rotation model negative velocities should be observed. Since the cloud velocity has very low velocity dispersion it is near the Sun and yet definitely isolated from the hydrogen of the plane. Intermediate positive velocity clouds are rather rare but have also been observed by Smith (1963), Prata (1964) and Cugnon (1968) whose cloud parameters are compared with those of da Rocha Vieira (1971) in table 5.3. Typical cloud sizes observed by da Rocha Vieira are, small clouds R_{o}=12-17 pc and larger clouds R_{o}=20-70 pc. They are located some 1-4 kpc from the L.S.R. with densities between 4 and 7 atoms cm^{-3}, mean velocity dispersions of $\sim$2.5 km sec^{-1} and column densities $N_H=3.7 - 8.5\ 10^{20}$ atoms cm^{-2}.

5.2.4 The small scale hydrogen structure the Galaxy

At intermediate latitudes $b = \begin{matrix}+26.4 & +21.4 & +16.4 & +11.4\\ -23.6, & -18.6, & -13.6, & -8.6\end{matrix}$ Gronigen astronomers Takakubo & van Woerden (1966), Takakubo (1967) observed a wide grid ($\Delta\ell=10^{o}$) of profiles with a 2 km sec^{-1} receiver bandwidth and 0.6^{o} aerial beam width. As observed in other experiments the profiles showed considerable structure indicative of a possible resolution of the contributions from individual interstellar clouds. The profiles were analysed into Gaussian components, following least-squares methods on an electronic computer. Figure 5.7a illustrates a typical profile broken down into twenty one Gaussian components which are represented by thin crosses of various kinds, by superposition they form the profile shown here by dots. The profile can be seen to be well represented by the four components drawn as thick crosses (full curve). Superposition or blending of components in groups equivalent to four regions in the sky where the 21 Gaussians have been observed are shown in figure 5.7b. The regions lie at b$\sim+23.4^{o}$, ℓ around 0^{o} (group C)

Table 5.3: Cloud parameters of intermediate positive velocity clouds observed in four different regions of the sky

Reference		ℓ^o	b^o	σkm sec^{-1}	v_r km sec^{-1}	$N_H \times 10^{-21}$ atoms cm^{-2}
Smith	(1963)	40.5	15	16.4	90.8	2.18
Prata	(1964)	2.2	-4	10.1	114.6	1.86
Cugnon	(1968)	349	+3	11.2	52.4	4.25
da Rocha Vieira	(1971)	306.5	+2.5	5.5	57.0	4.74

Table 5.4: The mean values of the parameters τ_o, σ_v and N_H for the clouds grouped by Takakubo (1967) according to their velocity dispersions, The proportion by mass of each group present in the sample of clouds observed is also given.

Group	ALL	S	M	L
Range of velocity dispersions	—	$\sigma_v \leq 3$km sec^{-1}	$3 < \sigma_v \leq 7$km sec^{-1}	$\sigma_v > 7$km sec^{-1}
$\langle\tau_o\rangle$	0.147	0.155	0.195	0.086
$\langle\sigma_v\rangle$	6.31	2.20	4.50	12.73
$\langle N_H\rangle \times 10^{-21}$ cm^{-2}	4.15	2.03	4.90	5.56
Proportion of total mass	1	0.163	0.415	0.422

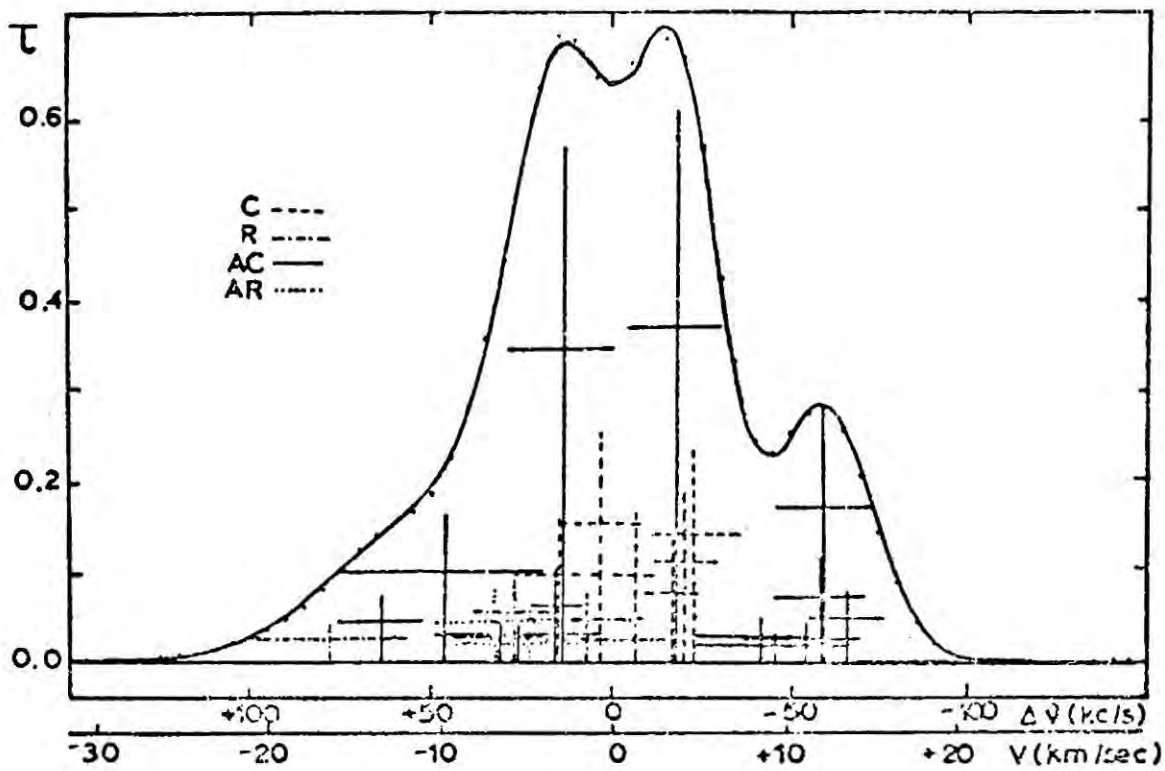

Figure 5-7a) Twenty one Gaussians are represented by thin crosses of various kinds, by superposition they form the profile shown here by dots. The four component drawn as thick crosses give a very good representation (full curve) of the dotted profile. The four regions of the sky where the 21 Gaussians have been observed are distinguished by different types of line see figure 5-7b.

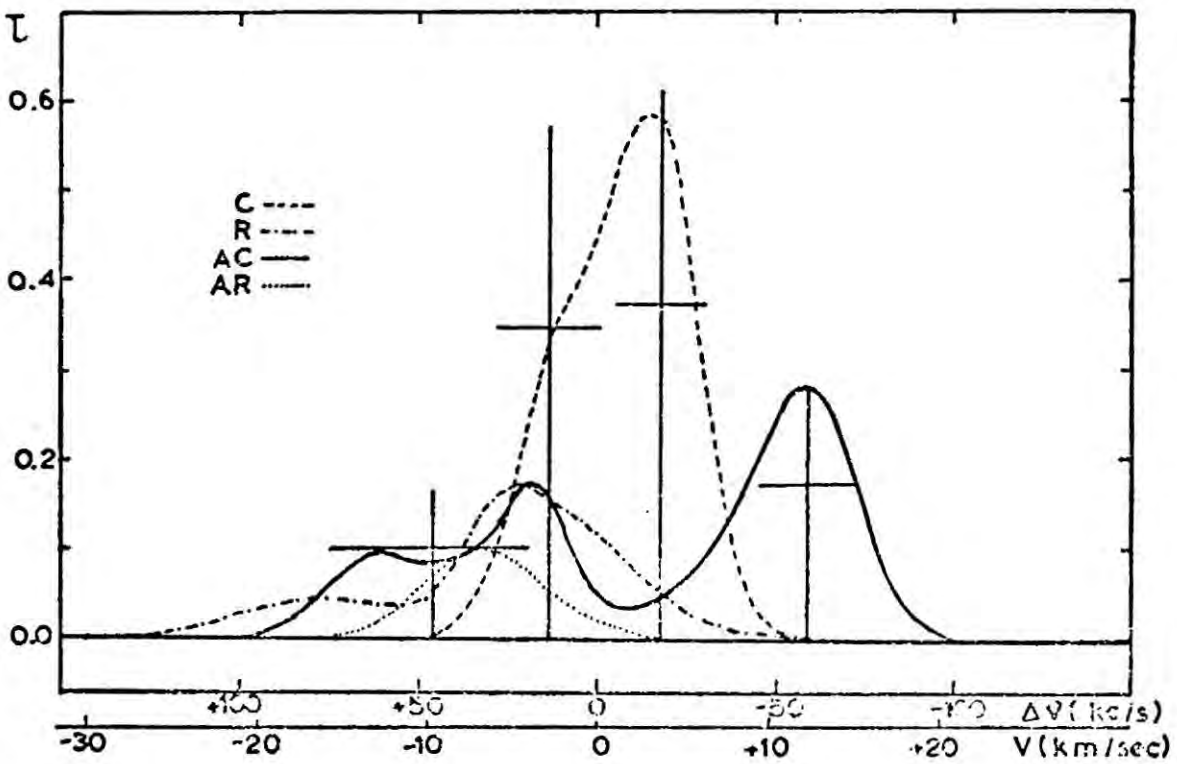

Figure 5-7b) Superposition of groups of Gaussian components the 21 Gaussians in figure 5-7a are here superposed in four groups according to the regions of the sky where they were observed. These regions lie at b=23.4 ℓ around 0°(C), 90°(R). 180° (AC), 270°(AR). The partial relationship of the four heavy components reproduced from figure 5-7a and the four superpositions is in evidence.

6 components, 90^{o}(R) 4 components, 180^{o}(AC) 9 components and 270^{o}(AR) 2 components. The profile can be interpreted in terms of four clouds of large angular extent or 21 clouds in four groups in different parts of the "sky," thus illustrating the problems encountered using the Gaussian component technique.

Figure 5.8 is a typical summary of the Gaussian components of 21 cm profiles observed at $b=16.4^{o}$ in this particular case. Each Gaussian component is represented by a rectangle whose height is proportional to the central optical depth τ_o, and whose halfwidth is the same as the velocity dispersion, σ_v, of the component. Thus the area of the rectangle is proportional to the surface density, N_H, of the hydrogen atoms in the component. The abscissae at which the centres of the rectangle are plotted mark the velocities, v_r of the components, after correction for the standard solar motion. The "clouds" were arbitrarily divided into groups according to their velocity dispersions. The mean values of τ_o,σ_v, and N_H together with their proportions by mass are listed in Table 5.4.

Conclusions reached by the authors are as follows:

a) Components of group S are clouds whilst those in group M are blends of two or more clouds. Group S show the local velocity field near to the Sun. The mean distance above the galactic plane, $<|z|>$ for clouds is found to be 78 pc.

b) Group M gives information on the velocity field in a larger domain with $<|z|>=105$ pc. Schmidt (1957) concludes from 21 cm observations in 8 directions 5^{o} apart, that the total thickness of the gaseous layer is 220 pc which is twice $<|z|>$ quoted for the M component. Thus the M group shows the general characteristic properties of the gas layer containing interstellar clouds represented by the components in group S which refer to a more limited region of space.

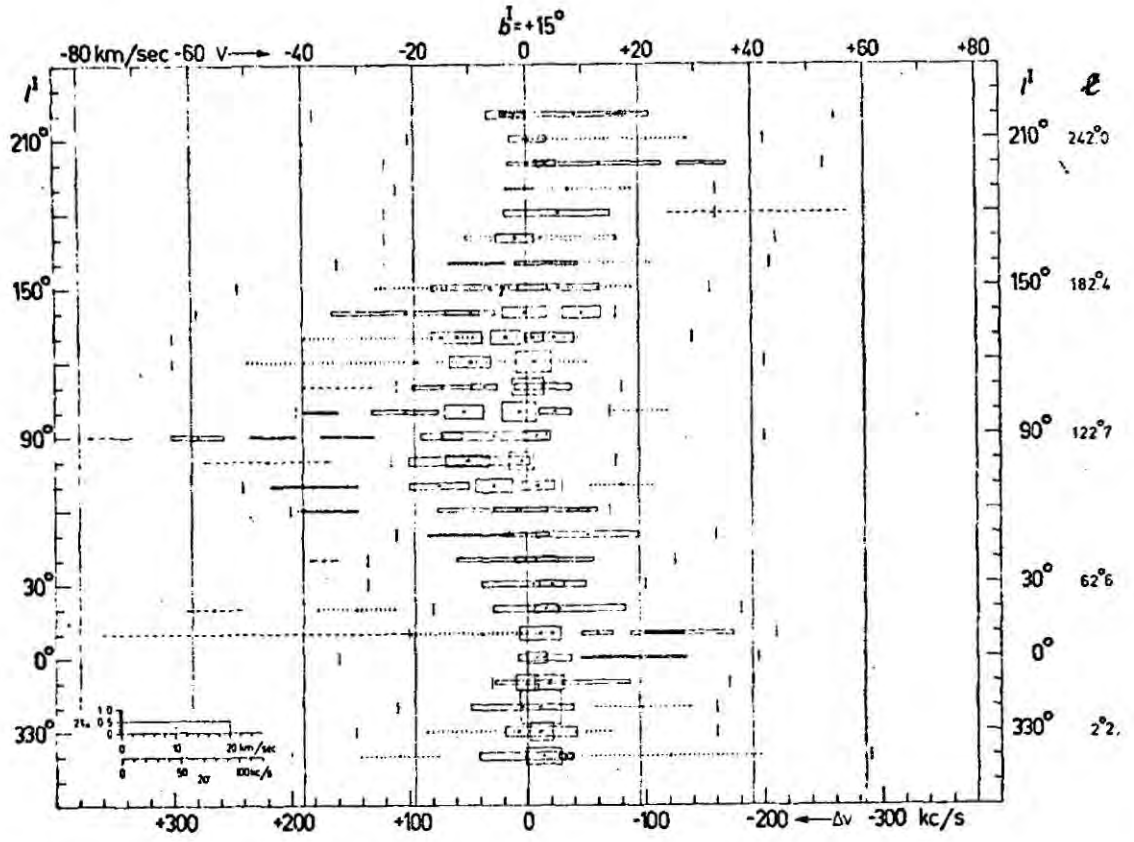

Figure 5-8 Gaussian components of 21 cm profiles observed at $b^{I}=+15^{\circ}$ (Takakubo 1967) The radial velocities, V, of the Gaussian components with respect to the local standard of rest are plotted versus the galactic longitude ℓ. Each component is represented by a rectangle with a dot at its centre. The position of the dot shows the longitude, ℓ, of observation and the radial velocity, V , of the component; the height of the rectangle is proportional to the centre optical depth, τ_o; its width indicates (twice) the velocity dispersion, σ, hence the area of the rectangle is proportional to N_H the number of hydrogen atoms per column of 1 cm^2 cross section in the component. The scales of τ_o and σ are shown in the lower left corner of the diagram.

Components significantly affected by stray radiation are shown dotted. Dashed lines represent components for which the parameters were obtained by eye estimate. Small vertical bars indicate the frequency (or velocity) intervals in which the profiles were analysed. Some profiles may contain components outside the interval shown here. Numerical values of the parameters are given in Table I of Takakubo and van Woerden (1966).

c) The components of group L have different properties to those of S and M and the effect of differential rotation does not explain their large dispersions. It is suggested that these wide components are produced by gas in the transition region between the disk and the halo, as observed by Dieter (1964).

In a previous paper Takakubo (1963) performed some model calculations on the same observational data discussed above assuming all the radiation in the profile to be produced by gas concentrated into spherical interstellar clouds of equal size R_c=3-4 pc, and uniform density n_H=14 atoms cm^{-3}. It was found that clouds had masses of 55 $M_\odot$, the number of clouds along the line of sight k was 11 kpc^{-1} with the fraction of space occupied by clouds f=0.05. In his model II Takakubo assumed that the radius and density of the clouds were inversely proportional but the results were not significantly different. Because of the arguments for a tenuous gas layer not being single clouds as explained above Takakubo (1967) suggested that the parameters f, N_o k and n_H ought to be reduced by a factor of 0.6.

A very detailed survey of low velocity 21 cm emission has been made at the National Radio Astronomy Observatory in Green Bank by Heiles (1967). The region bounded by $\ell \sim 100^\circ$-140° and $b \sim 13^\circ$-17° has been mapped using a 300 foot telescope and a 100 channel autocorrelation receiver. The beam width of the antenna at this wavelength is 10', the velocity resolution <1 km sec^{-1} the total range of velocities observed was about 50 km sec^{-1}, and the antenna sensitivity about 1°. The hydrogen was seen to lie in two sheets some 300-500 pc from the L.S.R. a fact supported by the results of Lodén (1961) and Elvius (1956) who both observed absorbing dust concentrated at the same two distances, 300 and 500 pc. Heiles (1967) proposes two models for the spacial distribution of the two sheets of hydrogen, however a more detailed examination of the two sheets, that has since been made by Ames

and Heiles (1970) using both 21 cm radio data and optical spectra of stars in that region of the sky, has led to the conclusion that the sheets are $\lesssim$10 pc thick, they approach one another and are in fact colliding supersonically in one region. Figure 5.9 shows the spacial extent of the sheets. The sheets have sharp boundaries and are of greater extent in longitude than in latitude and spread beyond the boundaries of the observed region. If the depth of the sheet in the line of sight is 10 pc then a typical density in the sheet is 1 hydrogen atom cm^{-3}. The two sheets are closer together at higher than at lower latitudes.

The over-all distribution of hydrogen with position and velocity can be separated into three components, a background component, which alone produces a profile changing slowly with position and having a large velocity dispersion, and two "velocity peaks" which characterise most of the line profiles of the region. Within these peaks (the sheets) appear smaller structures which are classified according to size: large concentrations or clouds, and small concentrations or cloudlets. If it is assumed that all the gas is at a distance of 500 pc, 50-70% of the mass is background, the remainder is contributed by the sheets. About 18% of the gas in the sheets is in the form of cloudlets. The sheet furthest away from L.S.R. (the high velocity sheet, H.V.S.) appears to be more patchy than the sheet nearest to the L.S.R. (the low velocity sheet, L.V.S.).

Altogether 13 large gas concentrations (or clouds for descriptive reasons only because their densities are only a factor of two above their surroundings and in that sense are not strictly standard interstellar clouds) defined as having a radius R$\geq$7pc and 815 cloudlets with radius <7pc were observed inside the two sheets.

The mass, hydrogen density and velocity dispersion were calculated for each cloud and cloudlet. These properties are listed for all clouds

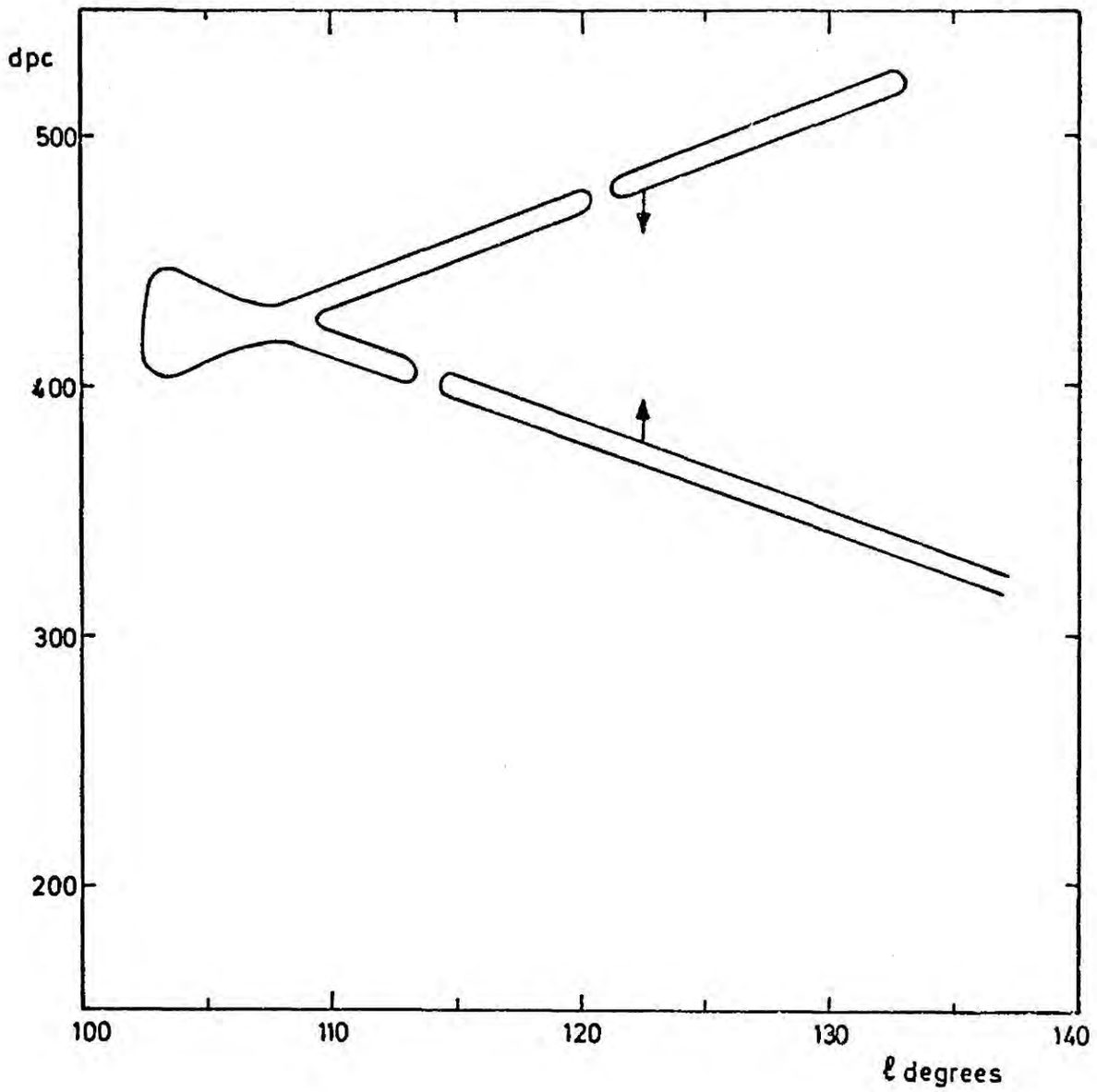

Figure 5-9 The distribution in distance d pc and longitude ℓ^{o} of the two sheets of neutral hydrogen - preferred model of Heiles (1967). Ames and Heiles (1970) confirmed this picture.

and for a sample of 45 of the 815 cloudlets in table 5.5 and table 5.6 respectively. In the calculations the hydrogen has been assumed optically thin, the presence of molecular hydrogen has been neglected and the objects have been taken as spherical. Self gravitation is completely negligible in these clouds but some are so large that tidal effects from the z component of the galactic gravitational field helps to contain these objects.

Two regions in the H.V.S. are best described as "groups of clouds" superposed on the background of excess density. The properties of these group clouds within each group are given in table 5.5 (the first 3 concentrations belong to the first group; the following 3 to the second group). Self gravitation is unimportant in the group clouds and they are similar to the clouds observed in radio absorption spectra in the galactic plane, Clark et al (1962) and Clark (1965), but they are less dense. This fact could be regarded as a selection effect because absorption spectra highlight cold clouds of large optical depth. The group clouds are similar to the "standard interstellar clouds" found by Dieter (1964, 1965) near the galactic poles, however, her clouds were slightly smaller and less dense. Cloudlets reside inside these group clouds which have a velocity $\lambda^{\text{width,}}$ u km sec^{-1}, two or three times that of its associated cloudlets, a difference probably due to large scale or macroscopic motion.

The cloudlets appear to be immersed in the slowly varying substratum of the velocity sheets. Sometimes they appear to coalesce probably because their number density is quite high. Figure 5.10 shows the cloud size, mass and hydrogen density distributions for the 815 cloudlets. Cloudlets were selected for measurement by the following criteria: (a) the cloudlet had to be distinguishable from the surrounding cloudlet. (b) The cloudlet was accepted as real, not simply noise, if it was visible on at least three neighbouring contour maps. Because of blending the true number of cloudlets

Table 5.5 Parameters of gas concentrations

	Radius R_o pc	Mass M $M_\odot$	hydrogen density n_H cm^{-3}	velocity* width u km sec^{-1}	$n_H^{2/3} R_o$ pc cm^2
	7	280	4	3.6	17.8
	11	1200	6	3.0	36.3
	8	430	5	4.5	24.4
	10	1400	8	4.2	40.0
	15	4000	7	4.2	53.5
	10	3500	2.1	1.2	16.4
	13	1000	2.7	3.9	24.9
	15	1400	2.7	4.2	28.8
	36	5000	0.7	2.4	4.6
	11	4000	2.0	1.7	17.5
	20	6000	4	3.9	50.4
§	40	16000	1.5	3.9	52.3
†	15	2800	5	3.7	43.8
MEAN	16.2	3620	3.9	3.4	31.6

§ merged profile

† isolated profile

* velocity width in km sec^{-1}, taking the velocity distribution as exp - $(\frac{v}{u})^2$; the value of u of the receiver passband is 0.63 km sec^{-1}.

Table 5.6 Parameters of cloudlets

Radius $R_o$pc	Mass M $M_\odot$	Hydrogen density n_H cm^{-3}	Velocity width u km/sec	$n_H^{2/3} R_o$pc cm^2
2.9	7.9	1.8	1.3	4.3
3.0	7.1	1.6	1.3	4.1
2.0	1.7	1.4	0.8	2.5
2.0	2.1	1.6	1.0	2.7
3.4	24.6	3.6	2.4	8.0
2.5	5.8	2.2	1.3	4.2
3.8	29.5	3.4	1.6	8.6
3.6	10.1	1.4	1.3	4.5
2.8	6.2	1.8	1.5	4.2
1.9	2.1	1.8	0.8	2.8
3.7	13.8	1.8	1.2	5.5
3.2	4.8	1.0	0.8	3.2
4.5	22.1	1.4	1.2	5.7
4.7	21.4	1.2	1.9	5.3
3.8	11.2	1.4	1.0	4.8
2.7	5.0	1.6	1.3	3.7
2.1	4.1	2.8	1.5	4.2
2.8	8.8	2.4	1.4	5.0
2.1	3.3	2.2	1.2	3.6
2.7	4.8	1.6	1.0	3.7
2.9	6.0	1.4	0.9	3.6
1.9	1.7	1.4	1.0	2.4
3.1	7.4	1.6	1.4	4.2
2.5	8.2	3.2	1.4	5.4
2.8	10.6	3.0	1.1	5.8
1.9	3.2	2.8	1.3	3.8
4.9	53.9	2.8	1.5	9.7
1.5	0.7	1.2	0.9	1.7
2.9	8.8	2.0	1.1	4.6
1.9	2.9	2.6	1.1	3.6
3.2	16.1	3.0	1.2	6.7
3.2	12.7	2.4	1.4	5.8
2.7	3.2	1.0	0.9	2.7
2.4	3.4	1.4	1.1	3.0
3.1	14.2	3.0	1.3	6.5
1.4	1.3	2.8	1.2	2.8
2.4	6.5	2.8	1.0	4.7
1.8	1.9	2.0	1.0	2.9
2.5	3.9	1.4	1.0	3.1
4.1	15.6	1.4	1.1	5.1
3.4	11.6	1.8	1.2	5.0
2.3	4.4	2.2	1.3	3.9
2.9	6.1	1.4	1.4	3.6
2.4	3.1	1.4	1.0	3.0
2.3	2.4	1.2	1.1	2.6
MEAN 2.8	9.0	2.0	1.2	4.4

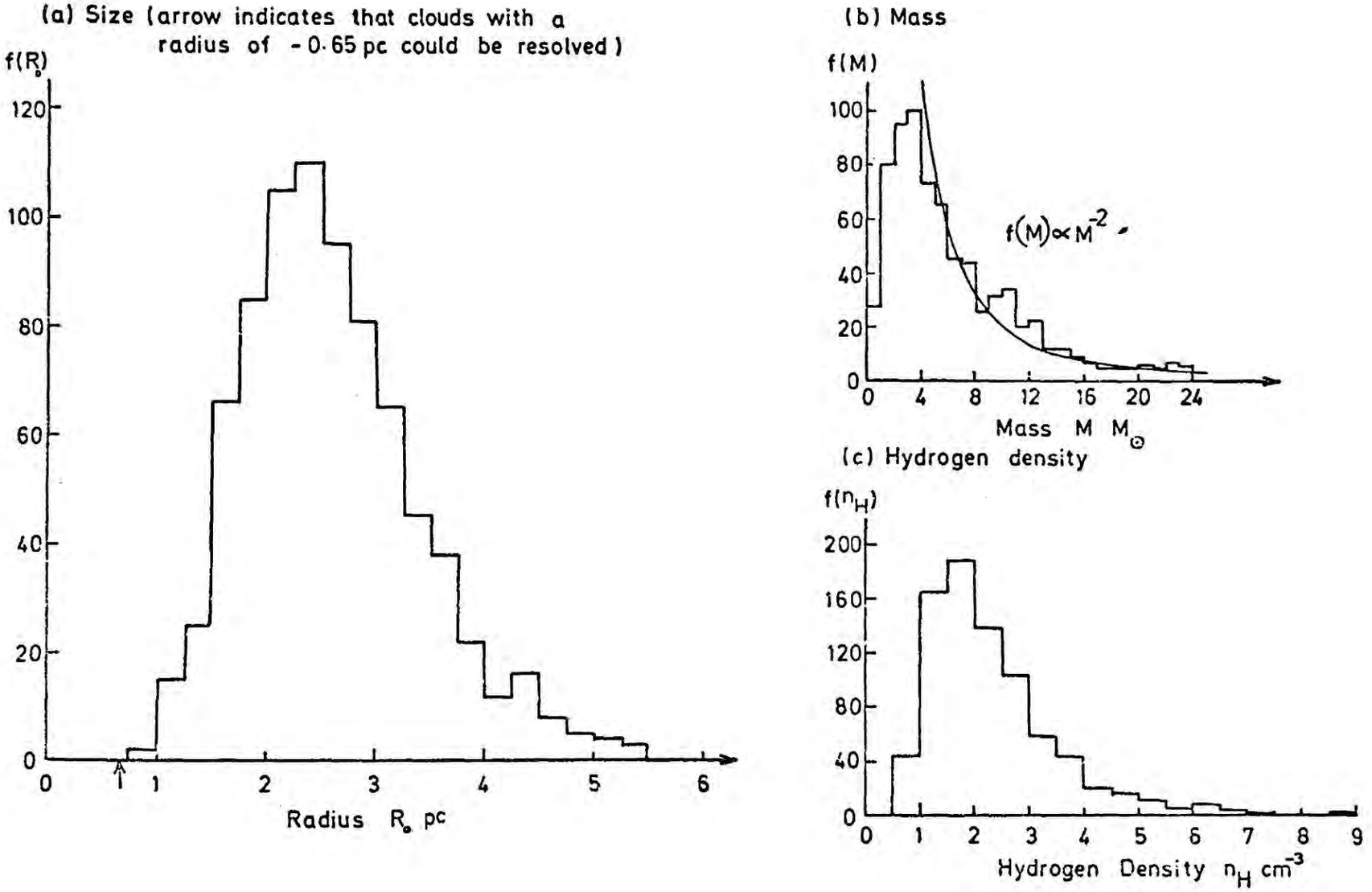

Figure 5-10 The size, mass and hydrogen density distributions of cloudlets, Heiles (1967).

is larger by perhaps a factor of two. If the size spectrum of the cloudlets is universal a correlation would be expected between angular size and velocity if the velocity is correlated with distance as would occur if differential galactic rotation were important, such a correlation was not observed.

Some theoretical interpretations of the interstellar velocity field might expect equipartition in the cloudlets so that mass and velocity would be correlated, again no such correlation was found. However, the density within cloudlets (about twice that of the background gas of the sheets) varies only a little, see figure 5.10c, and therefore the mass and radius are well correlated, see figure 5.11. Fitting a straight line to the points using Gauss' method the relationship between mass and radius was found to be $M=R_o^{3.3\pm0.8}$ for both clouds and cloudlets.

The internal velocity dispersion is typically 1.2 km sec^{-1} which yields an upper limit of 100°K for the gas temperature. Self gravitation of the cloudlets is a completely negligible binding force unless molecular hydrogen is several hundred times more abundant than atomic hydrogen when they might be expected to disperse very quickly. The fact that there are so many cloudlets indicates their stability. Explanations consistent with observational evidence, a) they are cool objects in pressure equilibrium with their surroundings or b) they are purely turbulence elements.

Verschuur (1970) observed the Zeeman splitting of the 21 cm line in a number of neutral hydrogen clouds. He found a correlation between the magnetic field of a cloud and its neutral hydrogen density, the evidence is shown in figure 5.12. The reason why points fall beneath the straight line $H_o=1.27\ 10^{-6} n_H^{2/3}$, where H_o is in gauss and n_H in hydrogen atoms cm^{-3} is because only one component of the field in the Zeeman data is observed and therefore the upper envelope of the points should describe the history

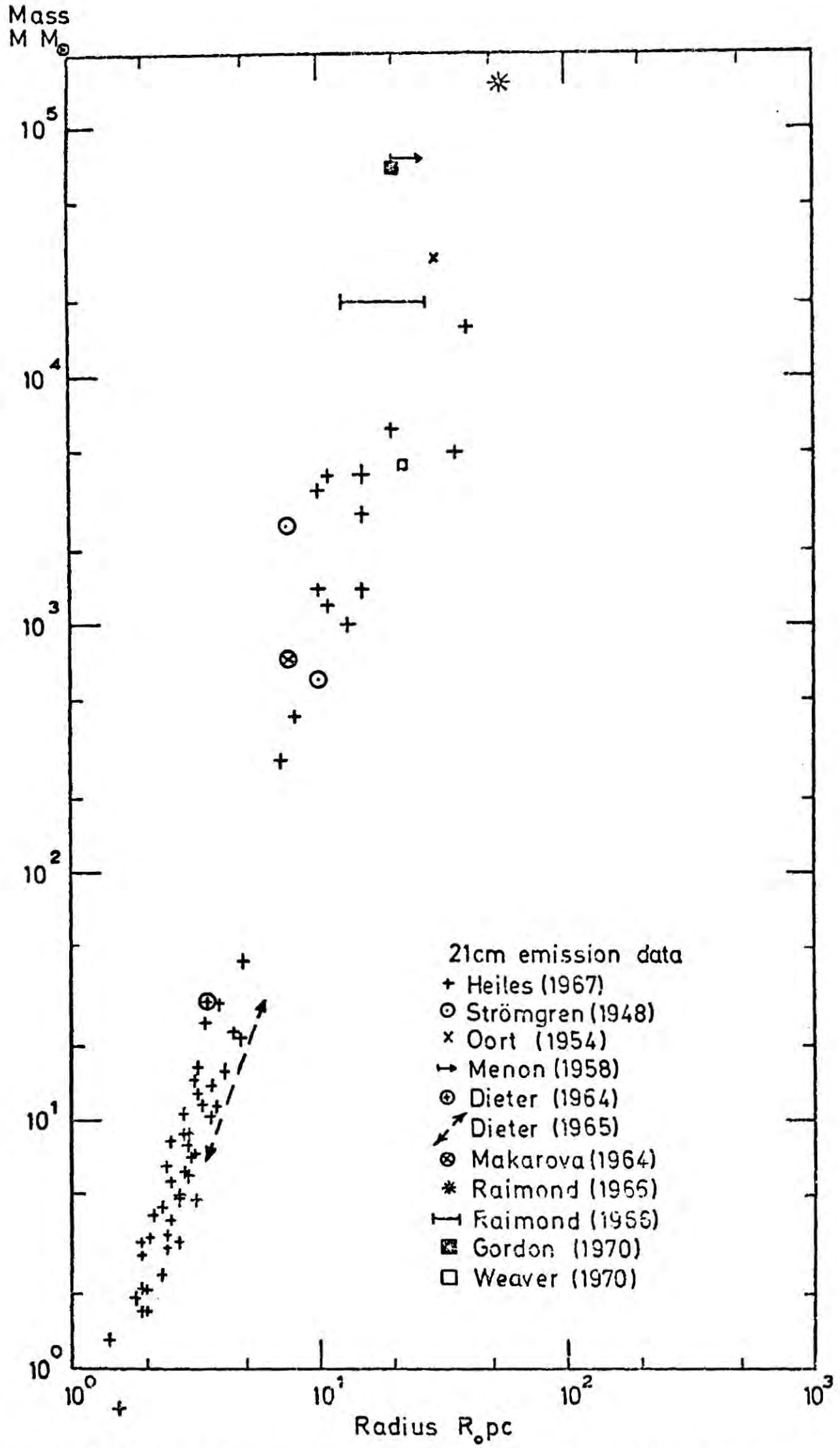

Figure 5-11 The cloud mass as a function of cloud size. The data suggest that there is a direct correlation between the mass and radius of cloudlets as well as clouds.

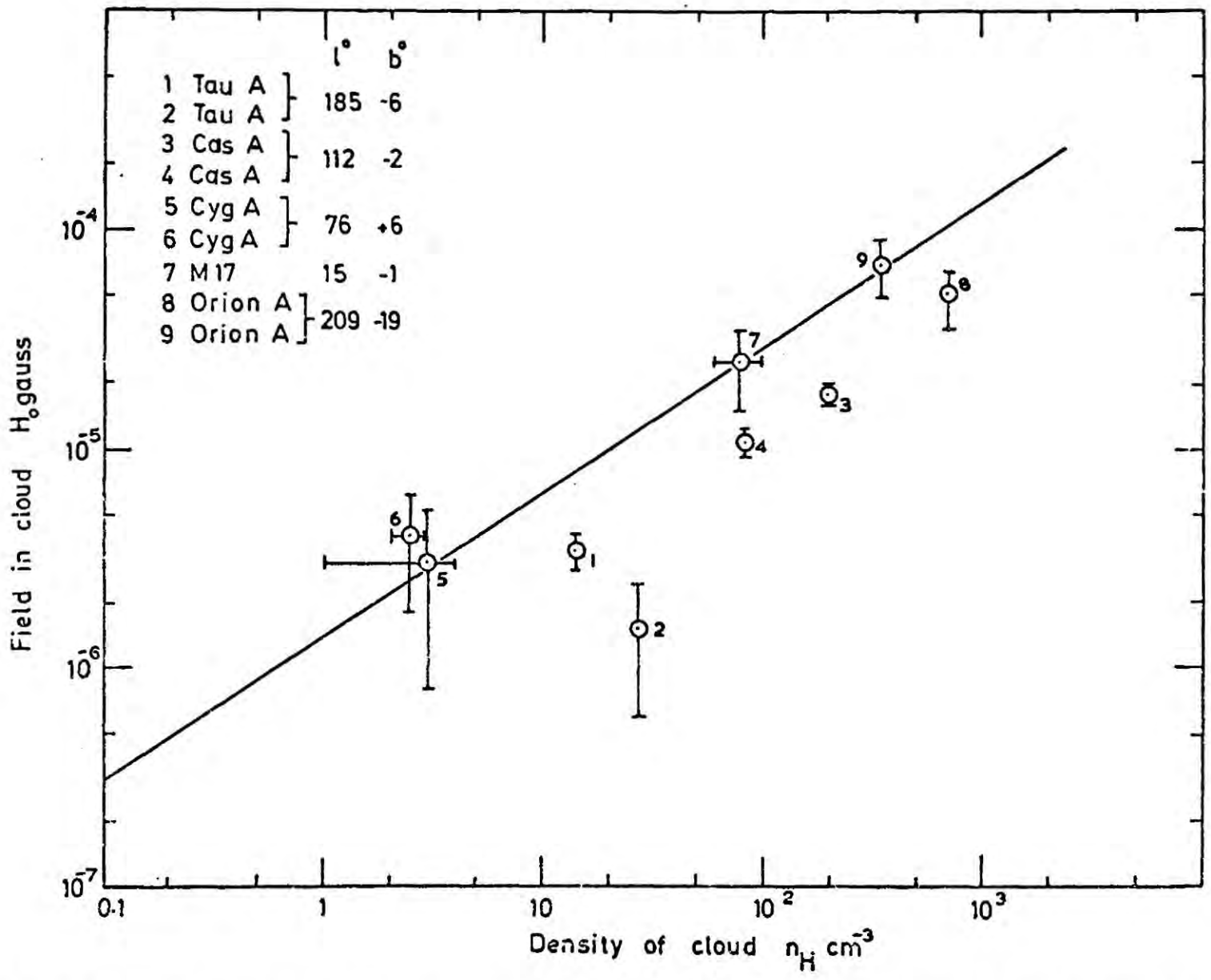

Figure 5-12 Magnetic fields in neutral hydrogen clouds as a function of their density, Verschuur (1970). The straight line is defined by

$$H_o = 1.27\ 10^{-6}\ n_H^{\frac{2}{3}} \text{ gauss.}$$

of the field strength in a contracting cloud. This relationship suggests that clouds contract isotropically with a "frozen-in" magnetic field, i.e. density is inversely proportional to the radius cubed and conservation of magnetic field lines gives magnetic field inversely proportional to the square of the radius, thus giving $H_o \propto n_H^{2/3}$. Obviously clouds are not spheres and it is unphysical to have uniform contraction, but this is acceptable as a first order approximation. Assuming $H_o \propto n_H^{2/3}$ and using the data of Heiles (1967) the quantity $n_H^{2/3} R_o \propto H_o R_o$ was calculated (column 5 in table 5.5 and 5.6). The distribution of $n_H^{2/3} R_o$ was finally established by scaling down the clouds with respect to the cloudlets by a factor of $\frac{45}{815}$ i.e. the ratio of the sample number to the actual number of cloudlets observed. A "best fit" to this data was found to be a normal or Gaussian distribution for cloudlets plus a constant for the clouds. However, it is thought unphysical that there are always equal numbers of clouds of size $\gtrsim$7 pc. A decrease in the number of clouds with increase in cloud size is more logical. For this reason the data beyond a value of $n_H^{2/3} R_o$ of 7 pc cm^2 was fitted with a power law in the differential form. The resultant distribution was found to be

$$f(p_o) = \underbrace{0.243 \exp - \frac{(p_o - 4.08)^2}{2.974}}_{\text{best fit to cloudlets}} + \underbrace{0.053}_{\text{scaling factor}} \times \underbrace{0.233\ p_o^{-1.3}}_{\text{"best fit" to clouds}}$$

where $p_c = H_o R_o \propto n_H^{2/3} R_o$

The experimental distribution for $n_H^{2/3} R_o$ (in the form of a histogram) and the "best fit" to that data is shown in figure 5.13.

A plot of $p_o = n_H^{2/3} R_o$ as a function of R_o (figure 5.14) indicates a very weak dependence of the field on cloud size. A least squares fit yields $p_o = 1.3 R_o^{1.2 \pm 0.1}$ and since $H_o = 1.27\ 10^{-6}\ n_H^{2/3}$ the magnetic field in the

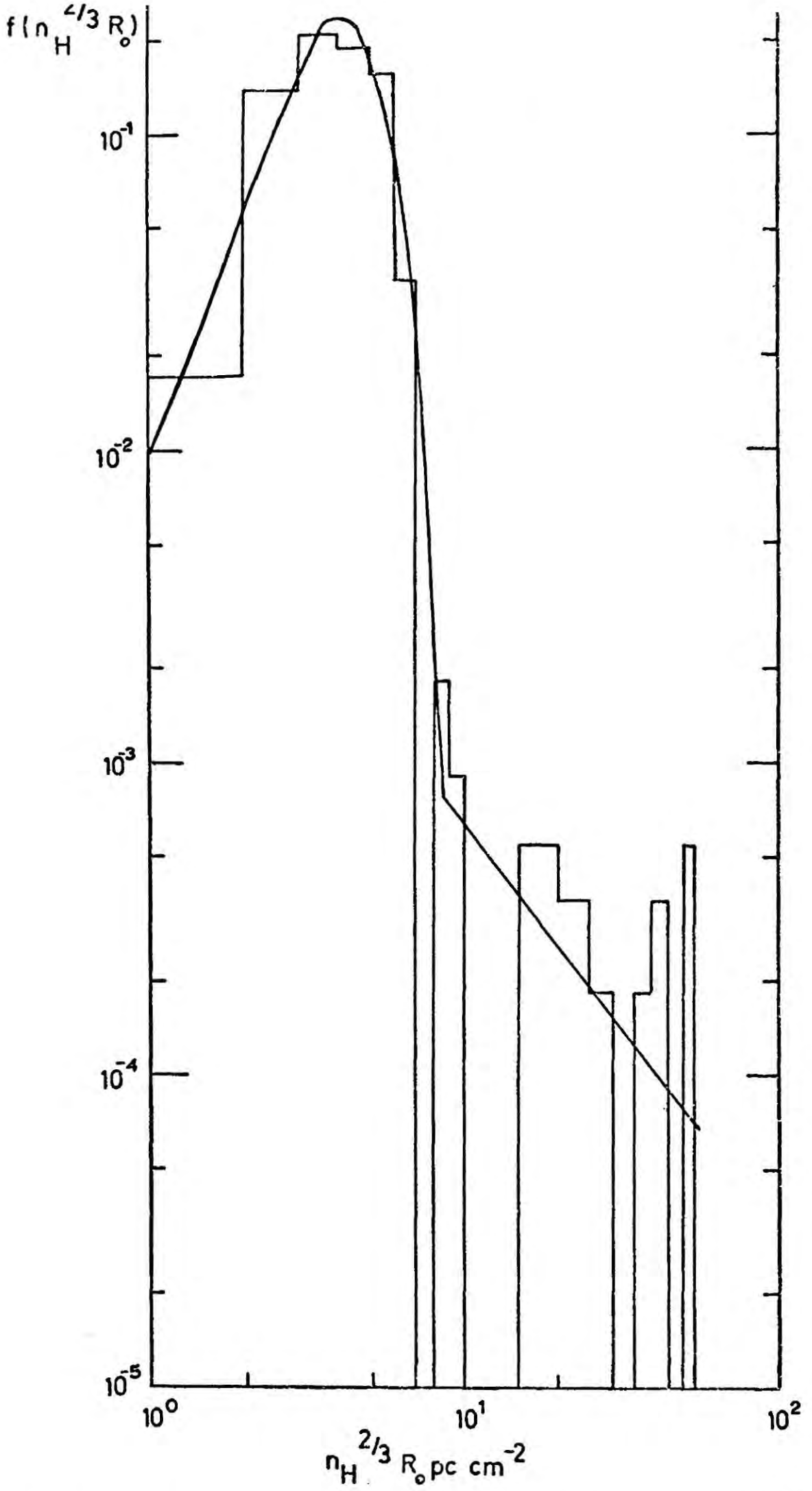

Figure 5-13 The histogram represents the distribution of $n_H^{2/3} R_o$ measured experimentally by Heiles (1967). The full line is the adopted "best fit" to the data.

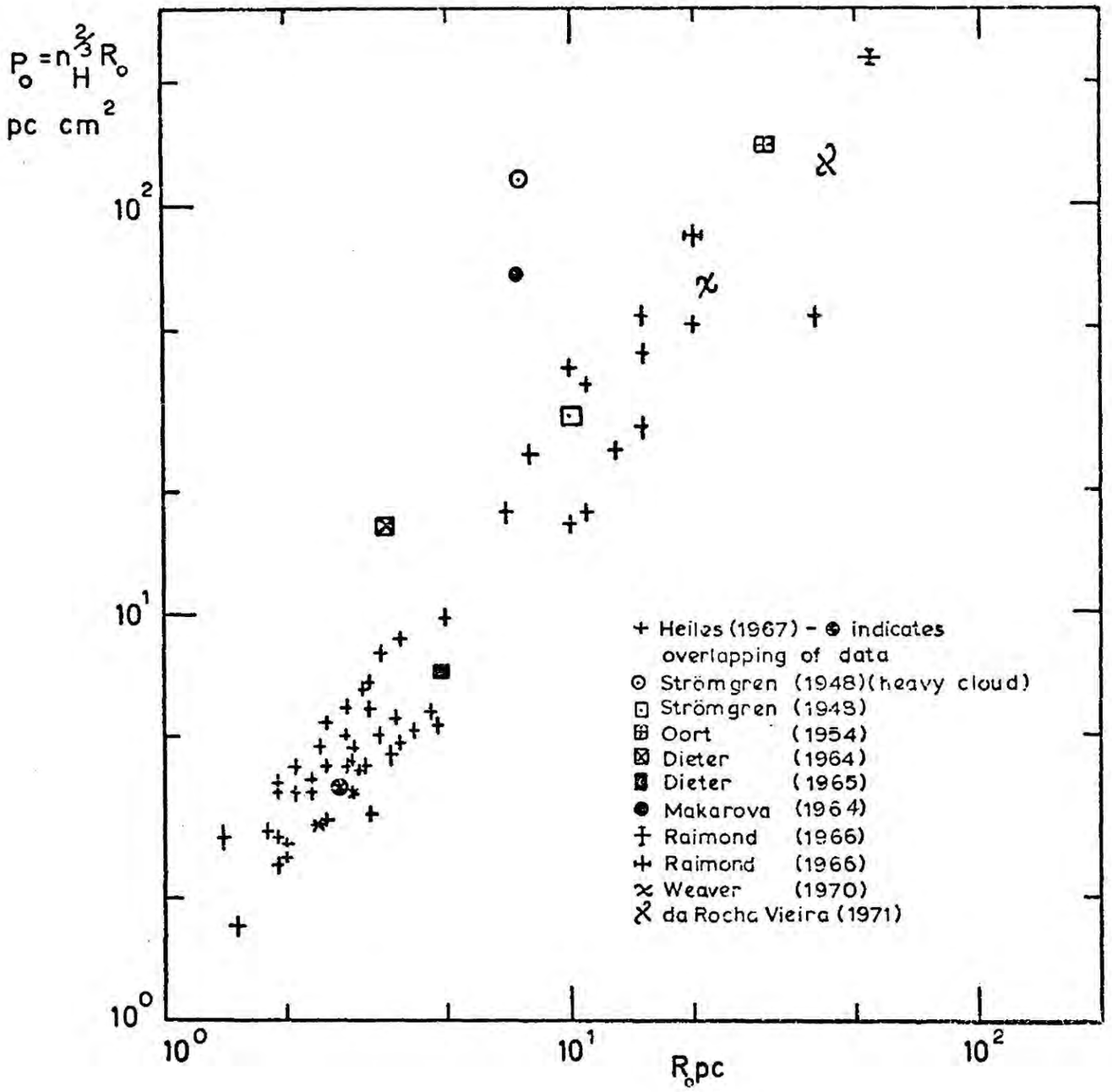

Figure 5-14 The direct correlation between R_o pc and p_o pc cm^2 for both cloudlets and clouds is found to be $p_o = 1.3\ R_o^{1.2\pm0.1}$ for the experimental data of Heiles (1967). Also plotted are the values of p_o as a function of R_o for clouds observed by other physicists (see inset).

cloudlets and clouds in gauss is given by the expression $H_o = 1.65\ 10^{-6} R_o^{0.2\pm0.1}$

Weaver and Williams (1970) used the Hat Creek observations to test Heiles observations. Their observations are summarised below.

a) a few concentrations resembling "standard" clouds ($R_o \sim 10$pc, $n_H \sim 6$ hydrogen atoms cm^{-3} and masses $\sim 10^3\ M_\odot$)

b) a small number of gas concentrations of larger dimensions ($R_o \sim 20$ pc, $n_H \sim 2$ hydrogen atoms cm^{-3} and masses $\sim$few $10^3\ M_\odot$) and

c) very many cloudlets with $R_o \sim 2$pc, $n_H \sim 2$H atoms cm^{-3} and masses $\sim 4 M_\odot$.

The region of the sky observed was $\ell = 44^\circ - 54^\circ$ $b = -4^\circ - -10^\circ$ at a distance of $\sim$750 pc from the L.S.R.. Careful examination reveals the existence of numerous concentrations or cloudlets of small angular extent and narrow velocity dispersion, a variety of gas concentrations of larger angular extent but small velocity dispersion. The numerical data for these various concentrations or density fluctuations are in excellent agreement with Heiles (1967). A typical large concentration at $\ell = 47^\circ$ and $b = -6^\circ$ at $v_r = 14.8$ km sec^{-1} i.e. at a distance of 750 pc possessed the following characteristics:

$R_o \sim 22$pc

$\langle n_H \rangle$ = 5 hydrogen atoms cm^{-3}

mass $\sim 4500\ M_\odot$

$\sigma_v \sim 3.2$ km sec^{-1}

The general background in which each concentration occurred was 0.5-1.0 hydrogen atoms cm^{-3}. It is observed that clouds are not gravitationally bound but form and evaporate with time.

5.3 Neutral hydrogen -21 cm absorption

Radiation from a source that emits over a wide continuum can be absorbed in a narrow frequency range as it passes through neutral hydrogen lying in the propagation path. Hydrogen line emission is present whenever absorption

lines are observed and therefore the recorded profile, being a mixture, is often difficult to analyse.

Figure 5.15 shows diagrammatically the composition of an absorption profile. The degree of absorption can only be derived when the emission profile that would have been recorded if there had been no absorption, is known. This profile is the "expected profile" and has to be estimated by interpolating between profiles observed at points just away from the source whose radiation is being absorbed. The irregularities in the 21 cm emission profiles discussed in the earlier part of this chapter illustrate the uncertainty imposed on the expected profile. What is more, problems are encountered because of the angular scale differences, limited by the scale of the antenna beam width in the case of emission and by the source diameter in the case of absorption.

Despite these difficulties absorption experiments provide a wealth of information, the main applications are:-

(a) Because the effective solid angle of a small source is much less than that of any antenna beam yet available, a higher resolution can be obtained to study cloud structure of the interstellar medium.

(b) The absorbing hydrogen must always be in front of the source. Therefore, if we know the approximate location of the hydrogen, limits can be placed on the distance of the source. Similarly, if the source is at a known distance, this can be used to locate the absorbing hydrogen. If the source is behind some and in front of other hydrogen concentrations in the same line of sight it becomes particularly useful.

(c) Absorption observations provide the only method for determining the spin temperature (for theory see appendix (iv)) of any concentration of hydrogen when measurements of both absorption and emission brightness

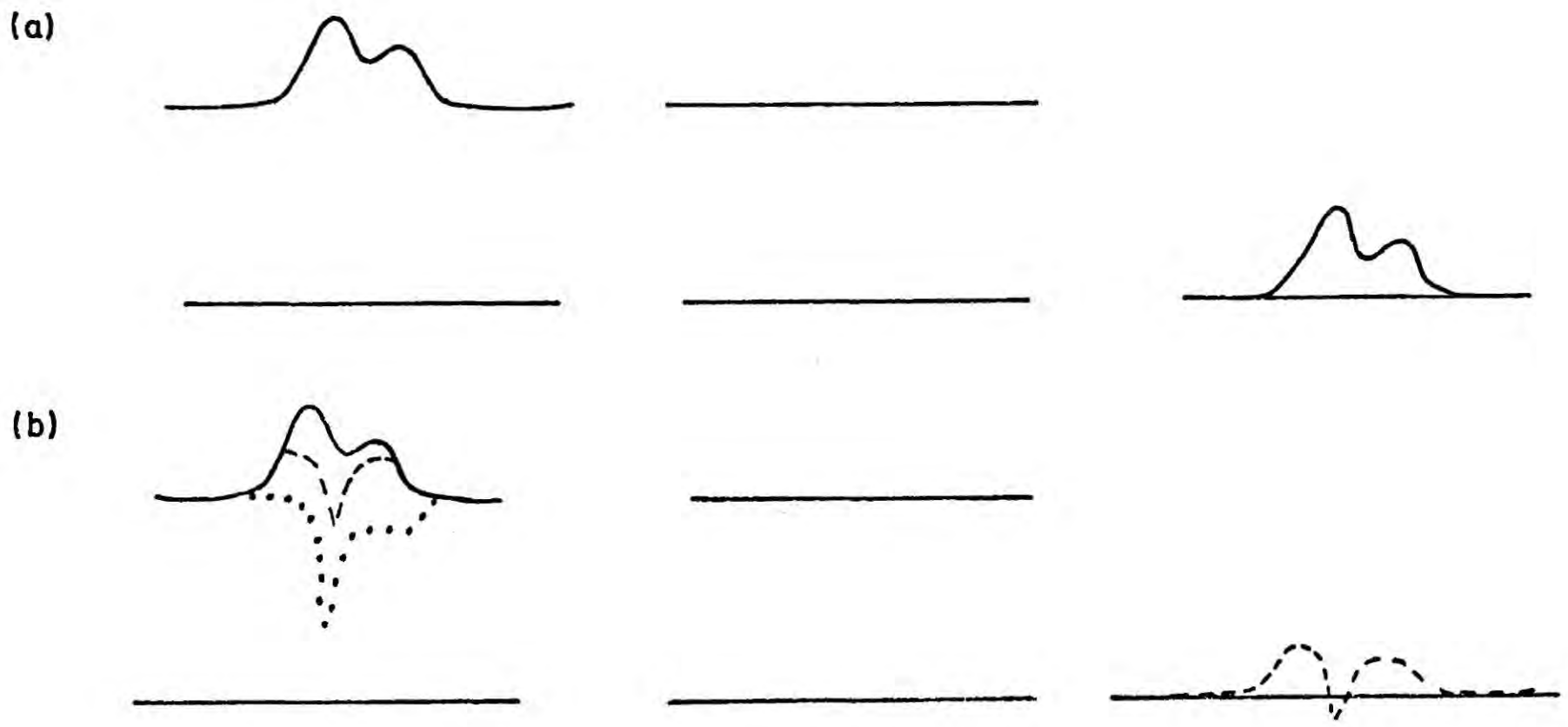

Figure 5-15 The composition of an observed absorption profile from the combination of the line and continuum radiation (a) without absorption (nearby continuum source in front of all the hydrogen) (b) with absorption (source beyond some of the hydrogen) — line emission in the absence of absorption ... continuum source spectrum attenuated by hydrogen absorption at the same frequencies - - -observed profile, combination of absorption and emission.

temperatures are needed. The optical depth and the spin temperature can then be separated.

(d) Absorption techniques provide the most sensitive method for detecting hydrogen at very low temperatures, for example, in the intergalactic gas.

The first absorption observations were reported by Hagen and McClain (1954) and Hagen, Lilley and McClain (1955). Soviet astronomers have published studies of 21 cm absorption in the spectra of the galactic centre source, Ryzkova et al (1963 , 1964) and Egorova (1963 , 1964) and of several other sources, Bystrova et al(1964a, b, 1965)and the source W49 was studied by Akabane and Kerr (1965) but the bandwidths were 17 and 8 km sec^{-1} respectively, much too large for detailed study.

At the Paris Symposium in 1958 the first detailed absorption study was reported by Muller (1958). The velocity resolution was 1 km sec^{-1} and he studied four strong radio sources Cas A, Tau A, Cyg A and Ori A. The cloud components had the following characteristics:-

	Range
Optical depth τ	0.07(Cas A) - 1.4 (Ori A)
R.M.S. velocity km sec^{-1}	1.0 (Tau A) - 2.6 (Cas A)
N_H atoms cm^{-2}	$2\ 10^{19}$ (Cyg A) - $4.1\ 10^{21}$ (Cas A)

Clark et al (1962) investigated the spectra of twelve sources with a velocity resolution of 1.3 km sec^{-1}. Most spectra contain one or more deep absorption components $\tau>0.5$. For these opaque clouds Clark derived the following parameters: R_o = 7.5 pc, n_H = 20 cm^{-3}, mass = 1000 $M_\odot$ in close agreement with Heiles (1967).

Clark (1965) observed the brightness distributions across five intense radio sources, Cas A, Tau A, Sgr. A, Ori A and M17 (Omega Nebula) in

detail. His analysis, made by resolving the features of the 21 cm absorption lines into Gaussian components, supplied radial velocities v_r, central optical depths τ_o, velocity dispersions σ_v and hydrogen surface densities N_H assuming a gas temperature of 100°K. The angular scale enabled n_H the hydrogen density, and M, the mass of the cloud, to be calculated. Finally, the distance to the cloud was derived from the radial velocity using the differential galactic rotation model. The hydrogen densities ranged from 1.2 atoms cm^{-3} to 680 atoms cm^{-3}, which was the case for a small dense cloud in front of Orion A. The mean hydrogen density was 11 atoms cm^{-3}. Cloud masses ranged from 2.6 $M_\odot$ to $\sim$1000 $M_\odot$, a heavy cloud causing a deep line in Cas A. The mean mass was 115 $M_\odot$. Surface densities range from 4 10^{19} to >90 10^{19} atoms cm^{-2} which represents a cloud in Sgr A. The mean surface density was 6 10^{20} atoms cm^{-2} ignoring the cloud in Sgr. A. Clark also observed the spectra of ten weak sources and with a similar analysis to that above provides information on the optical depth and velocity dispersion. Figure 5.16a shows the distribution of central optical depths τ_o of both the strong and weak sources (the dotted line refers to the five strong discrete sources only). In making the histogram, components for which only an upper limit in optical depth is known were excluded. These would tend to fill in the right hand portion somewhat. The distribution law is an exponential with an exponent of the order of unity (plotted in the diagram). Figure 5.16b illustrates the distribution of velocity dispersions which range from 0.5 km sec^{-1} to 6.5 km sec^{-1} with a mean 1.94 km sec^{-1}.

Correcting appropriately for incomplete resolution of components in the analysis, Clark derived a line density, k=4.1 kpc^{-1} for clouds of all optical depths in the galactic plane. There is, however, some evidence that the density is up to twice this in the local arm.

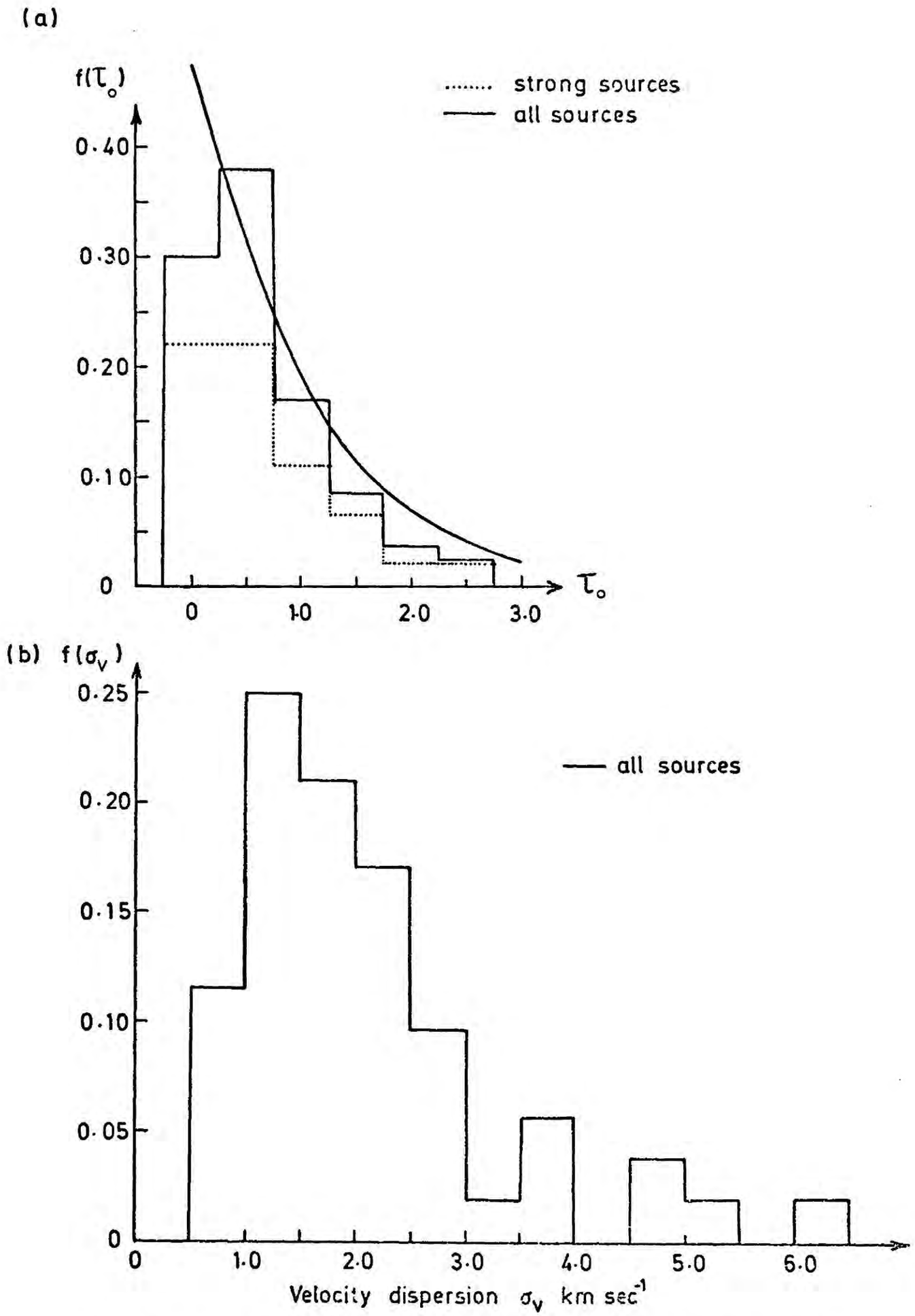

Figure 5-16 The distribution of (a) central optical depths, and (b) velocity dispersion measured by Clark (1965).

21 cm absorption spectra are known to be different in dispersion from emission spectra. Clark suggests that the hydrogen seen in emission is at a high temperature and therefore has a very low absorption coefficient (a temperature >1000^{o}K is sufficient to make hydrogen invisible in the absorption spectrum) whilst hydrogen seen in absorption is somewhat cooler than 100^{o}K. This dual nature of the interstellar medium can therefore be looked at in terms of a "raisin pudding" model where the "pudding", the hot hydrogen, is the intercloud medium in which the "raisins", the cold denser hydrogen, the clouds, are embedded. In such a model the clouds are in pressure equilibrium with the interstellar medium with 50% cloud to intercloud medium. The mechanism for stopping the clouds from expanding into the surrounding medium is heating and ionisation by homogeneous flux of low energy cosmic rays balanced by radiative cooling. (Other models based on the same conclusion are discussed in section 5.7).

An absorption line study of the galactic neutral hydrogen at 21 cm wavelength has been made by Hughes et al (1971). They used 97 sources of which all but four are believed to be extragalactic. Measurable absorption was detected in 64 cases. In the analysis no attempt was made to resolve them into Gaussian components because the number of components required for each profile is by no means uniquely determined. Therefore, the analysis was limited to the total optical depth of the most prominent absorption feature. Figure 5.17 shows the distribution of the peak value of optical depth τ for 119 features listed in his paper. As can be seen the form of the distribution is exp-τ in good agreement with Clark (1965). Optical depths >0.5 were found only within 20^{o} of the galactic plane, except in the region of the Cetus arc where values up to 1.4 occur. The highest galactic latitude at which absorption was detected was 75^{o} for Virgo A.

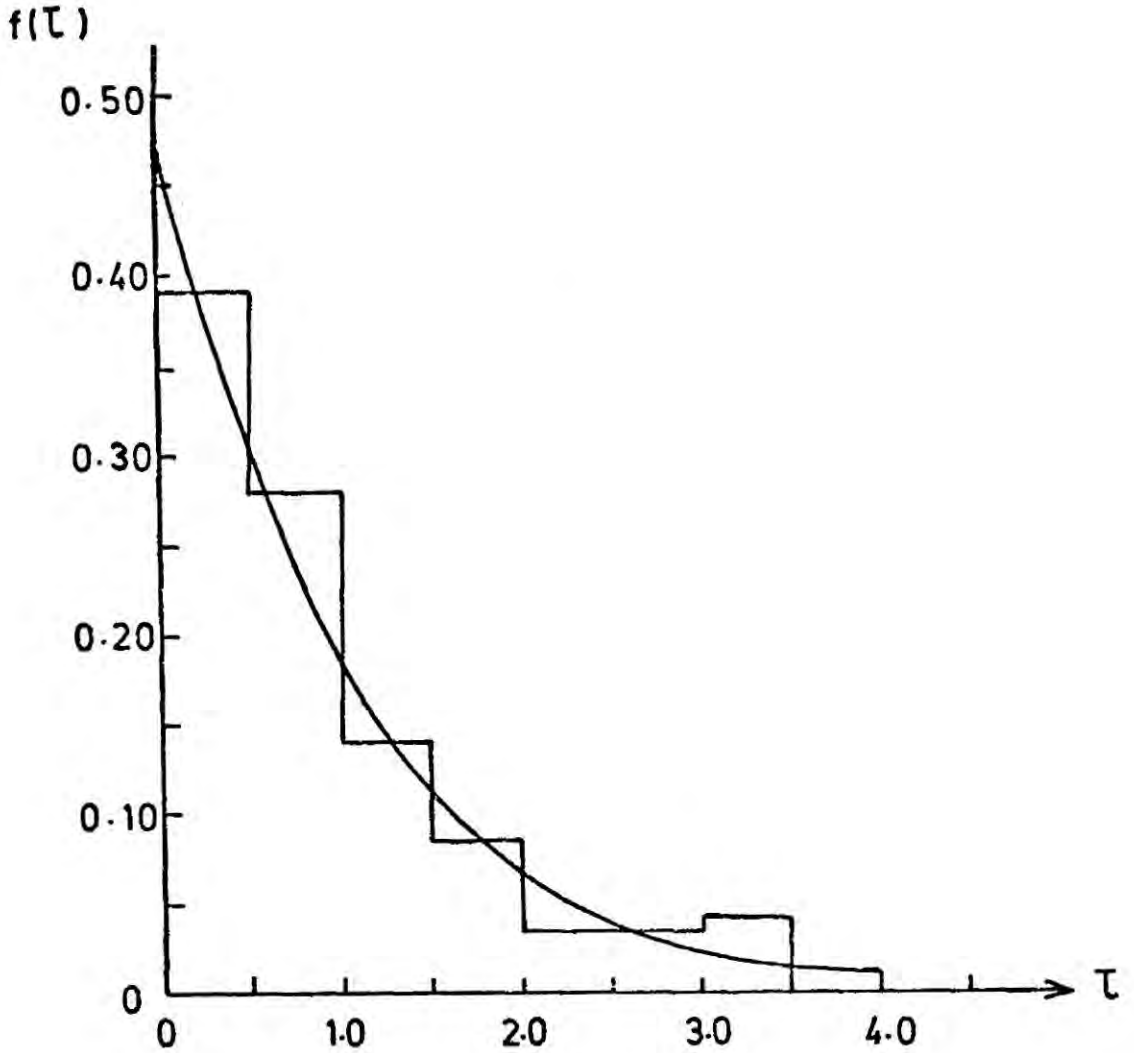

Figure 5-17 The distribution of the peak value of optical depths τ, measured by Hughes et al (1971) is shown to be well approximated by an exponential i.e. $f(\tau) = e^{-\tau}$.

The dual nature of the interstellar medium was evident and the mean temperature of the cool absorbing gas was found to be $71\pm9^{\circ}K$ after correction was made for the effects of the surrounding hot gas. The highest lower limit for the temperature of the hotter gas was estimated to be $600^{\circ}K$ but there was evidence of a temperature of a few hundred degrees Kelvin. With the assumption that the interstellar gas has such a two temperature structure it is found that for a line of sight close to the galactic plane 7.5% of neutral atomic hydrogen is in the cool state. For the general vicinity of the Sun the result is 36-45% depending on the ratio of the temperature of the two states of the gas and this is probably also a good estimate for the Galaxy as a whole.

Generally, the random motions of the cool clouds were found to lie between 1 and 6 km sec^{-1} whilst velocities as high as 8 or 9 km sec^{-1} occurred for 3C88 and 3C98 both of which lie very close to the anticentre longitude.

The most recent survey of 21 cm absorption has been made using the Parkes hydrogen-line interferometer. Radhakrishnan et al 1972a gives the details of the instrumentation, Radhakrishnan et al 1972b provides data on 35 extragalactic sources. 21 cm absorption measurements on 41 galactic sources north of declination -48° is dealt with by Radhakrishnan et al 1972c and on low latitude sources south of declination -46° by Goss et al (1972). Fitting of Gaussian components enabled estimates of physical parameters of what might well be individual clouds of neutral hydrogen, to be made. Experimental results are in reasonable agreement with those of Clark (1965) and Hughes et al (1971) and a statistical treatment of the absorbing H_{I} concentrations in the galactic disk made by Radhakrishnan and Goss (1972) lead to the conclusion that the mean value for N_H/T_g is $1.5\ 10^{19}$

atoms cm^{-1} $^oK^{-1}$. The spin temperature for cold gas is 60-80^{o}K and for hot gas >750^{o}K. A line of sight along the plane intersects on the average a minimum of 2.5 concentrations kpc^{-1}.

5.4 Neutral hydrogen associated with galactic clusters and OB stars

Many studies have been made of the neutral hydrogen content of galactic clusters and associations. Raimond (1966) as an introduction to his own extensive work on two associations in Monoceros discusses most of the early work on this subject, only a brief summary will be given here.

The main difficulty encountered in investigations of this type is to separate the hydrogen connected with a cluster or an association from the effect of background irregularities. Some of the earlier studies can be criticized from this point of view, either for too low a telescope resolution or for insufficient exploration of the background surrounding the cluster.

Drake (1958) observed appreciable neutral hydrogen in all but the oldest cluster of five, as indicated in the table below.

Table 5.7 Observations of Drake (1958)

Cluster	age $\times 10^{-6}$ years	Mass of hydrogen M_H $M_\odot$
hX Persei	3	7400
Pleiades	150	470
Coma Berenices	700	27
Praesepe	1000	26
M67	5000	<18

He found that the ratio of the mass of the neutral hydrogen in the cluster to the total mass in the cluster increased with age of the cluster

which supports the hypothesis that the H_I masses are residues of the primordial gas masses from which the clusters were originally formed.

Dieter (1960) found 31 out of 40 cases when hydrogen and OB associations were coincident. However, the distance to the association obtained from optical measurements did not always agree with the distance suggested by the velocity of the hydrogen as calculated using the galactic rotation model.

In 1963 Davies and Tovmassian selected clusters of small diameters (10'-20') and used a large telescope to cut down errors due to background irregularities. They reported neutral hydrogen at the position of four galactic clusters out of five and they found that more massive clusters retained a greater proportion of their gas. Large cloud complexes were observed in the region of Taurus by Oort (1954), Burke et al (1963a,b) and Garzoli et al (1966) whilst the Perseus region has been examined in detail by Grahl (1960). Raimond (1966) made a detailed study of a large region in Monoceros when he identified 11 concentrations of neutral hydrogen of a rather discrete character. Three of these appeared to be related to Monoceros II with a total mass of neutral hydrogen $\sim$200,000 $M_\odot$ an order of magnitude greater than the estimated stellar mass of the associated cluster NGC 2264. On Mon I, two clouds in different velocity ranges covered the areas shown in figure 5.18. The total mass of hydrogen was found to be 150,000 $M_\odot$ with an over-all diameter of 110 pc and an average density of 8.5 hydrogen atoms cm^{-3}.

The Orion region has been studied by Strömgren (1948), Menon (1958) and more recently by Gordon (1970). Estimates of the size, density and mass of clouds of hydrogen are compared with the 21 cm emission data discussed previously in table 5.8. Menon reports the presence of a ring

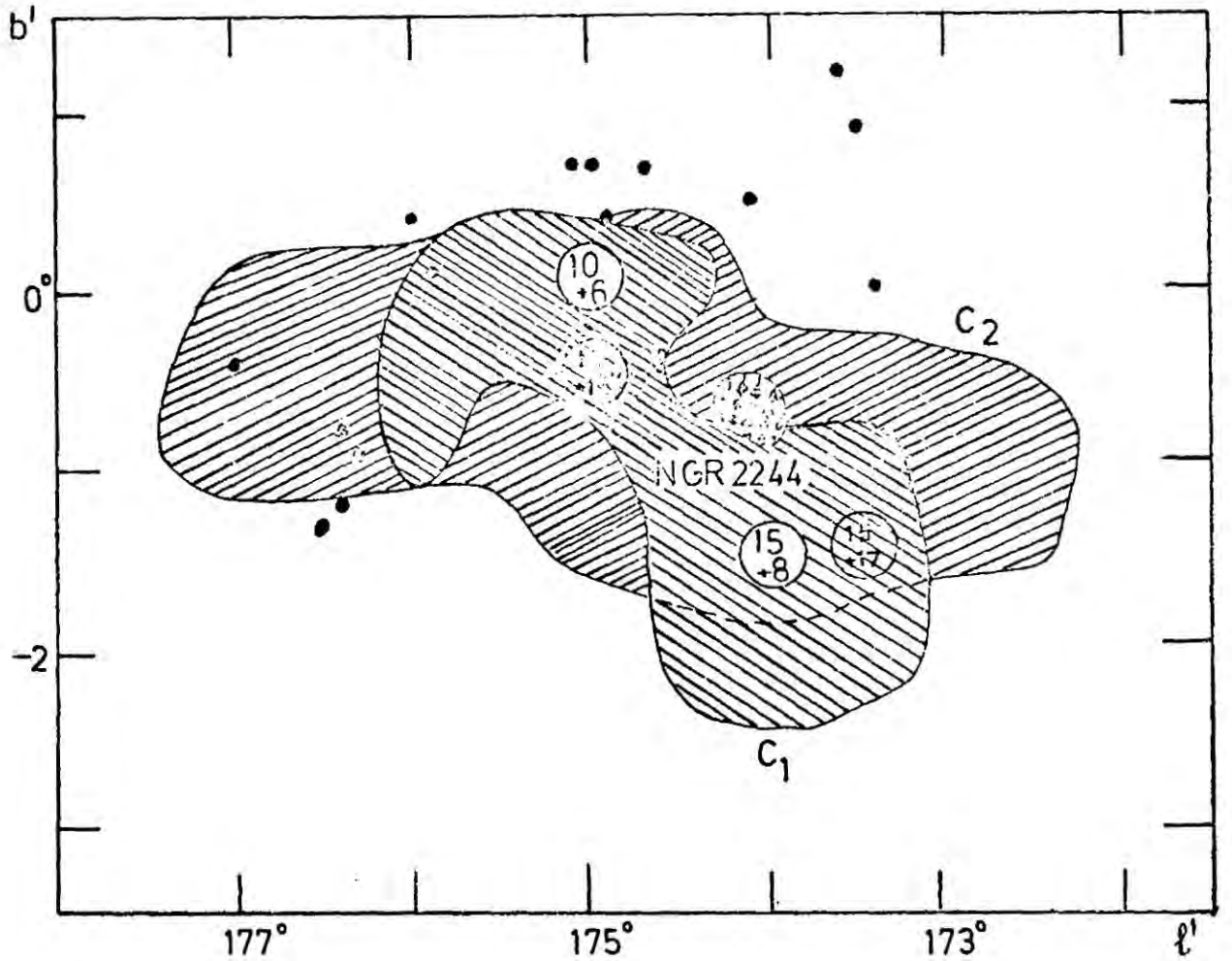

Figure 5-18 Two hydrogen clouds C_1, C_2 (hatched areas) in the region of the cluster NGC2244 (Raimond 1966). For the two clouds, the upper number of the ringed pairs (hatched circles) indicates the maximum surface density of hydrogen atoms in units of 10^{20} cm^{-2}; the lower number indicates the radial velocity of the peak. Secondary maxima (open circles) are also indicated. The average surface density over the hatched area is half the peak value in each instance. The cluster (cross checks) and some members of the association I Mon (filled circles) are also shown.

Table 5.8 Cloud Parameters obtained from 21 cm emission and absorption experiments
(† R.M.S. random radial velocity)

Reference	Year	R_o pc Radius	n_H cm^{-3} Density of H_I	M $M_\odot$ Mass of H_I	$N_H \times 10^{-20}$ cm^{-2} Column Density of H_I	T °K Temperature of cloud	N_o kpc^{-3} Number of clouds per unit volume	k kpc^{-1} Number of clouds per unit distance along the line of sight	T_o Optical depth	σ_v km sec^{-1} Velocity dispersion	Comments
Strömgren	1948	7.5	60	2,500	28				3	4	Particularly heavy cloud in front of χ^2 Ori
Strömgren	1948	10	6	600	8	125	$2\ 10^4$	7	0.4	4	'Average' interstellar cloud data from extinction and from optical interstellar absorption lines 1% of space occupied by clouds
Strömgren	1948	5					10^5	7			5% of OB2 stars are actually located in clouds
Helfer	1955									3.5	
Hulst van de, Muller & Oort	1954							8			Inverse correlation between interstellar absorption and atomic hydrogen abundance
		5-20									Median size of H_{II} found to be 5 pc
Oort	1954	30	10	30,000	18						Large cloud complexes e.g. in Taurus
Heeschen	1955				45-58	120				6.2-9.9†	Hot clouds(galactic centre)
Heeschen	1955				2-5	40				2.1-2.7†	Cold clouds(galactic centre
Verontsov-Velyaminov	1955	1.5-400									

Table 5.8 continued

Reference	Year	R_o pc	n_H cm^{-3}	M $M_\odot$	$N_H \times 10^{-20}$ cm^{-2}	T °K	N_o kpc^{-3}	k kpc^{-1}	T_o	σ_v km sec^{-1}	Comments
		Radius	Density of H_I	Mass of H_I	Column Density of H_I	Temperature of cloud	Number of clouds per unit volume	Number of clouds per unit distance along the line of sight	Optical depth	Velocity dispersion	
Menon	1958	>20		73,000							H_I associated with Orion Nebula. Mass of ionized hydrogen 31000 $M_\odot$
Prönik	1959	20						18-20			Number of clouds kpc^{-1} up to Cas A.
Kaftan -Kassim	1961										Expanding cloud of hydrogen near the solar system. Hydrogen associated with OB stars
Davis	1962	4-324									Neutral hydrogen in front of OB stars
Dieter	1964	3.5	10	30						4-8	North galactic pole. H_I at a distance of 100 pc
Dieter	1965	3.5c-6c	$1.5c^{-1}$-$2.2c^{-1}$	$7c^2$-$30c^2$	0.37-0.6					2-2.3	South galactic pole. H_I at a distance 100c pc where c~1
Makarova	1964	7.5	27	735	11	62	$6.5\ 10^4$	10	2	5	σ =1.9 km/sec. 21 cm profiles for intervals 10° along galactic equator profiles decomposed into Gaussian components which numbered 200.
Garzoli et al	1966				11-29						H_I located in Taurus indirect evidence for a significant amount of molecular hydrogen

Table 5.8 continued

Reference	Year	R_o pc	n_H cm^{-3}	M $M_\odot$	$N_H \times 10^{-20}$ cm^{-2}	T °K	N_o kpc^{-3}	k kpc^{-1}	T_o	σ_v km sec^{-1}	Comments
		Radius	Density of H_I	Mass of H_I	Column Density of H_I	Temperature of cloud	Number of clouds per unit volume	Number of clouds per unit distance along the line of sight	Optical depth	Velocity dispersion	
Menon	1958	>20		73,000							H_I associated with Orion Nebula. Mass of ionized hydrogen 31000 $M_\odot$
Prönik	1959	20						18-20			Number of clouds kpc^{-1} up to Cas A.
Kaftan -Kassim	1961										Expanding cloud of hydrogen near the solar system. Hydrogen associated with OB stars
Davis	1962	4-324									Neutral hydrogen in front of OB stars
Dieter	1964	3.5	10	30						4-8	North galactic pole. H_I at a distance of 100 pc
Dieter	1965	3.5c-6c	1.5c^{-1} - 2.2c^{-1}	7c^2-30c^2	0.37-0.6					2-2.3	South galactic pole. H_I at a distance 100c pc where c∿1
Makarova	1964	7.5	27	735	11	62	6.5 10^4	10	2	5	σ =1.9 km/sec. 21 cm profiles for intervals 10° along galactic equator profiles decomposed into Gaussian components which numbered 200.
Garzoli et al	1966				11-29						H_I located in Taurus indirect evidence for a significant amount of molecular hydrogen

Table 5.8 continued

Reference	Year	R_o pc	n_H cm^{-3}	M $M_\odot$	$N_H \times 10^{-20}$ cm^{-2}	T °K	N_o kpc^{-3}	k kpc^{-1}	T_o	σ_v km sec^{-1}	Comments
		Radius	Density of H_I	Mass of H_I	Column Density	Temperature of cloud	Number of clouds per unit volume	Number of clouds per unit distance along the line of sight	Optical depth	Velocity dispersion	
Raimond	1966	55	8.5	150,000						3.4	Two H_I clouds associated with Mon I
Raimond	1966	12.5-27.5	4-13	20,000							Three clouds associated with Mon II
Heiles	1967	1.4-4.9 7-36	1.0-3.6 0.7-8	1.3-54 280-16000		<100	$3.5\ 10^5$ $6.5\ 10^3$			0.8-2.4 1.2-4.5	Cloudlets / Clouds } inside 2 sheets of H_I 10 pc thick ∿500 pc from LSR. ∿1% space occupied by clouds
Linblad	1967										H_I in galactic anticentre
Riegel & Jennings	1969	<50				<42					Unusually cold cloud <1kpc from the Sun
Gordon	1970	20		70,000	16-29						H_I in the Orion Region
Weaver & Williams	1970	22	5	4,500						3.2	Large concentration centred at ℓ=47° b=-6°; 750 pc from L.S.R. background density 0.5-1.0 H atoms cm^{-3}
da Rocha Vieira	1971	12-74	4.9-7		7.9-11					2.5-3.8	H_I in a region in Centaurus
Knapp & Verschuur	1972	400 300		0.20 0.11	0.05-1.27 0.06-0.49	24 17			0.2-2.0 0.2-2.2		} Two large clouds looked at in extreme detail

of hydrogen expanding around the Orion nebula at a velocity of 10 km sec^{-1}. Such expanding rings of hydrogen gas are commonly observed around clusters e.g. by Wade (1957) and Davies & Tovmassian (1963).

Kaftan Kassim (1961) found that the density of neutral hydrogen increased at the positions of OB associations and gave evidence of an expanding H_I region around the association Vl Cygni.

Goldstein et al (1966) observed the 21 cm emission line of atomic hydrogen at 63 adjacent positions in Serpens and Libra.

5.5 Dark clouds and reflection nebulae

Several catalogues of objects recognised as assemblies of solid particles have been compiled. In particular, Lynds (1962) published such a catalogue of dark nebulae compiled from a study of the red and blue prints of the National Geographic Palomar Observatory Sky Atlas. A statistical treatment of the data revealed that ∿49% of the sky is obscured by dust clouds in the area within 1^{o} of the galactic plane. The dark clouds were found predominantly along the Goulds belt. Figure 5.19 gives the histograms of the distribution in angular size of the clouds grouped according to their opacities. The arrows indicate the mean values for the respective opacity group. If it is assumed that the clouds are uniformly distributed in the Gould belt assumed to be at a constant distance from the L.S.R. over the entire range in galactic longitude, then these histograms illustrate the distributions of the true physical sizes of the clouds in reasonable agreement with Heiles (1967). However, all but 3 of 48 dust clouds surveyed in the 21 cm line by Heiles (1969) did not obviously display their presence in H_I but most probably in molecular hydrogen or frozen hydrogen mantles on dust grains. Therefore,

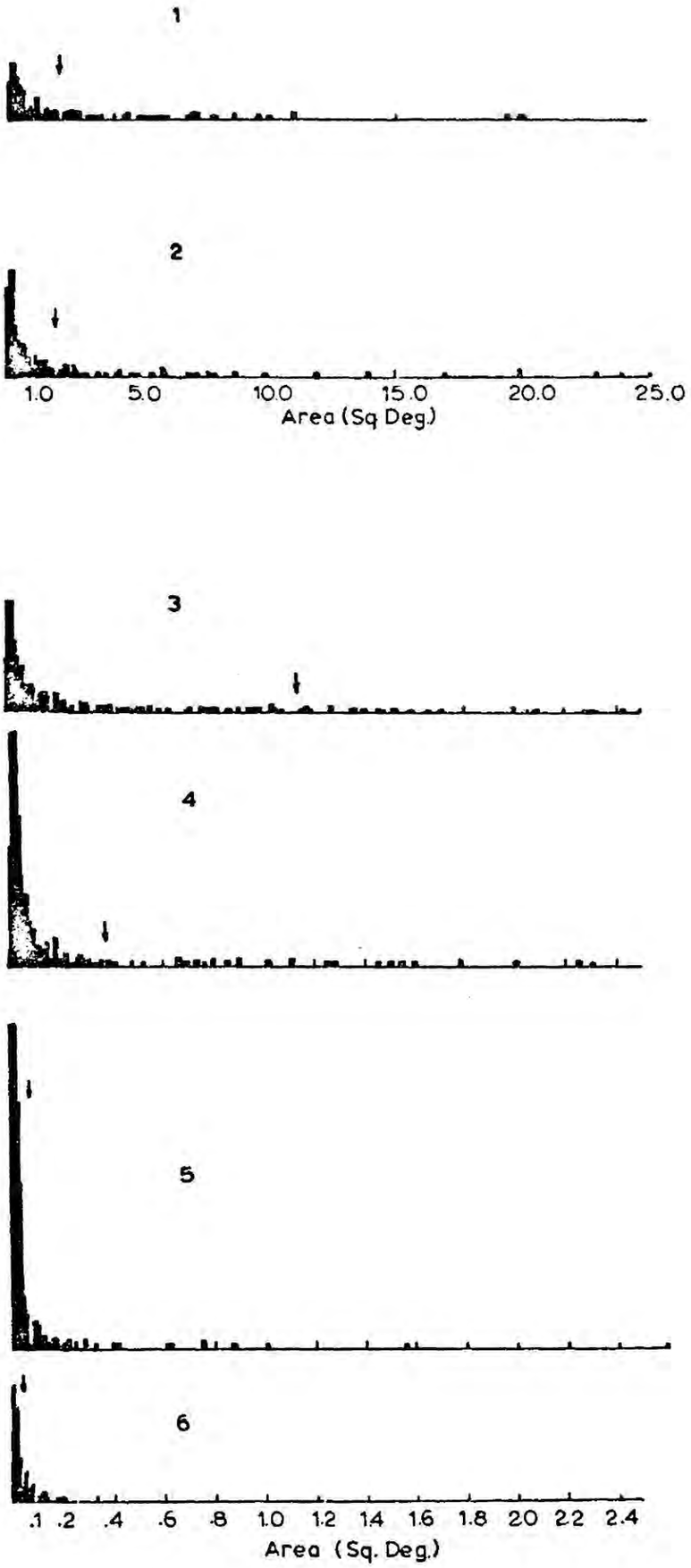

Figure 5-19 Histogram for clouds of opacity 1, 2, 3, 4, 5 and 6 (clouds of small area could easily be missed in a visual inspection for opacity groups 1 and 2).

there is no reason why the distribution of neutral hydrogen clouds and dust clouds should be the same.

Neckel (1966) determined the space distribution of absorbing matter from measures of colour-excesses of stars and galactic clusters. He found large dust clouds 100 pc-1000 pc in size and the average thickness of the dust layer to be ∿40 pc. Scheffler (1966, 1967a, 1967b) discussed the distribution of the sizes of colour excess and derived a cloud model allowing two types of clouds small ones, with radii 1.5 pc mass 25 $M_{\odot}$, line density of 5 kpc^{-1} and large areas with radii 12.5 pc, mass 15,000 $M_{\odot}$ and line density 0.5 kpc^{-1}.

5.6 Models of the interstellar structure

There are two distinct types of model calculations in which theoretical astrophysics research groups are engaged. The first is involved with the manipulation of experimental data to hypothesise cloud parameters. A number of such models have already been dealt with previously and these along with those of Blaauw (1952), Münch (1961), Terauti (1963) and Spitzer (1968a) are summarized in table 5.9. The second is a purely theoretical treatment under the guidance of experimental implications to hypothesise mechanisms to explain the actual formation and stability of the cloud and intercloud media.

The earliest attempt at a description of the interstellar gas dynamics, consistent with observations, was that by Oort (1954). The basic element of the scheme was the interstellar "cloud" a region of high density moving freely through an intercloud medium of low density and high temperature. Such clouds frequently appear in descriptive models of interstellar gas being consistent with a variety of observations of interstellar neutral hydrogen, calcium ions, and dust particles, Spitzer (1968a). Oort supposes

Table 5.9 Model Parameters

Reference	Year	R_o pc	n_H cm^{-3}	M $M_\odot$	$N_H \times 10^{-20}$ cm^{-2}	T_s °K	N_o kpc^{-3}	k kpc^{-1}	f	σ_v km sec^{-1}	Comments
		Radius	Density of hydrogen	Mass of hydrogen	Column density of hydrogen	Temperature of cloud	Number of clouds per unit volume	Number of clouds per unit distance along line sight	fraction of space occupied by clouds	Velocity dispersion	
Blaaw	1952	3	20	46				8-12		5±1	Velocity distribution of interstellar clouds—derives parameters from statistical model
Hulst van de	1958	a)Orion arm 9	1.5				$5\ 10^5$		1	5	
		b)Perseus arm 17.5					$4\ 10^4$		1	5	
Münch	1961	5	3	40							
Terauti	1963	8	4.6	264	2.3		$7\ 10^4$	14	0.14		Spherical cloud and shell of double size and half density
Takakubo	1963	3.4	14	55	3		$3\ 10^5$	11	0.05		System of spherical clouds of equal size and uniform density
Kahn and Dyson	1965	1	100			100					Interior H_I cloud free from magnetic field Large scale galactic magnetic field strength ∿3 μgauss
Scheffler	1967a	1.5	70	25	6			5			From statistics of visual extinction "small clouds"

Table 5.9 continued

Reference	Year	R_o pc	n_H cm^{-3}	M $M_\odot$	N_Hx10^{-20} cm^{-2}	T_s ^oK	N_o kpc^{-3}	k kpc^{-1}	f	σ_v km sec^{-1}	Comments
Scheffler	1967b	12.5	70	15,000	55			0.5			From statistics of visual extinction "compact big clouds"
Spitzer	1968a	7	10	400	4		$5\ 10^4$	8	0.07		"Standard" cloud
Spitzer	1968a	15	20	7,000	18		10^3	0.7	0.007		"Large" cloud from statistics of colour excess
Spitzer	1968a	4	100	800	25						"Intermediate size dark cloud"
Hjellming et al	1969	a) cloud b) inter-cloud				10^3 50					
Falgarone and Lequeux	1972	a) cloud b) inter-cloud	0.29 0.155		1.5 1.4 at b=90^o	70-80 10^4		3 3		4-5 6.4±0.9	

each cloud to be in approximate hydrostatic equilibrium, its internal pressure balancing external pressure plus self gravitation thus maintaining the cloud's identity for long periods. The clouds undergo collisions with each other thus changing their mass, momentum and energy.

The life cycle for clouds was as follows: A small region of high density is compressed by the surrounding hot gas of an expanding H_{II} region which causes it to accelerate outward undergoing inelastic collisions with other clouds in the vicinity. At first, the "cloud" is so small, self gravitation is unimportant, but coalescence occurs thus increasing the cloud size to the point where self gravitation becomes significant and finally dominant. The cloud is then gravitationally unstable and undergoes a rapid collapse and subject to gravitational fragmentation. The final result is a group of young stars, the brighter of which ionise the hydrogen gas remaining in the cloud to form H_{II} regions and thereby regenerate small clouds as before to continue the cycle.

This model was formulated mathematically with simplifying assumptions by Field (1965) with the result that the cloud mass spectrum was found to be approximately a $M^{-3/2}$ law. However, in Field's private communication with Heiles, he indicated that an inverse square power law best fits the data in the range 6-20 $M_{\odot}$. The question of the shape of the mass spectrum will be dealt with in more detail in section 7.2.3 where it will be used to establish a distribution of cloud sizes assuming that the magnetic fields in the clouds are constant and $M \propto R_o^{3.3}$.

Spitzer (1968b)summarised the properties of H_I regions and interpreted them in terms of dense cool clouds in pressure equilibrium with a rarefied, hot intercloud medium. Hayakawa (1961) showed that low-energy cosmic rays are quite effective in heating the interstellar medium, and

Field (1962) proposed that cosmic ray heating could produce a neutral intercloud medium of high temperature.

Pikel'ner (1967), Field et al (1969), Hjellming et al (1969) and McCray and Buff (1972) constructed models based on these ideas. Bergeron and Souffrin (1971) and Habing and Goldsmith (1971) developed similar two phase models but with X-rays instead of cosmic rays as the heating.

Finally Schwartz (1972) demonstrates that interstellar H_I regions suddenly heated above equilibrium temperatures favour the growth of density enhancements as medium relaxes back to equilibrium. The clouds formed in this way had "typical" interstellar clouds of size 1-10 pc but the cloud temperature $T \lesssim 20^{\circ}K$ is in disagreement with observations, (e.g. Hughes et al 1971 with a mean cloud temperature of $70-80^{\circ}K$). However, this same problem is encountered with the steady state model. Field et al (1969) suggested that a depletion of carbon on dust grains would alleviate this problem.

5.7 Conclusion

The development of the theory of the 21 cm hydrogen emission was necessary to obtain an understanding of the experimental data. Successful interpretation of the data was possible by using the galactic rotation model to establish how far the hydrogen under observation was from the L.S.R. This meant that a picture of the Galaxy on both a large and small scale could be established. Figure 5.20 illustrates the large scale distribution of hydrogen in the galactic plane; arms with hydrogen denser by a factor of 3 compared with the interarm regions, spiralling from the galactic centre. The arms, expanding outwards, are not continuous: suffering irregular breaks where the hydrogen gas projects above or below the plane. On average, the properties of the clouds above and

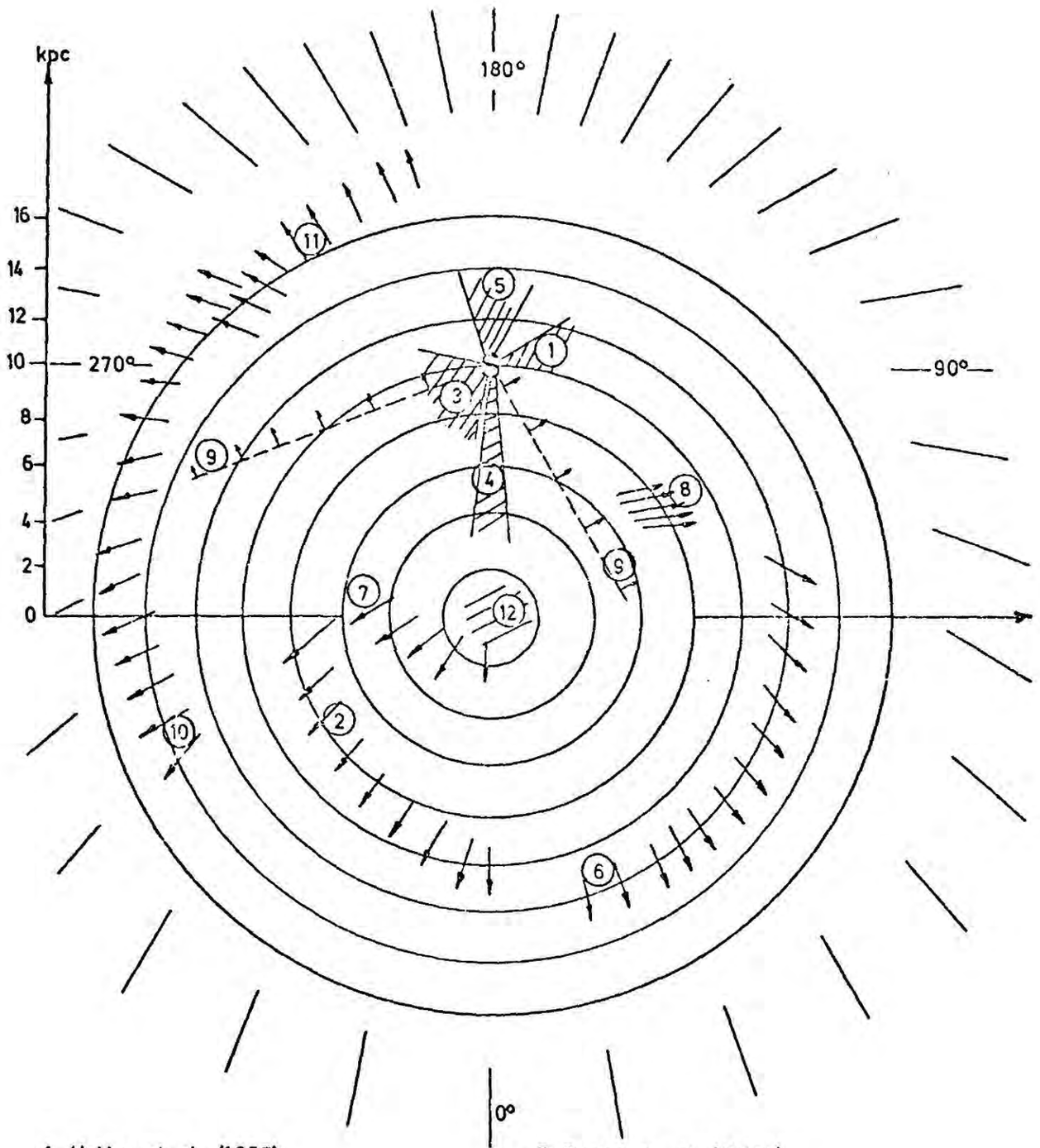

Figure 5-20 The large scale distribution of hydrogen in the galactic plane. The spiral structure, characteristic of our Galaxy, is illustrated.

below the galactic plane are the same yet layers of gas which are not connected with the plane have been shown to lie above the plane. It is believed that a huge mass of hydrogen, with a density $\leq\frac{1}{10}$ of the average hydrogen density in the plane, forms a halo around the galactic disk. There is evidence of high velocity gas condensing from the halo into the disk.

The structure of hydrogen on a small scale is very complex. Table 5.8 serves as a summary of the 21 cm emission data of the small scale structure of the Galaxy. The data reveals ranges of cloud sizes from 0.5 - 400 pc, hydrogen densities from 0.7 - 60 hydrogen atoms cm^{-3} and masses from 0.1 - 73,000 $M_\odot$. The standard cloud with a size $R_o \sim 7$ pc $n_H \sim 10$ cm^{-3}, $M \sim 400$ $M_\odot$ developed by Spitzer (1968a) is not typical since the data in general reveal a deficiency of clouds of this size, egs. Heiles (1967).

For the problem of diffusion at hand it was necessary to establish the H_oR_o distribution for the clouds inside the spiral arms. Verschuur in his experiments on Zeeman splitting showed empirically that the magnetic field, H_o is proportional to $n_H^{2/3}$, the two thirds power of the hydrogen density in the cloud, thus making it possible to establish the distribution H_oR_o via the hydrogen density. This was more convenient because the difficulties encountered when trying to measure weak fields render it quite impossible to ascertain the magnetic fields in the clouds to within an acceptable accuracy, whilst hydrogen density measurements are taken with relative ease.

Only one experiment, that performed by Heiles (1967), has been carried out in sufficient detail to enable further development of the diffusion model. He used instruments with a resolution high enough to be able to observe cloudlets with a size less than the smallest cloudlet

found to exist. Basically, Heiles finds two classes of hydrogen concentrations: small clouds or cloudlets which have sizes 1 pc$\lesssim R_o \lesssim$7 pc; and clouds, having sizes 7 pc$\lesssim R_o \lesssim$36 pc. The cloudlets are approximately 10^3 times more abundant than clouds. On the whole, the hydrogen densities within his cloudlets and clouds vary only slightly about a mean density $\bar{n}_H \sim 2.5$ cm^{-3}, suggesting a mean magnetic field $\bar{H}_o \sim 3.2$ gauss if the empirical result of Verschuur (1970) is correct. The distribution of cloud masses is not inconsistent with a power law of m^{-2} also observed by Field (private communication with Heiles 1967).

It was found necessary to adopt Heiles data and use it to define the distribution of H_oR_o as accurately as possible. The 21 cm emission data obtained by other experimenters was, however, not ignored completely, but used to try to "confirm" some of the observations of Heiles. When possible, the data parameters appearing in table 5.8 were plotted in figures 5.11 and 5.14 along with those of Heiles for comparison. It can be seen that they are in agreement with $M \propto R_o^{\alpha}$ with $\alpha = 3.3$ which seems to suggest an almost constant density, however the correlation between R_o and $p_o (= n_H^{2/3} R_o)$ is not as strong, even when the particularly heavy cloud in front of χ^2 Ori observed by Strömgren (1948) is ignored.

As a result of a careful analysis of the data of Heiles (1967) two physical models for the interstellar medium were developed. The first, Model A, assumes that the hydrogen density is constant, the distribution of cloud masses if $f(M)dM \propto M^{-2}$ and $M \propto R_o^{+3.3 \pm 0.8}$. The second, Model B, uses the more detailed analysis of the data when the distribution for H_oR_o reduces to the sum of a gamma function, representing cloudlets, and a power law, representing clouds.

Absorption data has led to the development of the idea of the dual nature of interstellar matter, cold dense hydrogen clouds in pressure

equilibrium with a hot less dense intercloud medium. On average, cloud parameters egs. temperatures, optical depths, and sizes are in agreement with 21 cm emission data. However, absorption data seems to be biased towards the observation of clouds with high densities and masses.

Analysis of 21 cm hydrogen data almost always assumes spherical clouds and yet a visual examination of contour maps reveals filamentary structures except on a very small scale ($R \lesssim 4$ pc) irrespective of their position in the Galaxy.

Dust has been found associated with hydrogen both having cloud sizes of the same order of magnitude. Large H_I clouds are found associated with star clusters a fact in support of the theory of Verschuur (1970) stating that stars have condensed from hydrogen. Visual opacity measurements (Lynds, 1962) suggest a similar type of distribution of clouds to that of Heiles.

Finally, statistical modelling based on experimental data has been reasonably successful but the theoretical understanding of mechanisms which are responsible for the existence of clouds is by no means complete.

Chapter 6 Magnetic fields in our Galaxy

6.1 Introduction

Magnetic fields have an important influence on the interstellar gas whilst at the same time the motion of the gas partly determines the structure of the magnetic field. The energy density of cosmic rays of energy above $5\ 10^6$ eV is comparable to the energy density of random motions in the gas as well as to the magnetic energy density. The gas, magnetic fields and cosmic rays are thus dynamically coupled and should really be treated as one system.

The preceeding chapter developed a 3-D picture of the distribution of matter, hydrogen, dust and stellar bodies, inside the Galaxy. It is the aim of this chapter to identify with the galactic structure and substructure, the structure of the magnetic fields; it is these fields which dominate the motion of cosmic rays. Immediately it is evident that both a large scale magnetic field, associated with the spiral arm and interarm features, and a small scale magnetic field component, associated with the clouds, cloudlets and supernovae, exist within the Galaxy.

Information about the magnetic field strengths and/or its orientation in space has been obtained from experimental measurements of the Zeeman effect, interstellar polarization, Faraday rotation measures, dispersion measures and synchrotron radiation and each of these will be dealt with in turn.

The synchrotron flux measurements of discrete sources, Ilovaisky and Lequeux (1972), will be used to calculate the associated magnetic field. After a discussion of how coherent the field is across the source, an estimate of the total number of supernova remnants (S.N.R.) in the Galaxy will be made. The distribution of H_R for S.N.R. will be calculated and compared with that of cloudlets and clouds, Heiles (1967).

Finally, the last paragraph of this chapter will be devoted to a discussion on how significant these regions of very high magnetic fields are with respect to the clouds and cloudlets in terms of diffusion of cosmic rays.

6.2 The Zeeman Effect

Bolton and Wild (1957) suggested that the magnetic fields inside clouds of neutral hydrogen are strong enough to cause Zeeman splitting of the 21cm line seen in absorption against strong radio sources. In the direction of a weak magnetic field the 21cm line is seen to be split into left and right-hand circularly polarized components, the frequency of the splitting being proportional to the line of sight component of the magnetic field and equal to 2.8 MHz gauss.$^{-1}$

In a field of 1-10 μgauss, typical of interstellar clouds, the total splitting is only a small fraction of the line widths and therefore experimental techniques for measuring the degree of splitting, hence the line of sight magnetic field, are sensitive to the direction of the polarization of the two components. The difference ΔI in the intensity of the left and right-hand circularly polarized radiation for all frequencies across the absorption line is measured. Assuming the line has a Gaussian profile the maximum value of ΔI is related to the frequency shift $\Delta\nu$ by the relationship: $\Delta\nu = 0.7\nu_{\frac{1}{2}} \frac{\Delta I_{max}}{I}$ where $\nu_{\frac{1}{2}}$ is the halfwidth and I the depth of the line (Galt et al 1960). $\Delta\nu$ is related to H_ℓ, the line of sight component of the magnetic field and therefore in order to calculate the absolute field strength the direction of the field must be established by other means.

Using the above technique, Galt et al (1960) detected no interstellar magnetic field for which an upper limit of 50 μgauss was given. By using low noise receivers and switches the sensitivity of this technique

was improved by a factor of ten (Davies et al 1963a). Six absorption features in the strong radio sources Cassiopeia A, Cygnus A, Taurus A and Sagittarius A and one emission feature, Dec=+10^1 and R.A.=4^h 20^m, were studied (Davies et al 1963b and Davies and Shuter 1963c) with the following results. For the four major absorption features shown in figure 6.1 the best fitting H_ℓ component was $\lesssim 7$ μgauss. The four results were combined to provide a best fit to a circular field parallel to the spiral arms of -6.8 ± 3.2 μgauss (the error quoted is two standard deviations and represents 95% confidence limits. The negative sign indicates a field direction towards the L.S.R.). However, a slightly better fit to the data was obtained with a field of -10 μgauss inclined at an angle of 20° to the neutral hydrogen spiral arms. The line of sight magnetic fields predicted by this model (shown in brackets in figure 6.1) are seen to compare favourably with those observed experimentally in three regions. Verschuur (1968) observed a line of sight magnetic field of 10-12 μgauss in the Perseus arm in the direction of Cassiopeia A, a value confirmed by Davies et al (1968). Verschuur (1969) found $\bar{H}_\ell$ = -3.5 ± 0.7 μgauss in the Perseus arm in the direction of Taurus A, and a field of $\lesssim$ 1, 2.5 and 4.8 μgauss in the Orion arm, (local arm). The results of Verschuur are consistent with a field in a clockwise direction around the spiral arm observed from the North galactic pole.

Finally, the work by Verschuur (1970) dealt with in the previous chapter, attempted to show that the magnetic strength is related to the hydrogen density within the cloud, by the relation $H_o = 1.27\ n_H^{2/3}$ μgauss. This predicts a mean field strength of 2 μgauss and 3 μgauss for the cloudlets and clouds of Heiles (1967) respectively, but denser clouds with correspondingly higher fields do exist. For example, the cloud observed by Clark (1965) in front of Orion A had a density of 680 atoms cm^{-3} which would possess a field of ~100 μgauss if Verschuur's empirical relationship is true.

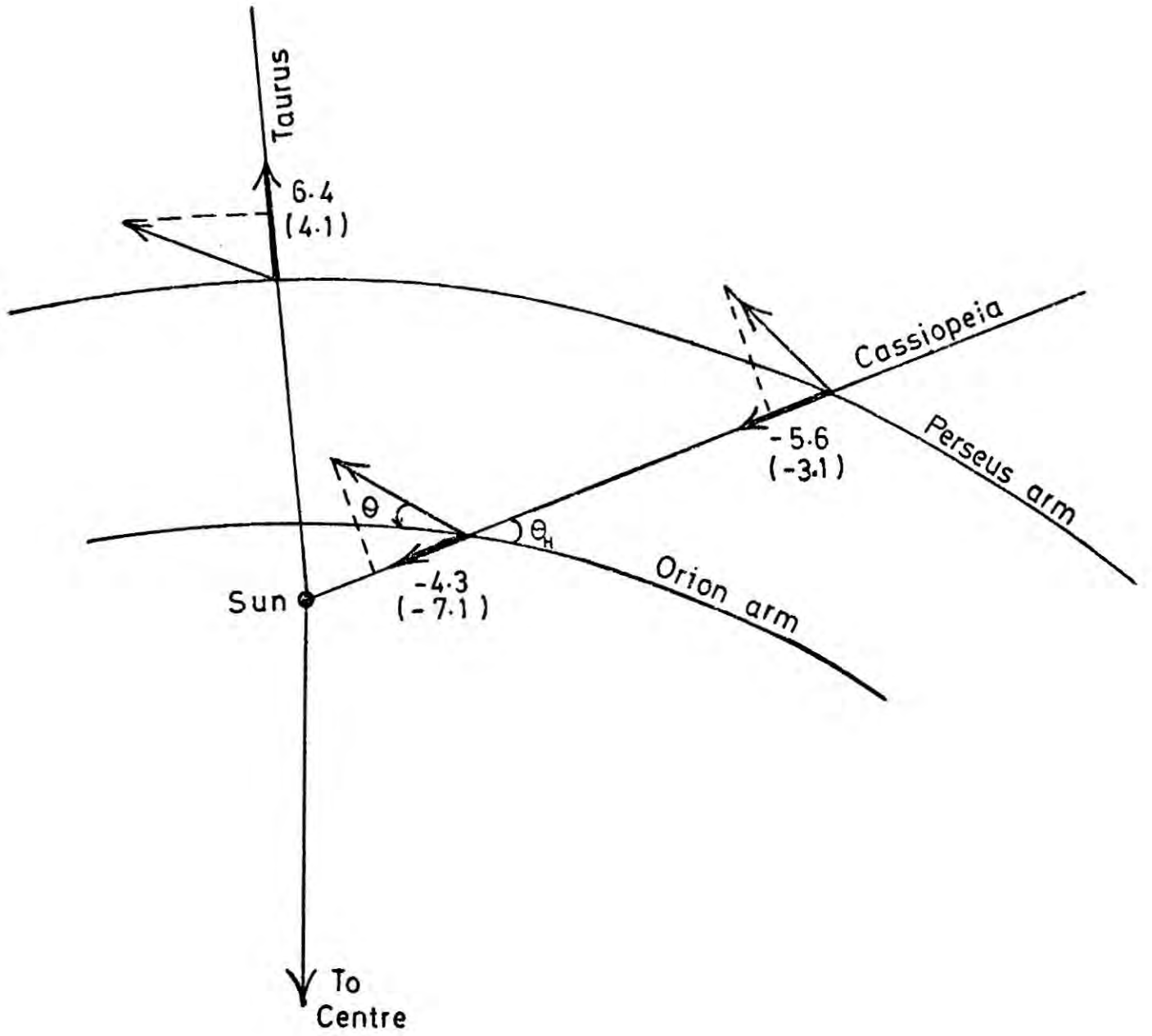

Figure 6.1 The observed magnetic field components (heavy lines) in three regions compared with the components expected for a field of 10 μgauss directed anticlockwise around the Galaxy and making an angle $\theta=20^{o}$ with the circular spiral arms. The expected components in the line-of-sight are given in brackets.

6.3 Interstellar Polarization

Interstellar polarization is caused by dust grains of asymmetric structure which are lined up by an interstellar magnetic field. Davis and Greenstein (1951) assumed elongated dust grains containing mostly compounds of hydrogen with 12% of iron by weight. He found that a magnetic field strength of 10 μgauss was sufficient to align grains of size 10^{-5} - 3 10^{-5}cm, with the short axis of rotation along the magnetic field lines, to produce the observed ratio of polarization to colour excess. The theory predicts uniform magnetic fields, with interstellar matter of constant temperature and composition and the polarization is proportional to the square of the magnetic field.

Henry (1958) developed similar models with the result that grains will be practically completely aligned for fields much greater than 50 μgauss for graphite flakes, 30 μgauss for paramagnetic grains (both grain types of size 4 10^{-6}cm) and 1.2 μgauss for ferrites and 0.013 μgauss for iron grains (both grain types of size 2 10^{-5}cm).

Davis and Greenstein (1951) concluded that the direction of the observed polarization vectors indicate a magnetic field parallel to the plane of the Galaxy over regions of several hundred parsecs being almost uniform along the spiral arm and perhaps making random whirls. This magnetic field orientation is consistent with polarization studies of 92 stars of Hoag (1953) and more recently by Seymour (1969) and Verschuur (1970) who analysed 550 stars.

However, studies of the optical polarization data of the local spiral arm Ireland (1961) and Mathewson (1968) indicate the presence of a helical field winding itself around the spiral arm. Mathewson (1968) combined his own polarization observations of 1800 local stars with those of Hiltner (1949) and Hall (1958) giving a total of over 7000 stars. He plotted the electric vectors as a function of their position in galactic space and found the best

fit to the data was a helical field component.

6.4 Faraday Rotation Measures

When a plane polarized radio wave of wavelength λ traverses an ionized medium containing a magnetic field the plane of polarization suffers a rotation through an angle ϕ numerically equal to

$$\phi \text{ radians} \approx 8.1\ 10^{11}\ \lambda^2 \int H_\ell n_e ds$$

Where λ is expressed in cms, H_ℓ is the longitudinal component of the magnetic field in gauss, n_e the electron density of the medium in cm^{-3} and ds, the element along the line of sight in pc in which the rotation occurs. Most extragalactic radio sources show some plane polarization at least at the decimeter and centimeter wavelength. Measurements of the observed position angle of the plane of polarization of the radiation from a given radio source plotted as a function of the square of the wavelength defines the Rotation Measure $\propto \int H_\ell n_e ds$. Typical values lie between 10 and 100 radian m^{-2}. The use of many sources gives the Rotation Measure (R.M.) in various directions. A negative value of the R.M. indicates a line of sight component of the field directed away from the L.S.R.

The electron density n_e and the distance ds over which Faraday rotation occurs must be established to calculate the magnetic field. Since the Faraday rotation of the ionosphere is two orders of magnitude less than the observed R.M. and the position angles show little variation at different times of the day or night (Cooper and Price 1962) the ionosphere can be assumed insignificant. Most of the observed Faraday rotation is either in the vicinity of the source or in our Galaxy. Seielstad et al (1964) observed R.M. increasing with decreasing galactic latitude suggesting that the rotation was mainly due to our Galaxy, however Gardner et al (1969b) showed very different R.M.'s were observed from two adjacent sources, some few degrees

DURHAM UNIVERSITY SCIENCE 3 AUG 1974 SECTION LIBRARY

apart, indicating intrinsic Faraday rotation in the sources. A large number of experiments have studied the R.M.'s of extragalactic sources to determine the field strength as well as the orientation of the large scale galactic field.

Davies (1968) studied the R.M.'s of extragalactic sources within 10^{o} of the galactic plane. He found that the best fit to the data was given by the expression R.M. = 17 $|\cos b|$ $\cos(\ell-100^{o})$ assuming a uniform magnetic field in the direction $\ell=100^{o}$, a value differing by 30^{o} from the direction of the Orion arm, but permeating a uniform layer of gas of constant electron density n_e. The layer of hydrogen has a thickness equal to 200pc (a value obtained from 21 cm data, Schmidt (1957) and one which is consistent with other measurements, see Chapter 9). Mills (1970) concludes that the mean value for n_e is $0.062cm^{-3}$ out to z=100pc in the local spiral arm thus giving a value of 3 μgauss for the magnetic field strength, however, it must be emphasised that the mean value of n_e is most uncertain.

Mitton (1972) presents a summary of 195 extragalactic sources whose R.M.'s have been reliably determined, 23 from Berge and Seilstad (1967), 42 from Gardner et al (1969a), 88 from Reinhardt and Theil (1970) and 39 newly determined R.M. These data provide a more uniform coverage of the sky than any previous analyses although there is still a lack of sources in the region $260^{o}<\ell<360^{o}$, $|b|<30^{o}$ as indicated by figure 6-2 where each source is plotted according to its position in galactic co-ordinates. The area of the circle is proportional to the magnitude of the rotation measure. Open circles indicate a negative R.M. equivalent to a field away from the observer and vice versa for the closed circles. There are substantial regions of the sky where the R.M. is predominantly positive (bottom left) or negative (bottom right) with the average R.M. decreasing towards the

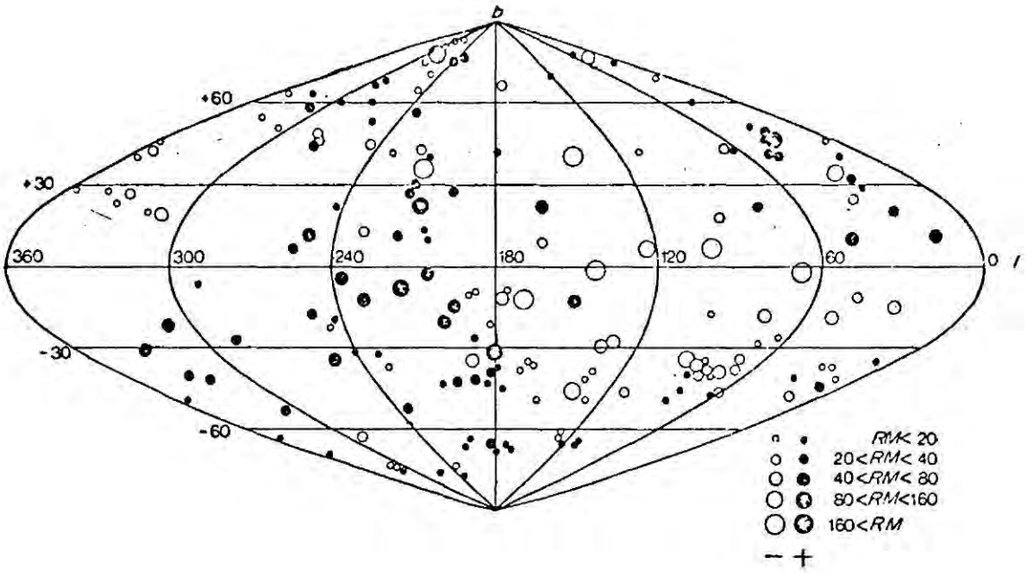

Figure 6-2 The galactic distribution of the rotation measures of 192 extragalactic radio sources.

galactic poles, in agreement with the galactic magnetic field model proposed by Mathewson and Nicholls (1968). Five sources well away from the galactic plane have rotation measures exceeding 100 radians m^{-2}. There is strong evidence in support of this rotation being intrinsic to the source. Omitting these sources and considering those 65 sources whose $|b|>65^{o}$ (high latitude sources reflect the large scale magnetic field component best) the mean rotation measure was believed to be $|R.M.|<10$ radians m^{-2} when the possible grouping effects of sources was taken into account. Assuming a path length of 5kpc, $\langle n_e H_\ell \rangle \lesssim 2.5\ 10^{-3} cm^{-3}$ μgauss. Most sources are <10% linearly polarized even at high frequencies. Burn (1966) showed that for this polarization 20% of the field is coherent. Using the equipartition argument of Scheuer (1967) the total magnetic field strength was found to be 50 μgauss giving a large scale coherent field of 10 μgauss. However, a field of $H_\ell<25$ μgauss is obtained using the de Young and Axford (1967) model which hypothesises a value for $n_e = 10^{-4} cm^{-3}$ and a $H_\ell<2.5$ μgauss taking the Mills and Sturrock (1969) model which formulates a value for $n_e = 10^{-3} cm^{-3}$. This lower value seems inconsistent with the polarization observations.

Gardner and Davies (1966) observing 86 sources found a longitudinal field with a reversal in the direction of the field for $b > +20^{o}$. Superimposed on this field there is evidence of a field anomaly possibly associated with Goulds belt (Davies 1968) and could be interpreted as a local helical field component. A longitudinal field is consistent with the data of Berge and Seielstad (1967) for 79 sources and Gardner et al (1967) for 133 sources, but as more and more rotation measures are determined more irregularities in the overall pattern appear. Theilheim and Langhoff (1968) formulated a quasi-longitudinal field model with the Sun 85pc below the plane, the magnetic field directed along the spiral arm suffers a

direction reversal above and below the plane. Mathewson and Nicholls (1968) were able to explain the observed change in field direction with a model in which a helical field is a localised perturbation of a general longitudinal field directed along the spiral arm towards $\ell=90^{\circ}$.

A later chapter will give evidence for an ellipse of hydrogen in which the solar system is situated; it appears that the local field anomaly is associated with this ellipse.

Because the position where the rotation of the plane polarized light occurs and the electron density in that region of space are both ill defined, the R.M. of extragalactic sources give very unreliable magnetic field strengths, although the field orientation can successfully be determined. This problem is overcome by using pulsars as the source of polarized radio emission when the dispersion measure equal to the line integral of the electron density to the source $D = \int n_e ds$, where s is the distance to the source in pc and n_e is the electron density in cm^{-3}, is determined. Therefore, $\bar{H}_{\ell} = \frac{\int n_e H_{\ell} ds}{\int n_e ds}$ defines the line of sight component of the magnetic field strength. Faraday rotation measures of pulsars have been made by Smith (1968), Lyne and Rickett (1968), Staelin and Reifenstein (1969) and Shitov (1971). Dispersion measures have been determined by Taylor (1969), Davies (1969), Goldstein and James (1969) and Davies and Large (1970). However the most comprehensive survey has been carried out by Manchester (1972) who finds that his data are consistent with a simple longitudinal field of strength $\sim$3.5 μgauss directed along the local spiral arm towards $\ell=90^{\circ}$ but he found no indication of a local helical component of the field.

A comprehensive survey of the same data by Roberts (1973) found that the pulsar data were consistent with a Theilheim type field provided that the solar system is sufficiently far below the galactic plane.

6.5 Synchrotron Radiation

6.5.1 Cosmic electrons in interstellar magnetic fields

When a relativistic electron gyrates in a magnetic field of strength H, it emits radiation with a specific intensity $I_\nu \propto H^{1+\alpha}\nu^{-\alpha}$ where $\alpha = (\frac{\gamma-1}{2})$ and γ is the spectral index of the differential energy spectrum for electrons. The theory of synchrotron emission is outlined in appendix (v). In a field of ∿1-10 μgauss, electrons of energy 10^9 eV are responsible for radiation of frequency range 10-400 MHz (equation v-2).

If the electron spectrum is known, then by measuring the synchrotron emission at various frequencies it is possible to evaluate the magnetic field strength. Figure 6-3 summarises the differential flux of cosmic ray electrons measured in the neighbourhood of the Earth, and relevant details of the experiments are found in table 6-1. Because of solar modulation, the spectrum below an energy ∿3 GeV deviates from the power law which is true for $E \geq 3$ GeV. What is more the degree of solar modulation varies over a period of eleven years, the solar cycle. A period of minimum solar modulation occurred in 1965-1966 as indicated in figure 6-3 where the measurements of Beedle and Webber (1967) and L'Heureux (1967) show a greater abundance of electrons of energy ≤2 GeV arriving at the Earth than the measurements made since that time. The power low fitted to the data of Zatsepin (1971) (beyond the region where the solar modulation is important) gives the following differential spectrum; $n_e(E) = 95 \pm 12\, E^{-2.70\pm0.05}$ $(m^2 \text{sec sr GeV})^{-1}$ which is in good agreement with that measured by Anand et al (1969) :- $n_e(E) = 126\ E^{-2.62\pm0.05}$ $(m^2 \text{sec sr GeV})^{-1}$. Using the more recent result of Zatsepin and assuming that this electron density extends throughout the whole of interstellar space, the value obtained for K is $7.03\ 10^{-17}$ $cm^{-3}erg^{-1}$ and for γ, 2.7.

By measuring the specific intensity over a known distance L of space at a particular frequency the magnetic field is calculated using

Table 6-1 Details of the experiments performed to establish the differential electron energy spectrum in the energy range 10^{-1}-10^{3} GeV

	Reference	Year Experiment Performed		Electron detector
✚	Bleeker et al 1969	1966-1968	Balloon	5 scintillation counters and lead glass $\check{C}$ counter
✚	Bleeker et al 1969	April-May 1968	OGO5	"
✚	Beedle et al 1969	1968-1969	Balloon	Gas $\check{C}$ detector-lead glass spectrometer
✚	Nishimura et al 1969	1968	Balloon	emulsion chamber
✚	Meyer, Muller 1971	1970	Balloon	Gas $\check{C}$ detector-lead glass spectrometer
✚	Silverberg et al 1971	April 1969 Nov. 1970	Balloon	Ionization spectrometer
✚	Marsden P.L. et al 1971	1968	ESRO 11	Gas $\check{C}$ detector + 2 scintillation counters in lead sandwich
✚	Swaneburg et al 1971	1968	OGO5	5 scintillation counters and lead glass $\check{C}$ counter
⋮	Anand et al 1968b	1968	Balloon	emulsion-lead sandwich
✚	Anand et al 1968a			
✚	Zatsepin 1971	1969 1970	Balloon	scintillation telescope
✚	L'Heureux 1967	1960-1964 1964-1966	Balloon	energy-loss vs range counter telescope energy-loss vs total energy counter telescope
■	Beedle, Webber 1967	1966	Balloon	scintillation counter telescope and gas C detector

I Demodulated spectrum taken by Davies (1965)

II Demodulated spectrum as calculated by Anand, Daniel and Stephens (1968b)

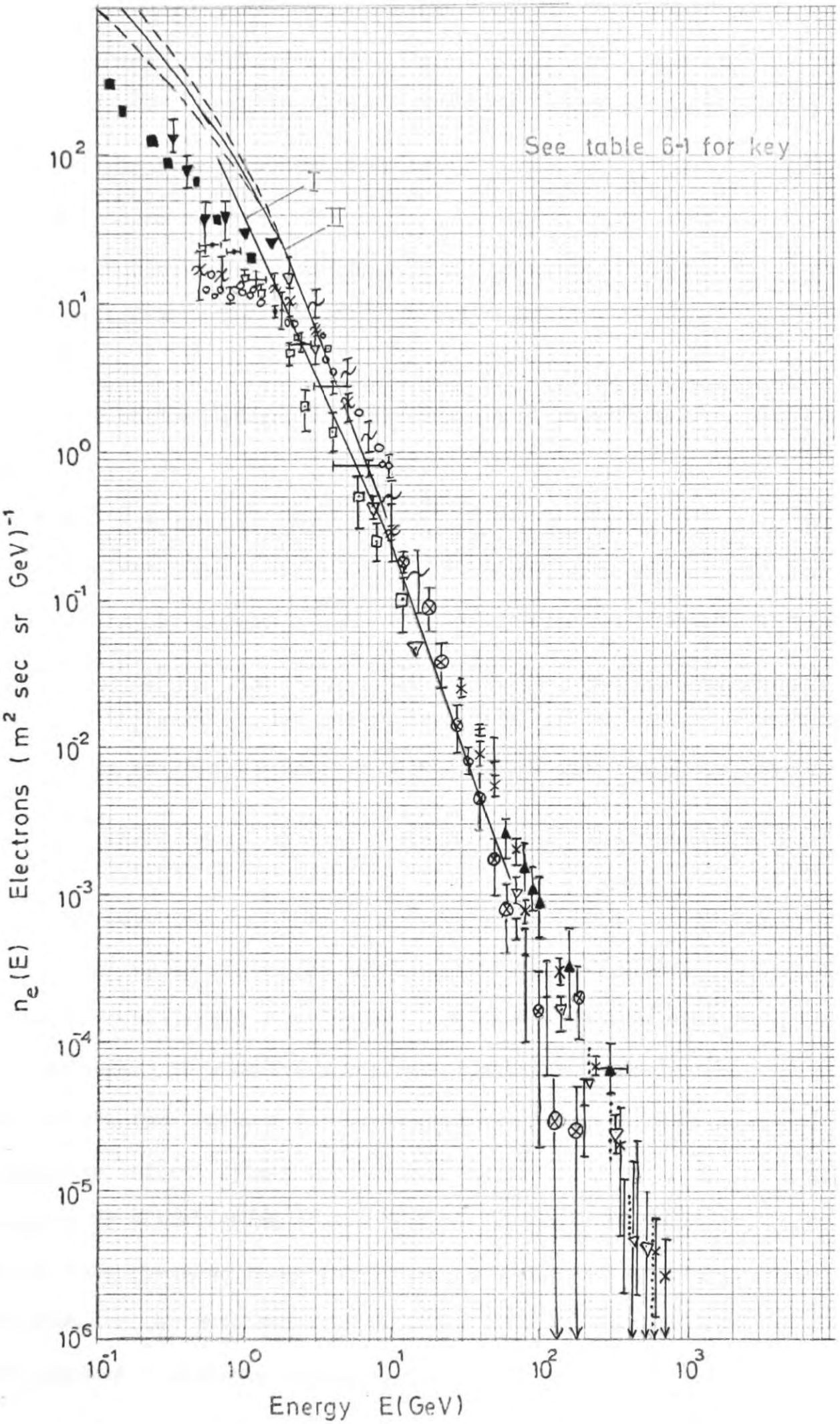

Figure 6-3 The differential electron energy spectrum.

$$I_\nu = 1{\cdot}36 \times 10^{-22}(6.26\ 10^{18})^{\frac{\gamma-1}{2}} H^{(\frac{\gamma+1}{2})} \nu^{-(\frac{\gamma-1}{2})} \alpha(\gamma)\ KL$$

$$\text{ergs sec}^{-1}\ \text{Hz}^{-1}\ \text{cm}^{-2}\ \text{sr}^{-1}$$

which follows from equation v-4.

Alternately if the brightness temperature is measured experimentally, equation v-5 defines the magnetic field, i.e. $T_b = 3.26\ 10^{36} I_\nu \nu^{-2}$.

Earlier measurements of synchrotron emission by Mills (1959), Baldwin (1958), Davies and Hazard (1962) and Davies (1965) show the presence of a halo field of ∿6-7 μgauss and superimposed on this is a disc field of ∿30 μgauss. Such high fields can be explained because at that time the electron spectrum was ill defined by measurements in the energy region in which solar modulation was important for example the solid line marked I in figure 6-3 was that used by Davies (1965). The synchrotron measurements appear to be overestimated because of experimental inadequacies and incorrect estimates of the path lengths. Also, associated with the regions where appreciable synchrotron emission occurs, are S.N.R. which are themselves sources of cosmic rays. This increase in electron density is not taken into account in the derivation of the magnetic field.

The most reliable work on synchrotron emission of the Galaxy has been carried out by Anand, Daniel and Stephens (1968b). Figure 6-4 is a schematic diagram of the Galaxy showing the different regions of space considered for the analysis. Figures 6-5 along with table 6-2 summarise the experimental data in the four regions (a) north galactic halo, (b) halo minimum, (c) anticentre and (d) galactic ridge, of the sky analysed. The brightness temperature distribution of the halo minimum and the north halo within errors have the same shape but differ in absolute magnitude by ∿0.3. The spectrum for the anticentre is slightly flatter than that for the halo but has comparable absolute intensities. The slope varies from about ∿0.3 at

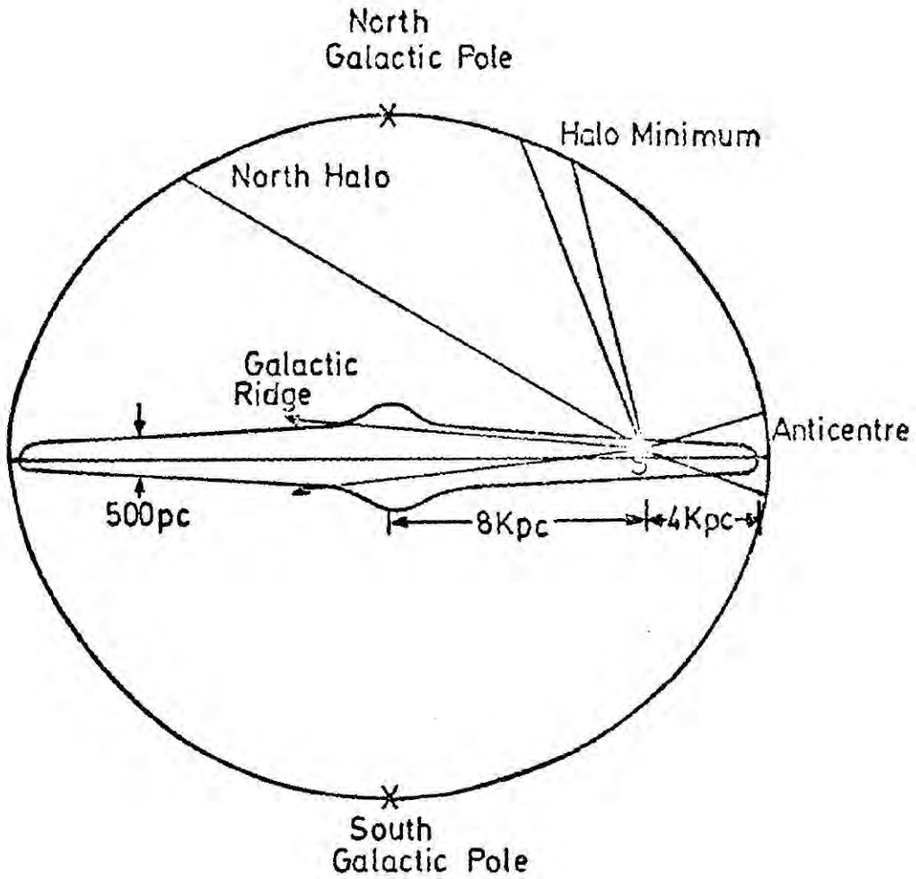

Figure 6-4 A schematic diagram of the Galaxy showing the different regions of space considered for the analysis Anand, Daniel and Stephens (1968b). (Not to scale).

Table 6-2

Radio flux data used in the analysis for the Galactic Ridge

Reference	Year	Frequency νMHz	Beam Width	Flux J_ν watt $m^{-2} sr^{-1} Hz^{-1}$ $x10^{21}$
Baldwin	1955	81.5	$2^\circ x15^\circ$	21.0
Hill et al	1958	86	$0^\circ.8x0^\circ.8$	17.0
Kraus and Ko	1955	250	$1^\circ x8^\circ$	11.2
Seeger et al	1960	400	$2^\circ x2^\circ$	8.7
Seeger et al	1965	400	$2^\circ.2x1^\circ.7$	9.7
Large et al	1961	408	$0^\circ.7x0^\circ$	8.35
Piddington and Trent	1956	600	$3^\circ x3^\circ$	8.9
Moron	1965	610	$0.5^\circ x0.5^\circ$	5.9
Denisse	1955	900	$0.8^\circ x0.8^\circ$	5-35
Wilson and Burton	1960	960	$0.8^\circ x0.8^\circ$	4.2
Westerhaut	1958	1390	$0.6^\circ x0.6^\circ$	3.2
Mathewson et al	1962	1440	$1^\circ x1^\circ$	3.04
Penzias and Wilson	1966	4080	$0.7^\circ x0.7^\circ$	1.28

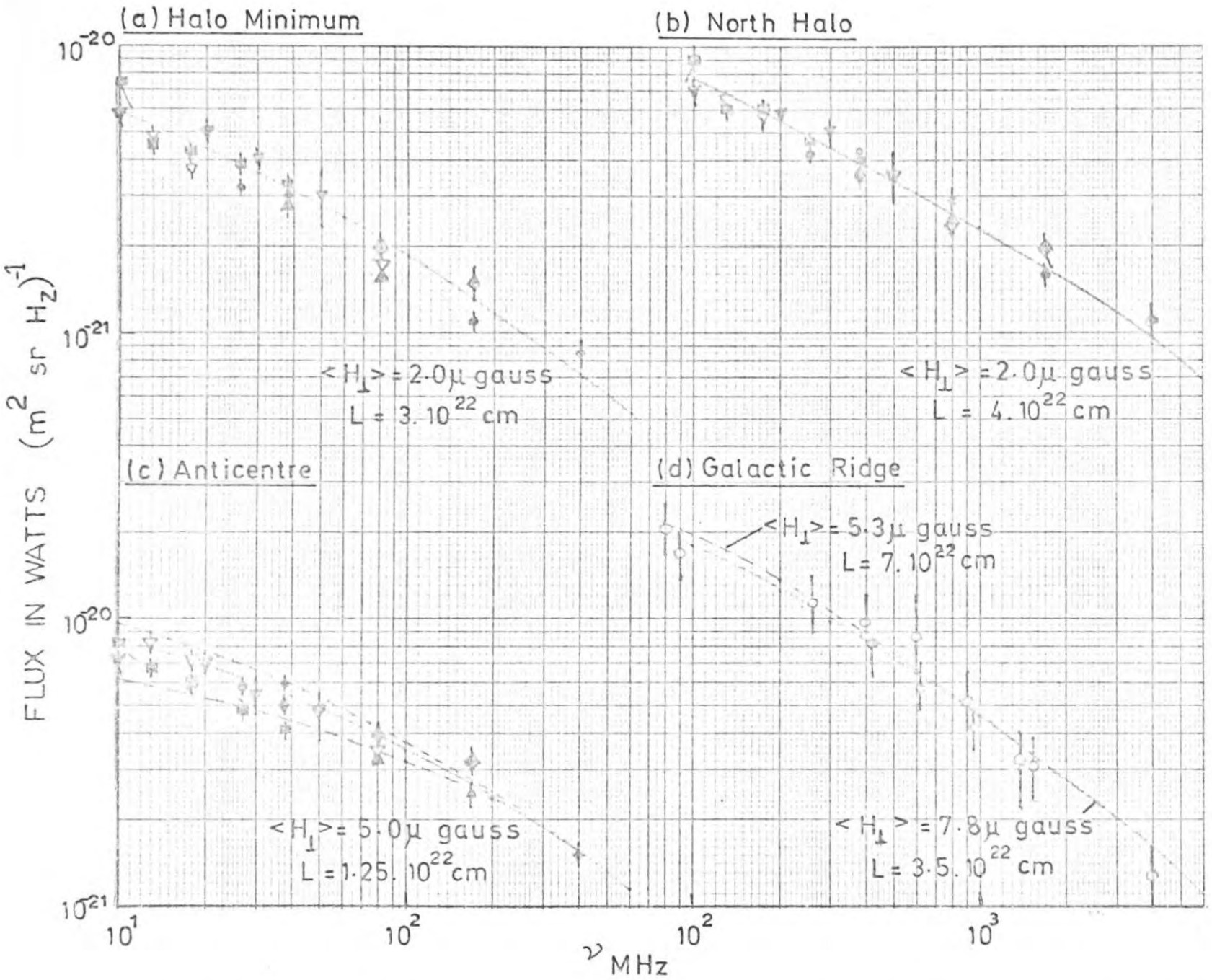

- ♦ Costain 1960
- • Turtle et al 1962
- ■ Andrew 1966
- ▲ Purton 1966
- ▽ Bridle 1967
- ▼ Parthasarathy & Lerfald 1965
- o Narrow angle beam surveys see table. 6-2

Figure 6-5 Radio brightness distributions in the directions a) Halo minimum, b) North Halo, c) Anticentre, d) Galactic Rigde. The solid curves were obtained using the electron spectrum II given in figure 6-3 and the dotted lines correspond to the dotted lines of figure 6-3.

the lowest frequencies to ∿0.8 at the highest frequencies. The fluxes plotted in figure 6-5 d have been carefully selected to avoid radiation from the galactic nucleus and any possible thermal radiation from the corona. Within experimental uncertainties this spectrum has a shape the same as that for the anticentre but with an intensity ∿6 times larger, also the slope is constant at ∿0.8 out to a frequency of 400 MHz.

Since the electrons with energy ≥5 GeV in the direction of the anti-centre are expected to have the same spectrum as those in the vicinity of the earth it is possible to select a particular value for the field and a unique smoothly varying electron spectrum to match the observed radio spectrum. Taking the value of L=4kpc in the anticentre direction a field of 5 μgauss was found to best fit the electron spectra (solid line figure 6-3) and the radio spectrum (solid line figure 6-5c). To show the sensitivity of the method on the electron spectrum used, the dotted lines in figure 6-5c illustrate the radio spectrum that would result from two slightly different electron spectra indicated by dotted lines in figure 6-3 but for the same L and H. Extending the calculations to the other parts of the Galaxy the best fit to the data are shown in figures 6-5a, 6-5b and 6-5e with fields and path lengths summarized in table 6-3.

6.5.2 Cosmic electrons in magnetic fields in discrete sources

Section 6.5.1. dealt with synchrotron radiation due to relativistic electrons, with an energy distribution the same as that observed at the Earth, moving in the interstellar fields. However, there are relatively small regions in the Galaxy where the synchrotron radiation is orders of magnitude higher than the general background emission. Associated with these regions are radio sources, super nova remnants, nebulae, or a mass of highly ionized H_{II} and the increase in synchrotron emission is caused

Table 6-3

For each of the regions of space considered, the magnetic field strength and the path length derived for the best fit to the radio synchrotron data (solid lines figure 6-5) for an assumed but unique electron energy spectrum (curve II figure 6.3)

Region of space	Assumed path length $Lx10^{-22}$ cm	Deduced magnetic field H μgauss
(a) Halo minimum	3.0	2.0
(b) North Halo	4.0	2.0
(c) Anticentre	1.25	5.0
(d) Galactic Ridge	3.5	7.8

by the high magnetic field associated with the body as well as an excess of electrons probably produced by the source. The angular size ϕ, of these sources is generally small and usually the spectral density of the emission flux defined as the energy flux per unit frequency range incident along the normal per unit area

$$F_\nu = \int_o^\phi I_\nu d\nu$$

is measured instead of I_ν, the specific intensity.

Because the linear dimension L cm is small compared with its distance away d cm, the absolute magnitude of the field strength and the relativistic electron concentration can be considered constant over the volume of the source. Thus equation v-4 reduces to

$$F_\nu = 1.36\ 10^{-22}(6.26\ 10^{18})^{\frac{\gamma-1}{2}}\ H^{\frac{\gamma+1}{2}}\ \nu^{-(\frac{\gamma-1}{2})}\ \alpha(\gamma)\ \frac{K_V}{d^2} \qquad 6\text{-}1$$

where $K_V = K_e V$ is the coefficient in the electron energy spectrum with respect to the total volume of the source $V = \frac{\pi L^3}{6}$. Assuming the electron energy spectrum is of the form

$$n_e(E)\ dE = K_V E^{-\gamma} dE \qquad 6\text{-}2$$

in the energy range E_1 and E_2 equivalent to a radio frequency ν_1 and ν_2 respectively. Substitution of K_V from 6-1 in 6-2 yields the total number of electrons in the specific energy range.

Assuming

(i) the magnetic field energy in the source and the energy of the relativistic particles (all cosmic rays) are in the first approximation equal

ie $W_{CR} = W_H = \frac{H^2}{8\pi}$

(ii) the total energy of all cosmic rays W_{CR} is simply proportional to the energy of the relativistic electrons W_e, measured experimentally

ie $W_{CR} = \kappa W_e$

the magnetic field strength is found to be

$$H = \left[48\kappa\ A(\gamma,\nu)\ \frac{F_\nu}{d\phi^3}\right]^{\frac{2}{7}} \qquad 6\text{-}3$$

where $\phi = \frac{L}{d}$ is the angular size of the source,

$$A(\gamma,\nu) = \begin{cases} \frac{2.96\ 10^{12}}{(\gamma-2)a(\gamma)}\nu^{\frac{1}{2}}\left[\frac{y_1(\gamma)\nu}{\nu_1}\right]^{\frac{\gamma-2}{2}}\left\{1-\left[\frac{y_2(\gamma)\nu_1}{y_1(\gamma)\nu_2}\right]^{\frac{\gamma-2}{2}}\right\} & \text{If } \gamma \geq 2 \\ 1.44\ 10^{13}\nu^{\frac{1}{2}}\ln\left[\frac{y_1(\gamma)\nu_2}{y_2(\gamma)\nu_1}\right] & \text{If } \gamma = 2 \\ \frac{2.96\ 10^{12}}{(2-\gamma)a(\gamma)}\nu^{\frac{1}{2}}\left[\frac{y_2(\gamma)\nu}{\nu_2}\right]^{\frac{\gamma-2}{2}}\left\{1-\left[\frac{y_2(\gamma)\nu_1}{y_1(\gamma)\nu_2}\right]^{\frac{2-\gamma}{2}}\right\} & \text{If } \gamma < 2 \end{cases}$$

ν_1 and ν_2 are the frequency extremes of the observed radio band in which the spectral index $\alpha = (\frac{\gamma-1}{2})$ has a constant value and $y_1(\gamma)$, $y_2(\gamma)$ and $a(\gamma)$ are defined in table 6-4.

Hence, a direct determination of the field strength can be made provided that the source's spectrum, angular size, distance away and the constant of proportionality κ is known. Only the latter is uncertain and really there is no reliable method of determining κ. Usually it is set equal to 100 but for the Crab nebula a value $\kappa \leq 1$ and for the radio Galaxy Virgo A, κ is low, according to Shklovsky (1963). In the present analysis the magnetic field strength is calculated in units of $\kappa^{2/7}$ with a maximum possible error of a factor of 3.7 in the resultant field.

A recent paper of Ilovaisky and Lequeux (1972) lists 116 galactic radio sources along with their position in galactic co-ordinates ℓ and b, angular size ϕ, flux density at 1000 MHz, distance from the L.S.R. dkpc, distance from the galactic centre r kpc, height above the plane zpc and the linear dimension of the source Lpc. Except for those sources analysed by

Table 6.4 The numerical values for $\alpha(\gamma)$, $y_1(\gamma)$ and $y_2(\gamma)$ as a function of γ

γ	1	1.5	2	2.5	3	4	5
$\alpha(\gamma)$	$2.83\ 10^{-1}$	$1.47\ 10^{-1}$	$1.03\ 10^{-1}$	$8.52\ 10^{-2}$	$7.42\ 10^{-2}$	$7.25\ 10^{-2}$	$9.22\ 10^{-2}$
$y_1(\gamma)$	0.8	1.3	1.8	2.2	2.7	3.4	4.0
$y_2(\gamma)$	$4.5\ 10^{-4}$	$1.1\ 10^{-2}$	$3.2\ 10^{-1}$	10^{-1}	$1.8\ 10^{-1}$	$3.8\ 10^{-1}$	$6.5\ 10^{-1}$

Milne (1971a) where a value of the spectral index α of the radio source spectrum is defined at 1000 MHz, α was set equal to 0.5. Assuming α is constant over the emitting frequency range of 10 - 10,000 MHz for all sources the magnetic field strength in units of $\kappa^{2/7}$ was calculated using equation 6-3. When the radio spectrum was known in detail a more accurate magnetic field strength was calculated for example the field for Sagittarius A, the source at the galactic centre, H_o = 34 μgauss, Downes and Maxwell (1966) and for the Crab Nebula a field H_o = 250 μgauss, Baldwin (1971).

6.5.3 Coherence of the magnetic field across radio sources

To find out if radio sources play any part in the diffusion of cosmic rays it is necessary to establish the degree of coherence of the field across the source and to compare the density distribution of $H_o R_o$ of radio sources with that of cloudlets and clouds.

Conway (1971) combined optical and radio measurements of polarization to find the configuration of the magnetic field throughout the Crab Nebula. In the central portion of the nebula the E vectors are aligned roughly parallel to the major axis indicating a magnetic field predominantly along the minor axis. Surrounding the central area there are a series of 'fans' in each of which the E vectors are arranged radially about the centre and the percentage polarization is as high as 50%. The 'fans' are related to prominent filaments which according to Woltjer (1957) (1958) are seats of powerful currents the magnetic field of which is arranged radially around the filament throughout a considerable volume. These properties are illustrated in figure 6-6 where the radio polarization of the Crab Nebula at a wavelength of 11cm (Conway, 1971) are plotted. The bar lines are proportional in length to the polarized intensity mI. Figure 6-7 shows the projected directions of magnetic field in IC443, the contours are the

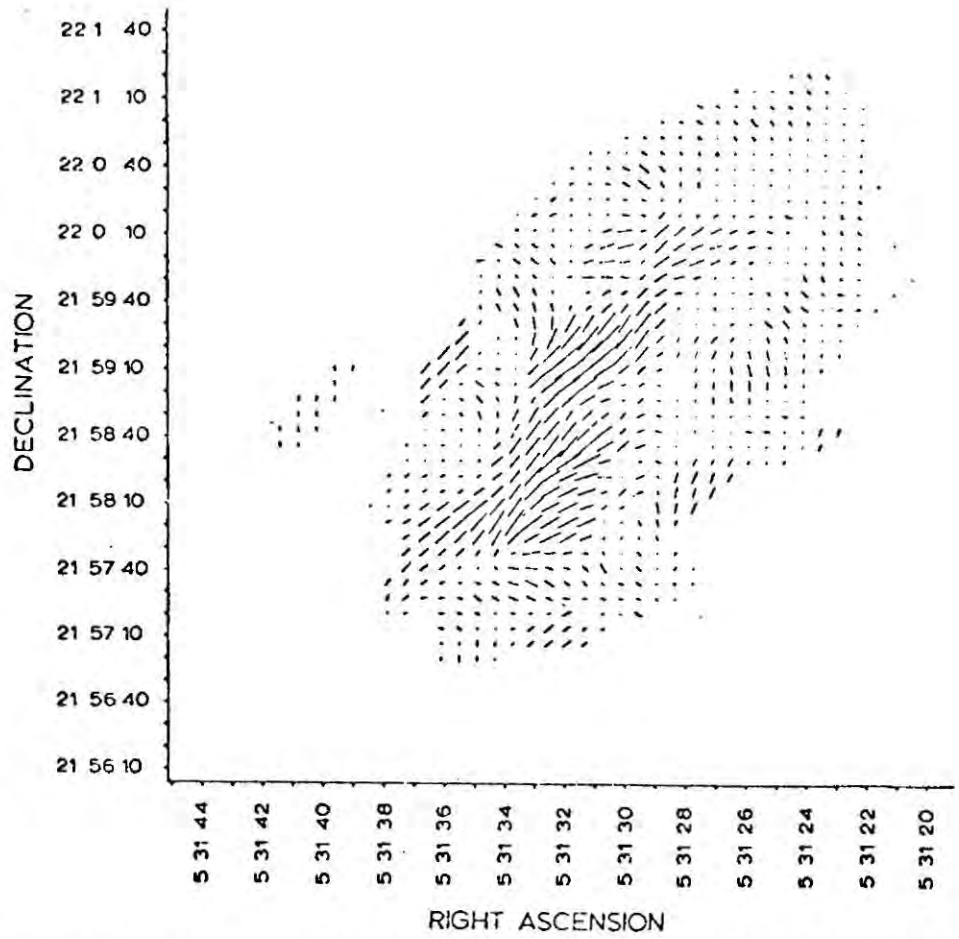

Figure 6-6 Radio polarisation of the Crab Nebula at λ-11cm. The bar lines are proportional in length to the polarized intensity mI. The beam is 8" x 14", with the larger dimension roughly parallel to the major axis of the nebula.

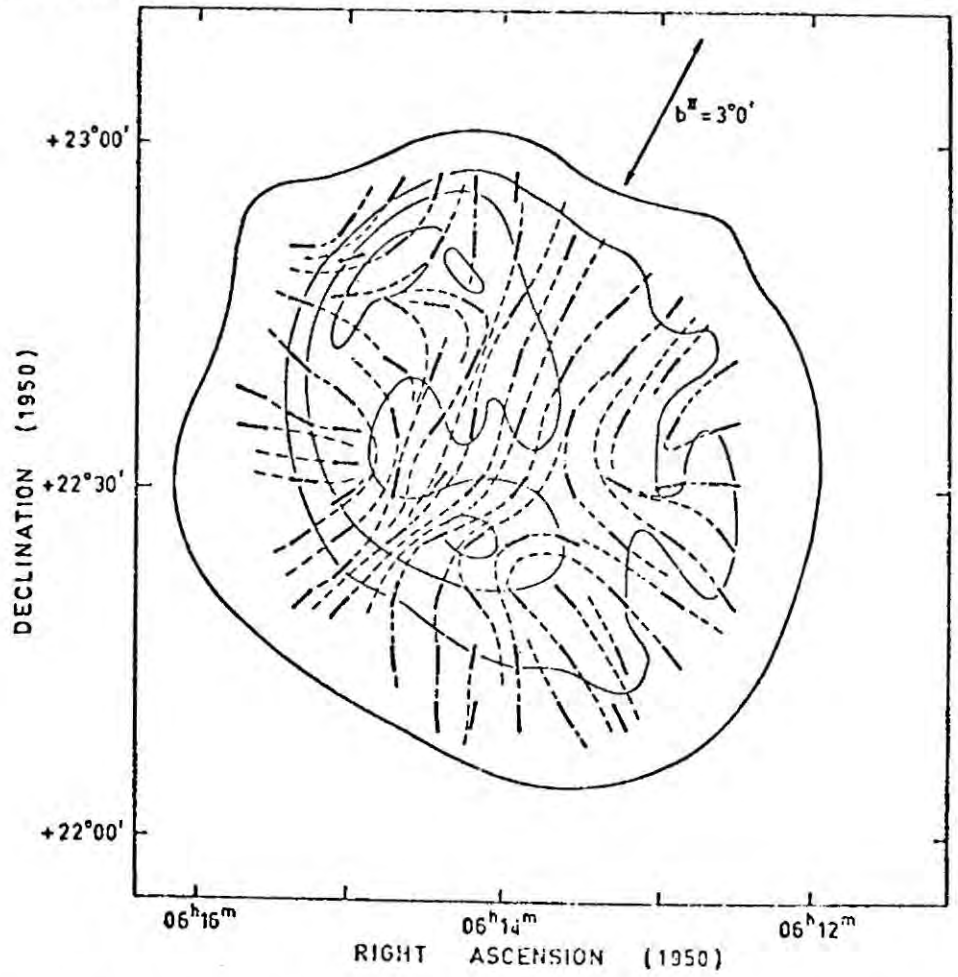

Figure 6-7 The projected directions of magnetic field in IC443; the contours are 5000 MHz isotherms. The magnetic field is predominantly radial Milne (1971).

5000 MHz isotherms, as measured by Milne (1971b). The magnetic field is predominantly radial.

Both the optical and radio polarisation measurements show that the magnetic field is reasonably coherent over the area occupied by the source.

6.6 The role played by SNR in cosmic ray diffusion

6.6.1 Density distribution of SNR

The 116 radio sources analysed above are plotted in figure 6-8 to show their position in galactic longitude and the distance from the L.S.R. They are thought to be a representative sample of the total number $\mathcal{N}$ in the Galaxy. Two values of $\mathcal{N}$ were considered. The first was calculated by assuming that the density of sources within 4 kpc of the solar system is typical of the rest of the Galaxy. The diameter of the Galaxy is thought to be $\sim$30 kpc and therefore the sampling area around the Sun is $\sim \frac{1}{14}$ of the total. Figure 6-8 shows that 41 sources lie within 4 kpc giving 574 for $\mathcal{N}$.

Ilovaisky and Lequeux (1972) in their statistical analysis of SNR found that most likely there are some 2500 SNR with a size less than 64 pc (maximum size measured experimentally) this is a factor of four higher than the previous estimate. Also in this work the density of SNR, with diameters D<30 pc and lying within 6 kpc of the Sun, was found to fall off with perpendicular distance z to the plane according to the expression

$$n(z) = n(0) \exp\left(\frac{-|z|}{90}\right), \quad z \text{ in pc}$$

This suggests that $\frac{\mathcal{N}}{e}$ of SNR lie within ±90 pc of the galactic plane. Assuming $\mathcal{N} = 2500$ the density of SNR was found to be $7\ 10^{-9}$. The resulting distribution for $H_o R_o$ μgauss pc is shown in Figure 6-9.

6.6.2 Density of cloudlets and clouds in the Galaxy

The cloudlets and clouds observed by Heiles (1967) were seen to be collected within two sheets which occupied approximately one tenth of the

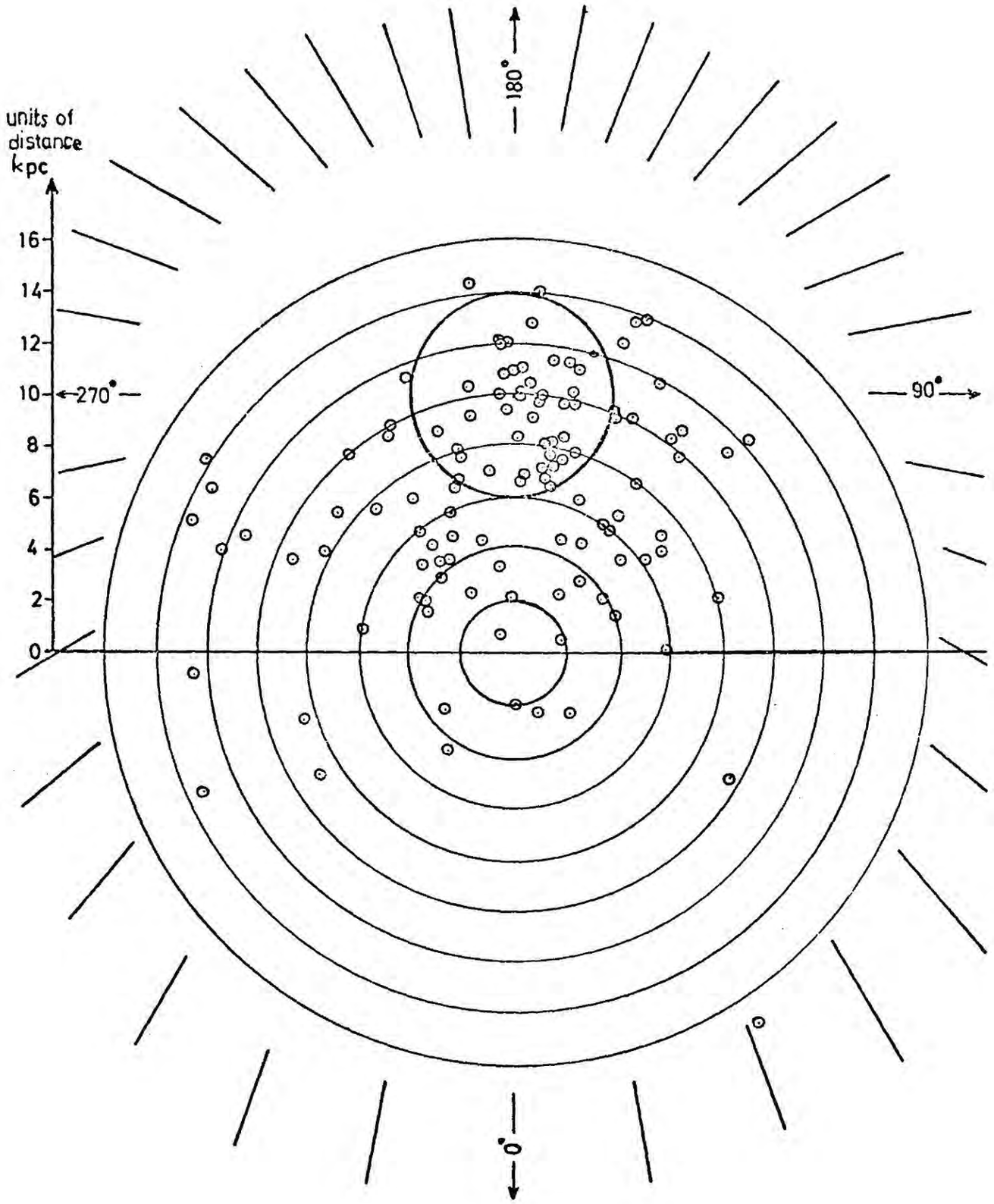

Figure 6-8 Sources analysed by Ilovaisky and Lequeux (1972).

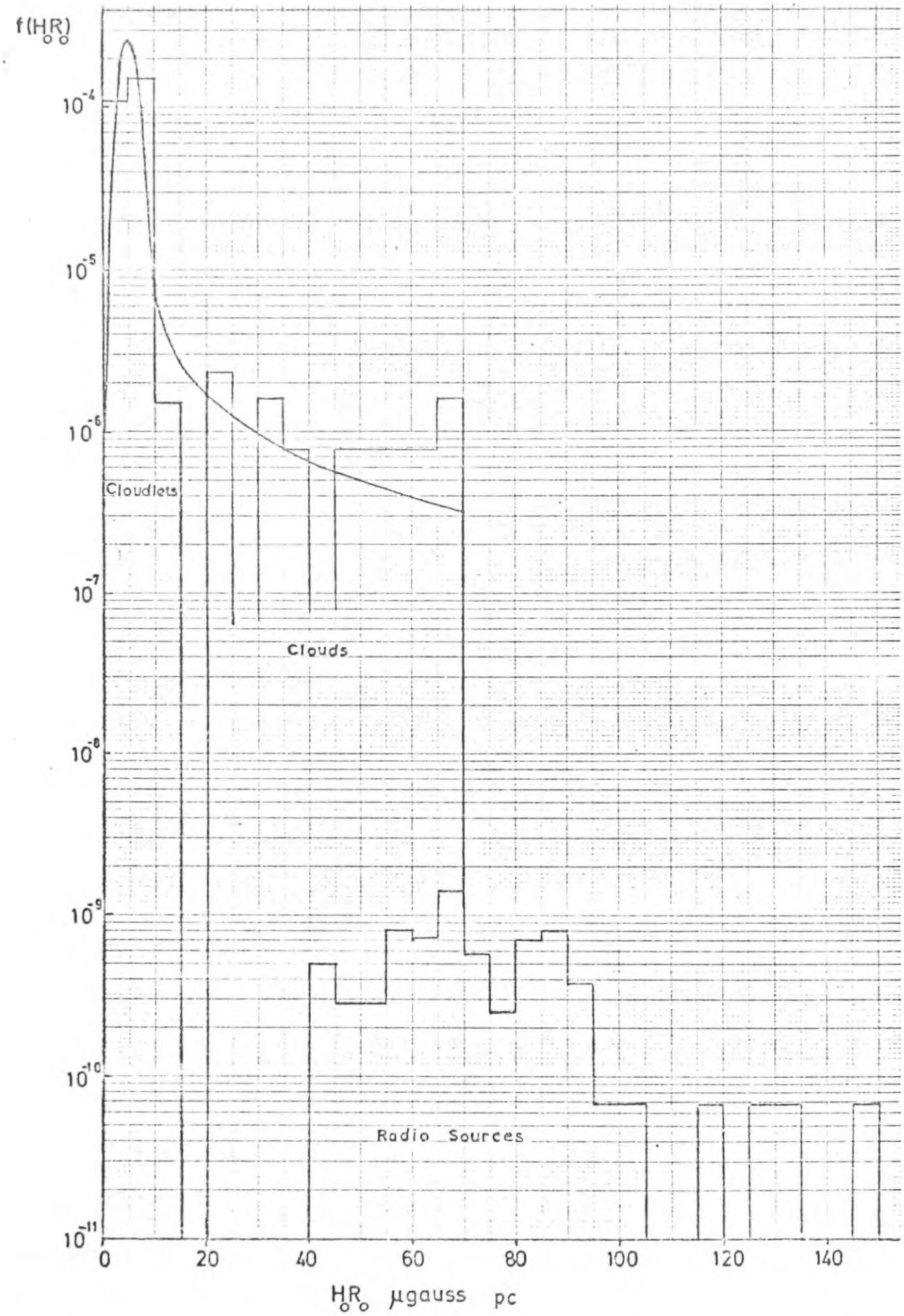

Figure 6-9 The distribution of H_oR_o for cloudlets and clouds, Heiles (1967), compared with that for radio sources Ilovaisky and Lequeux (1972).

total volume analysed. It is very unlikely that the distribution of H_oR_o figure 5-13 is typical of all other regions in galactic space but in the absence of any other data this has had to be used in order to make some progress with the present theory of diffusion of cosmic rays. A more realistic density for cloudlets and clouds in interstellar space as a whole was obtained by assuming that the 815 cloudlets and 13 clouds are distributed inside the total volume analysed by Heiles rather than being confined to the two sheets.

From figure 6-10 the volume was found to be $1.55\ 10^6$ pc^3 giving $5.26\ 10^{-4}$pc^{-3} and $9.68\ 10^{-6}$pc^{-3} for the density of cloudlets and clouds respectively. Using the relationship $H_oR_o = 1.27\ n_H^{2/3}R_o$ μgauss parsec the density distribution for cloudlets and clouds was recalculated and compared with that for SNR in figure 6-9.

6.6.3 Mean separation and mean free path of cloudlets, clouds and S.N.R.'s

The mean radii $\bar{R}$, for cloudlets, clouds and S.N.R.'s are 2.8, 16.2 and 24.6 pc respectively and their respective densities $\mathcal{N}$ have been shown to be $5.26\ 10^{-4}$, $9.68\ 10^{-6}$ and $7\ 10^{-9}$ pc^{-3}. The mean separations, $\bar{L}$, for cloudlets, clouds and S.N.R.'s are respectively 7, 15 and 475 pc defining $\bar{L} = \left(\frac{1}{\mathcal{N}}\right)^{1/3} - 2\bar{R}$. The mean free paths, $\bar{\lambda}$, for cloudlets, clouds and S.N.R.'s are found to be approximately 77, 125 and 10^5pc respectively provided that $\bar{\lambda} = 1/\mathcal{N}\pi\bar{R}^2$.

6.7 Conclusion

Measurement of the Zeeman splitting of the 21cm hydrogen line gives the line of sight component of the magnetic field only. The data are consistent with the local field of 1-5 μgauss spiralling around the Orion arm. A magnetic field of 3-10 μgauss is expected in the Perseus arm. The magnetic field inside a hydrogen cloud is related to the density by the empirical relationship $H_o = 1.27\ n_H^{2/3}$ μgauss.

No reliable value for the strength of the magnetic field is obtainable from interstellar polarization measurements because very little is known about

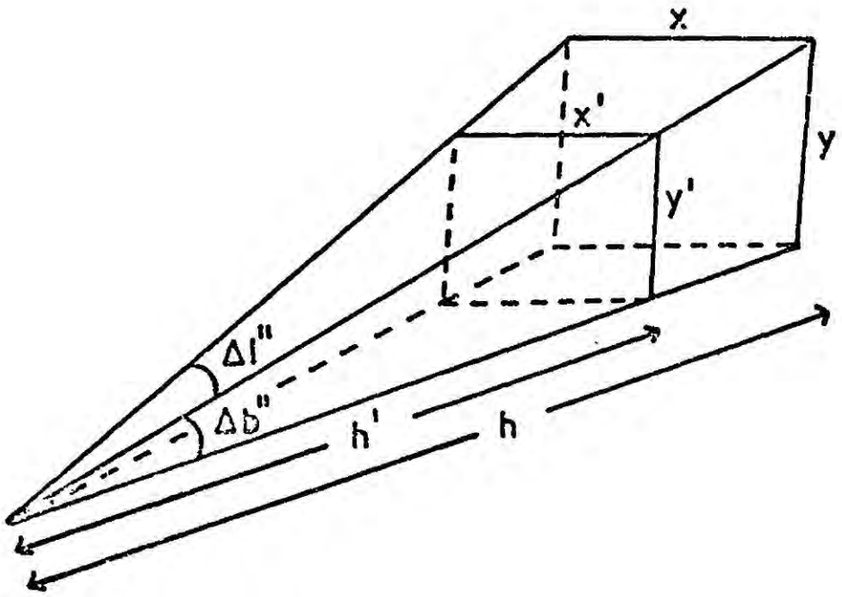

$$\text{Total Volume} = \frac{1}{3}(x\,y\,h - x'y'h')$$

$$= \frac{(2\pi)^2}{3}\,\Delta l\,\Delta b\,(h^3 - h'^3)$$

$\Delta l'' = 0{\cdot}11^c$, $\Delta b'' = 0{\cdot}011^c$, $h = 500\,pc$, $h' = 310\,pc$.

$$\underline{V = 1{\cdot}55\ 10^6\ pc^3}$$

Figure 6-10 The volume of space analysed by Heiles (1967).

the nature, distribution of sizes, and alignment mechanism of the grains. However, this method does prove successful for determining the orientation of the local magnetic field. A field strength of 3 μgauss is not inconsistent with experiment and the observations suggest two possible models for the orientation of the magnetic field. Either a "quasi-longitudinal" model in which the magnetic field lines are parallel to the spiral arms or a "helical" model in which the magnetic field helices wind round the spiral arm.

The derivation of magnetic fields from Faraday rotation measures is very unreliable because the region in space and the electron density where the rotation occurs are ill defined. However, a local field of 3 μgauss with a mean galactic field of 10 μgauss are typical, with 20% of the full scale field being coherent. Pulsar dispersion measures, together with Faraday rotation measures, predict a longitudinal field of 3.5 μgauss with a direction reversal above and below the plane. A helical magnetic field anomaly associated with the Gould Belt is probable.

Synchrotron measurements indicate a disc field decreasing with increasing distance from the galactic centre. A field of 7.8 μgauss is measured for the galactic ridge and 3 μgauss for the anticentre region. The halo field is 2 μgauss.

On average the magnetic field strength associated with a S.N.R. is a factor of five higher than the field strength of a cloudlet or cloud and the field is coherent over areas $\sim$500 pc^2. However, S.N.R. play no role in the diffusion of cosmic rays because (a) as seen from figure 6-9 the H_oR_o distribution of S.N.R. is insignificant compared with that for the cloudlets and clouds, Heiles (1967) and (b) the mean free path for cosmic rays colliding with S.N.R. being 10^5pc is three times the size of the Galaxy!

Chapter 7 Diffusion of cosmic rays in a physical Galaxy

7.1 Introduction

As a result of an extensive survey of the information available on the structure of the Galaxy it has been possible to conclude that only the work by Heiles (1967) provides the information on the small scale structure of hydrogen (in the form of clouds) within the spiral arms needed to make further developments with the diffusion model. It has been possible to derive the frequency distribution $f(H_oR_o)$, where H_o is the mean field in a cloud of radius R_o, from his results in two ways. The first, model A, is based on the assumption that the magnetic field in the clouds is constant and the mass distribution is a simple power law whilst the second, model B, takes into account the possibility of varying fields inside neutral hydrogen concentrations such that there are approximately a thousand times more clouds with a value of $p_o \sim 4$ pc cm^{-2} than clouds with a $p_o \geq 7$ pc cm^{-2}.

In this chapter the diffusion of cosmic ray protons inside these two physical media will be established and then the existence of heavy primaries in the primary radiation at energies in the region 10^9-10^{11} eV will be discussed in relation to the derivation of the modulated energy spectrum representing diffusion of cosmic ray primaries with mixed composition at an energy $\sim 10^{16}$ eV. The mean atomic mass as a function of energy predicted by the diffusion models will also be presented. An estimate will be made for the isotropy expected for the case of cosmic ray diffusion in a physical medium.

7.2 Diffusion of protons in a physical galactic medium

7.2.1 Definition of the mean free path for protons in a physical medium

We found in Chapter 5 that the magnetic clouds possess a spectrum of $H_oR_o \propto p_o$ therefore the mean free path can be written as

$$\frac{1}{\lambda(p)} = \int_0^\infty \int_0^\infty \pi\, n\,(R_o,p_o)\; R_o^{\,2}\; \bar{t}\;(p,p_o)\; dR_o\; dp_o \qquad 7.1$$

where $n(R_o,p_o)$ is the density of clouds of radius R_o and field strength H_o per (eV/c) per unit radius per unit volume, $\pi R_o^{\,2}$ is the geometrical cross section for a three dimensional treatment. $\bar{t}(p,p_o)$ represents the mean time for a cosmic ray of momentum p to escape from the spiral arm assuming that a uniform distribution of clouds with constant p_o (i.e. constant cloud size R_o and magnetic field H_o) to exist as the interstellar medium.

Defining the total area of all the clouds with the same scattering power as

$$A = \int_0^\infty \pi\, R_o^{\,2}\; n(R_o,p_o)\; dR_o$$

then since the total number of these clouds is defined by

$$f(p_o) = \int_0^\infty n(R_o,p_o)dR_o$$

and total area = total number x average area then

$$A = f(p_o)\; \pi\; \langle R_o^{\,2} \rangle$$

An analysis of Heiles data (figure 5.14) shows that $p_o = 1.3\; R_o^{1.2}$ which suggests a weak dependence of magnetic field H_o on the cloud size R_o i.e. $H_o = 1.65\; R_o^{0.2}$ μgauss. It follows that $R_o^{\,2} = 0.65\; p_o^{5/3}$. The integral 7.1 simplifies giving

$$\frac{1}{\lambda(p)} = 0.65\pi \int_0^\infty f(p_o)\; p_o^{5/3}\; \bar{t}(p,p_o)dp_o \qquad 7.2$$

which defines the mean free path as a function of momentum.

7.2.2 Derivation of the proton energy spectrum from the reciprocal mean free path

Because of the problems encountered in defining the absolute relationship between λ and D, an absolute time of escape for particles from the spiral arm is not obtainable. Consequently it is impossible to obtain the total flux of cosmic rays absolutely even if the cosmic ray production spectrum were known. It is sufficient here to assume that the cosmic ray intensity at the Earth $J(E)dE$ is proportional to $\frac{J_p(E)dE}{\lambda(E)}$ where $J_p(E)$ is the cosmic ray intensity at the source defined by equation 4.11 and $\lambda(E) = \lambda(300 p_o c) \propto \lambda(p_o)$. The resultant curve is then normalised to the experimental data at an energy remote from the "knee" at the low energy end. The energy is defined absolutely from the momentum p since $E = 300\ pc = 300\ H\ R$, which means that the $H_o R_o = p_o c$ values which are characteristic of the galactic medium define the energy of the cosmic ray it diffuses. Conversion of p_o pc cm^{-2} to energy in eV is obtained by multiplying by the factor $1.14\ 10^{15}$.

7.2.3 Model A

An analysis of Heiles data shows that the mean density of hydrogen in the cloudlets and clouds is 2 and 3.9 hydrogen atoms cm^{-3} respectively. It has been shown that the magnetic field is proportional to the two thirds power of the hydrogen density giving the mean fields for cloudlets and clouds to be 2 μgauss and 3 μgauss respectively. Because the fields differ only slightly the magnetic field is assumed to be constant and equal to 2.3 μgauss for cloudlets and clouds irrespective of their sizes.

Heiles (1967) gives the distribution of masses for cloudlets only (figure 5-10b). The most common of the masses are 3-4 $M_\odot$, the distribution falls off very rapidly and levels off beyond 12 $M_\odot$. The maximum

mass of any cloudlet observed was 24 $M_\odot$. Field (private communication with Heiles) finds that the mass spectrum of cloudlets is well approximated by an inverse square power law over the range 6-20 $M_\odot$ which is consistent with Saltpeter's (1955) initial luminosity function for stars, which also can be fitted fairly well over the range 9-25 $M_\odot$ by an inverse power law. As can be seen in figure 5.10b the distribution of cloudlets observed by Heiles (1967) is also well fitted by an inverse square power law over the mass range 6-24 $M_\odot$. However, the mass distribution for Heiles' clouds cannot be established with any degree of accuracy because of the limited number of clouds observed. Perry and Helfer (1972) in their statistical analysis of 21 cm data derived models of the density distribution of interstellar gas in small volumes of the spiral arms. They found that the cloud mass spectrum is very well described by a power law $f(M)dM \propto M^{-\beta}dM$ with $\beta=1.8\pm0.2$ for the Perseus arm and $\beta=2.0\pm0.2$ for the interarm features for cloud masses $10^3 \lesssim M \lesssim 10^6 M_\odot$. For the development of model A the mass distribution is assumed to be an inverse square power law consistent with experimental data.

The analysis of Heiles data figure 5.11 shows that $M \propto R_o^{3.3}$, therefore, since by definition

$$f(M)dM = f(R_o)dR_o$$

and $f(M)dM \propto M^{-2}\, dM$

$$f(R_o)dR_o = f(M)\left(\frac{dM}{dR_o}\right) dR_o$$

then $f(R_o)dR_o \propto R_o^{-4.3}dR_o$

since $p_o c = 300\, H_o R_o$ and H_o is constant $p_o \propto R_o$

and $f(R_o)dR_o = f(p_o)dp_o \propto p_o^{-4.3}\, dp_o$

This gives for the mean free path

$$\frac{1}{\lambda(p)} = 0.65\ \pi \int_{o}^{p_{o_{max}}} p_o^{-2.7}\ \bar{t}\ (p,p_o)\ dp_o \qquad 7.3$$

Assuming that the inverse square power law is valid for clouds as well as cloudlets, since the maximum sized cloud observed by Heiles was 36 pc and the mean constant field assumed is 2.3 μgauss then the upper limit of the integration is 83 μgauss pc or 65 pc cm^{-2}.

The integration 7.3 was performed by computer for different values of p/p_o. The reciprocal mean free path as a function of momentum is plotted in figure 7.1 and is marked by II-A.

For comparison the results for diffusion in an idealised medium are shown by the curve marked I, the statistical errors of $\pm\sigma$ of the numerical calculation are also shown. The effect of assuming that clouds have a constant field and a power law spectrum for cloud sizes: $f(R_o)dR_o = R_o^{-4.3}dR_o$ is to increase the curvature of the spectrum in the region of the "knee" compared with the spectrum representing diffusion in an idealised medium. The parameters defining the curve are $f_d = 0.56$, $\Delta\gamma\sim2$ and the position of the "knee" occurs at an energy $E_K\sim2\ 10^{15}$eV.

Model II-A has unfavourable characteristics, a) there is a very gradual transition region with $f_d = 0.56$, a value which is very much less than that observed experimentally ($f_d\sim1.0$) and, b) there is no indication of a change in slope other than $\Delta\gamma\sim2$ over any appreciable range in momentum. (Experimentally we observe a change of slope $\Delta\gamma\sim0.6$ over at least two decades in energy).

7.2.4 Model B

In section 5.2.4 the distribution of p_o found to be the "best" fit to the data of Heiles (1967) was

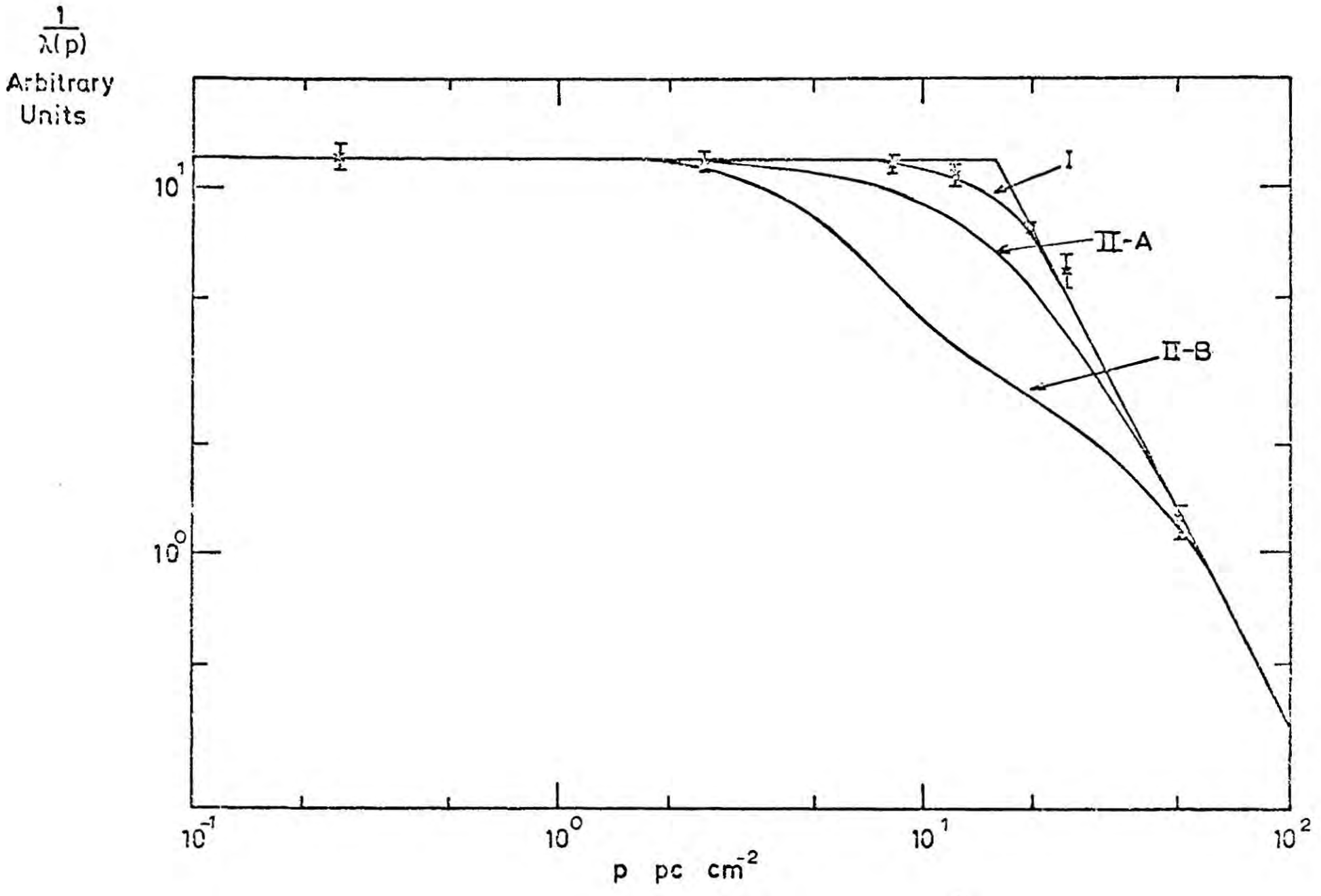

Figure 7-1 The reciprocal mean free path as a function of p pc cm^{-2} for diffusion of cosmic ray protons in an idealised medium (curve I) compared with that in a physical interstellar medium (curves marked II-A and II-B)

$$f(p_o) = 0.243 \exp - \left[\frac{(p_o-4.08)^2}{2.974}\right] + 0.053 \times 0.233\ p_o^{-1.3}$$

The Gaussian fits the data over a range of p_o defined by $0<p_o<6$ pc cm^{-2} and the power law fitted the data over a range of p_o defined by $6<p_o<54$ pc cm^{-2}. Therefore, the reciprocal mean free path is defined by the following integrand:

$$\frac{1}{\lambda(p)} = 0.65\pi \int_o^6 0.243 \exp - \frac{(p_o-4.08)^2}{2.974}\ p_o^{5/3}\ \bar{t}(p,p_o)dp_o + \int_6^{54} 0.053 \times$$

$$0.233\ p_o^{0.4}\ \bar{t}(p,p_o)dp_o \qquad 7.4$$

The solution of this integral was obtained by computer. The reciprocal mean free path for model B is plotted as a function of momentum in figure 7.1 and is marked by II-B. The characteristics of this curve are $f_d = 0.90$, $\Delta\gamma=0.79$ and the position of the "knee" occurs at an energy $E_K = 3.4\ 10^{15}$eV.

7.2.5 The discovery of important relationships between the characteristics of the energy spectrum implied by Model II-B and the shape of the p_o distribution

Plotted in figure 7.2 is the contribution of the two integrands defined by equation 7.4 to the total reciprocal mean free path which is also shown. From a study of the build up of the curve defined by $\frac{1}{\lambda\ (p)}$ with respect to the shape of the distribution $f(p_o)$ shown in figure 5.13, the following important conclusions have been drawn.

a) The curve marked G is effectively the result of integrating over cloudlets and the curve P, over clouds.

b) The position of the "knee" in the implied energy spectrum is mainly defined by the peak of the distribution $f(p_o)$. It follows that

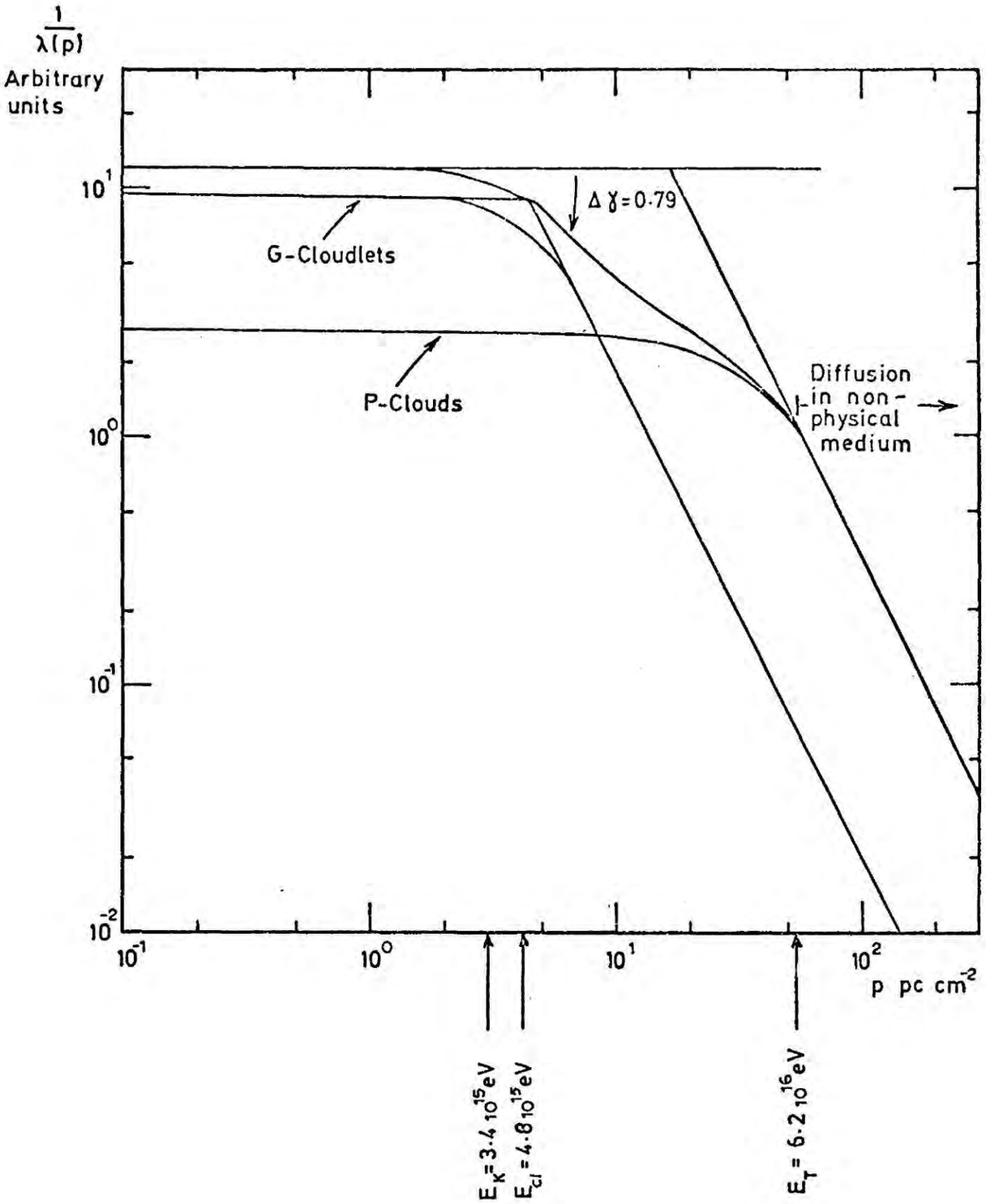

Figure 7-2 The reciprocal mean free path as a function of p for diffusion of cosmic ray protons in the physical medium defined by model II-B.

the energy at which the change of slope occurs due to circular hydrogen concentrations with magnetic fields H_o coherent over R_o pc is

$$E_{c\ell} = 300\ H_o R_o$$

Since the peak of the distribution for cloudlets occurs at $(n_H^{2/3} R_o) = 4.2$ pc cm^{-2}

$$E_{c\ell} = 4.8\ 10^{15} \text{eV}$$

c) The change of slope for the total spectrum occurs at a value of p_o=3 pc cm^{-2} i.e. $E_K = 3.4\ 10^{15}$eV indicating that clouds do have some, although small, influence on the position of the "knee".

d) The change of slope $\Delta\gamma$=0.79 and its linearity depends on the width of the Gaussian fitted to the cloudlets, the relative number of cloudlets $n_{c\ell}$with respect to the number of clouds n_c and the shortage of clouds with $p_o \sim 10$ pc cm^{-2}.

e) The maximum value of p_o observed experimentally defines the energy E_T at which the change of slope returns to $\Delta\gamma \simeq 2$, i.e. where diffusion returns to that defined by an idealised medium. $\Delta E = E_T - E_K$ gives the range of energy over which the change of slope of $\Delta\gamma$=0.79 is 'constant'. For Heiles data the maximum value for p_o is 54 pc cm^{-2} giving $E_T = 6.2\ 10^{16}$eV. It is very satisfactory to find that the geometric limit lies beyond this energy E_T implying total isotropy of cosmic rays up to this energy.

Finally, it is interesting to mention that provided there are present in the Galaxy, a) a large number of cloudlets with $H_o R_o \sim 4$-5 μgauss pc, b) the ratio $\frac{n_{c\ell}}{n_c} \sim 10^3$ and c) a shortage of clouds with $H_o R_o \sim 10$ μgauss pc an energy spectrum with favourable features would be obtained.

7.3 The diffusion of cosmic rays of mixed composition in a physical Galaxy

7.3.1 The theory for deriving the spectrum for mixed composition from the proton spectrum

Up to now we have only considered the case of diffusion of cosmic ray protons in the Galaxy. Direct experimental observations of cosmic rays at the top of the atmosphere reveal a mixed composition for cosmic ray primaries. As Peters (1961) has pointed out, the scattering process depends on the rigidity $R' = \frac{pc}{Ze}$ rather than momentum alone. For this reason, when we deal with cosmic rays of mixed composition, i.e. nuclei with different Z, the position of the knee moves to an energy/nucleus higher by the factor Z with respect to protons. Consider figure 7.3 where the abundance of cosmic rays of nuclear charge Z_1, Z_2, $Z_3 \ldots Z_i$ is respectively RA_1, RA_2, $RA_3 \ldots RA_i$ relative to protons ($Z = 1$, $RA_o = 1$). If the energy spectrum for protons is $J_o(E)$ then the spectrum for a mixed composition is defined at an energy E by

$$J_{MC}(E) = J_0(E) + RA_1 J_0(^{E}/_{Z_1}) + RA_2\, J_0(^{E}/_{Z_2}) + \ldots + RA_i J_0(^{E}/_{Z_i}) \quad 7.5$$

The effect of taking into account the possibility of there being a mixed composition is to decrease the change of slope occuring at the "knee".

7.3.2 The energy spectrum for mixed composition defined by the diffusion models II-A and II-B

In chapter 3 a critical review was made of the experimental work involved with establishing the relative abundance of cosmic ray primaries as a function of energy for energies ≤ 1 GeV. This knowledge is used to imply the chemical composition of cosmic rays at EAS energies because at these energies it is impossible to establish directly the chemical composition with any degree of accuracy.

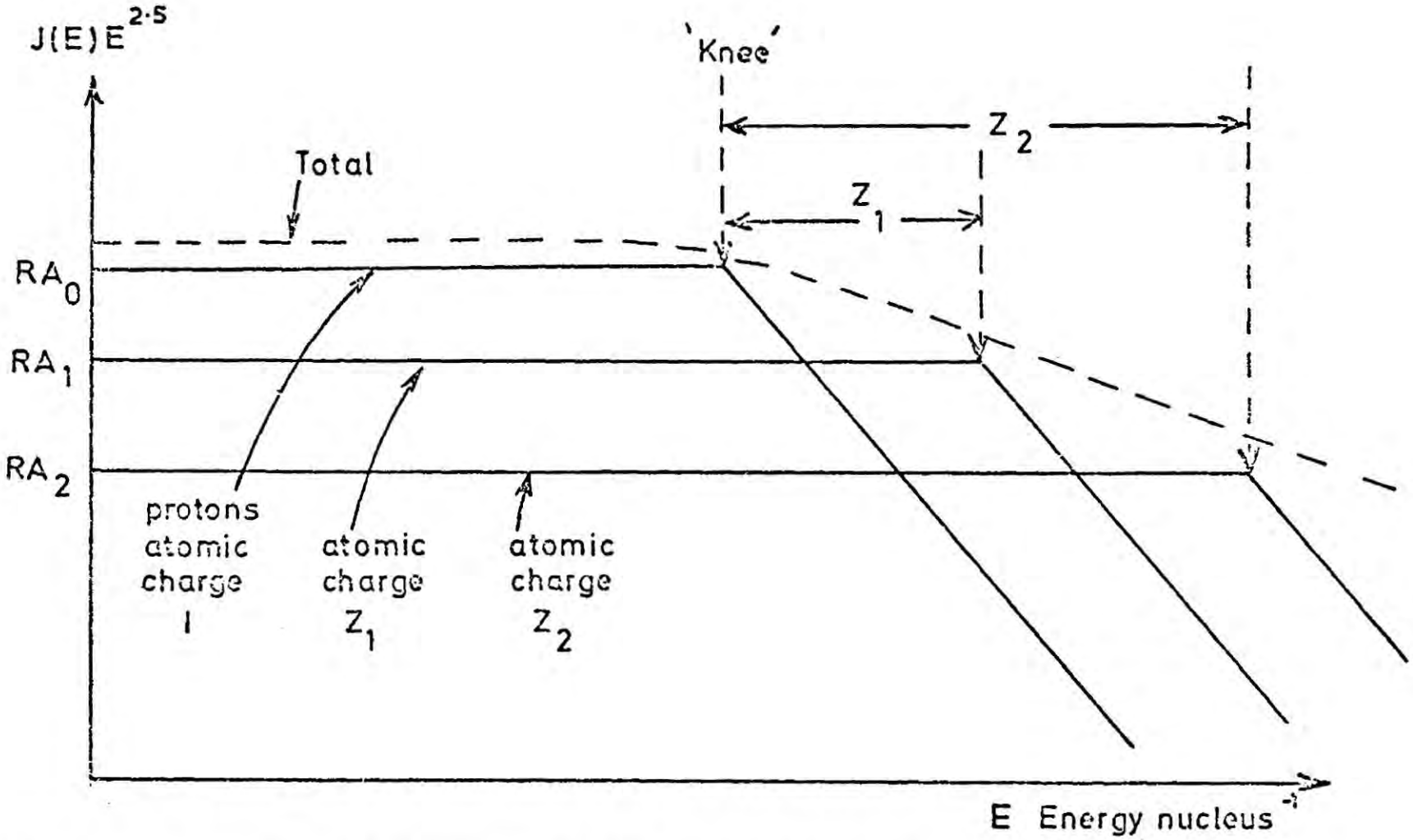

Figure 7-3 A schematic representation of the effect of galactic modulation of cosmic rays with atomic charges Z_1, Z_2, Z_3 ... Z_i and abundance relative to protons RA_1, RA_2, RA_3 ... RA_i respectively.

The best estimate for the relative abundances of cosmic rays with energies $\lesssim$1 GeV was defined by $p/\alpha = 18$ along with the relative abundance for individual elements $Z \gtrsim 2$ as determined by Cartwright et al (1971) listed in Table 3.5. However, two conflicting results exist with respect to the energy dependence of the relative abundances of certain elements present in the cosmic ray radiation below energies $\sim$1 GeV. These will be dealt with in turn.

(a) The earlier experimenters found that within experimental error the relative abundances of all elements in the primary cosmic radiation remain constant with energy. Therefore in a conservative model we assume the best estimate of the relative abundances observed at energies <1 GeV are the same at the energies with which we are involved in cosmic ray diffusion in the Galaxy. By evaluating equation 7.5 by computer the two differential energy spectra for mixed composition were established using the proton spectra defined by the models II-A and II-B respectively. These spectra are shown in figure 7.4 normalised to each other at positions remote from the "knee". The parameters that characterise these curves are for model II-A and II-B respectively f_d=0.92, $\Delta\gamma$=0.74, E_K=7.6 10^{15}eV, E_T=6.3 10^{16}eV and f_d=0.91, $\Delta\gamma$=0.58, E_K=4.8 10^{15}eV, E_T=1.2 10^{17}eV.

(b) The recent work of Balasubrahmanyan and Ormes (see chapter 3) claims that there is a slight dependence of the abundance of light to medium nuclei, i.e. $\frac{J(E)_L}{J(E)_M} \propto E^{0.14\pm0.07}$ where $J(E)_L$ and $J(E)_M$ are the cosmic ray intensities of light and medium nuclei respectively, as well as a strong dependence of the relative abundance of Fe with respect to C, i.e. $\frac{J(E)_{Fe}}{J(E)_C} \propto E^{0.52\pm0.15}$ for cosmic rays of energies $\gtrsim$2 GeV. Extrapolation of the spectra of the elements concerned to energies $\gtrsim 10^{14}$eV has the following effects: for the light nuclei, its energy dependence

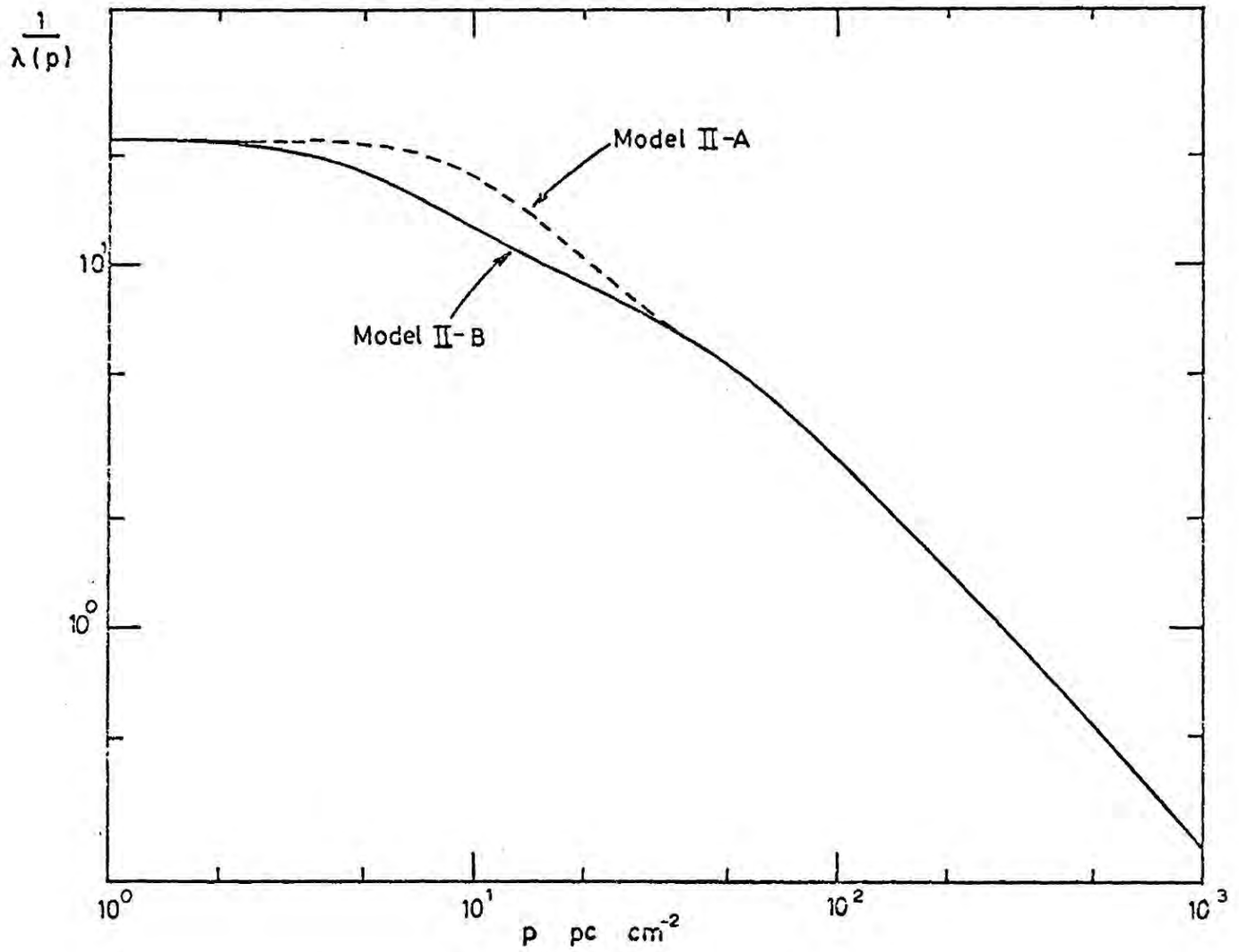

Figure 7-4 The reciprocal mean free path for cosmic rays of mixed composition as a function of p for models II-A and II-B.

with respect to medium nuclei can be ignored because the abundance of light nuclei is small compared with that of medium nuclei; however, the effect of extrapolation of the Fe spectrum is such that it crosses over that of the proton (assuming the spectral index for protons is the same as for carbon atoms) spectrum at $\sim 10^{13}$eV. This has drastic effects on the shape of energy spectrum beyond 10^{14}eV. Firstly the position of the knee will be shifted to 6.6 10^{16} eV which is in total disagreement with experiment. Secondly, and more important, the entire spectral shape will be modified by a factor $E^{0.52\pm0.15}$ i.e. $J_o(E) = J_o(E)\ E^{0.52} \times$ (Abundance of Fe with respect to protons). This would result in a power law with spectral index of 3.02 below the "knee" and 3.53 beyond the "knee", two statements in total disagreement with experimental observation. Also, the mean atomic mass for all cosmic rays beyond 10^{14}eV would be very close to that of Fe another fact considered to be inconsistent with observations made in EAS experiments.

In conclusion, if diffusion is to be responsible for the "knee" in the energy spectrum the iron spectrum must suffer a cut off at energies very much lower than 10^{13}eV. If this were so, then we rely on heavy elements other than Fe to keep the change of slope of $\sim$0.6 to energies $\sim 10^{17}$eV. Alternatively, the relative abundance of Fe with respect to C is only energy dependent over a small range in energy returning to a constant value before 10^{13}eV.

7.3.3 Mean atomic weight as a function of energy as defined by models II-A and II-B

The mean atomic weight $\bar{A}$ was established as a function of energy per nucleus by computer in the following way: at a particular energy/nucleus the products of the relative abundance and the atomic mass of each element were summed and the result divided by the sum of the relative

abundances of the elements. The $\bar{A} - E_o$ curve for each diffusion model II-A and II-B is shown in figure 7.5. Galactic modulation at low energies establishes a mean atomic weight of $\sim$7.2 this increases gradually beyond $\sim 2\ 10^{15}$eV in the case of model II-B and rather rapidly beyond $\sim 8\ 10^{15}$eV in the case of model II-A.

7.4 Some indication of the isotropy of cosmic rays for the spectra defined by cosmic ray diffusion

For model A the isotropy will be similar to the isotropy calculated for diffusion in an idealised medium, provided that the solar system does not lie too far from the centre of the spiral arm.

For model B however, where effectively there are a great deal more clouds with H_oR_o small than clouds with H_oR_o large, it is believed that because the smaller H_oR_o clouds will on average be closer together relative to the idealised medium the cosmic ray directions will be randomised even more and the anisotropy δ will be smaller than in the case of diffusion in an idealised medium. As cosmic ray energy increases the value of $\frac{1}{\lambda(p)}$ decreases by approximately a factor of ten before diffusion returns to that in an idealised medium (see figure 7.1) or alternatively because the ratio $^{n}cl/_{n_c}$ $\sim$1000 the average spacing between the large clouds increases by a factor of 10. This means that the anisotropy δ will increase by a factor of 100 to a value of $\sim 10^{-2}$ at $\sim 6 \times 10^{16}$eV. We conclude that the isotropy is consistent with experiment up to this energy.

7.5 Conclusions

The data survey of chapter 2 gave a working hypothesis for the development of the diffusion model, i.e. the characteristics of the differential energy spectrum implied from the integral size spectra of electrons and

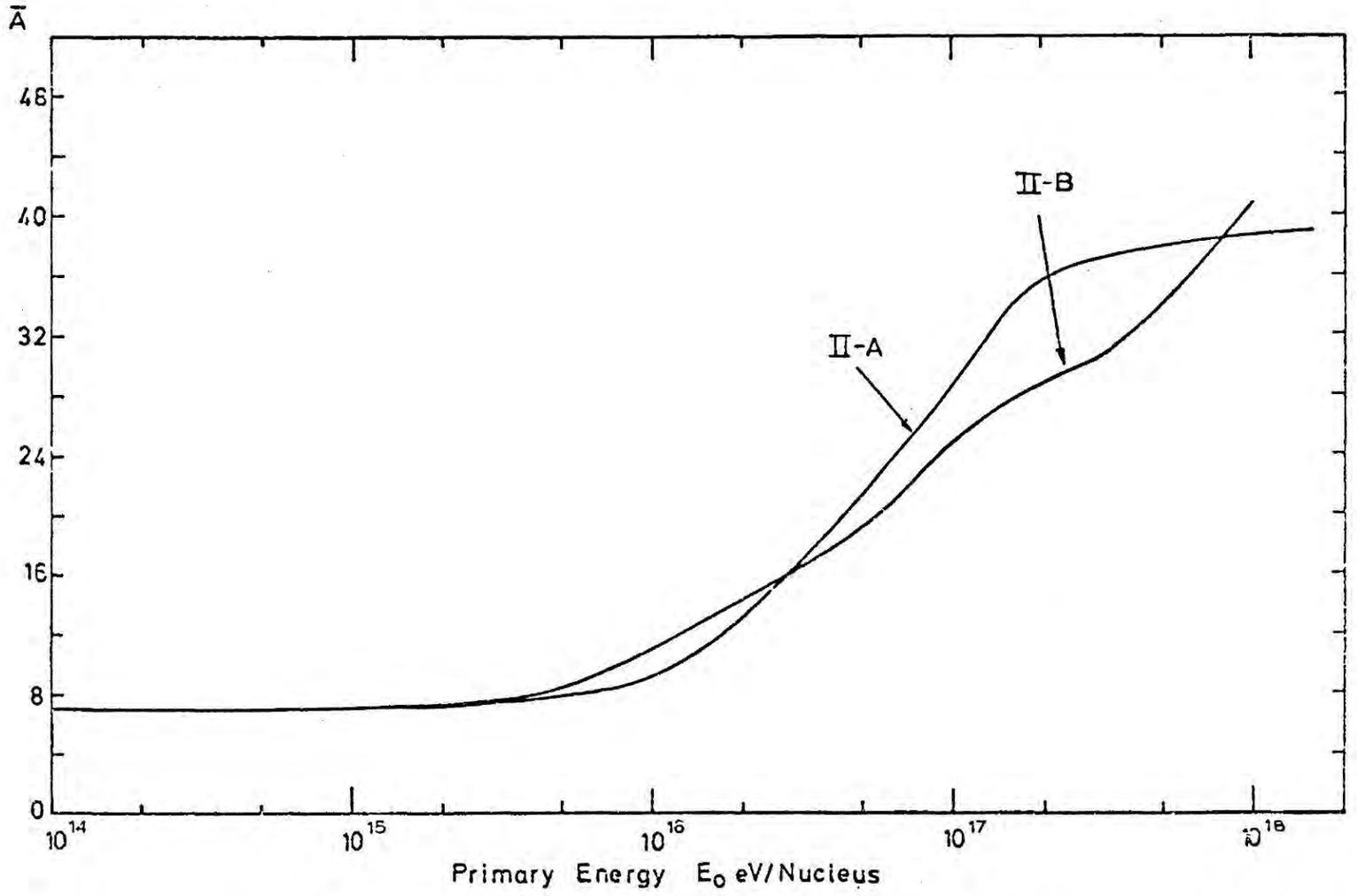

Figure 7-5 The mean atomic weight ($\bar{A}$) as a function of energy per nucleus for model II-A and II-B.

muons at sea level and electrons at mountain altitudes are $f_d \sim 1.0 \pm 0.1$, $\Delta\gamma \sim 0.6$ being constant over the largest possible range in energy i.e. $\log_{10} E_T/E_K$ is large, with the "knee" lying between ~3 10^{15}eV and ~10^{16}eV. Table 7.1 compares the latter with the parameters defined by the three diffusion models considered. Model I for only protons in an idealised interstellar medium, model II-A and II-B for both protons and cosmic rays with a mixed composition in physical interstellar media. In striving for a possible explanation of the observed energy spectrum for cosmic rays at the Earth the optimum diffusion model must be established.

The simple theoretical model along with model I are totally unsatisfactory for reasons given in the conclusions of chapter 4. Model II-A is based on the assumptions that the magnetic fields in all cloudlets and clouds is constant (i.e. the hydrogen density is constant) with a simple inverse square power law for the cloud mass distribution up to 36 $M_\odot$. The energy spectrum differs only in that it indicates an increase curvature in the region of the knee compared with that for diffusion in idealised medium, $f_d = 0.56$ and $\Delta\gamma \sim 2$ showing no characteristics exhibited by the experimental spectrum. Consideration of the presence of primary cosmic rays with atomic charges $Z>2$ along with galactic modulation gives marginal improvements in the sense that the 'f' factor increases to 0.92 i.e. the "knee" is sharpened and the change of slope decreases to 0.74 but this occurs only over a short energy range, i.e. $\log_{10}(E_T/E_K) = 0.92$ whereas a value in excess of ~ 2 is required to be in agreement with experiment.

Model II-B, which is based on the best possible interpretation of the experimental observations of Heiles (1967) however, shows very promising characteristics. Both the proton and the modulated spectrum

Table 7.1 Comparison of the parameters characterising the differential energy spectra defined by the various diffusion models

Model			f_d	$\Delta\gamma$	E_K eV	E_T* eV	$\log_{10} \frac{E_T}{E_K}$ †
Simple theoretical model			1	2	-	$E_T=E_K$	0
idealised galactic medium	Model I - protons		0.75	∿2	Depends on the assumed values of H_o and R_o	$E_T \sim E_K$	∿0
physical galactic medium	Model II-A	protons	0.56	∿2	$\sim 2\ 10^{15}$	$E_T \sim E_K$	∿0
		mixed composition	0.92	0.74	$7.6\ 10^{15}$	$\sim 6.3\ 10^{16}$	∿0.92
	Model II-B	protons	0.90	0.79	$3.4 10^{15}$	$6.2\ 10^{16}$	1.26
		mixed composition	0.91	0.58	$4.8\ 10^{15}$	$1.2\ 10^{17}$	1.40
"Experimental"			1.0 ± 0.1	0.6	$(3-10)10^{15}$	-	>2.00 Large

* Because the transition from the diffusion in a physical medium to diffusion in a non physical medium is gradual E_T is estimated at a point approximately in the centre of this energy region.

† A value of $\log_{10} \frac{E_T}{E_K} = 1$ implies that the change of slope $\Delta\gamma$ remains constant over one decade in energy, and in general for $\log_{10} E_T/E_K = n$, $\Delta\gamma$ is constant over n decades in energy.

have a relatively sharp transition region and the $\Delta\gamma$'s are approaching that implied by the size spectra and such a change of slope remains constant for over a decade in energy. The position of the "knee" is defined by model II-B to be at 3.4 10^{15}eV in the case of a pure proton spectrum and at 4.8 10^{15}eV for a spectrum with cosmic radiation of mixed composition. As indicated in chapter 2 it is difficult to establish the position of the "knee" in the experimental energy spectrum because of the uncertainties in the modelling of EAS development through the atmosphere, in the threshold energy of particles detected and the structure function fitted to the experimental observations. The other parameter which would cause a shift of the "knee" to a higher energy would occur if the dominant cloudlets had a value of ("magnetic field" x cloud size) greater than 4.2 pc cm^{-2}. Such a shift in the total H_oR_o distribution established by Heiles would result if say the sheets Heiles analysed were more distant from the L.S.R. or higher fields exist inside the concentrations. For these reasons the "knee" position is not critical and in fact it is the parameter which will be manipulated in the next chapter to obtain the best fit to the experimental data and to establish the physical implications of the present work.

On the whole, model II-B shows favourable characteristics for both proton and heavy spectra. It has been assumed in the above discussion that a one to one relationship exists between size and energy for both protons and heavies but this is not strictly true. In figure 7.6 then, the integral energy spectrum for protons and for mixed composition is plotted along with the corresponding differential spectra, (the mixed composition spectra are normalised to that for protons at 10^{14}eV). These represent the energy spectra defined by the diffusion of cosmic

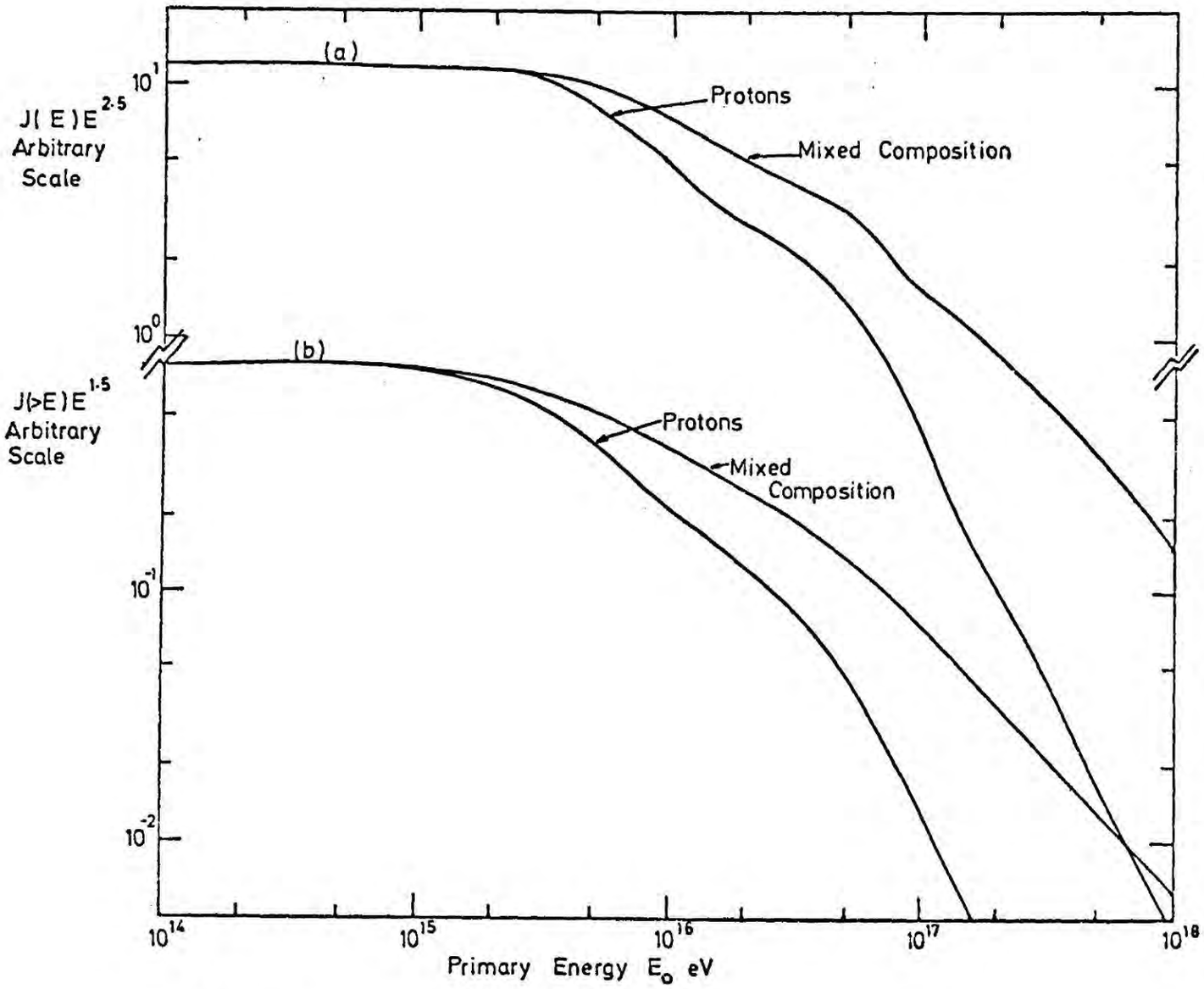

Figure 7-6 The energy spectra (a) differential and (b) integral for protons and for primaries of mixed composition, representing diffusion of cosmic rays in the Galaxy.

rays in the galactic medium defined by model II-B. Now that a reasonable model has been established it must be tested by comparing it directly with the integral size spectra. This will be achieved by using the EAS simulation data of Bradt et al (1965) de Beer et al (1966) and Dixon et al (1973) and the integral spectra plotted in figure 7.6.

Chapter 8 Application of the diffusion model to the shape of the size spectra of EAS in the region of the "knee"

8.1 Introduction

Figure 7.6 gives the integral energy spectrum for both primary protons and primary cosmic rays with a mixed composition. They define the diffusion of cosmic rays in an interstellar medium whose cloud sizes and magnetic fields were established from direct experimental observations, i.e. model B. Throughout this chapter, diffusion model B only is discussed with respect to the derivation of the theoretical size spectra. Subsequently, direct comparison is made with those measured experimentally at mountain altitudes and at sea level. When cosmic ray diffusion is referred to in this chapter it is to be assumed to be in an interstellar environment defined by model B and when mixed composition is referred to it is that defined by Cartwright et al (1971) and $p/\alpha = 18$ modulated according to charge Z, except when otherwise stated.

8.2 Derivation of the size spectra

The model calculations for the development of air showers in the atmosphere used to obtain the size spectrum from the energy spectrum are, Bradt et al (1965), de Beer et al (1966) and Dixon et al (1973). These will be dealt with in turn. The reader is referred to Chapter 2 for the details of the EAS simulation models and the results.

8.2.1 Bradt et al (1965)

These authors show that the energy E_o eV of the primary cosmic ray producing an EAS bears a linear relationship with $N_{e_{max}}$, the number of electrons in the shower at its maximum of development.

i.e. $E_o = 2\ 10^9\ N_{e_{max}}$ 8.1

Since showers with an energy in the range $2\ 10^{15} < E \leq 2\ 10^{17}$ eV

reach maximum development at mountain altitudes (depending on the zenith angle) this relationship can be applied to the spectrum over a size range of 10^6 - 10^8 particles. Bradt et al (1965) derived the integral size spectrum at maximum development (figure 2.8). Using equation 8.1 diffusion predicts the size spectrum for protons indicated as a full curve in figure 8.1a, the theoretical curve is normalised to the data at a value of $J(>N_{e_{max}})\ N_{e_{max}}^{1.5} \sim 0.4$ and the error bars indicate the experimental uncertainty. Provided a shift in the theoretical spectrum equivalent to a factor of ~ 0.5 in the electron size is made, good agreement is obtained with experiment up to a size of $\sim 10^7$ particles (dashed curve). An arbitrary shift in size is possible because renormalization of intensity is permitted. Such a shift could be accounted for if one assumes that the "knee" in the energy spectrum predicted by diffusion occurs at $\sim 2\ 10^{15}$ eV rather than at $4\ 10^{15}$ eV implying that the interstellar clouds with a value of $H_o R_o \sim 2$ pc cm^{-2} are most abundant, alternatively the E_o-N_e relationship could be overestimated by a factor of ~ 0.5, i.e. $E_o \sim 10^9\ N_{e_{max}}$ eV instead of $E_o = 2\ 10^9\ N_{e_{max}}$ eV. Both of these possible reasons for explaining the shift are not very satisfactory. In the first instance Heiles (1967) is quite confident that his instruments were of sufficiently high resolution to show that a sharp increase in the number of clouds from ~ 1 pc cm^{-2} to a maximum at ~ 4 pc cm^{-2} existed and therefore it must be assumed that the distance to the cloudlets and clouds was underestimated by a factor of two, a statement inconsistent with the measurements made by Ames and Heiles (1970). In the second case the fact that the relationship 8.1 has been derived independently by different physicists it seems difficult to accept that it is incorrect. However, if the "threshold" energy of the particles detected had been overestimated or the structure function fitted to the "raw" data was too steep, then a shift of x0.5 could be totally or partly explained.

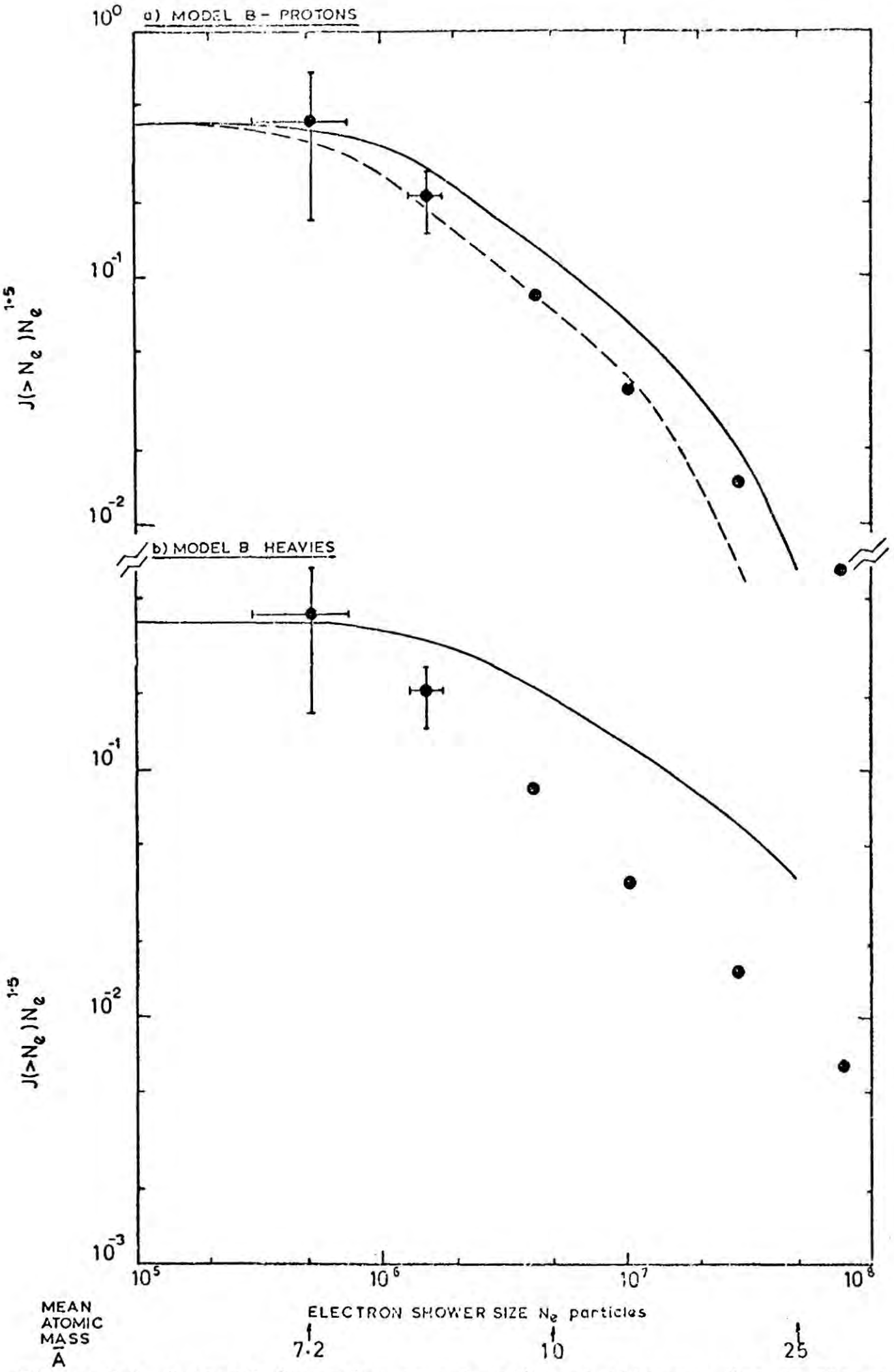

Figure 8-1 Integral intensity as a function of electron size at the maximum of development. The error bars indicate experimental uncertainty (Bradt et al 1965). The full curves are those predicted by the diffusion model together with the EAS simulation model of Bradt et al (1968) for (a) protons and (b) heavy nuclei. The dotted line represents a shift of x0.5 in size to establish a better agreement with experiment for diffusion of primary protons. The mean atomic mass as defined by the diffusion model B is indicated

Accepting the theory of superposition of showers and using the curve defining the mean atomic weight as a function of energy for the diffusion model, figure 7.5 , the size spectrum representing the diffusion of cosmic rays with mixed composition was derived. It is compared with the same experimental data in figure 8.1b. It can be seen that the fit is totally unsatisfactory, the change of slope being too small.

Although there is some indication that diffusion of cosmic ray protons might be the cause of the "knee" heavy primaries, according to Bradt's simulations, can be ruled out.

8.2.2 de Beer et al (1966)

For vertical showers at sea level the E_o-N_e relationships derived by de Beer et al for protons are plotted in figure 8.2 (see equations 2.1 and 2.2). Using figure 7.5 ($\bar{A}$ varying with energy for diffusion model B) and assuming the theory of superposition of showers, the E_o-N_e curves for cosmic rays with mixed composition were derived. These are plotted in figure 8.2. In general the average size of a shower initiated by a proton produces more particles than a heavy primary for a particular energy/nucleus.

The size spectra predicted by diffusion, using the simulations of de Beer et al, for protons and a mixed composition are shown in figure 8.3a and 8.3b respectively. Normalisation of intensity is made at the "peak" of the spectrum. In the spectra represented by full lines the horizontal scale is absolute.

It can be seen that using the simulations of de Beer et al a shift of x4 (dotted lines) is necessary in the spectrum representing diffusion of protons and even then agreement is not too good. The full lines enclosing the shaded area corresponds to the difference produced in the spectrum resulting from the calculation assuming the E_o-N_e curve for showers initiated by primaries of fixed energy or the E_o-N_e curve for mean primary energies for

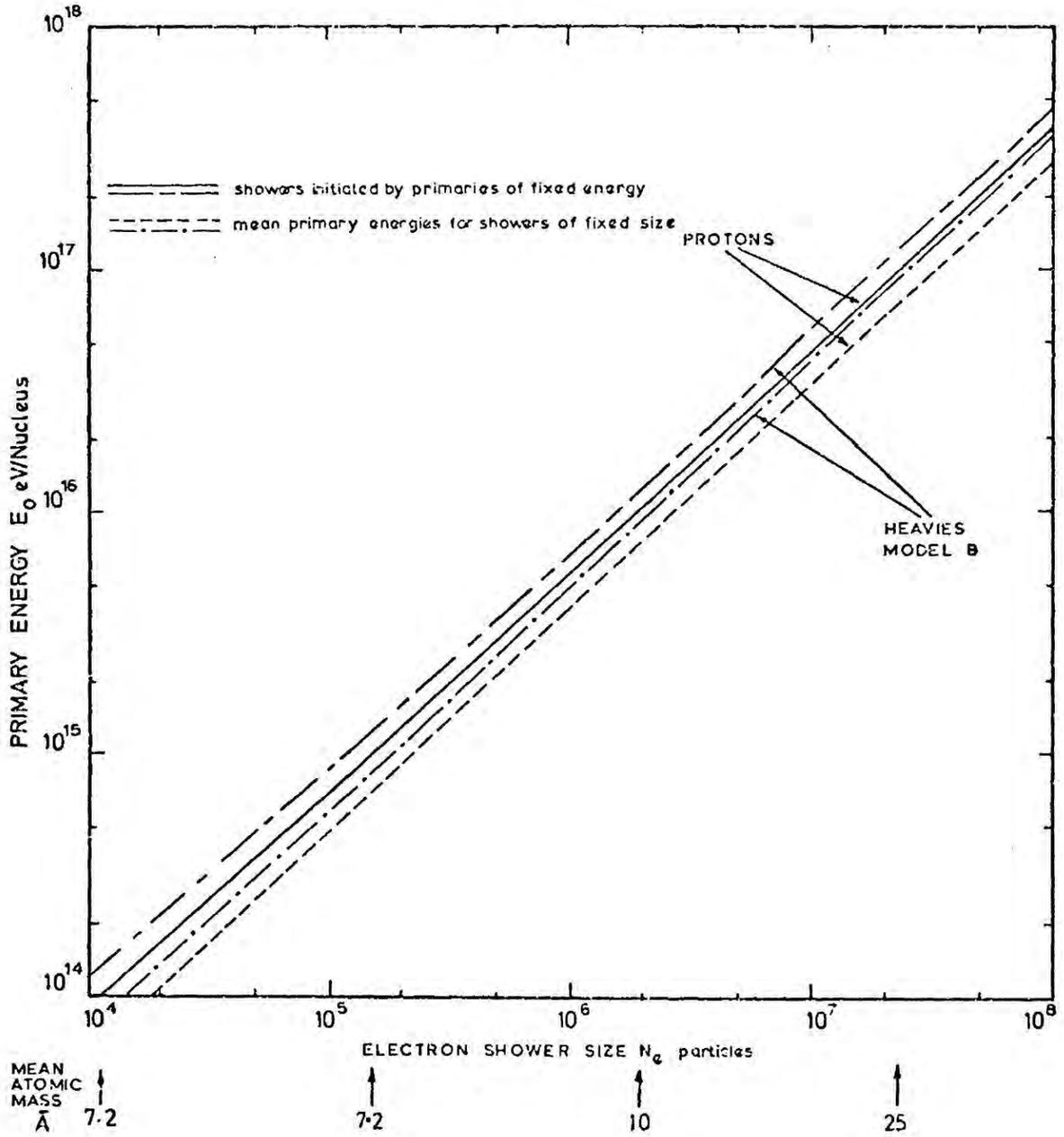

Figure 8-2 The E_o-N_e curves for vertical showers at sea level. Model I de Beer et al (1966).

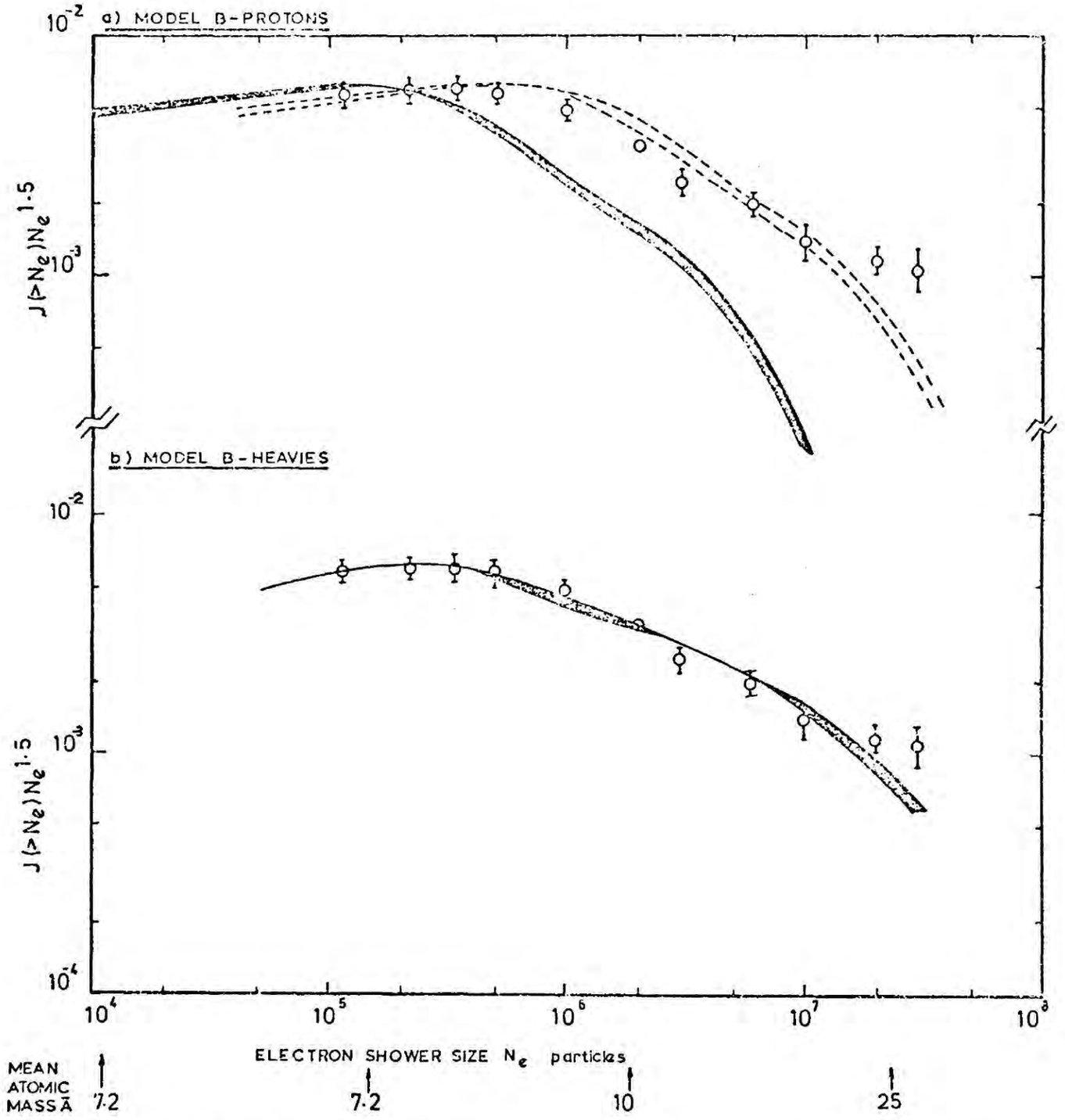

Figure 8-3 Integral electron size spectrum at sea level. The experimental data are those measured by MSU, Khristiansen et al (1972). The full curves bounding the shaded area are those spectra predicted by the diffusion model plus the shower simulation data of de Beer et al Model I (The spread is due to the different E_ρ-N_e curves shown in figure 8-2) (a) for proton primaries and (b) for heavy primaries. The dotted lines represent a shift of x4 in the size to establish a better agreement with experiment for diffusion of primary protons. The mean atomic mass as defined by diffusion model B is indicated at decade intervals below the size scale.

showers of fixed size. A shift of x4 would necessitate clouds with a value of $H_o R_o \sim 17$ pc cm^{-2} to be the most abundant elements or the distance to the elements overestimated by a factor of four, both facts are most unrealistic. Therefore, in this case we would have to argue that the simulations of EAS through the atmosphere carried out by de Beer et al have drastically underestimated the number of particles in the shower as it reaches the Earth or alternatively the threshold energy or structure function argument affecting the experimental data could assist in part, but not in full. For such a large shift to be accounted for, it is believed that all the above explanations contribute and have a cumulative affect.

The agreement of the theoretical curve derived from diffusion of cosmic rays with a mixed composition with experiment is, however, remarkable (see figure 8.3b). Normalisation of intensity was made at the peak "intensity" of the spectrum, whilst the size is absolute, i.e. no shift in electron size was necessary to make data comparison. It can be concluded then, that diffusion of cosmic rays with a mixed composition fully explains the cosmic ray size spectrum observed at sea level, over a size range $10^5 < N_e < 2\ 10^7$, provided we accept the theory of superposition of air showers along with the E_o-N_e curves for protons derived by de Beer et al.

8.2.3 Some important remarks - N_μ/N_e ratio

Using the EAS simulation results of Bradt et al diffusion of protons gives marginal agreement with the integral electron size spectrum measured experimentally at mountain altitudes whilst a mixed composition is totally unsatisfactory. The shower simulations of de Beer et al lead us to an entirely different conclusion. At sea level, the experimental integral electron size spectrum can be explained completely in terms of diffusion of cosmic rays with a mixed composition and galactic modulation,

whilst to obtain even just slight agreement with a spectrum representing diffusion of cosmic ray protons the shower size has to be adjusted by a factor of x4; a shift which can be explained by the cumulative effect of underestimation of the number of particles observed experimentally, the number of particles expected at the observation level for cosmic ray of a particular primary energy and of the size and magnetic fields of clouds observed in the Galaxy.

Just small variations in the E_o-N_e curves were seen to appreciably affect the size spectra they derive from the energy spectrum (e.g. the spreading observed in figure 8.3a due to the use of the different E_o-N_e curves represented by equations 2.1 and 2.2). The muon integral size spectrum established experimentally is at sea level for muons with an energy threshold of 10 GeV. There are many E_o-N_μ curves which could be used to establish the theoretical muon size spectrum from the energy spectrum for comparison with this experimental data. However, the E_o-N_μ curves are derived by different physicists who have assumed different modelling parameters and they are found to be quite different (see figure 2.1). If we applied these E_o-N_μ curves then the resultant spectra would present us with an impossible situation where any one of many theoretical spectra could be made to agree with the experimental data because arbitrary shifts are permitted. In the chaos there would be difficulties in finding basis for firm conclusions. No attempt was made at this stage to establish a muon spectrum representing diffusion of cosmic rays.

The N_μ/N_e relationship measured by EAS experiments is found to be always constant and therefore this arbitrary shifting of spectra is now constrained to the extent that a shift in the muon spectrum demands a corresponding shift in the electron size spectrum such that N_μ/N_e

remains the same, always.

It is believed that the earlier EAS simulations considered so far are rather naive, due to the inferior computer facilities available at that time, and therefore they have limited application. We look to the more complex model of Dixon et al (1973) which makes available the information required to make comparisons of the diffusion model (for proton as well as heavy primary cosmic rays) in the form of the integral size spectra for muons as well as electrons with different energy thresholds, at mountain altitudes as well as at sea level. This information will be used in the next section to enable the final conclusions to be drawn.

Firstly, with the knowledge so far obtained, an attempt will be made to bring into perspective the relative importance of the four possible explanations for the shift in the spectral size already proposed (see section 2.6).

(i) The position of the peak in the H_oR_o distribution is very pronounced and can confidently be believed to occur at the value of 4.2±1.2 pc cm^{-2} which would cause some 28% uncertainty in the position of the "knee". The distance to the cloudlets and clouds observed is more doubtful and a conservative estimate on the maximum possible positive shift in the "knee" is ∿30%. Any shift assumed to be due to the effective cloud size or due to changes in the effective value of H_oR_o will affect the size spectra equally at all altitudes.

(ii) Because of the observed spread in the multiplicity laws assumed to fit the experimental data, and the variations in the model parameters used, the E_o-N_e relationships established can alter the size by as much as 50% at large sizes. This factor will also affect the

size spectra by a constant factor for all altitudes.

(iii) The fitting of the structure function is a rather difficult parameter to deal with in the sense that it is not always assumed to be dependent on the age of the shower. Although not easily determined the error involved can be assumed small compared with the error due to the actual fitting of a particular structure function to the experimental data, an error which at the largest sizes dealt with here could be as much as 50%.

(iv) The E_o-N_e curves provided by Dixon et al (1973) figure 2.2 are seen to differ quite appreciably depending on the threshold energy of the particle detected, for example at sea level for showers initiated by primary protons of energy 10^{16}eV there would be approximately twice as many electrons with zero energy threshold than with an energy threshold of 10 MeV produced.

8.2.4 Dixon et al (1973)

Because the threshold energy of particles is an important factor and that for electrons detected by scintillators at mountain altitudes and by Geiger Muller tubes at sea level is not known absolutely, it is logical to commence analysis with the integral spectrum measured for muons with the known threshold energy of 10 GeV. Using the E_o-N_μ curve established by Dixon et al (1973) for proton showers arriving vertically at sea level (figure 2.2) the theoretical integral muon size spectrum was calculated, using the energy spectrum defined by diffusion (figure 7.6). The result is the solid curve shown in figure 8.4a, the size being an absolute quantity whilst normalisation of the theoretical curve to the data is made at a value of $J(>N_\mu)\ N_\mu^{\ 2} = 1.13\ 10^{-2}$. It can be seen that a shift of the curve through a factor of three in size is sufficient to get excellent

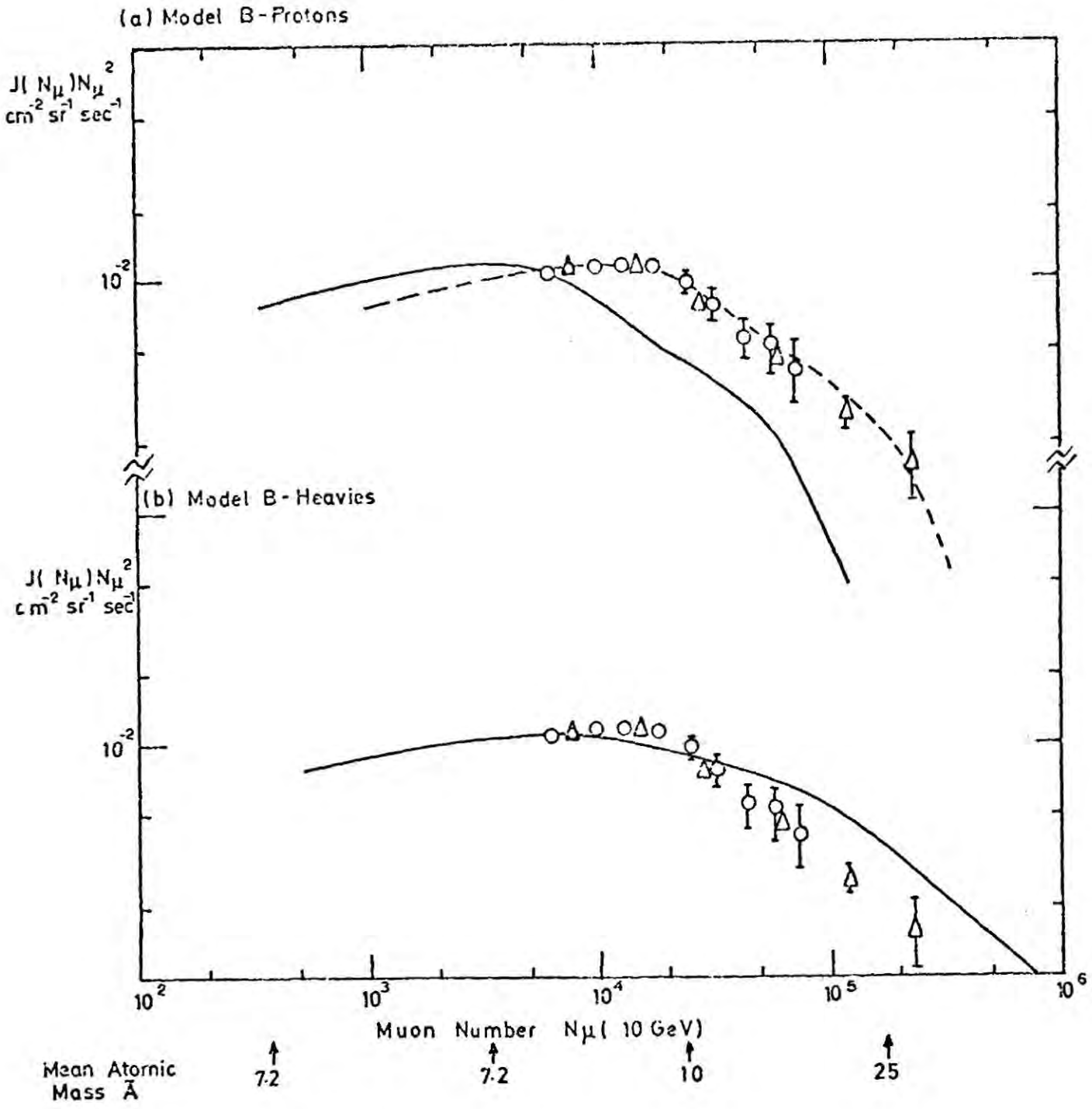

Figure 8-4 Integral size spectrum for muons with a threshold energy of 10 GeV at sea level. The experimental data are those of MSU (Δ), Tien Shan (◊) see Khristiansen et al (1972). The full lines are the actual spectra for (a) protons and (b) heavies as predicted by the diffusion model B and the shower simulation data of Dixon et al (1973). The dashed line is the spectrum predicted by the diffusion model B for protons shifted through a factor of x3 in muon size, thus giving a better fit to the experimental data. The mean atomic mass as defined by the diffusion model is indicated at decade intervals below the size scale.

agreement of the theory with experiment over the entire range in size.

Turver (1973, private communication) established the E_o-N_μ curve for muons (threshold energy 10 GeV) at sea level for primary cosmic rays with a mixed composition defined by figure 7.5. The resultant E_o-N_μ curve is plotted in figure 8.5 and $\bar{A}$ is indicated at decade intervals below the N_μ axis. Because showers tend to be more mature when considering break up of heavy nuclei by fragmentation, for low primary energies the number of muons at sea level would tend to be less and for high primary energies the number of muons to be more relative to the superposition model, the overall effect is to steepen the slope of the E_o-N_μ curve. The muon size spectrum representing the diffusion of cosmic rays with mixed composition is compared with the experimental data in figure 8.4b. The agreement can be seen to be totally unsatisfactory.

The simulations of Dixon et al predict that diffusion of protons in the spiral arm can account for the shape of the muon spectrum in the region of 10^4 particles. What is more, the shift needed to obtain the best fit has been established as a factor of three for muons. This means that the intensity for muons has to be altered by a factor of nine ($=N_\mu^2$). Because the N_μ/N_e ratio must remain the same, the necessary shift for the electron spectrum has therefore been directly established i.e. $N_e^{1.5} = 9$ or a shift equivalent to x4.3 in electron size.

Taking the E_o-N_e curves for proton primaries arriving at mountain altitudes obtained by Dixon et al for electron threshold energies $\geq$0 MeV and >1 MeV figure 2.2, the corresponding electron spectra were calculated. These are plotted as a full line ($\geq$0 MeV) and a dot-dashed line (>1MeV) in figure 8.6a. These two curves are normalised at $J(>N_e)\ N_e^{1.5} = 1.8$

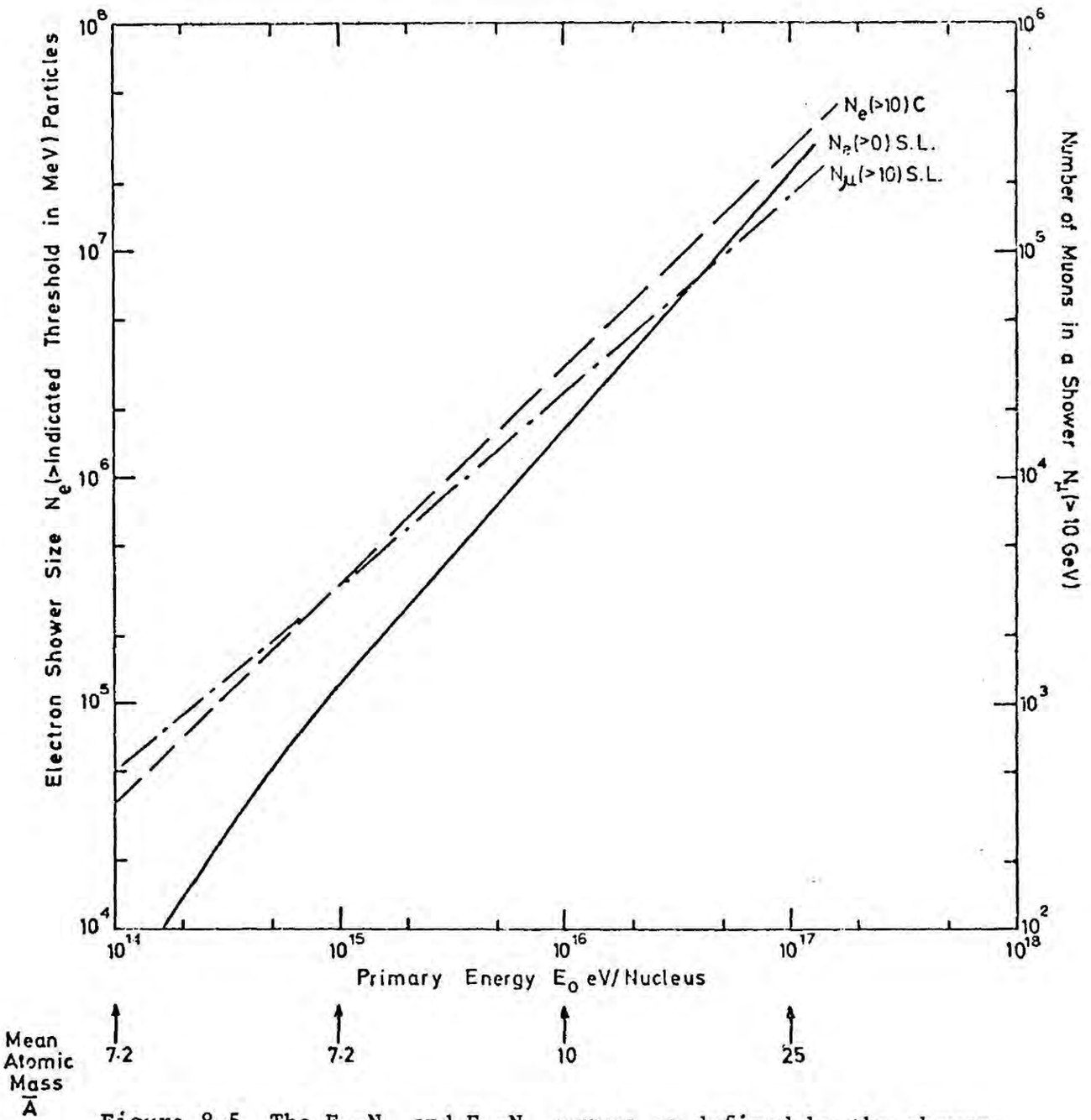

Figure 8-5 The E_o-N_e and E_o-N_μ curves as defined by the shower simulations, Turver (1973), for primaries with mixed composition for the stated threshold energy of the detected particles. The mean atomic mass as defined by the diffusion model is indicated at decade intervals below the energy scale.

whilst the electron sizes are absolute. An arbitrary shift of size is made to establish the goodness of the fit with the experimental data. This is shown as the smeared solid curve. The variation in the shape of the two curves representing the two threshold energies is due to the fact that the EAS simulation for the ≥0 MeV E_o-N_e curve is based on a one dimensional development of air showers according to approximation B, whilst the simulation for the >1 MeV E_o-N_e curve is based on a one dimensional development of air showers according to approximation A, plus results from the numerical treatment by Messel and Crawford (1969) of the shower when the energy of the secondary particle <56 GeV and these treatments are found to be different (Dixon et al 1973). It can be seen that the shape of the theoretical curve agrees well with experiment up to an electron size of 10^7 particles.

As a shift of 4.3 is needed, it can be estimated that electrons with a threshold energy ∿0.8 MeV were detected at Mount Chacaltaya.

The analysis was repeated assuming that primary cosmic rays have a mixed composition using the E_o-N_e curve derived by Turver (1973, private communication) see figure 8.5. The resulting spectrum shown in figure 8.6b is seen to be totally unsatisfactory.

The entire procedure was repeated to predict the theoretical curve for the electron size spectrum at sea level. The E_o-N_e curves for electron threshold energies ≥0 MeV, >1 MeV and >10 MeV assuming proton primaries, are shown in figure 2.2 (Dixon et al 1973). The E_o-N_e curve for electron threshold energy of ≥0 MeV assuming mixed composition for primary cosmic rays is plotted in figure 8.5 (Turver 1973). The resulting spectra are shown in figures 8.7a (protons) and 8.7b (heavies). It is found that diffusion of cosmic ray protons

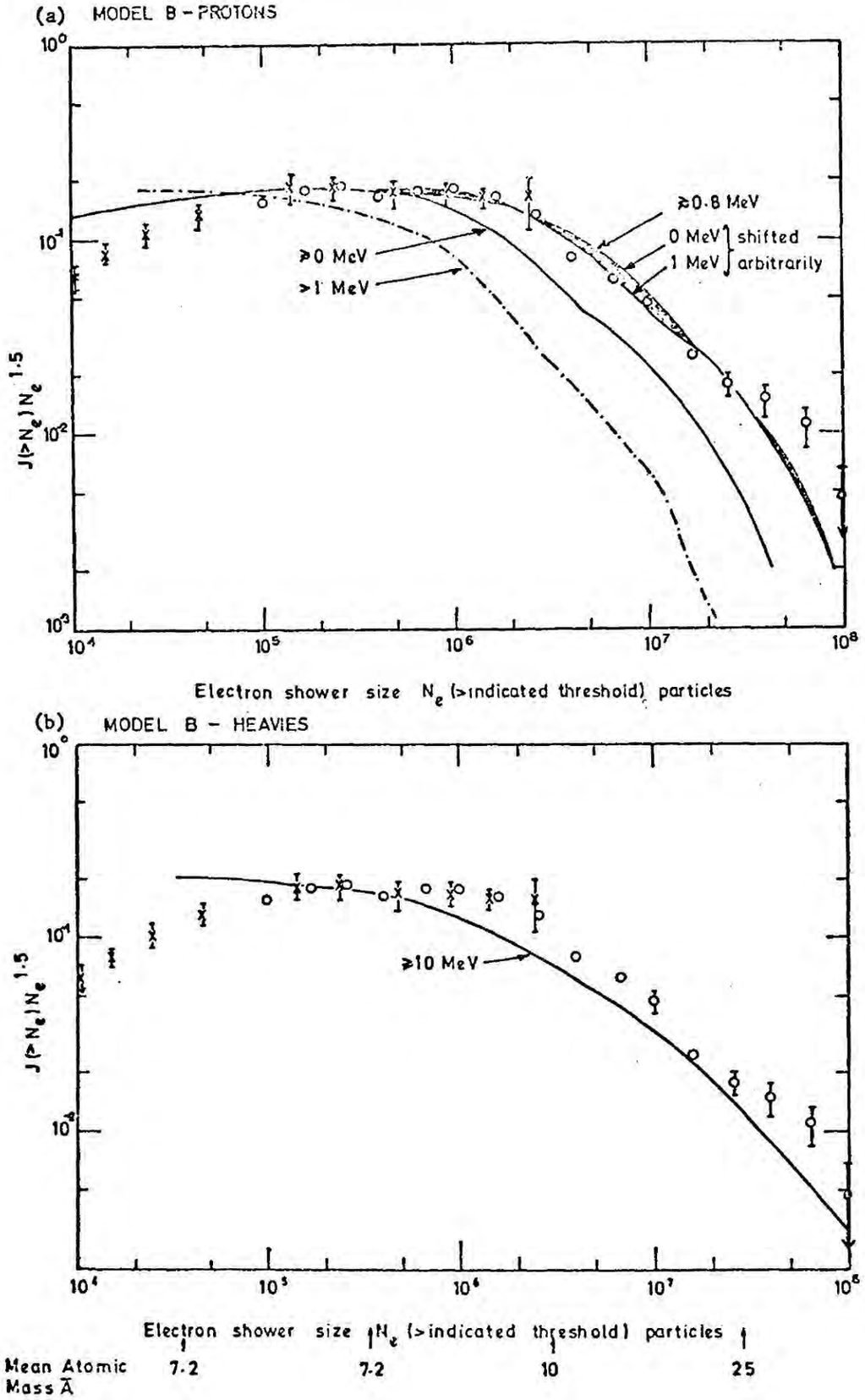

Figure 8-6 Integral electron size spectrum at mountain altitudes. The experimental data are those measured by Bradt et al (1965) at 530 gm cm^{-2} ($\bar{Q}$) and Amineva (1969) at 700 gm cm^{-2} ($\frac{1}{2}$). The full lines and the dot dashed line are the actual spectra for (a) protons and (b) heavy primaries as predicted by the diffusion model B and the shower simulation data of Dixon et al (1973) for the stated threshold energy of the particles detected. The shaded area is bounded by curves obtained by making an arbitrary shift in the proton spectra of the two threshold energies ≥0 MeV and >1 MeV. For the required shift of x4.3 the smeared curve represents a particle threshold energy ~0.8 MeV. The mean atomic mass as defined by the diffusion model is indicated at decade intervals below the size scale.

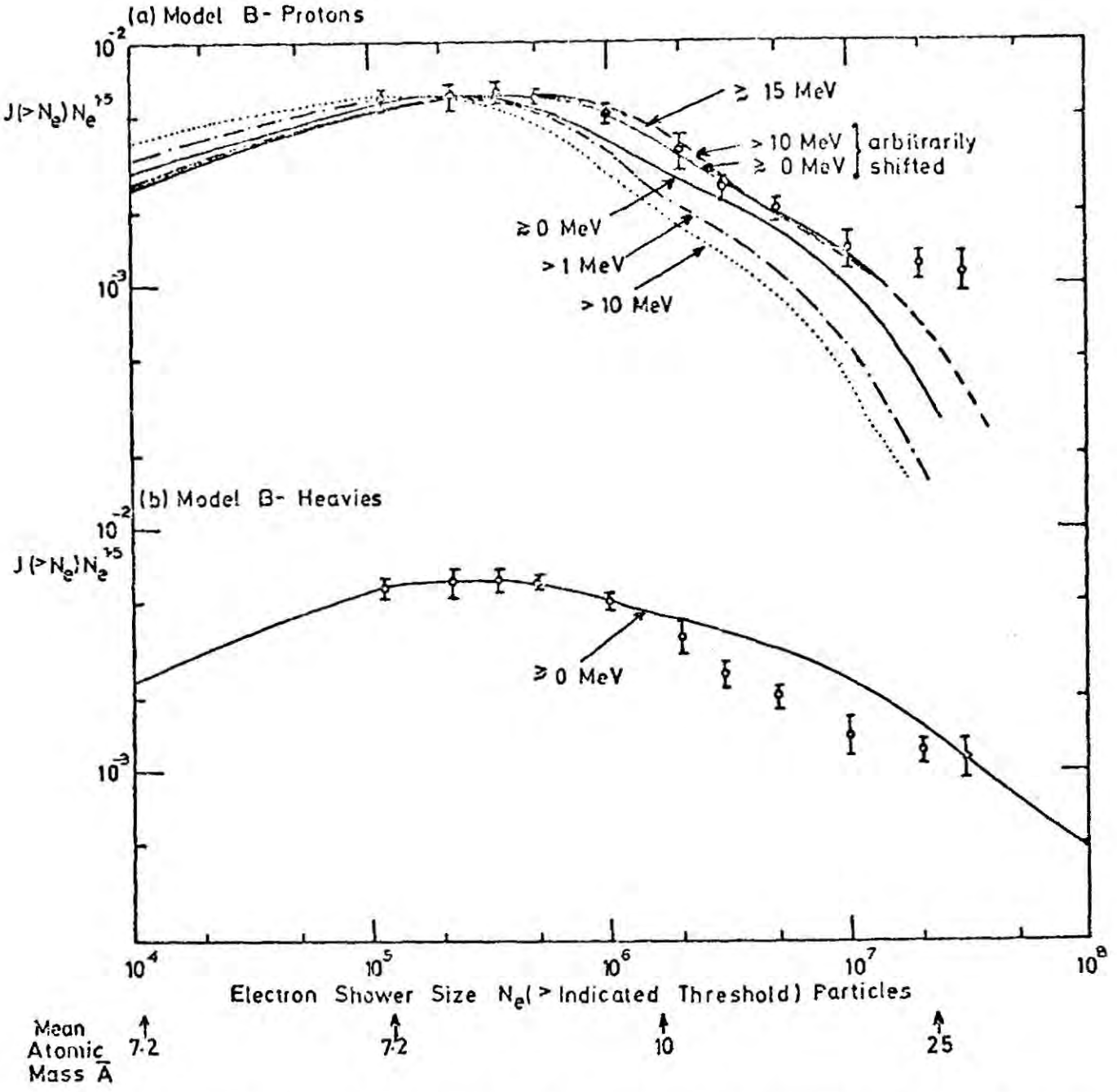

Figure 8-7 Integral electron size spectrum at sea level, the experimental data is the dot-dashed line and the dotted line are the actual spectra for (a) protons and (b) heavies as predicted by the diffusion model II-B and the shower simulation data of Dixon et al (1973) for the stated threshold energy of particles detected. The shaded area is bounded by curves obtained by making arbitrary shifts in the proton spectra representing the two threshold energies ≥0 MeV and >10 MeV. For the required shift of x4.3 the smeared curve represents a particle threshold energy ≥15 MeV. The mean atomic mass as defined by the diffusion model is indicated at decade intervals below the size scale.

can explain the shape of the electron size spectrum in the region of the "knee" provided that we assume that the threshold energy of the particles detected by the EAS array at Moscow State University was ∿15 MeV. Cosmic ray primaries with mixed composition would be totally unsatisfactory.

8.3 Conclusions

Diffusion of cosmic ray protons can explain the shape of the size spectrum for muons at sea level and for electrons at sea level and mountain altitudes provided we accept the simulation data of Dixon et al (1973) as being correct. The integral electron spectrum for showers at maximum development established experimentally at Mount Chacaltaya (Bradt et al 1965), can also be explained in terms of diffusion of cosmic ray protons. It is interesting to point out that the simulations of de Beer et al (1966) predicted a x4 shift in the theoretical proton spectrum to obtain agreement (although only marginal) with experiment. This shift is consistent with that predicted by the Dixon et al (1973) simulations. It is possible to conclude that the simulations of de Beer et al give a result that is consistent with Bradt et al and Dixon et al.

This analysis predicts that the air shower array at Mount Chacaltaya detects electrons with energy threshold of ∿0.8 MeV in agreement with experiment (section 2.5.6) and that at MSU detects electrons with a threshold energy of ∿15 MeV. And to account for the shift required to obtain agreement with the data the calculations predict that the clouds observed by Heiles (1967) are probably further away, the EAS simulations are probably underestimating the number of particles produced in a shower and perhaps the structure functions fitted to the experimental data are too flat.

Chapter 9 Neutral hydrogen in the solar neighbourhood

9.1 Introduction

It is important to establish the position of the solar system in the Orion arm because of the anisotropy problems encountered with cosmic ray diffusion when the solar system is not at its centre (for details see chapter 4). So far we have assumed that the Earth lies in the centre of the Orion arm and ignored any possibility of the Earth being nearer the edges of the spiral arm or even close to or inside a hydrogen cloud supporting a magnetic field. If the solar system lay inside a cloud then no significant anisotropy would be expected; however, an anisotropy might be experienced if the solar system lay close to a cloud configuration whose fields might be such that some screening of cosmic rays of certain energy would be experienced.

Information on the position of the solar system with respect to the hydrogen in the Orion arm is sparse because it is quite impossible to obtain any distance measurement for 21 cm emission. The problem is caused by the inability to differentiate between random cloud motion and motion due to galactic rotation. Some experimental observations of the distribution of matter in the solar neighbourhood will be dealt with in this chapter in order to establish the location of the solar system.

As a consequence of this study, the evidence of the existence of an ellipse of hydrogen enables a simple model, which leads to another way of interpreting the shape of the primary energy spectrum of cosmic rays in the region of the "knee", to be developed.

9.2 Position of the solar system with respect to the local hydrogen

A magnetic field study of Theilheim and Langhoff (1968), see

section 6.4 for details, suggested that the solar system lies beneath the plane by a distance of ∿85 pc. Kerr and Westerhaut (1965) suggest that the Galaxy is a fairly tightly wound spiral with arms which are circular in form. The pattern has many irregularities and although these occur in the line profiles their position in the galactic plane is by no means certain. The Sun lies in the inner side of the Orion arm. This conclusion is consistent with the observations of van de Hulst et al (1954) and Morgan et al (1953) who also showed that the hydrogen density between the Orion arm and the inner arm, the Perseus arm some 2 kpc distant, was ≤0.1 atoms cm^{-3}.

Later, Bok (1959) collected data from a wide variety of sources and built up a picture for the distribution of matter in the vicinity of the Sun, see figure 9.1. Bok noted the widespread disagreement, but concluded that continuity of the Carina and Cygnus portions of the arm through the Sun was an important and real feature of the pattern. The assumption that the Sun is positioned approximately at the centre of the local spiral arm is consistent with this picture, shown in figure 9.1, of Bok (1959).

9.3 Pitch angle of the Orion arm at the position of the solar system

Mills (1958,1959) in his 3½ meter survey of the Milky Way region found a number of "steps" in the distribution of the radiation with galactic longitude, and suggested that these might represent tangential spiral arms. This result implies emission in a direction along the arm, whereas it would be expected that the radiation, which is of a synchrotron type, would show a preference for directions perpendicular to magnetic field and hence spiral arms. As a result of further investigation of his observations he fitted a 2-start regular spiral to his

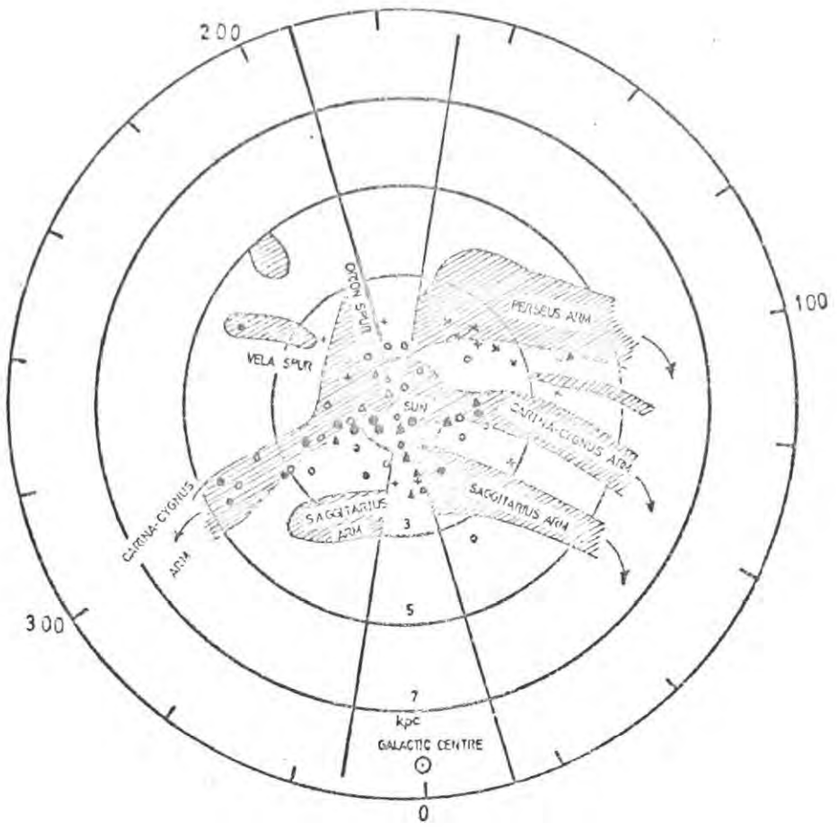

Figure 9-1 The local spiral structure of the Galaxy (Bok 1959) The shaded regions define the areas of H_I, • cepheids high concentration, · cepheids low concentration ○ OB associations, × radial velocities, ▲ H_{II} regions and + galactic clusters.

pattern of steps. The Orion arm lay in a direction defined by $\ell=80^{o}$ (Cygnus maximum) $\ell=262^{o}.4$ (Vela-Puppis maximum) at the Sun. This observation is consistent with the results of Bok (1959).

9.4 Thickness of the galactic disk

9.4.1 The thickness of the neutral hydrogen layer in the Galaxy

Schmidt (1957) obtained values for the neutral hydrogen layer thickness at a series of tangential points on the northern side of the Sun-centre line. He found an average value of 220 pc for the thickness between half density points. The fact that the thickness at tangential points appeared to be fairly constant over the range of longitude covered by his observations he felt justified in making the assumption of a constant layer thickness existing over the whole region inside and at the position of the Sun. A much lower value has been suggested by other physicists. A typical value of $\bar{z}_{\frac{1}{2}}=120$ pc for the arm at 3 kpc from the centre and for the high velocity material throughout the inner region was reported by Rougoor and Oort (1960) and Kerr (unpublished). Farther out from the Sun the thickness increases considerably, e.g. Habing (private communication) indicates that beyond R=12 kpc the thickness is many hundreds of parsecs. Kerr (1969) suggests that the half density thickness of the neutral hydrogen layer runs from 100 pc in the first 350 pc from the galactic centre to 120 pc in the 4 kpc expanding arm, 200 pc in the vicinity of the Sun, a value of $\sim$750 pc is reached at 15 kpc from the galactic centre.

The model of Falgarone and Lequeux (1972) indicates that the $\bar{z}_{\frac{1}{2}}$ is almost constant out to $\sim$5 kpc from the galactic centre increasing gradually out to $\sim$10 kpc and rapidly beyond, a result not inconsistent with the observations of Schmidt, Habing and Kerr. Falgarone and Lequeux show that tl thickness of the cloud system close to the Sun is 330 pc. The equivalent

thickness of the intercloud medium is 585±100 pc assuming a Gaussian shape.

9.4.2 Layer thickness for other constituents of the interstellar medium

Detailed studies of population I cepheids, Walraven, Muller and Oorsterhoff (1958) obtained a dispersion in the z component of ±65 pc for 160 cepheids whose positions were specified in terms of an early 21 cm result for the galactic pole derived by Westerhout (1957). Petit (1960) obtained a value of ±68 pc for a list of 191 cepheids. These results correspond to values for thickness between half density points of 153 and 160 pc respectively.

The layer thickness for optically observed H_{II} regions does not appear to have been worked out with the same precision but is ∿150 pc. Westerhout (1958) has considered the thickness of the layer of ionised hydrogen which is mainly responsible for the continuous spectrum radiation at 22 cm. A thickness of 200 pc is consistent with the observed brightness distribution.

9.5 Evidence of the hydrogen having a filamentary structure in the solar neighbourhood

Davies (1958) measured drift curves at 21 cm across regions in Auriga and Cygnus and he observed six elongated regions at a temperature cooler than the surroundings. The Auriga cloud had a kinetic temperature of $60^{\circ}K$, velocity dispersion 5 km sec^{-1} whilst the Cygnus clouds had a kinetic temperature $\leq 25\text{-}60^{\circ}K$ with a velocity dispersion of 6.5 km sec^{-1}. There was also evidence of cool dense neutral hydrogen regions lying between the bulk of the galactic neutral hydrogen emission and the Sun. McGee and Murray (1961) observe that hydrogen is predominantly horizontally stratified parallel to the galactic plane. Da Rocha Vieira 1971 found atomic hydrogen in the region of Centaurus. Clearly visible were three elongated features parallel to the galactic plane at heights ∿200 pc above the plane.

9.6 Existence of a sub-system in the local spiral arm

Gould (1879) indicated that the brighter stars,which could be observed with the naked eye , in the northern and southern Milky Way formed a belt inclined at an angle of 20^{o} to the galactic plane. This observation was confirmed by the work of Shapely (1919) who showed that the stars formed a sub-system of the Galaxy localised within several hundred parsecs of the Sun. The Gould Belt consisting of B stars,which were observable with the naked eye, lay within 200 pc of the Sun. He indicated that bright Be stars showed the same spatial distribution as the B stars. Reflection nebulae indicate a system inclined at 20^{o} to the galactic plane. The following parameters were given for the sub-system: north pole $\ell=202.^{o}2$, $b=72.^{o}6$, centre $\ell=272.^{o}2$, $b=-4.^{o}4$, radius $\sim$500 pc and mass $\sim 10^{8}$ $M_{\odot}$

Lynds (1962) published a catalogue of dark nebulae compiled from the blue and red Palomar sky survey prints. The catalogue is accompanied by statistics of angular sizes and opacities. The dark clouds are found predominantly along Goulds Belt. Dorschener and Gürtler (1963, 1966) and van den Bergh (1966) have published catalogues of reflection nebulae based on the sky survey, and made statistics of these objects. Van den Bergh list 13 associations of reflection nebulae which tend to fall in the Gould's Belt.

The 21 cm method is imprecise for tracing the nearby spiral structure however, observations at middle and high latitudes can reveal the general properties of the local gas. Three extensive surveys have been made of 21 cm radiation away from the Milky Way strip. The first was carried out by the Carnegie Institution group in Washington DC (Erickson, Helfer and Tatel, 1959 ; Erickson and Helfer, 1960), the second in Sydney (McGee, Murray and Pawsey, 1961 ; McGee and Murray, 1961) and the third at Jodrell Bank (Davies, 1960) . The details of these experiments are outlined in table 9.1.

Table 9.1 Surveys of hydrogen 21 cm emission in the solar neighbourhood

Reference	Year	Beam width degrees	Band width kc/s	Region	Sampling interval	Form of Presentation of data
Davies	1960	1.5 x 1.7	100, 25	Whole sky lat. δ=53°N	≤5°	B_{int} map
Erickson & Helfer	1960	1.8 x 2.5	12	Whole sky lat. δ=59°N $\|b\|>20°$	ℓ,b,10°	Profiles
McGee & Murray	1961	2.2	38	Whole sky lat. δ=34°S	ℓ,30°,b,2°	Sky maps, N_H, v at max

Davies (1960) showed that a number of neutral hydrogen clouds coincide in position with dust complexes. The major feature of the distribution is the excess of neutral hydrogen in the position of the local system (Gould's Belt) of early type stars and dust. The system ($\sim 10^5$ $M_\odot$) appears to represent a later formation in the local spiral arm.

McGee, Murray and Pawsey (1961), McGee and Murray (1961) found that the observed distribution in the neutral hydrogen in the solar region was such that the minima were displaced from the galactic poles by $\sim 30^\circ$ implying the existence of a rough connection with the plane of the local system of stars, the Gould's belt, but McGee & Murray (1961) point out that there is closer agreement with the plane of galactic magnetic field in the solar vicinity as derived by Shain (1957) from optical polarization measurements. In addition to general stratification of the hydrogen there are some particular regions of higher density such as the spur in Scorpius-Ophiuchus and the region Gemini-Taurus-Orion. These are generally related to known areas of optical obscuration and are presumably nearby cloud complexes of dust and gas. In low latitudes differential rotation effects show up clearly but there are also additional motions of a systematic nature which cannot be completely separated from differential rotation in the absence of a distant scale. The most recognisable effects according to McGee & Murray are an outward flow with a mean velocity of 6 km sec^{-1} in the approximate directions of the centre and anti-centre. Helfer (1961) has also analysed the velocity field of the local gas and has derived an expression for the velocity-distance relation which best fits the Carnegie observations. Lilley and Heeschen (1954) found a correlation between neutral hydrogen gas and dust in southern parts of the sub system. Braes (1963) found a peak intensity over the whole region at 6 km sec^{-1} with explanation as either due to outward motion of the adopted LSR pro-

posed by Kerr or more probably by a nearby cloud of hydrogen receding from the Sun.

Lindblad (1967) observed 21 cm H_I features which were quite extensive in longitude indicating close proximity to the Sun. One in particular can be seen in emission over a longitude range about 80°-250°. All the information presented in this chapter so far is consistent with a model proposed by Lindblad (1967) which explains the observed distribution of hydrogen in the solar neighbourhood.

He shows that the neutral hydrogen in the solar neighbourhood is in the form of an ellipse which is expanding with the dimensions 1300x560 pc with its centre 270 pc from the Sun as shown in figure 9.2. The thickness of the neutral hydrogen ring is $\sim$10 pc, the kinetic energy of the expansion at present is $>10^{51}$ ergs, the total mass of hydrogen involved is 3×10^{6} $M_{\odot}$. The velocity of expansion, if at the speed of sound, is consistent with a temperature for interstellar gas of $\sim2500^{\circ}$K. The ring appears to be the remains of a large explosion, possibly a type III supernova, in the neighbourhood of the Sun. These supernovae occur at a rate of about once every 10^{7} years and liberate $\sim10^{53}$ ergs. The age of the ellipse of hydrogen is 65×10^{6} years which is short enough not to be dispersed by normal galactic rotation.

9.7 Simple model for explaining the shape of the energy spectrum in the region of the "knee"

On the assumption that the ellipse of hydrogen proposed by Lindblad (1967) does exist, some interesting hypotheses are possible.

Plotted in figure 9.2 are the sheets of hydrogen observed by Heiles (1967). The 500 pc distant sheet is seen to be coincident with the hydrogen observed by Lindblad (1967) and which forms part of the ring

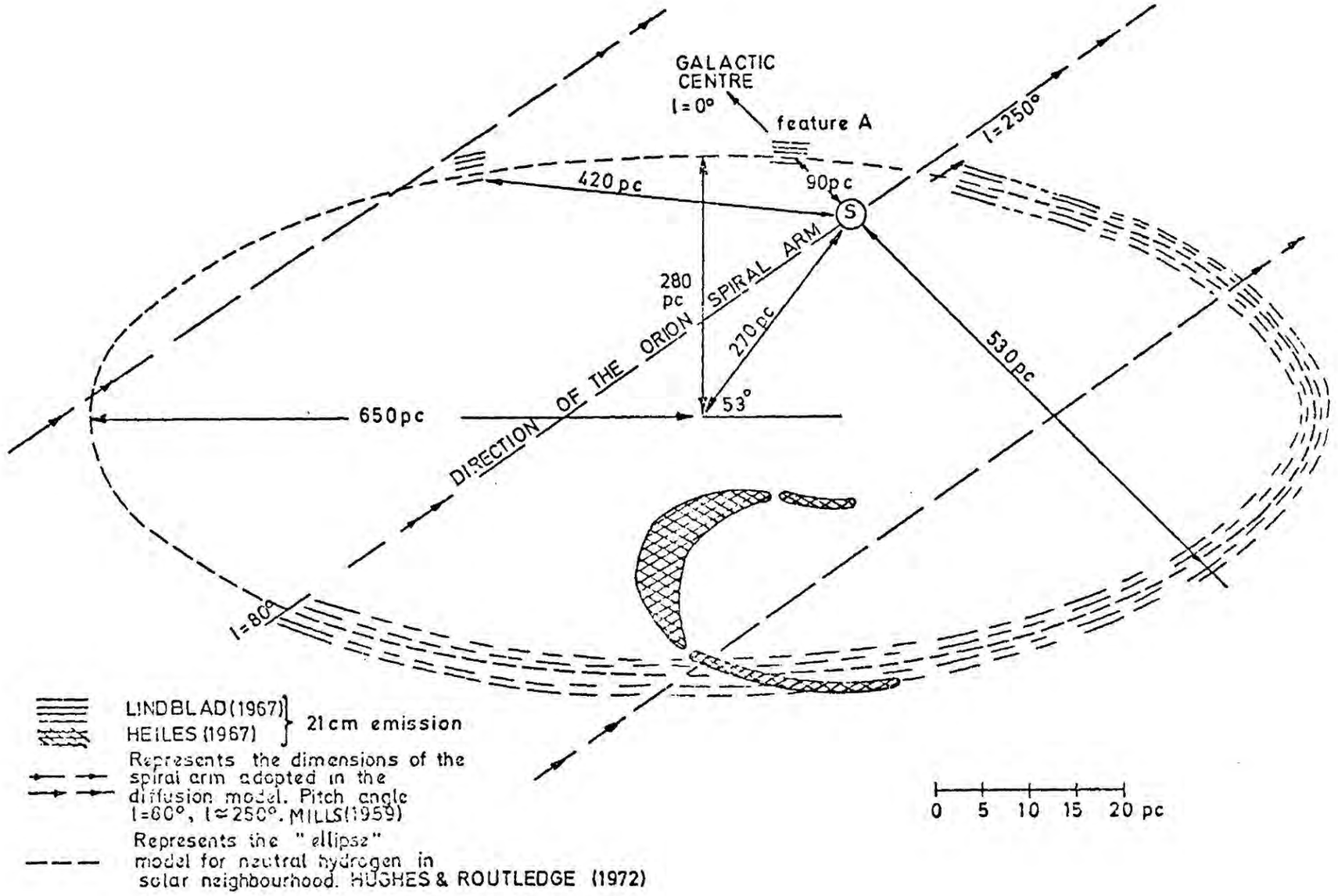

Figure 9-2 The distribution of hydrogen in the solar neighbourhood.

(S marks the position of the Sun.)

of hydrogen. Lindblad (1967) proposed a value of 10 pc for the thickness of the shell which is consistent with the measured width of 10 pc for the sheets of hydrogen,Ames and Heiles (1970). This filamentary nature of the hydrogen in the region of the solar neighbourhood has, in the earlier sections of this chapter, been shown to be a common feature. Although actual distances to these filaments are unknown, they can be considered, along with the 330 pc and 500 pc sheets of Heiles (1967) and the stars and dust present in the Gould belt system to represent the shock wave-front of the type III supernova explosion considered by Lindblad.

The volume of interstellar matter enclosed by the ring of hydrogen, assuming the half density thickness to be 330 pc (a value obtained from the model of Falgarone and Lequeux , 1972) is $V=\pi abz=\pi x1300x560x330=7.55\ 10^{8}\ pc^{3}$. Because the density of cosmic rays is observed to be $\sim$1eV cm^{-3} then the total energy involved, if the entire volume inside the ellipse possessed this density, is $\sim 2\ 10^{64}$ eV or $3\ 10^{52}$ ergs. We can conclude that a type III SN explosion would yield sufficient energy to give the observed cosmic ray density.

The major axis of the ellipse lies $\sim 30^{o}$ to the direction of the spiral arm. It is evident that the elliptical shape could have been due to the stretching of the initially spherical orientation of the shock front (made up of interstellar matter) caused by the explosion, by the magnetic fields associated with the local spiral arm. It can be seen in figure 9.2 that the hydrogen which is obviously not symmetrically orientated as in the diagram, lies approximately in the direction of the spiral arm (Mills, 1958, 1959 and Bok, 1959).

The simple model, shown schematically in figure 9.3, is then developed as follows.

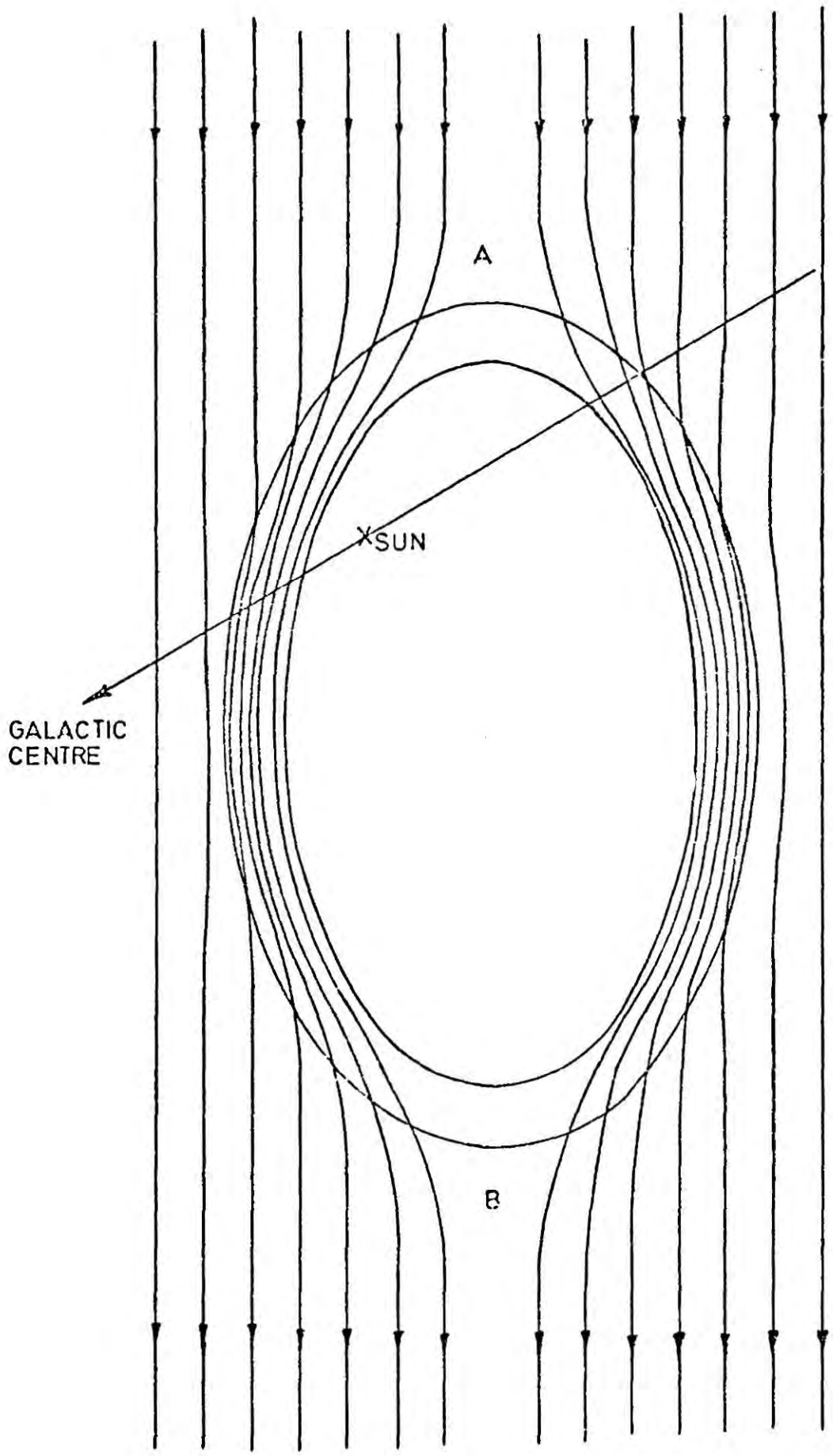

Figure 9-3 A schematic representation of the type of distortion in the magnetic field expected if an ellipse of hydrogen, dust, stellar matter etc. existed as a subsystem in the spiral arm in the solar neighbourhood.

A magnetic field ∿3 μgauss (see chapter 6) is frozen into the ring of hydrogen with the field lines directed approximately along the length of the ellipse, due to the effect of the large scale magnetic fields in the local spiral arm.

Because the thickness of the shell is 10 pc and E=300 HR then those cosmic rays of energy ≳3 10^{16}eV only are allowed to escape from the ellipse or enter the ellipse from the other parts of the Galaxy.

At the edges of the ellipse at points A and B an equilibrium is built up between the diffusion of cosmic rays of all energies out of and into the ellipse where streaming could occur.

Cosmic rays of energy ≲3 10^{16}eV are effectively trapped inside the ellipse due to the fact that the magnetic field frozen into the shell acts as a reflecting boundary giving complete randomisation of the cosmic rays arriving at the Earth even though the Sun, in this model lies closer to the hydrogen in the galactic centre than anticentre direction.

Cosmic rays of energy ≳3 10^{16} eV escape from the ellipse with little probability of returning.

We have a situation, then, where the energy spectrum up to the "knee", occuring at an energy ∿10^{16}eV, is explained in terms of cosmic rays produced by the SN type III "bang" some 10^{7} years ago and the cosmic rays beyond the energy of the "knee" are either galactic or extragalactic origin. The change of slope would be accounted for because it would be assumed that the cosmic rays produced by the super-nova explosion exhibit their production spectrum only whilst the cosmic rays from sources outside the ellipse will be modified by passing through the interstellar medium or even by a different production spectrum at their source.

Complete isotropy of cosmic rays at low energies is assured by multiple reflections from the walls of the ellipse, and at high energies provided the galactic sources are evenly spread about the ellipse. Of course there is no problem with isotropy of cosmic rays of extragalactic origin.

It is interesting to repeat the words of Hughes and Routledge (1972) who have put forward quite convincing evidence in support of the existence of the ellipse of hydrogen first suggested by Lindblad (1967): "The explosion might have been so great that even though at the time the Sun was probably about 1 kpc away, the resulting flux of cosmic ray particles together with other forms of radiation and the effects of the ensuing shock wave which passed through the solar system (or through which the Sun passed) may have been severe enough to leave a record on the lunar surface or on the surfaces of other planets and satellites in the solar system. Two facts which might be significant in this regard are the catastrophic change in the terrestial flora and fauna that occurred with the close of the Mesozoic Era, approximately 65 10^6 years ago and which has been attributed to a supernova explosion (Russel and Tucker, 1971) and the possible "contamination" of the lunar surface with carbon compounds observed in recent studies of lunar samples".

Even though a simple calculation predicted the position of the "knee" in this simple "ring of hydrogen" model to be 3 10^{16}eV it will probably be slightly lower than this due to the lack of continuity of the ring and possible irregularities in its absolute thickness.

The degree of smearing in the region of the "knee" is also a function of these irregularities. It is stressed that this model is rather naive but sufficient to propose physical arguments to explain the shape of the cosmic ray energy spectrum.

9.8 Conclusions

The position of the Sun at the centre of a circular spiral arm of radius 300 pc the value which was adopted in the diffusion model has been shown to be consistent with experimental observations of the inter-cloud medium, in the solar neightbourhood, Mills (1959), Bok (1959).

The primary cosmic ray energy density can be accounted for in terms of a type III super nova explosion which occurred $\sim 10^7$ years ago, and the shape of the energy spectrum in the region of 10^{16}eV is explained due to the existence of a shell of hydrogen enclosing the solar neighbourhood which prevents the escape of cosmic rays of energy $\lesssim 10^{16}$eV and allows the escape of cosmic rays of energy $\gtrsim 10^{16}$eV.

Chapter 10 Conclusion

The diffusive propagation of cosmic rays from the "cloud" approach as a possible explanation of the shape of the cosmic ray energy spectrum in the region of several 10^{15} eV, observed at the Earth has not been pursued by many physicists. The main reasons have been due to the expected E^2 dependence of mean free path arising from the small angle multiple scattering at "high"† cosmic ray energies, Ginzburg and Syrovatskii (1964), and also the problems encountered by having to ensure that cosmic rays of all energies arrive isotropically at the Earth.

In the case of an idealised interstellar medium, the characteristic E^2 dependence occurs after only a short transition region present about an energy of $\sim 3\ 10^{15}$ eV for clouds with constant magnetic fields of 3 μgauss coherent over dimensions of about 1 pc. The fact that the clouds do not have constant dimensions and/or magnetic field strengths formed the basis for the development and subsequent success of the present author's treatment of cosmic ray diffusion in the interstellar medium.

If the distribution of H_oR_o is considered to follow a linear, power or exponential law then no significant improvement over diffusion in an idealised medium was obtained. The effect was to cause smearing over a larger range of energy, the range and degree of smearing depending respectively on the range of values of H_oR_o and the type of law considered. The work of Kota (1973) was based on an analytical treatment of cosmic ray diffusion. In order to obtain soluble integrals two simple power laws were fitted to the H_oR_o distribution developed by the author from the results of Heiles (1967). A power law with a positive slope over the range $1 \leq p_o \leq 4$ pc cm^{-2} and a negative power law for $p_o \geq 4$ pc cm^{-2} were used. The results of the calculations gave an energy spectrum which was unsatisfactory,

---

† for definition see section 4.4.2

there was substantial smearing over approximately one and a half decades in energy but no change of slope other than that due to the characteristic E^2 dependence which occurred beyond the wide transition region was in evidence.

The numerical treatment performed by the author has given conclusive evidence that provided clouds with small values of H_oR_o are more abundant, by a factor $\sim 10^3$, than clouds with large values then favourable characteristics are obtained for the energy spectrum in the region of the "knee". The shape, position of the "knee", the absolute value for the change of slope and the range of energy over which this change of slope remains before it assumes the value of two, characteristic of an idealised medium, are dependent on the shape of the H_oR_o distribution adopted for calculation. It has been shown that that implied by direct experimental observations, Heiles (1967), has been responsible for the success of the diffusion model.

The energy spectrum representing diffusion of cosmic ray protons in this physical medium is shown in figure 7-6.

Cosmic ray primaries have been observed directly at energies below $\sim 10^{11}$ eV and they are known to possess atomic masses greater than unity. A detailed survey of the relative abundances of cosmic rays obtained experimentally at these energies was made and used as the basis to predict the galactic modulated energy spectrum representing diffusion of cosmic rays with a mixed composition at EAS energies. This is also plotted in the integral and differential form in figure 7-6.

Having made the predictions for the two energy spectra based on cosmic ray diffusion they were put to test by comparing with the experimental observations of cosmic rays observed at the Earth. This was achieved by using the simulations of EAS propagation through the atmosphere made by Bradt et al (1965), de Beer et al (1966) and Dixon et al

(1973). It was shown that diffusion of cosmic ray protons in the interstellar medium between the source and the Earth provided adequate explanation of the size spectra of muons and electrons observed at sea level as well as electrons at mountain altitudes up to an energy of 10^{17} eV. The energy spectrum at the top of the atmosphere predicts that the "knee" occurs at $3.4\ 10^{15}$ eV.

(It must be stressed that the derivation of the size spectra from the energy spectra predicted by diffusion for comparison with the experimental observations relies on simulations of EAS through the atmosphere which themselves are open to question. For this reason the implications of chapter 8 are to be regarded qualitatively).

The question of lack of isotropy of cosmic rays has been shown not to arise below energies $\sim 5\ 10^{16}$ eV, for the case of diffusion of protons in an idealised medium, constant cloud size R_o=1pc, constant field H_o=3 μgauss, provided that the Earth is at the centre of the spiral arm. At and beyond these energies one can argue that sources in particular regions of the Galaxy emit more strongly at these energies than sources in the other regions but this is rather unlikely. Alternatively it can be argued that the presence of "bands" of hydrogen of the appropriate thicknesses strategically positioned could act as reflecting boundaries causing randomisation of cosmic ray directions arriving at the Earth; although a more attractive theory, again rather unlikely. However, throughout the development of the model for diffusion in a physical interstellar medium, only that part of the curve below that energy where problems of anisotropy arise has been considered.

A suggestion for the origin of the "knee" has been put forward as an interesting alternative to cosmic ray diffusion. This is based on the possibility of cosmic rays with energies below the "knee" being produced by a supernova explosion type III which occurred 65×10^6 years ago some

170 pc distant from the Sun and those beyond the "knee" are from other parts of the Galaxy. The change of slope would then be either a consequence of the fact that the production spectrum for cosmic rays, with energy below that defined by the "knee", of the type III supernova is different to the production spectrum of cosmic rays, with energies above the "knee", by galactic sources or alternatively it is believed that cosmic rays of all energies have the same production spectrum then the change of slope would be due to the fact that below the "knee" cosmic rays are of local origin and those above have their energy spectrum modified during their journey through interstellar matter.

The basic diffusion model calculations in an idealised medium assume constant step lengths between consecutive cloud deflections, an assumption which is unphysical. The introduction of, say, an exponential or power law for the distribution of step lengths would have been chosen with no real experimental support. The adoption of a value L=10 pc however, was not without physical reasoning. The numerical value was derived by considering that some 10^3 clouds existed in the region of space some 10^6 pc^3 observed by Heiles, but also it is known that there exists in the Galaxy an overall, large scale magnetic field associated with the spiral arms of the Galaxy which no doubt affects the cosmic ray in between the "collisions" with the small scale irregularities. The effect of a large scale field, then, would be to confine the cosmic ray a lot longer in the spiral arm. This is exactly what the effect of assuming a constant step length between collisions has - i.e. it pushes the cosmic ray into a "back and forwards" or "circular type" motion providing the cosmic ray with less chance of progressing towards the edge of the spiral arm which would not be the case if the step length had an exponential form for example.

In addition, the width of the spiral arm was chosen to be 600 pc on the basis of the value given by Ilovaisky and Lequeux (1972) for the half density height of the interstellar medium of the galactic disk in the region of the solar system whereas it was thought that a value nearer to that given for the half density height for clouds equal to $\sim$200 pc (Schwartz (1957) etc) would be more appropriate. However, choosing the higher value does in fact also help to compensate for not considering the presence of a magnetic field between the clouds. In other words, the latter two points effectively increase the value of G, thus increasing the geometrical cut off energy discussed in section 4.4.3.

Suggestions for further development of the diffusion model would be to take into account the presence of a full scale magnetic field of $\sim$3 μgauss as well as a distribution of step lengths, furthermore the fact that the z distribution of cloud and interstellar medium is Gaussian and the possibility of the presence of hydrogen masses in the vicinity of the Sun which could help to isotropise the directions of the "high" energy cosmic rays could also be considered.

The part played by a halo surrounding the disk of the Galaxy was ignored because there is no direct and conclusive experimental evidence that the halo does in fact exist. If indeed it does exist, it is believed to possess only a very weak magnetic field with very little internal structure in the form of clouds. Even if completely random weak fields exist then it is believed that the halo would take little part in the cosmic ray diffusion process except perhaps at very low energies. A situation where the halo could act as a reflecting boundary returning cosmic rays escaping from the disk is unlikely and therefore the "no return" condition assumed in the diffusion model is still valid. In the event of the existence of a halo being proved this would open up another

avenue for the development of the diffusion model.

The diffusion model developed in this thesis was based on experimental observations and details were taken care of by adopting a numerical treatment of the problem using a computer. These facts together are responsible for its success. The inevitable cut off in the spectrum occurring at $\sim 10^{17}$ eV where diffusion breaks down and is characteristic of the E^2 effect makes it necessary to assume that cosmic rays beyond this energy are of extragalactic origin when no problems of isotropy will be encountered. No indication of their possible composition can be made.

Appendix (i) The effect of fluctuations in the mean electron size on the differential and integral size spectra

(i) - 1 Distribution of electron number at sea level for a particular primary energy.

The frequency distribution for the number of electrons expected at sea level for a proton primary of energy 4 10^{14} eV, arriving vertically at the Earth, is shown in figure (i) - 1. The datum, in the form of a histogram, is taken from the model I calculations of de Beer et al (1966). The electron distribution increases in width with increasing zenith angle θ and with decreasing primary energy, E_o. This is because an increase in θ and a decrease in E_o is equivalent to observing an older shower at a point away from its maximum and the fluctuations are more pronounced. The electron distribution is sharpened for heavy primaries due to energy sharing between the nucleons. Assuming that a heavy initiated shower of mass A is equivalent to the superposition of A showers each with A times smaller energy, then for the adopted model (de Beer et al 1968):-

$$\left(\frac{\sigma}{\bar{N}_e}\right)_A = \left(\frac{\sigma}{\bar{N}_e}\right)_p \quad A^{-\frac{1}{2}}$$

where σ is the standard deviation and $\bar{N}_e$, the mean number of electrons in the shower. For the shower in figure (i) - 1, $\bar{N}_e = 7.2\ 10^4$ particles and $\theta = 0^o$, de Beer et al (1968) gives a value of 0.55 for $\frac{\sigma}{\bar{N}_e}$.

Popowa (1969) found that in general the distribution of electron size expected at sea level is best fitted by a gamma function. The general expression for a gamma function is:

$$f(x) = \frac{q^p}{\Gamma(p)} \quad x^{p-1} \exp(-qx)$$

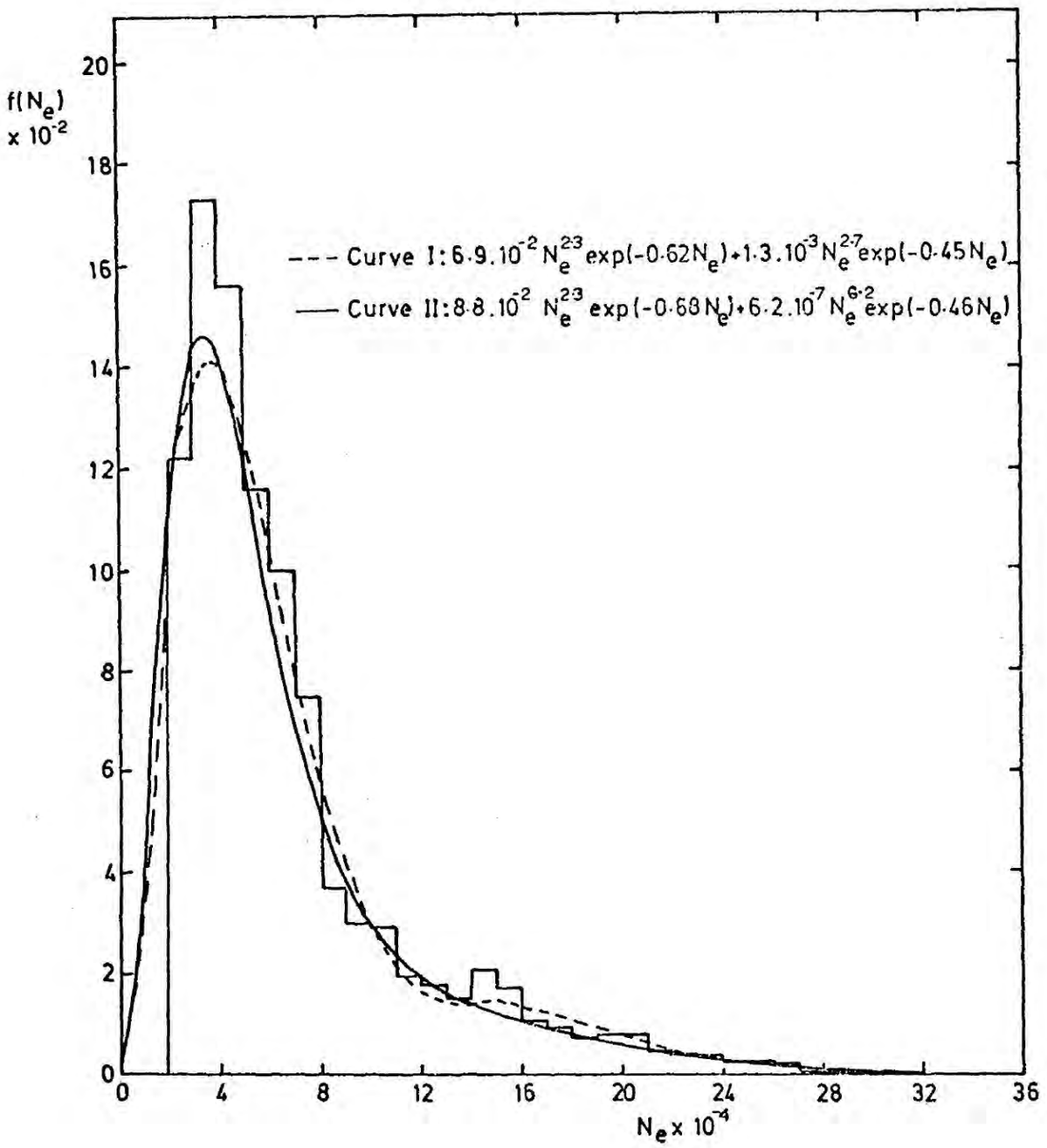

Figure (i)-1 The electron size distribution expected at sea level for a cosmic ray of energy 4 10^{14}eV as established by the Model I air shower simulations of de Beer et al (1966).

The first moment: $\int_0^\infty f(x)dx = 1$ is equivalent to normalisation, from the second moment the mean of the distribution $\bar{x} = \int_0^\infty x\, f(x)dx$ is obtained. The standard deviation is calculated in the normal way and finally the maximum of the distribution x_{max} is obtained such that the conditions $\frac{d}{dx} f(x) = 0$ and $\frac{d^2}{dx^2} f(x) < 0$ are fulfilled. This gives $\bar{x} = \frac{p}{q}$ and $\sigma^2 = \frac{p}{q^2}$ and so for the electron size distribution putting $x = N_e$ we get

$$f(N_e) = \frac{\left(\frac{\bar{N}_e}{\sigma^2}\right)^{\left(\frac{\bar{N}_e}{\sigma}\right)^2}}{\left(\Gamma\left(\frac{\bar{N}_e}{\sigma}\right)^2\right)} \quad N_e^{\left(\left(\frac{\bar{N}_e}{\sigma}\right)^2 - 1\right)} \quad \exp - \left(\frac{\bar{N}_e}{\sigma^2}\right) N_e$$

$$\text{and } N_{e_{max}} = \frac{p-1}{q} = \frac{\bar{N}_e^2 - \sigma^2}{\bar{N}_e} \qquad \text{(i) - 1}$$

The best fit, curve I in figure (i) - 1, is the sum of two gammas; the first with origin at 0 and peak at $4\ 10^4$ particles and the second with origin at $1.1\ 10^5$ particles and peak at $1.5\ 10^5$ particles. However, when the fluctuations so represented were folded into the Greisen spectrum the resultant equations were insoluble. To obtain workable formulae two gammas had to be fitted to the distribution such that their origins were each at zero. This fit is marked by II in figure (i) - 1 and was obtained in the following way. The "principal" gamma function was fitted assuming the peak of the distribution to be at $3.4\ 10^4$ particles and assuming $\frac{\sigma}{\bar{N}_e} = 0.55, \bar{N}_{e_c} = 4.87\ 10^4$ particles from equation (i) - 1 and $\sigma_c = 2.68\ 10^4$ particles. The "principal" gamma function is therefore $f_c(N_e)\, dN_e = 1.03\ 10^{-1}\ N_e^{2.30} \exp(-0.68\ N_e) dN_e$ normalised to unity. Subtracting the

distribution from the histogram and applying the theory of Gaussian statistics the mean size of the remaining histogram was found to be $\bar{N}_{e_m} = 1.56\ 10^5$ particles with a standard deviation $\sigma_m = 5.83\ 10^4$. The "minor" gamma function is therefore $f_m(N_e)\ dN_e = 4.3\ 10^{-6}\ N_e^{6.21} \exp(-0.46N_e)\ dN_e$ normalised to unity. The total area beneath the distribution of N_e is equivalent to 100 showers. The ratio of the area beneath the minor to that of the principal is $\frac{1}{6}$. Giving:

$f_T(N_e)dN_e = 8.8\ 10^{-2} N_e^{2.3} \exp(-0.68 N_e) + 6.2\ 10^{-7} N_e^{6.2} \exp(-0.46 N_e)\ dN_e$

as the adopted fit to the distribution. This equation is for one particular size distribution produced by a shower of unique energy. The general formula valid for all showers is:

$$f(N_e,\bar{N}_e)\ dN_e = \left[\frac{19}{\bar{N}_{e_c}}\left(\frac{N_e}{\bar{N}_{e_c}}\right)^{2.3} \exp\left(-3.3\,\frac{N_e}{\bar{N}_{e_c}}\right) + \frac{1.3\ 10^3}{\bar{N}_{e_m}}\left(\frac{N_e}{\bar{N}_{e_m}}\right)^{6.12} \times \exp\left(-7.1\ \frac{N_e}{\bar{N}_{e_m}}\right)\right] dN_e$$

(i)-2 The relationship between shower size and primary energy

In EAS work, the shower "size" is defined as the total number of particles of all types which would be detected and counted at sea level by a huge detector covering the entire shower front. In practice only a fraction of the area is sampled and the total number of particles is inferred by the use of a "structure function" see section 2.4.1 Since electrons constitute the bulk of the particles little error is introduced by equating the electron size with the actual shower size. de Beer et al (1966) predict from their model I calculation that the

relationship between primary energy E_o and the mean electron size $\bar{N}_e$ of a shower is given by

$$E_o = 9.5\ 10^{13} \left(\frac{\bar{N}_e}{10^4} \right)^{0.91} \text{ eV} \qquad \text{(i) - 2}$$

This expression predicts a primary energy of $5.7\ 10^{14}$eV instead of $4\ 10^{14}$eV for the shower in figure (i) - 1 because the mean size defined by the histogram is $7.16\ 10^4$ particles. This discrepancy of a factor $\sim 3/2$ in energy is due to the inaccuracies in taking data from published work.

(i) - 3 The calculations performed to establish the importance of the fluctuations in electron size.

The "knee" observed in the primary energy spectrum in the region of $\sim 10^{16}$eV appears to be a well established phenomenon. One of the first summaries of the differential spectrum was given by Greisen (1966a)

$$J_B(E_o)\ dE_o = 4\ 10^{18}\ E_o^{-2.6}\ dE_o \quad \text{below the "knee"}$$

and $$J_A(E_o)\ dE_o = 10^{28}\ E_o^{-3.2}\ dE_o \quad \text{above the "knee"}$$

where E_o is in eV. Equating these two spectra the "knee" is found to be $\sim 5\ 10^{15}$eV. Using equation (i) - 2 this energy spectrum is converted to a size spectrum such that

$$J_B(\bar{N}_e)\ d\bar{N}_e = 1.05\ 10^2\ \bar{N}_e^{-2.5} \text{ below the "knee"}$$

and

$$J_A(\bar{N}_e)\ d\bar{N}_e = 1.82\ 10^5\ \bar{N}_e^{-3.0} \text{ above the "knee"}$$

the "knee" occurring at $8.5\ 10^5$ particles. Given that $f_T(\bar{N}_e, N_e)\ dN_e$ represents the total electron size distribution and assuming that the width of the distribution is the same for all sizes, the effect of the

fluctuations in the electron size distribution can be established by performing the following integration:-

$$J(N_e)dN_e = \int_o^k (f_T(\bar{N}_e,N_e)\ J_B(\bar{N}_e)dN_e)\ d\bar{N}_e + \int_k^\infty (f_T(\bar{N}_e,N_e)\ J_A(\bar{N}_e)dN_e)\ d\bar{N}_e \quad \text{(i) - 3}$$

Because, in fact, $f_T\ (\bar{N}_e,N_e)$ is the sum of two functions the integration above is carried out in two independent steps, i.e. for each of the two gamma functions.

Figure (i) - 2 assists in understanding the effect of dividing the two electron size distribution into two components. Each gamma function has a mean size which is related directly to the primary energy of the total shower because their E_o-$\bar{N}_e$ relationship is modified by the factor equal to the ratio of the mean size of the gamma to that of the total distribution. The situation now is to divide the Greisen energy spectrum into two parts and weight each according to the areas beneath the two gamma functions. Also because the E_o to $\bar{N}_e$ relationship is different for each gamma function the position of the "knee" in the size spectrum is shifted. The E_o versus $\bar{N}_e$ relationship, the gamma function, the size spectrum above and below the "knee" and the "knee" position as calculated for each component of the electron size distribution are given in table (i) - 1.

The integration defined by equation (i) - 3 was effectively, performed twice because $f_T(\bar{N}_e,N_e) = f_c\ (\bar{N}_e,N_e) + f_m\ (\bar{N}_e,N_e)$. The results are shown in figure (i) - 3 where the differential size spectrum with and without fluctuations for each component of the integration is plotted. The sum of the two component spectra gives the Greisen spectrum (differential) along with the estimated fluctuations. The integral size

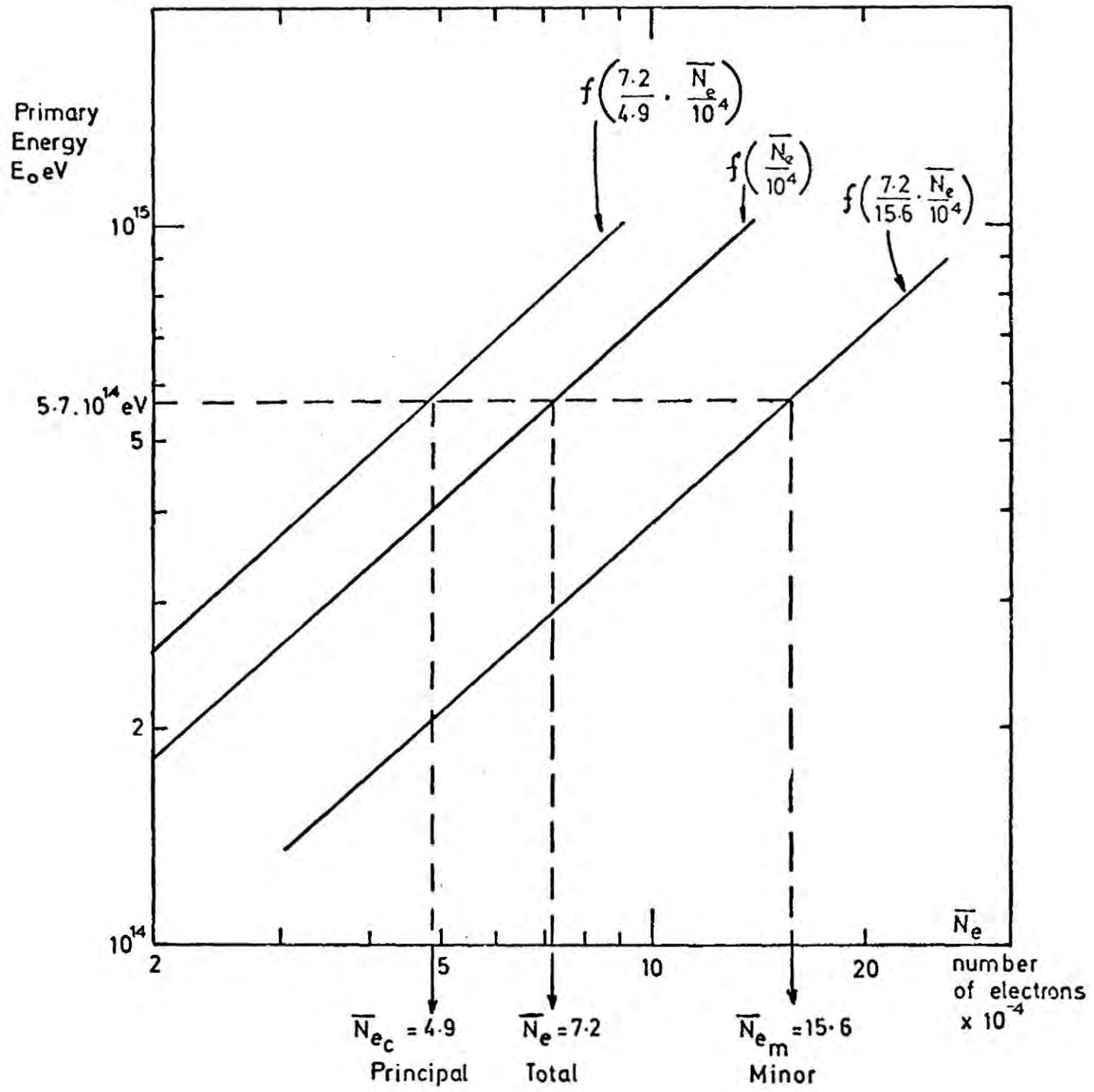

Figure (i)-2 A schematic representation of the relationship between the mean electron size $\bar{N}_e$ of the total shower and the effect of dividing the total distribution of the shower into two gamma functions.

Table (i) - 1 A summary of the information needed to perform the integrations

	Principal	Minor	Total
E_o versus $\bar{N}_e$	$E_c = 9.5\ 10^{13}\left(\frac{\bar{N}_{e_c}}{10^4} \cdot \frac{7.2}{4.9}\right)^{0.91}$	$E_m = 9.5\ 10^{13}\left(\frac{\bar{N}_{e_m}}{10^4} \cdot \frac{7.2}{15.6}\right)^{0.91}$	$E_o = 9.5\ 10^{13}\left(\frac{\bar{N}_e}{10^4}\right)^{0.91}$
$f(\bar{N}_e, N_e)dN_e$	$\frac{19}{\bar{N}_{e_c}}\left(\frac{N_e}{\bar{N}_{e_c}}\right)^{0.30} \exp - \left(3.3\ \frac{N_e}{\bar{N}_{e_c}}\right)$	$\frac{1.3\ 10^{13}}{\bar{N}_{e_m}}\left(\frac{N_e}{\bar{N}_{e_m}}\right)^{6.12} \exp - \left(7.1\ \frac{N_e}{\bar{N}_{e_m}}\right)$	Histogram
Size Spectrum Below the knee $f_B(\bar{N}_e)\ d\bar{N}_e$ without fluctuations	$52\ \bar{N}_{e_c}^{-2.456}$	$47\ \bar{N}_{e_m}^{-2.456}$	$105\ \bar{N}_e^{-2.456}$
Size Spectrum above the knee $f_A(\bar{N}_e)\ d\bar{N}_e$ without fluctuations	$7.2\ 10^4\ \bar{N}_{e_c}^{-3.002}$	$1.2\ 10^5\ \bar{N}_{e_m}^{-3.002}$	$1.8\ 10^5\ \bar{N}_e^{-3.002}$
knee position k particles	$5.75\ 10^5$	$1.83\ 10^6$	$8.47\ 10^5$

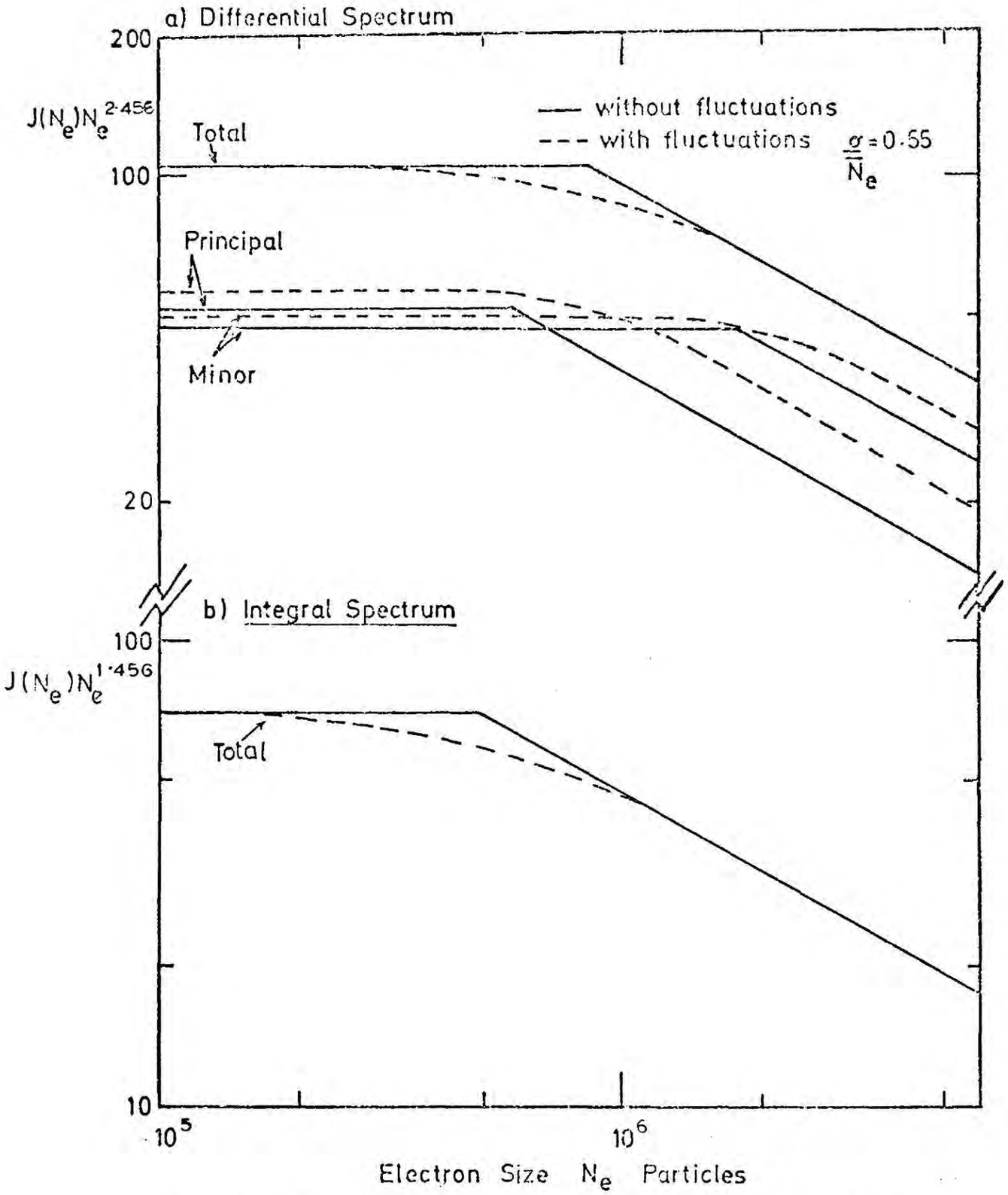

Figure (i)-3 (a) the differential and (b) the integral size spectrum for cosmic rays with fluctuations (dotted line) and without fluctuations (solid line).

spectrum with and without fluctuations for the total spectrum is also plotted.

In this treatment it is assumed that the value of $\frac{\sigma}{\bar{N}_e}$ is constant for showers of all energies. This is known not to be strictly the case. The recent Monte Carlo calculations of Dixon et al (1973) show that the quantity $\frac{\sigma}{\bar{N}_e}$ changes from 0.8 for a cosmic ray primary of energy 10^{15}eV down to 0.35 at 10^{18}eV (see also de Beer et al (1968) Adcock et al (1968)). In fact in the opinion of Hillas (private communication) $\frac{\sigma}{\bar{N}_e}$ can reach a value as high as 2 at low energies. The sensitivity of the "smoothing" in the region of the "knee" as a function of $\frac{\sigma}{\bar{N}_e}$ was established by assuming that the electron size spectrum at sea level for a particular primary cosmic ray energy is best represented by a single gamma function of the form:-

$$f(\bar{N}_e, N_e)\, dN_e = \frac{\Gamma(\gamma+2)}{(\gamma+1)^{(\gamma+2)}} \left(\frac{N_e}{\bar{N}_e}\right)^{\gamma} \exp\left(-(\gamma+1)\left(\frac{N_e}{\bar{N}_e}\right)\right) \frac{dN_e}{\bar{N}_e}$$

where $\gamma = \left(\frac{\bar{N}_e}{\sigma}\right)^2 - 1$

This function along with the Greisen spectrum (defined in column 3 table (i) - 1) was substituted in equation (i) - 3 and the integration was performed for values of $\frac{\sigma}{\bar{N}_e}$ = 0.4, 1.0 and 2.0. The results are shown in figure (i) - 4 where both the integral and differential spectra are plotted.

(i) - 4 Conclusion

Even for a fractional uncertainly of $\frac{\sigma}{\bar{N}_e}$ = 2.0 in the mean electron size at sea level, for showers of all energies, there seems to be little smearing in the region of the "knee" in the size spectrum. Appearing in

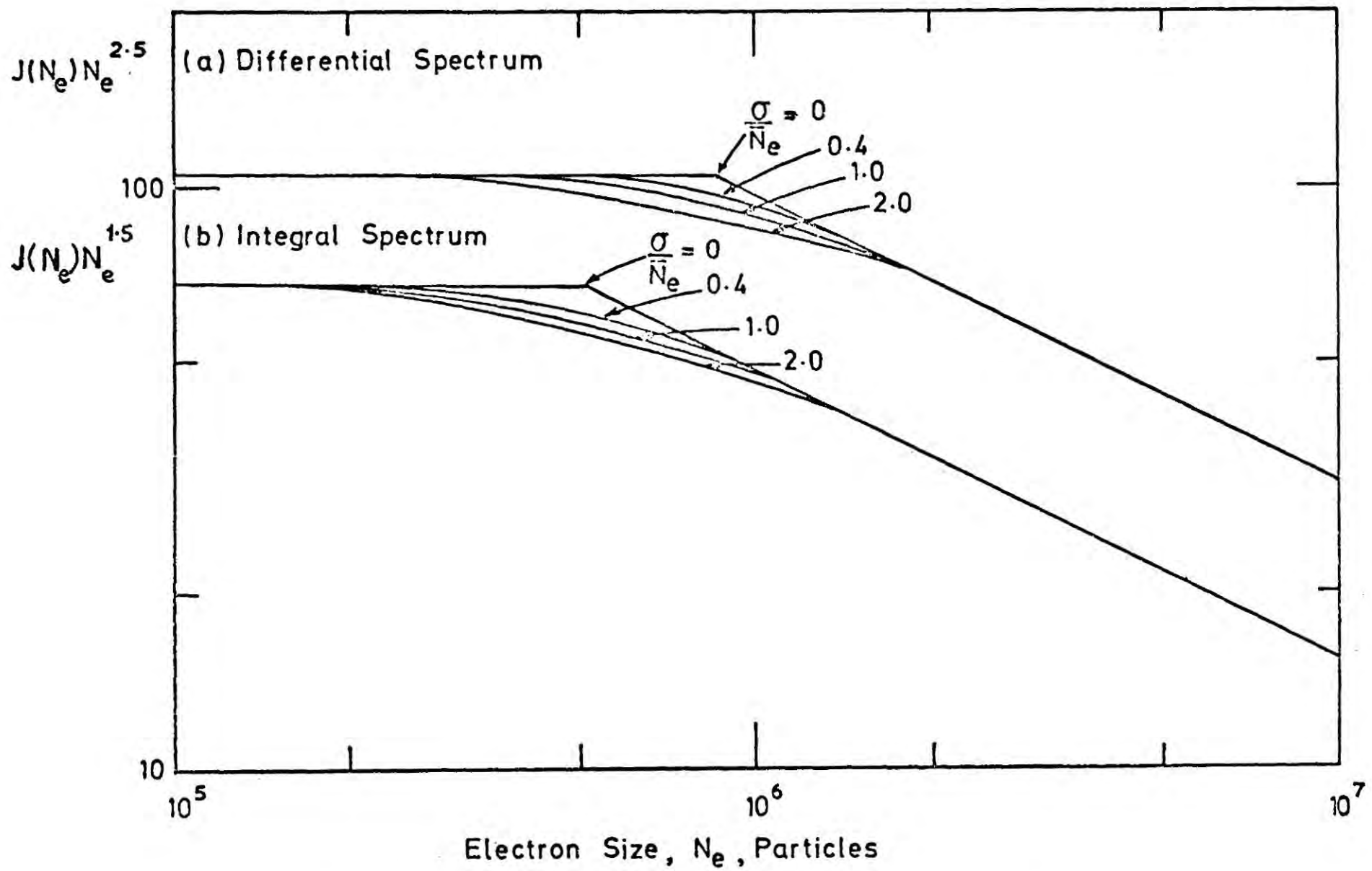

Figure (i)-4 The effect of fluctuations in the electron size distribution at sea level (a) and (b) are the differential and integral spectra respectively.

figures (i) - 3 and (i) - 4 are the integral spectra derived from the differential spectra also plotted in the figure. Although small, some additional smearing is obtained by converting from a differential to an integral size spectrum. We have dealt here with fluctuations expected in showers initiated by primary protons, for a mixed composition the electron size distribution at sea level is always narrower than that for protons of the same primary energy arriving at the same zenith angle and therefore the effect of fluctuations is always less.

For measurements at sea level in the region of interest it seems that a value of $\frac{\sigma}{\bar{N}_e}$ = 0.55 de Beer et al (1968) is most realistic. Assuming this value for $\frac{\sigma}{\bar{N}_e}$ then the results of the above calculations (see figure (i) - 3) predict the following:-

Spectral type	f* factor†	Range of smearing
Differential	0.86	$2.5\ 10^5 < N_e < 1.6\ 10^6$
Integral	0.84	$1.5\ 10^5 < N_e < 1.1\ 10^6$

(† for definition of factor f* see section 2.5.2) and we can conclude that fluctuations in electron size have little affect on smearing in the region of the "knee".

Appendix (ii) Theory of Diffusion

The following has been derived by Kota (1973) independently of the author.

For a 2-D model for diffusion, assume circular clouds with radius R_o and a homogeneous field H_o inside. Assume the particle crosses a cloud from the x direction, it will be deflected through an angle β depending on its Larmor radius R and impact parameter $R_o \sin\alpha$. It can be seen from figure (ii)-1 that

$$\text{Tan}\ \frac{\beta}{2} = \frac{R_o \text{Cos}\alpha}{R+R_o \text{Sin}\alpha} = \frac{p_o \text{Cos}\alpha}{p+p_o \text{Sin}\alpha}$$

Where p is the momentum of the particle and $p_o = 300\ H_o R_o/c$ and $p=300\ H_o R/c$. If the particle has the velocity components $v_x=v$ and $v_y=0$ then after scattering on a cloud, the mean values of the velocity component $v = v \langle\text{Cos}\beta\rangle$ where $\langle\text{Cos}\beta\rangle$ is the value of $\text{Cos}\beta$ averaged over the impact parameter and $v_y=0$ since the magnetic field is directed randomly up and down.

Defining the mean free path, $\lambda(p)$ by the equation

$$\frac{1}{\lambda(p)} = 2\ n(R_o,H_o)\ R_o \left[1 - \langle\text{Cos}\beta\rangle\right]$$

where $n(R_o,H_o)$ is the density of clouds of radius R_o and field strength H_o and $2R_o$ is the geometrical cross section in a two dimensional model. $\langle\text{Cos}\beta\rangle$ can be calculated by averaging on the impact parameter as follows:

$$\text{Cos}\beta = 1 - \frac{2\left(\frac{p_o}{p}\right)^2 \text{Cos}^2\alpha}{1+\left(\frac{p_o}{p}\right)^2 + 2\left(\frac{p_o}{p}\right) \text{Sin}\alpha}$$

$$\langle\text{Cos}\beta\rangle = \frac{1}{2} \int_{\frac{-\pi}{2}}^{+\frac{\pi}{2}} \text{Cos}\beta(\alpha)\ \ \text{Cos}\ \alpha\ d\alpha$$

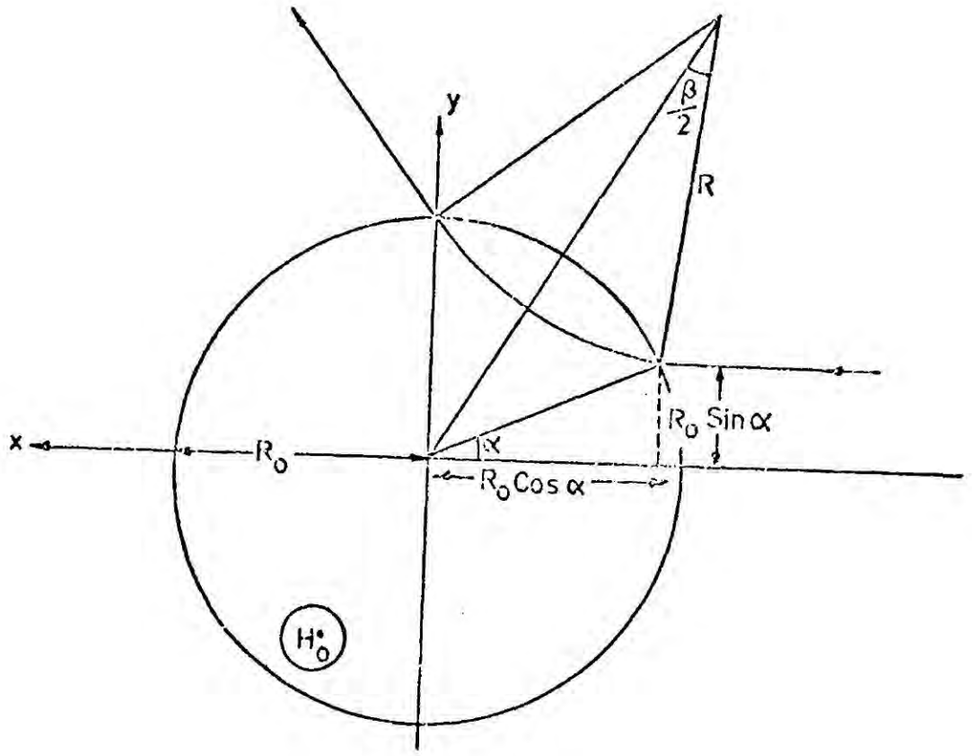

Figure (ii)-1 The trajectory of a cosmic ray particle across a cloud with radius R_o pc and field strength H_o μgauss

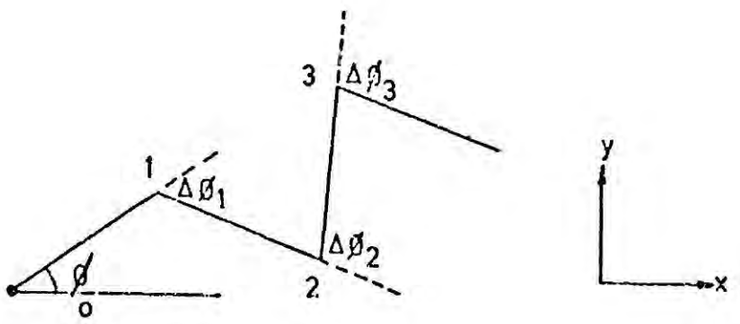

Figure (ii)-2 Schematic representation of a cosmic ray particle travelling equal distances between successive interactions

and

$$\frac{1}{\lambda(p)} = 2\, n(R_o,H_o)\, R_o \frac{p_o}{p}\left[\frac{p^2+p_o^2}{2pp_o} - \frac{(p+p_o)^2(p-p_o)^2}{(2pp_o)^2}\ln\left|\frac{p+p_o}{p-p_o}\right|\right]$$

for a uniform distribution, i.e. $n(R_o,H_o)$ is a constant this expression reduces to a form that agrees accurately with the equivalent curve obtained numerically by the author (plotted in figure 4.5).

Consider equal distances between subsequent scatterings ℓ which take place in equal times τ since the particle is assumed to travel at a constant speed v. The distribution of the angle of scatter is assumed symmetric for negative and positive deflection angles $\Delta\phi$ i.e. $f(\Delta\phi)= f(-\Delta\phi)$. To calculate the particles mean square displacement after time $n\tau$ in a particular direction (x axis) consider figure (ii)-2. Let the particle start at an angle ϕ_o to the x axis. Then after a time $k\tau$ the particles angle to the x axis is

$$\phi_k = \phi_o + \Delta\phi_1 + \Delta\phi_2 + \ldots\ldots + \Delta\phi_k$$

The displacement in the x direction is

$$\Delta X = \sum_{i=o}^{n-1} \ell_i \cos\phi_i$$

where ℓ_i and ϕ_i are the path length and the angle to the x axis between the ith and (i+1)th scatterings.

For isotropic scattering the particle completely forgets its original direction after one scattering. In the case of non-isotropic scattering, however, more scatterings are needed to randomise the direction distribution. Obviously after the first scattering

$$\begin{aligned}\langle\cos\phi_1\rangle &= \langle\cos(\phi_o+\Delta\phi_1)\rangle \\ &= \cos\phi_o \langle\cos\Delta\phi_1\rangle - \sin\phi_o \langle\sin\Delta\phi_1\rangle \\ &= \cos\phi_o \langle\cos\Delta\phi_1\rangle\end{aligned}$$

Since $\langle \mathrm{Sin}\Delta\phi_1 \rangle = 0$ as the positive and negative scattering angles are equally probable. The subsequent scatterings are independent so we have after the nth scattering

$$\langle \mathrm{Cos}\phi_n \rangle = \mathrm{Cos}\phi_o \langle \mathrm{Cos}\Delta\phi \rangle^n$$

The particle's direction can be regarded as randomised when $\langle \mathrm{Cos}\Delta\phi \rangle^n$ is very small. In the case of isotropic scattering it occurs after a single scattering, ($\langle \mathrm{Cos}\Delta\phi \rangle = 0$ for isotropic scattering). At high energies however, the deflection angle decreases so $\langle \mathrm{Cos}\Delta\phi \rangle$ approaches 1. Thus more scatterings are necessary to randomise the particle direction. Roughly we put

$$n \propto \frac{-1}{\ln \langle \mathrm{Cos}\Delta\phi \rangle}$$

if $\langle \mathrm{Cos}\Delta\phi \rangle^n$ has to be below a limit.

The mean square displacement is

$$(\Delta X)^2 = \sum_{i=o}^{n-1} \sum_{j=o}^{n-1} \ell_i \ell_j \, \mathrm{Cos}\phi_i \, \mathrm{Cos}\phi_j \qquad \text{(ii)-1}$$

Since the distance between the scatterings is fixed, we have $\langle \ell_i \ell_j \rangle = \ell^2$ and $\langle \mathrm{Cos}\phi_i \, \mathrm{Cos}\phi_j \rangle$ is calculated in the following way:

Using trigonometrical identities

$$\mathrm{Cos}\phi_i \, \mathrm{Cos}\phi_j = \frac{1}{2} \left[\mathrm{Cos} \, (\Phi_j - \Phi_i) + \mathrm{Cos} \, (\Phi_j + \Phi_i) \right] \qquad \text{(ii)-2}$$

for $j \geq i$, we obtain

$$\langle \mathrm{Cos}(\phi_j - \phi_i) \rangle \equiv \langle \mathrm{Cos}(\Delta\phi_{i+1} + \Delta\phi_{i+2} + \ldots + \Delta\phi_j) \rangle = \langle \mathrm{Cos}\Delta\phi \rangle^{j-i} \qquad \text{(ii)-3}$$

and

$$\mathrm{Cos}(\phi_j + \phi_i) \rangle \equiv \langle \mathrm{Cos}(2\phi_o + 2\Delta\phi_1 + \ldots + 2\Delta\phi_i + 2\Delta\phi_{i+1} + \ldots + \Delta\phi_j)$$

$$= \mathrm{Cos}\, 2\phi_o \langle \mathrm{Cos}2\Delta\phi \rangle^i \langle \mathrm{Cos}\Delta\phi \rangle^{j-i} \qquad \text{(ii)-4}$$

Hence using (ii)-2, 3 and 4

$$\langle \cos\phi_i \cos\phi_j \rangle = \frac{1}{2}\left[\langle \cos\Delta\phi\rangle^{j-i} + \cos 2\phi_o \langle \cos 2\Delta\phi\rangle^{i}\langle \cos\Delta\phi\rangle^{j-i}\right]$$

and (ii)-1 becomes

$$\langle \Delta X^2\rangle = \ell^2 \left[(n+\cos 2\phi_o \left\{\frac{1-\langle \cos 2\Delta\phi\rangle^n}{1-\langle \cos 2\Delta\phi\rangle}\right\}) \left(\frac{1}{1-\langle \cos\Delta\phi\rangle} - \frac{1}{2}\right)\right.$$

$$\left. - \frac{\langle \cos\Delta\phi\rangle}{1-\langle \cos\Delta\phi\rangle} \left(\frac{1-\langle \cos\Delta\phi\rangle^n}{1-\langle \cos\Delta\phi\rangle} + \cos 2\phi_o \left\{\frac{\langle \cos\Delta\phi\rangle^n - \langle \cos 2\Delta\phi\rangle^n}{\langle \cos\Delta\phi\rangle - \langle \cos 2\Delta\phi\rangle}\right\}\right) \right] \qquad \text{(ii)-4}$$

For large n i.e. after many scatterings

$$\langle \Delta X^2\rangle \approx \ell^2 \, n \left[\frac{1}{1-\langle \cos\Delta\phi\rangle} - \frac{1}{2}\right]$$

$$\langle \Delta X^2\rangle = \ell v t \left[\frac{1+\langle \cos\Delta\phi\rangle}{2(1 - \langle \cos\Delta\phi\rangle)}\right] \qquad \text{(ii)-5}$$

Diffusion theory defines the diffusion coefficient such that $\langle \Delta X^2\rangle \approx 2Dt$ and therefore the diffusion coefficient corresponding to the two dimensional diffusion model becomes

$$D = \ell v \left[\frac{1+\langle \cos\Delta\phi\rangle}{4(1-\langle \cos\Delta\phi\rangle)}\right] \qquad \text{(ii)-6}$$

Inspection of equation (ii)-4 shows that $\langle \Delta X^2\rangle$ in fact depends on ϕ_o, the direction in which the particle starts from its original position. The mean square displacement in the x direction is greater when the particle starts in the x direction. However, the larger n is the slighter the dependence on ϕ_o becomes. In fact the contribution of ϕ_o is responsible for the anisotropy. A particle starting in the x direction requires less time to reach a certain distance than does a particle starting in the y direction.

Appendix (iii)

Formation of hydrogen emission lines

Equation of transfer of radiation along a line of sight

$$\frac{dI_\nu}{dr} = j_\nu - K_\nu I_\nu \qquad \text{iii-1}$$

Where I_ν = specific intensity, ν = frequency of the radiation

r = distance from L.S.R. to volume coefficients of emission and absorption j_ν and K_ν respectively.

Solution

$$I_\nu = \int_o^\infty j_\nu \exp\left(-\int_o^r K_\nu \, dr'\right) dr \qquad \text{iii-2}$$

Rayleigh Jean's formula

$$T_b = \frac{I_\nu c^2}{2k\nu^2} \qquad \text{iii-3}$$

relates the brightness temperature to the observed intensity. The emission coefficient can be expressed in temperature units (degrees per centimeter)

$$J_\nu = \frac{j_\nu c^2}{2k\nu^2} \qquad \text{iii-4}$$

Kirchoff's law $J_\nu = K_\nu T_s$ iii-5

relates the emission and absorption coefficients through the spin temperature T_s.

Substitution of iii-3 and iii-4 in iii-2 gives

$$T_{b\nu} = \int_o^\infty T_s K_\nu \exp\left(-\int_o^r K_\nu \, dr'\right) dr \qquad \text{iii-6}$$

$$= \int_o^{\tau_\nu'} T_s \exp(-\tau_\nu) \, d\tau_\nu \qquad \text{iii-7}$$

where $\tau_\nu = \int_o^r K_\nu \, dr'$ iii-8

is the optical depth to a distance r at frequency ν and τ_ν' is the optical

depth to infinity along the line of sight.

If the spin temperature is constant along the line of sight

$$T_{b\nu} = T_s \, (1-\exp(-\tau_\nu')) \qquad \text{iii-9}$$

which is a general relation for an emission line. When T_s is non uniform, an analagous but more complex expression is required.

To calculate the number of emitting atoms: the atomic absorption coefficient a_ν expressed in terms of K_ν by the relation

$$K_\nu = a_\nu (n_o - n_1 \frac{g_o}{g_1}) \qquad \text{iii-10} \; *$$

where n_o and n_1 are the number of atoms in the two sublevels and g_o and g_1 are their weights related by the Boltzmann formula

$$\frac{n_1}{n_o} = \frac{g_1}{g_o} \exp\left(-\frac{h\nu_{10}}{kT_s}\right) \qquad \text{iii-11}$$

For radio waves $h\nu << T_s$ therefore equation iii-10 becomes

$K_\nu = a_\nu n_o \frac{h\nu}{kT_s}$. True absorption is largely compensated by stimulated emission and the effective absorption coefficient is dependent on the small residual variation of the relative populations with excitation temperature T_s. The smallness of the population variation in this case can be seen from the following examples for hydrogen:

T_s °K	10	100	1000
$\frac{n_1}{n_o}$	2.9806	2.9981	2.9998

The absorption coefficient a_ν is related to the transition probability A_{01} by

$$a_\nu = A_{01} \frac{c^2}{8\pi\nu^2} \frac{g_1}{g_o} f(\nu)$$

where $f(\nu)\, d\nu$ is the probability that a transition occurs in the frequency range ν and $\nu+d\nu$.

*Milne, E.A. Hdb. d. Ap., 3 chap.2, 159 (1930).

Substituting numerical values for hydrogen the total number of ground level atoms in unit frequency interval (1c/s) in a cylinder of cross-section $1cm^2$ extending along the whole line of sight

$$n \approx 4n_o = 3.88 \times 10^{14} T_s \tau_\nu$$

In velocity units, number of atoms in an interval 1 km sec^{-1} is

$$n_\nu = 1.823 \times 10^{18} T_s \tau_\nu$$

If the gas is optically thin i.e. $\tau << 1$, the number of atoms can be derived from the observed brightness temperature without the knowledge of T_s since $T_b = T_s \tau$.

The integrated brightness B_{int} is the total number of atoms in the line of sight at all velocities - this is effectively the area under the observed line profile

$$B_{int} = \frac{2k}{\lambda^2} \int \tau_\nu \, d\nu$$

numerically

$$N_H = 1.823 \times 10^{18} B_{int}$$

where B_{int} has units $1^oK \times 1$ km sec^{-1}.

When gas is optically thin, the line profile must be replaced by a plot of optical depth against velocity for a constant value of spin temperature T_s. Therefore giving

$$N_H = 1.823 \; 10^{18} T_s \int_{-\infty}^{\infty} \tau \, d\nu$$

In general, we can only obtain the value of the total number of atoms in a column of unit cross section in a unit frequency or velocity range. The atoms cannot be located along the line of sight nor can a space density be derived unless further information is sought. Hydrogen mass is determined from the number of atoms in a unit column when a limited concentration of gas is at known distance.

The natural width of the 21 cm line is $5 \; 10^{-16}$ c/s and therefore the width of the observed profile is entirely due to Doppler broadening at

1420.4 mc/s a radial velocity of v km sec^{-1} produces a frequency shift of -4.74v kc/s. The broadening is due partly to thermal motions of the atoms inside a single hydrogen cloud but mainly due to larger scale motions of the clouds or cloud complexes.

The hydrogen atoms are moving with a Maxwellian velocity distribution corresponding to a kinetic temperature T_k. The line produced by these atoms is Gaussian in shape with a width between half intensity points equal to

$$\delta v = 1.67 \frac{\nu}{c} \sqrt{\frac{2kT_k}{m}}$$

where m is the mass of a hydrogen atom.

$$\delta \nu = 1.015 \sqrt{T} \quad \text{kc/s}$$

$$\delta \nu = 0.215 \sqrt{T} \quad \text{km sec}^{-1}$$

Generally a number of thermally spread clouds one behind the other are observed with different radial velocities. The profile is therefore quite complex in the Milky Way region but quite simple outside where the width determines mainly the velocity dispersion of the gas clouds. Near the galactic equator the line is considerably broadened by mass motions of cloud complexes, including galactic differential rotation and systematic departures from circular motions.

Appendix (iv)

The formation of absorption lines

If a source emits a line profile with the same velocity as a body of gas in its vicinity the optical depths are additive and there is no formal difference from the instance where all the gas is in a single concentration. The continuum background emission from either a small-diameter discrete source occupying only part of the antenna beam or a broadly distributed source such as the Milky Way, will add to the total received intensity but will be partially absorbed when passing through the gas. The brightness temperature at frequency ν is given by

$$T_{b\nu} = T_s \, (1-\exp(-\tau_\nu)) + T_o \exp(-\tau_\nu)$$

The first term represents emission from the gas concentration (appendix iii-9) and the second term the attenuated radiation from the background whose brightness temperature is taken as T_o, considered independent of frequency over the small range occupied by the line. ΔT the excess brightness temperature at the line frequency compared with that outside the line is the contribution from line emission

$$\Delta T = T_{b\nu} - T_o = (T_s - T_o)\,(1-\exp(-\tau_\nu))$$

when $T_s > T_o$ - line appears in emission

$T_s < T_o$ - line appears in absorption

Absorption measurements can give optical depth τ of a body of gas without the spin temperature T_s which is not true in the case of emission. However n, the number of atoms in unit column and T_s cannot be separated in the absorption case whereas they can be for an optically thin emitting gas.

When the same cloud is observed at adjacent points in both emission and absorption it is possible to derive T_s and τ separately hence n can be calculated. However, the method is limited by the extent to which the cloud can be taken as uniform from point to point.

Appendix (v)

Synchrotron Radiation

Cosmic electrons in interstellar magnetic fields

A relativistic electron gyrating in a magnetic field emits radiation with a wide angular distribution, with a maximum perpendicular to the direction of the acceleration, in the electrons rest frame. In the laboratory frame, where the relativistic energy of the electron exceeds its rest mass energy, emission is in a very narrow cone in the direction of the instantaneous velocity of the particle Vladimirsky (1948) showed that the energy radiated in 1 second in the frequency interval ν and $\nu+d\nu$ by a relativistic electron moving in a magnetic field is given by

$$P(\nu,E)\ d\nu = \frac{16e^2H}{mc^2} \cdot\ p(\frac{\nu}{\nu_o}) \qquad \text{v-1}$$

where H is the magnetic field strength, e and m the electronic charge and mass respectively, c the velocity of light and $p(\frac{\nu}{\nu_m})$ is defined by the distribution of figure v-1. He shows that radiation is mainly in the peak of the spectrum, therefore if the frequency at maximum intensity $\nu_m = \frac{1}{3}\ \nu_c$ then

$$\nu_c = \frac{3eH_\perp}{4\ mc} \left(\frac{E}{mc^2}\right)^2 \qquad \text{v-2}$$

where $H_\perp$ is the component of the magnetic field $\underline{H}$ perpendicular to the particle velocity.

If the particle density $n_e(E)dE$ for energetic electrons within an energy range dE is given by the power law observed experimentally for cosmic ray electrons i.e.

$$n_e(E)dE = KE^{-\gamma}dE \qquad \text{v-3}$$

assuming (a) the magnetic fields are randomly orientated and the electron radiation can be considered practically isotropic

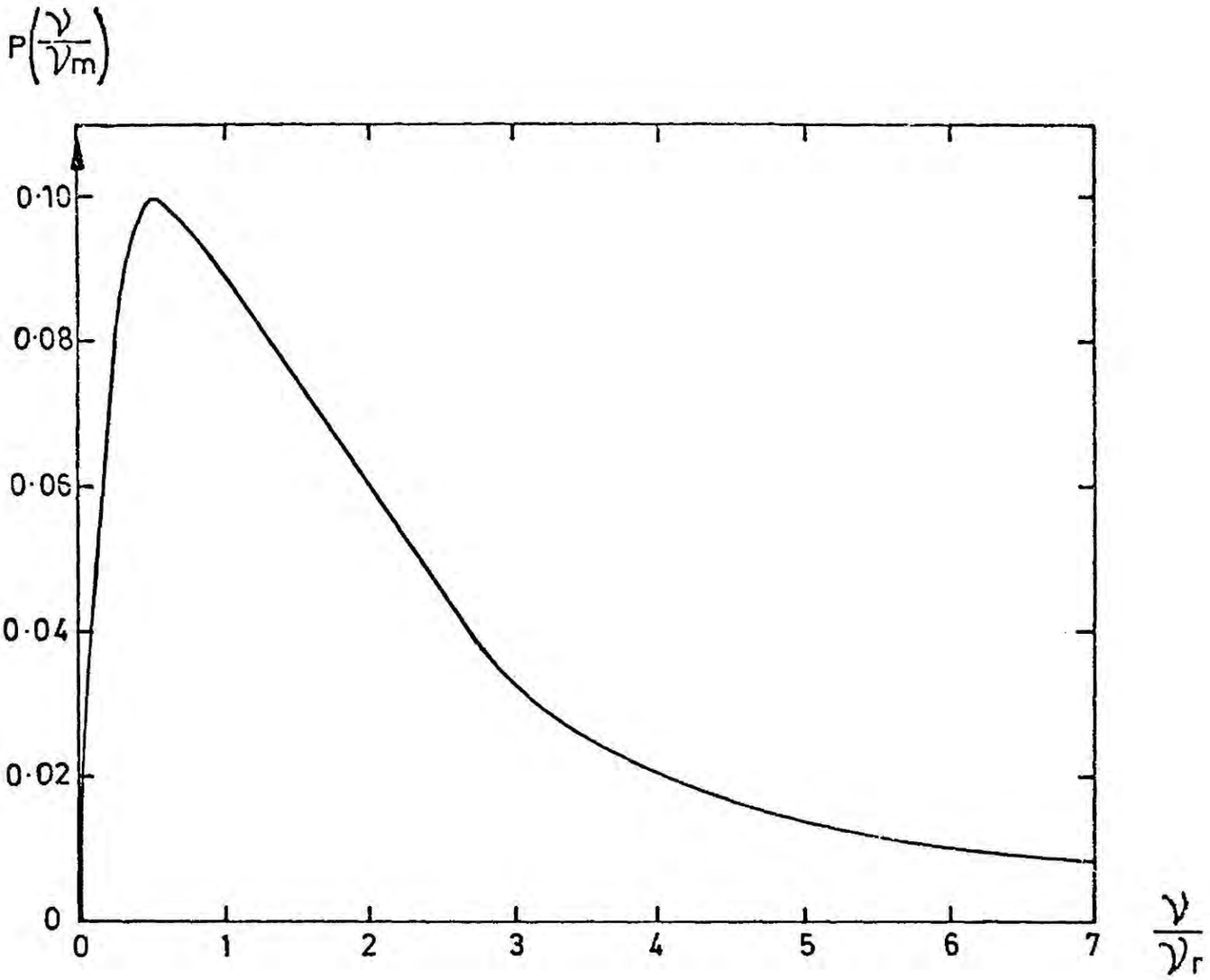

Figure (v)-1 The function $p(\frac{\nu}{\nu_m})$

(b) the total rate of emission of energy j_ν (ergs sec^{-1} cm^{-3} Hz^{-1}) is uniform over distance L

(c) there is negligible absorption over distance L.

The specific intensity

$$I_\nu = \frac{L}{4\pi}\int_o^\infty P(\nu,E)\, n_e(E)\, dE = \frac{Le^3H_\perp}{mc^3}\left(\frac{3eH_\perp}{4\pi m^3c^5}\right)^{\frac{\gamma-1}{2}} \frac{Ka(\gamma)}{\nu^{\frac{\gamma-1}{2}}} \qquad v\text{-}4$$

where $a(\gamma)$ takes the values 0.283, 0.147, 0.103, 0.0852, 0.0742, 0.0725 and 0.0922 for values of γ=1, 1.5, 2, 2.5, 3, 4 and 5 respectively.

For measurements in the radio spectrum I_ν is often replaced by the brightness temperature T_b defined as the temperature at which $B_\nu(T_b)$, the Planck function, equals the observed specific intensity $I(\nu)$ and since $\frac{h\nu}{kT}<<1$ at all radio frequencies the expansion of $B_\nu(T_b)$ with neglect of second and higher order terms yields

$$I_\nu = \frac{2\nu^2 kT_b}{c^2} \qquad v\text{-}5$$

where k is Boltzmanns constant and it follows that

$$T_b = \frac{Le^3H_\perp}{2mk}\left(\frac{3eH_\perp}{4\pi m^3c^5}\right)^{\frac{\gamma-1}{2}} \frac{Ka(\gamma)}{\nu^{2+\left(\frac{\gamma-1}{2}\right)}} \qquad v\text{-}6$$

Acknowledgements

The author wishes to thank Professor G. D. Rochester for making available the facilities of the Physics Department of the University of Durham and also the Science Research Council for its financial support.

She wishes to thank Professor A. W. Wolfendale for his constant guidance throughout the three years of research prior to the writing of this thesis.

The invaluable discussions with J. Wdowczyk, J. L. Osborne and J. Kota are acknowledged with gratitude.

The author wishes to thank her colleagues at the University of Lódz, Poland for their hospitality shown during her four weeks stay there in 1971.

The number of hours spent by Mrs. P. Russell and Mrs. A. Gregory drawing diagrams is appreciated. Mrs. D. Philpot is thanked for accepting the mammoth task of typing this thesis and doing it so well.

Finally, the author wishes to thank her husband, Ian, for the patience and help he gave during the developments of the computer programmes referred to in this thesis and for operating the computer during the off-peak hours in the week and at weekends.

REFERENCES

ADCOCK, C., et al., 1968, J. Phys. A (Proc. Phys. Soc.), (2), 1, 82.

ADCOCK, C., et al., 1969, J. Phys. A (Gen. Phys.), (2), 2, 574.

AKABANE, K. and KERR, F. J., 1965, Aust. J. Phys., 18, 91.

AMES, S. and HEILES, C., 1970, Ap. J., 160, 59.

AMINEVA, T. P., et al., 1969, Izv. An. U.S.S.R. ser. Phys., 33, 1508.

ANAND, K. C., et al., 1968a, Phys. Rev. Lett., 20, 764

ANAND, K. C., DANIEL, R. R. and STEPHENS, S. A., 1968b, Proc. Indian Acad. Sci., 67, 267.

ANAND, K. C., et al., 1968c, Can. J. Phys., 46, S 652.

ANAND, K. C., et al., 1969, Proc. 11th Int. Conf. on Cosmic Rays, (Budapest), OG-41, Acta.Phys. Acad. Hung., 29, Supp. 1, 229, (1970).

ANDREW, B. H., 1966, M.N.R.A.S., 132, 79.

ANDREWS, D., et al., 1971, Proc. 12th Int. Conf. on Cosmic Rays (Hobart), 3, 995.

ANTONOV, R. A., et al., 1971, Proc. 12th Int. Conf. on Cosmic Rays (Hobart), 6, 2194.

ASEIKIN, V. S., et al., 1971, Proc. 12th Int. Conf. on Cosmic Rays, (Hobart), 6, 2152.

BALASUBRAHMANYAN, V. K., et al., 1966, J. Geophys. Rev., 17, 1771.

BALASUBRAHMANYAN, V. K. (and ORMES, J. F.), 1972, Preprint X-661-72-447, Goddard Space Flight Centre, Greenbelt, Maryland.

BALASUBRAHMANYAN, V. K. (and ORMES, J. F.), 1973, Nat. Phys. Sci., 241, 95.

BALDWIN, J. E., 1955, M.N.R.A.S., 115, 684.

BALDWIN, J. E., 1958, Paris Symposium Radio Astronomy (I.A.U. Symposium No. 9) edited. R. N. Bracewell, Stanford University Press, Stanford, Paper 82, 460, (1959).

BALDWIN, J. E., 1971, I.A.U. Symposium No. 46, "The Crab Nebula" edited by R. D. Davies and F. G. Smith, Dordrecht Riedel Publishing Company, Dordrecht-Holland, 22.

BARADZEI, L. T., et al., 1964, Trudy Fian, 26, 224.

BEEDLE, R. E.,and WEBBER, W. R., 1967, Proc. 10th Int. Conf. on Cosmic Rays, (Calgary), MOD-81, Can. J. Phys., 46, S1014, (1968).

BEEDLE, R. E., et al., 1969, Proc. 11th Int. Conf. on Cosmic Rays (Budapest), OG-22, Acta. Phys. Acad. Sci. Hung. 29, Suppl. 1, 131.

de BEER, J. F., et al., 1966, Proc. Phys. Soc., 89, 567.

de BEER, J. F., et al., 1968a, Proc. 10th Int. Conf. on Cosmic Rays, (Calgary), Can. J. Phys., 46, S737.

de BEER, J. F., et al., 1968b, Proc. 10th Int. Conf. on Cosmic Rays, (Calgary), Can. J. Phys., 46, S185.

de BEER, J. F., et al., 1968c, J. Phys. A (Proc. Phys. Soc.), (2), 1, 72.

de BEER, J. F., et al., 1969, J. Phys. A (Gen. Phys.), (2), 2, 354.

BEHR, A., 1959, Nach. Akad. Wissensch. Göttingen Math. Phys. Kl., 185.

BELL, C. J., et al., 1971, Proc. 12th Int. Conf. on Cosmic Rays (Hobart), 3, 989.

BEREZINSKII, V. S.,and ZATSEPIN, G. T., 1969, Phys. Lett., 28B, 423.

BEREZINSKII, V. S.,and ZATSEPIN, G. T., 1971, Sov. J. Nuc. Phys., 13, 453.

BERGE, G. L.,and SEIELSTAD, G. A., 1967, Ap. J., 148, 367.

BERGERON, J.,and SOUFFRIN, S., 1971, Astron. Ap., 11, 40.

van den BERGH, S., 1966, A. J. 71, 990.

BLAAUW, A., 1952, B.A.I.N., 11, 459.

BLEEKER, J. A. M., et al., 1969, Proc. 11th Int. Conf. on Cosmic Rays, (Budapest), OG-34/35, Acta, Phys. Acad. Sci. Hung., 29, Supp. 1, 209, (1970), also OG-36, Acta. Phys. Acad. Sci. Hung., 29, Supp. 1, 217, (1970).

BOK, B. J., 1959, Observatory, 79, 58.

BOLTON, J. G. and WILD, J. P., 1957, Ap. J., 125, 296.

BOLTON, J. G., et al., 1958, Pub. A.S.P., 70, 544.

BOTHE, W. and KOLHÖRSTER, W., 1929, Z. Phys., 56, 751.

BRADT, H. V., et al., 1965, Proc. 9th Int. Conf. on Cosmic Rays (London) 2, 715.

BRADT, H. V. and RAPPAPORT, S. A., 1968, Phys. Rev., 164, 1567.

BRAES, L. L. E., 1963, B.A.I.N., 17, 132.

BRIDLE, A. H., 1967, M.N.R.A.S., 136, 219.

BURKE, B. F., et al., 1958, Paris Symposium on Radio Astronomy (I.A.U. Symposium No. 9) edited R. N. Bracewell, Stanford University Press, Stanford, Paper 72, 374, (1959).

BURKE, B. F., et al., 1963a, I.A.U.-U.R.S.I. Symposium No. 20 Australia Academy of Science, Canberra, Australia, article 32, 131, (1964).

BURKE, B. F., et al., 1963b, I.A.U.-U.R.S.I. Symposium No. 20 Australia Academy of Science, Canberra, Australia, article 43, 183, (1964).

BURN, B. J., 1966, M.N.R.A.S., 133, 67.

BUTLER BURTON, W., 1966, B.A.I.N., 18, 247.

BYSTROVA, N. V., et al., 1964a, Izv. glav. astr. Obs. Pulkove, 23, No. 5, 111.

BYSTROVA, N. V., et al., 1964b, Izv. glav. astr. Obs. Pulkove, 23, No. 5, 116.

BYSTROVA, N. V., et al., 1965, Izv. glav. astr. Obs. Pulkove, 24, No.2, 202.

CACHON, A., 1962, Proc. 5th Interamerican Seminar on Cosmic Rays, 2, 39.

CARTWRIGHT, B. G., et al., 1971, Proc. 12th Int. Conf. on Cosmic Rays (Hobart), OG-63, 1, 215.

CHUDAKOV, A. E., et al., 1960, Proc. Int. Conf. on Cosmic Rays (Moscow), II, 46.

CLARK, B. G., et al., 1962, Ap. J., 135, 151.

CLARK, B. G., 1965, Ap. J., 142, 1398.

CLARK, G., et al., 1963, Proc. 8th Int. Conf. on Cosmic Rays, (Jaipur), 4, 65.

CLAY, J., 1928, Proc. Amsterdam Acad., 31, 1091.

COCCONI, G., et al., 1961, Lawrence Radiation Laboratory High Energy Physics Study Seminars, No. 28, part 2, UCID-1444, 1.

COMSTOCK, G. M., et al., 1969, Ap. J., 155, 609.

CONTOPOLOUS, G., and STRÖMGREN, B., 1965, Tables of Plane Galactic Orbits New York, N.A.S.A., Institute for Space Sciences.

CONWAY, R. G., 1971, I.A.U. Symposium No. 46, "The Crab Nebula", edited by R. D. Davies and F. G. Smith, Dordrecht Reiedel publishing company Dordrecht-Holland, 292.

COOPER, B. F. C., and PRICE, R. M., 1962, Nature, 195, 1084.

COSTAIN, C. H., 1960, M.N.R.A.S. 120, 248.

COWSIK, R., 1966, Proc. 9th Int. Conf. on Cosmic Rays (London), 2, 656.

CUGNON, P., 1968, B.A.I.N., 19, 363.

DANILOVA, T. V., DENISOV, E. V., and NIKOLSKII, S. I., (1964), Sov. Phys. J.E.T.P., 19, No. 5, 1056.

DAUDIN, J., et al., 1956, Nuovo Cimento, 3, 1017.

DAVIES, J. G., and LARGE, M. I., 1970, M.N.R.A.S., 149, 301.

DAVIES, R. D., 1958, Paris Symposium Radio Astronomy (I.A.U. Symposium No. 9) edited R. N. Bracewell, Stanford University Press, Stanford, Paper 68, 355 (1959).

DAVIES, R. D., 1960, M.N.R.A.S., 120, 483.

DAVIES, R. D., and HAZARD, D., 1962, M.N.R.A.S., 124, 147.

DAVIES, R. D., et al., 1963a, M.N.R.A.S., 126, 343.

DAVIES, R. D., et al., 1963b, M.N.R.A.S., 126, 353.

DAVIES, R. D., and SHUTER, W. L. H., 1963c, M.N.R.A.S., 126, 4, 369.

DAVIES, R. D.,and TOVMASSIAN, H. M., 1963, M.N.R.A.S., 127, 45
also M.N.R.A.S., 127, 61.

DAVIES, R. D., 1965, Proc. 9th Int. Conf. on Cosmic Rays (London), 1, 35.

DAVIES, R. D., 1968, Nature, 218, 435.

DAVIES, R. D., et al., 1968, Nature, 220, 1207.

DAVIES, R. D., 1969, Nature, 223, 355.

DAVIS, L. Jnr.,and GREENSTEIN, J. L., 1951, Ap. J., 114, 206.

DAVIS, R. J., 1962, Smithsonian Contributions to Astrophysics, 5, 209.

DEDENKO, L. G., 1964, Zurn. Eksp. Teor. Fiz., 46, 1859.

DENISSE, J. F., 1955, Comptes Rendus, 240, 278.

DELVAILLE, J., et al., 1962, J. Phys. Soc. Japan 17, Suppl.,III-2-1, 76.

DICKINSON, G. J.,and OSBORNE, J. L., 1973, private communication

DIETER, N. H., 1960, Ap. J., 132, 49.

DIETER, N. H., 1964, A. J., 69, 288.

DIETER, N. H., 1965, A. J., 70, 552.

DIETER, N. H., 1972, Astron. and Ap. Suppl. Ser. 5. 21.

DIXON, H. E. et al., 1973, Proc. 13th Int. Conf. on Cosmic Rays (Denver), 4, 2473

DIXON, H. E. et al., 1973a, private communication.

DIXON, H. E. and TURVER, K. E., 1973, private communication.

DRAKE, F. D., 1958, Paris symposium Radio Astronomy, (I.A.U. Symposium No. 9) edited R. N. Bracewell, Stanford University Press, Stanford, Paper 70, 366, (1959).

DORSCHNER, J.,and GÜRTLER, J., 1963, Astr. Nachr., 287, 257.

DORSCHNER, J.,and GÜRTLER, J., 1966, Astr. Nachr., 289, 57.

DOWNES, D.,and MAXWELL, A., 1966, Ap. J. 146, 653.

DURGAPRASAD, N., et al., 1970, Phys. Rev., D1, 1021.

EFIMOV, N. N., KRASIL'NIKOV, D. D.,and NIKOLSKII, S. I., 1968, Izv. An. U.S.S.R. Ser. Phys., 32, 399.

EGOROVA, T. M., 1963, A.J.(U.S.S.R.), 40, 382 (=Sov. Astr. A. J., 7, 290).

EGOROVA, T. M., 1964, Izv. glav. astr. Obs. Pulkove, 24, 77.

ELLIOT, H., et al., 1969, Proc. 11th Int. Conf. on Cosmic Rays (Budapest) OG-95, Acta. Phys. Sci. Hung. 29, Supp. 1, 491.

ELVIUS, T., 1956, Stockholm Obs. Ann., 19, 3.

ERICKSON, W. C., HELFER, H. L.,and TATEL, H. E., 1958, Paris Symposium Radio Astronomy (I.A.U. Symposium No. 9) edited R. N. Bracewell, Stanford University Press, Stanford, Paper 73, 390, (1959).

ERICKSON, W. C.,and HELFER, H. L., 1960, A. J., 65, 1.

FALGARONE, E.,and LEQUEUX, J., 1972, private communication.

FAN, C. Y., et al., 1967, Proc. 10th Int. Conf. on Cosmic Rays (Calgary) Can. J. Phys., 46, S549, (1968).

FERMI, E., 1951, Phys. Rev., 81, 683.

FIELD, G. B., 1962, Interstellar Matter in Galaxies edited L. Woltjer, (New York: W. A. Benjamin, Inc.), 48.

FIELD, G. B., 1965, Ap. J., 142, 568.

FIELD, G. B., et al., 1969, Ap. J. Lett.,155, L149.

FREIER, P. S., (and Waddington, C. J.), 1967, Proc. 10th Int. Conf. on Cosmic Rays (Calgary) Can. J. Phys., 46, S578, (1968).

FOMIN, YU A., and KHRISTIANSEN, G. B., 1964, Sov. Phys., J.E.T.P., 19, 1445.

FOMIN, YU A. and KHRISTIANSEN, G. B., 1970, Unpublished.

GALT, J. A., et al., 1960, M.N.R.A.S., 120, 187.

GARCIA MUNOZ, M.,and SIMPSON, J.A., 1969, Proc. 11th Int. Conf. on Cosmic Rays (Budapest), OG-66, Acta. Phys. Sci. Hung., 29, Suppl. 1, 317, 1970.

GARCIA MUNOZ, M., et al., 1971, Proc. 12th Int. Conf. on Cosmic Rays (Hobart), OG-62, 1, 209.

GARDNER, F. F.,and DAVIES, R. D., 1966, Aust. J. Phys. 19, 129.

GARDNER, F. F., et al., 1967, Nature, 214, 371.

GARDNER, F. F., et al., 1969a, Aust. J. Phys., 22, 79.

GARDNER, F. F., et al., 1969b, Aust. J. Phys., 22, 107.

GARZOLI, S. L., et al., 1966, Ap. J., 145, 79.

GARZOLI, S. L., 1970, Astron. and Ap., 8, 7.

GILER, M., et al., 1969, Proc. 11th Int. Conf. on Cosmic Rays (Budapest) EAS-40, Acta, Phys. Sci. Hung., 29, Suppl. 3, 545, 1970.

GINZBURG, V. L., and SYROVATSKII, S.I., 1964, "The Origin of Cosmic Rays", Pergamon Press, 1064.

GINZBURG, V. L., and SYROVATSKII, S. I., 1971, Lebédev Physical Institute, Theoretical Department Preprint No. 77.

GLOEKLER, G. (and JOKIPII, J. R.), 1967, Ap. J. 148, L41.

GOLD, T., 1969, Nature, 221, 25.

GOLDSTEIN, S. J., Jnr., et al., 1966, A. J., 71, 297.

GOLDSTEIN, S. J., and JAMES, J. T., 1969, Ap. J., 158, L179.

GOOREVICH, L., 1971, Proc. 11th Int. Conf. on Cosmic Rays, (Hobart), EAS-14, 3, 983.

GORDON, C. P., 1970, A. J., 75, 914.

GOSS, W. M., et al., 1972, Ap. J. Suppl. Ser. No. 203, 24, 123.

GOULD, B. A., 1879, Uranometria Argentina, 335.

GRAHL, B. H., 1960, Mitt. Univ. - Sternw Bonn, No. 28.

GREISEN, K., 1960, Annual Review of Nuclear Science 10, 63.

GREISEN, K., 1966, Phys. Rev. Lett., 16, 748.

GREISEN, K., 1966a, Proc. Int. Conf. on Cosmic Rays, (London), 2, 609.

GRIEDER, P. K. F., 1969, Proc. 11th Int. Conf. on Cosmic Rays (Budapest), EAS-43/1, Acta. Phys. Acad. Sci. Hung., 29, Suppl. 3, 563, 1970.

GRIEDER, P. K. F., 1971, Proc. 12th Int. Conf. on Cosmic Rays (Hobart), EAS-11, 3, 970.

GRIGOROV, N. L., et al., 1971, Proc. 12th Int. Conf. on Cosmic Rays, (Hobart), OG-51, 5, 1746.

GUNN, J.E. and OSTRIKER, J. P., 1969, Phys. Rev. Lett., 22, 728.

HABING, H. J., and GOLDSMITH, D. W., 1971, Ap. J., 166, 525.

HAGEN, J. P., and McCLAIN, E. F., 1954, Ap. J., 120, 368.

HAGEN, J. P., LILLEY, A. E. and McCLAIN, E. F., 1955, Ap. J., 122, 361.

HAGGE, D. E., et al., 1967, Proc. 10th Int. Conf. on Cosmic Rays, (Calgary), Can. J. Phys., 46, S539, (1968).

HALL, J. S., 1958, Publications U. S. Naval Observatory, 17, part iv.

HAYAKAWA, S., 1961, Pub. Astr. Soc. Japan, 13, 184.

HEESCHEN, D. S., 1955, Ap. J., 121, 569.

HEILES, C., 1967, Ap. J. Suppl. Ser., 15, 97.

HEILES, C., 1969, Ap. J., 156, 493.

HELFER, H. L., et al., 1955, Ap. J., 121, 585.

HELFER, H. L., 1961, A. J., 66, 160.

HENRY, J., 1958, Ap. J., 128, 497.

HESS, V. F., 1912, Physik. Zeitschr. 13, 1804, see also "Cosmic Rays", A. M. Hillas, Pergamon Press, part 11, 139.

HILL, E. R., et al., 1958, Aust. J. Phys., 11, 530.

HILLAS, A. M., 1966, Proc. 9th Int. Conf. on Cosmic Rays (London), 2, 758.

HILLAS, A. M., 1967, Proc. 10th Int. Conf. on Cosmic Rays (Calgary), Can. J. Phys., 46, S623, (1968).

HILLAS, A. M., 1971, private communication.

HILLAS, A. M., 1971a, Proc. 12th Int. Conf. on Cosmic Rays (Hobart), EAS-18, 3, 1001.

HILLAS, A. M., 1971b, Proc. 12th Int. Conf. on Cosmic Rays (Hobart), EAS-19, 3, 1007.

HILTNER, W. A., 1949, Ap. J. 109, 471.

HINDMANN, J. V., and KERR, F. J., 1970, Aust. J. Phys. APS18.

HJELLMING, R. M., et al., 1969, Astron. and Ap., 2, 202.

HLAVAC, T., et al., 1969, Proc. 11th Int. Conf. on Cosmic Rays (Budapest), OG-100, Acta, Phys. Sci. Hung. 29, (1), 521.

HOAG, A. A., 1953, A. J., 58, 42.

HÖGLUND, B., 1963, Arkiv. Für Astronomi, Bd. 3, nr. 19, 217.

HUGHES, M. P., et al., 1971, Ap. J. Suppl. Ser. 200, 23, 323. see also Obs. Owens Valley Rad. Obs. 2.

HUGHES, V. A.,and ROUTLEDGE, D., 1972, A. J., 77, 210.

HULST, H. C., van de, 1958, Rev. Mod. Phys., 30, 913.

HULST, H. C., van de,(MULLER, C. A. and OORT, J. H.), 1954, B.A.I.N., 12, 117.

ILOVAISKY, S. A. and LEQUEUX, J., 1972, Astron. and Ap., 18, 169 and 20, 347.

IRELAND, J. G., 1961, M.N.R.A.S., 122, 461.

JOHNSON, J. H.,and STREET, J. C., 1933, J. Frank. Inst., 215, 239 and Phys. Rev., 43, 381.

JULIUSSON, E., et al., 1972, Phys. Rev. Lett., 29, 445.

KAFTAN-KASSIM, M. A., 1961, Ap. J., 133, 821.

KAHN, F. D., 1954, B.A.I.N., 12, 187.

KAHN, F. D. and DYSON, J. E., 1965, Astron. and Ap., 3, 47.

KERR, J. F., 1963, I.A.U.-U.R.S.I. Symposium No. 20, Australian Academy of Science, Canberra, Australia, article 44, 187, (1964).

KERR, F. J., 1968, "Nebulae and Interstellar Matter" ed. B. M. Middlehurst and L. H. Aller, Stars and Stellar Systems Vol. VII, Chicago, Chicago University Press, Ch. 10, 575.

KERR, F. J., 1969, Rev. Astron. and Ap., 7, 39.

KERR, F. J.,and WESTERHAUT, G., 1965, "Galactic Structure", edited A. Blaauw and M. Schmidt, Stars and Stellar Systems, Vol. V, Chicago, Chicago University Press, Ch. 9, 167.

KHRISTIANSEN, G. B., 1964, Thesis, Moscow.

KHRISTIANSEN, G. B., et al., 1972, European Symposium on Cosmic Rays, Paris (this unpublished work summarises the experiments done at Moscow State University and at Tien Shan over a number of years).

KNAPP, G. R. and VERSCHUUR, G. L., 1972, A. J., 77, 717.

KOLOMEETS, E. V., et al., 1969, Proc. 11th Int. Conf. on Cosmic Rays, OG-98, Acta, Phys. Sci. Hung. 29, Suppl. 1, 513.

KOTA, J., 1973, private communication.

KRAFT, R. P., 1965, "Galactic Structure", ed. A. Blaauw and M. Schmidt, Stars and Stellar Systems Vol. V, Chicago, Chicago University Press, Ch. 8, 157.

KRAFT, R. P., and SCHMIDT, M., 1963, Ap. J., 137, 249.

KRASILNIKOV, D. D., 1973, Proc. 13th Int. Conf. on Cosmic Rays (Denver), 4, 2393.

KRAUS, J. D. and KO, H.C., 1955, Nature, 175, 159.

KUILENBURG, J., van, 1972, Astron. and Ap. Suppl. Ser. 5, 1.

KWEE, K. K., MULLER, C. A., and WESTERHAUT, G., 1954, B.A.I.N., 12, 211.

LAL, S., 1967, Nuovo Cimento, 48, 466.

LAPIKENS, J., et al., 1971, Proc. 12th Int. Conf. on Cosmic Rays (Hobart) 1, 316.

LARGE, M. I., et al., 1961, M.N.R.A.S., 123, 113.

L'HEUREUX, J., 1967, Ap. J., 148, 399.

LEZNIAK, J. A., et al., 1969, Proc. 11th Int. Conf. on Cosmic Rays (Budapest), OG-68, Acta. Phys. Sci. Hung. 29, Suppl. 1, 375, see also Lezniak, J. A., and Webber, W. R., (1971).

LEZNIAK, J. A., and WEBBER, W. R., 1971, J. Geophys. Res., 76, 1605.

LILLEY, A. E., and HEESCHEN, D. S., 1954, Pub. Nat. Acad. Sci. 40, 1095.

LILLEY, A. E., 1955, Ap. J., 121, 559.

LINDBLAD, P. O., 1967, B.A.I.N., 19, 34.

LINDBLAD, P. O., et al., 1972, Astron. and Ap., 24, (2), 309,

LINSLEY, J., 1963, Proc. 9th Int. Conf. on Cosmic Rays (Jaipur), 4, 77.

LODEN, L. O., 1961, Stockholm Obs. Ann., 21, No. 7.

LYNDS, B. T., 1962, Ap. J. Suppl. Ser., 7, 1.

LYNE, A. G., and RICKETT, B. J., 1968, Nature, 219, 1339.

MAKAROVA, S. P., 1964, A. J. U.S.S.R., 41, 608, (= Sov. Astr. A. J., 8, 485, 1965).

MANCHESTER, R. N., 1972, Ap. J. 172, 43.

MARSDEN, D. J., et al., 1971, Proc. 12th Int. Conf. on Cosmic Rays (Hobart), EAS-20, 3, 1013.

MARDSEN, P. L., et al., 1971, Proc. 12th Int. Conf. on Cosmic Rays (Hobart), OG-34, 1, 110.

MATHEWSON, D. S., et al., 1962, Aust. J. Phys., 15, 354.

MATHEWSON, D. S., 1968, Ap. J. Lett., 153, L47.

MATHEWSON, D. S. and NICHOLLS, D.C., 1968, Ap. J. Lett., 154, L11.

McCRAY, R., and BUFF, J., 1972, Ap. J. Lett., 175, L65.

McCUSKER, C. B. A., 1963, Proc. 8th Int. Conf. on Cosmic Rays (Jaipur), 4, 35.

McCUSKER, C. B. A., 1969, Proc. 11th Int. Conf. on Cosmic Rays (Budapest), EAS-34, Acta. Phys. Acad. Sci. Hung, 29, Suppl. 3, 377, 1970.

McGEE, R. X., and MURRAY, J. D., 1961, Aust. J. Phys., 14, 260.

McGEE, R. X., MURRAY, J. D. and PAWSEY, J. L., 1961, Nature, 189, 957.

MENON, T. K., 1958, Ap. J., 127, 28.

MESSEL, H., and CRAWFORD, D. F., 1969, Electron-Photon Shower Distribution Function Tables for Lead, Copper and Tin absorbers. Pergamon Press Ltd.

MEYER, P., and MULLER, D., 1971, Proc. 12th Int. Conf. on Cosmic Rays (Hobart), OG-36, 1, 117.

MILLS, B. Y., 1958, Paris Symposium Radio Astronomy (I.A.U. Symposium No. 9), edited R. N. Bracewell, Stanford University Press, Stanford, paper 79, 431, (1959).

MILLS, B. Y., 1959, Pub. A.S.P., 71, 267.

MILLS, B. Y., 1970, I.A.U. Symposium No. 38, "The Spiral Structure of our Galaxy", edited W. Becker and G. Contopoulos, Dordrecht Reidel Pub. Company, Dordrecht-Holland, 178.

MILLS, D. M. and STURROCK, P. A., 1969, Ap. Lett., 5, L105.

MILNE, D.K., 1971a, I.A.U. Symposium No. 46, "The Crab Nebula", edited R. D. Davies and F. G. Smith, D. Reidel Pub. Company, Dordrecht-Holland, 248.

MILNE, D. K., 1971b, Aust. J. Phys., 24, 429.

MITTON, S., 1972, M.N.R.A.S., 155, 373.

MORGAN, W. W., et al., 1953, Ap. J., 118, 318.

MORON, M., 1965, M.N.R.A.S., 129, 447.

MULLER, C. A., 1958, Paris Symposium Radio Astronomy (I.A.U. Symposium No. 9), edited R. N. Bracewell, Stanford University Press, Stanford, Paper 69, 360 (1959).

MÜNCH, G., 1961, Ap. J. 133, 11.

NAGY, B., et al., 1970, Nature, 225, 1028.

NECKEL, Th., 1966, Z. Astrophys., 63, 221.

NIKOLSKII, S. I., 1963, Sov. Phys. USPEKHI, 78, 849.

NIKOLSKII, S. I., 1965, Sov. Phys. J.E.T.P., 24, 535.

NIKOLSKII, S. I., 1969, Izv. An. U.S.S.R. Ser. Phys., 33, 1383.

NISHIMURA, J., and KAMATA, K., 1950, Progr. Theor. Phys., 5, 899, 20, 22, 24, 25.

NISHIMURA, J., and KAMATA, K., 1951, Progr. Theor. Phys., 6, 628, 20, 22, 23, 24.

NISHIMURA, J.,and KAMATA, K., 1952, Progr. Theor. Phys., 7, 185, 20, 22, 24.

NISHIMURA, J.,and KAMATA, K., 1958, Progr. Theor. Phys., 6, 93.

NISHIMURA, J., 1967, Handbuch der Physik, ed. S. Flugg, 46, 1.

NISHIMURA, J., et al., 1969, Proc. 11th Int. Conf. on Cosmic Rays (Budapest), OG-43, Acta. Phys. Acad. Sci. Hung., 29, Suppl. 1, 239, 1970.

O'DELL, F. W., et al., 1961, Tokyo Conf. on Cosmic Radiation (I.U.P.A.P.), J. Phys. Soc. Japan Suppl. A III, 17, 23, 1962.

OORT, J. H., 1954, B.A.I.N., 12, 177.

OORT, J. H., KWEE, K. K., MULLER, C. A. and WESTERHAUT, G., 1954, Kon. Ned. Ak.v. Wetensch. (Verslagen), LXIII, 94.

OORT, J. H., 1963, Proc. I.A.U. Symposium No. 20, Australian Academy of Science, Canberra, Australia, Article 31, 130, (1964).

ORMES, J. F.,(and WEBBER, W. R.), 1965, Proc. 9th Int. Conf. on Cosmic Rays (London), 1, 349.

ORMES, J. F.,and BALASUBRAHMANYAN, V. K., 1969, Proc. 11th Int. Conf. on Cosmic Rays, TE-7, Acta. Phys. Acad. Sci. Hung., 29, Suppl. 4, 397, 1970.

ORMES, J. F., et al., 1971, Proc. 12th Int. Conf. on Cosmic Rays (Hobart), OG-55, 1, 178.

PAL, Y.,and PETERS, B., 1964, Kgl, Danske, Videnskab, Slskab. Mat-Fys. Medd., 33, No. 15, 1.

PARTHASARATHY, R.,and LERFALD, G. M., 1965, M.N.R.A.S., 129, 395.

PENZIAS, A. A.,and WILSON, R. W., 1965, Ap. J., 142, 419.

PENZIAS, A. A.,and WILSON, R. W., 1966, Ap. J., 146, 666.

PERRY, J. F. W.,and HELFER, H. L., 1972, Ap. J. 174, 341-360.

PETERS, B., 1961, Nuovo Cimento, 22, 800.

PETIT, M., 1960, Ann. d'Ap., 23, 710.

PIDDINGTON, J. A.,and TRENT, G. H., 1956, Aust. J. Phys., 9, 481.

PIKEL'NER, S. B., 1967, Astron. Zh 44, 1915 (Sov. Astron. A. J. 11, 737).

PINKAU, K., et al., 1969, Proc. 11th Int. Conf. on Cosmic Rays (Budapest), OG-61, Acta. Phys. Acad. Sci. Hung., 29, Suppl. 1, 291, 1970.

POPOWA, L., 1969, Thesis, Lodz.

PRATA, S. W., 1964, B.A.I.N., 17, 511.

PRŐNIK, I. I., 1959, Izv. Krymskoi Astrofiz Observ. 21, 276.

PURTON, C. R., 1966, M.N.R.A.S., 133, 463.

RADHAKRISHNAN, V., et al., 1972a, Ap. J. Suppl. Ser., 203, 24, 1.

RADHAKRISHNAN, V., et al., 1972b, Ap. J. Suppl. Ser., 203, 24, 15.

RADHAKRISHNAN, V., et al., 1972c, Ap. J. Suppl. Ser., 203, 24, 49.

RADHAKRISHNAN, V., and GOSS, W. M., 1972, Ap. J. Suppl. Ser., 203, 24, 161.

RAIMOND, E., 1966, B.A.I.N., 18, 191.

RATHGEBER, M. H., 1969, private communication.

REAMES, D. V.,and FITCHEL, C. E., 1966, Phys. Rev., 162, 1291.

REINHARDT, M.,and THIEL, M. A. F., 1970, Ap. Lett., 7, 101.

RIEGEL, K. W.,and JENNINGS, M. C., 1969, Ap. J., 157, 563.

ROBERTS, E., 1973, Thesis, Durham.

ROCHA VIEIRA, E. da, 1971, Ap. J. Suppl. Ser. No. 190, 22, 369.

von ROSENVINGE, T. T., et al., 1969, Ap. and Space Sci., 3, 80.

ROUGOOR, G. W.,and OORT, J. H., 1960, Proc. Nat. Acad. Sci. 46, 1.

ROZENTAL, I. L., 1952, Z.E.T.F., 23, 440.

RUSSEL, D.,and TUCKER, W., 1971, Nature, 229, 553.

RYAN, M. J., et al., 1971, Proc. 12th Int. Conf. on Cosmic Rays, (Hobart), OG-54, 1, 173.

RYAN, M. J., et al., 1972, Phys. Rev. Lett., 28, 985.

RYZKOVA, N. F.,et al., 1963, A. J. U.S.S.R., 40, 17 (= Sov. Astr. A. J. 7, 12).

RYZKOVA, N. F., et al., 1964, Izv. glav. astr. Obs. Pulkove, 23, 3.

SALPETER, E. E., 1955, Ap. J., 121, 161.

SCHEFFLER, H., 1966, Z. Astrophys., 63, 267.

SCHEFFLER, H., 1967a, Z. Astrophys., 65, 60.

SCHEFFLER, H., 1967b, Z. Astrophys., 66, 33.

SCHEUER, P. A. G., 1967, Plasma Astrophysics ed. P. A. Sturrock, Academic Press, New York, page 282.

SCHMIDT, M., 1957, B.A.I.N., 13, 247.

SCHMIDT, M.,and BLAAUW, A., 1965, "Galactic Structure". Stars and Stellar Systems Vol. V., Chicago.

SCHWARTZ, J., 1972, Ap. J., 175, 673.

SEEGER, C. L., et al., 1960, Phillips Technical Review, 21, 317.

SEEGER, C. L., et al., 1965, B.A.I.N., 18, 11.

SEIELSTAD, G. A., et al., 1964, Ap. J., 140, 53.

SEYMOUR, P. A. H., 1969, M.N.R.A.S., 142, 33.

SHAIN, G. A., 1957, A. J. U.S.S.R., 34, 3 (= Sov. Astron. A. J. 1, 1).

SHAPELY, H., 1919, Ap. J., 49, 311.

SHAPIRO, M. M., et al., 1971, Proc. 12th Int. Conf. on Cosmic Rays (Hobart), OG-64, 1, 221.

SHARPLESS, S., 1965, "Galactic Structure" ed. A. Blaauw and M. Schmidt, Stars and Stellar Systems Vol. V, Ch. 7, 131.

SHERMAN, N., 1953, Phys. Rev. 89, 25.

SHITOV, YU.P., 1971, Nature Physical Science, 229, 179.

SHKLOVSKY, I. S., 1956, Cosmic Radio Waves, Moscow State Publishing House - English translation by R. B. Redman and C. M. Varsavsky, Cambridge Massachusetts. Harvard University Press, 1960.

SHKLOVSKY, I. S., (1963), Astr. Zh. 40. 972, (Sov. Astron. A. J. No. 6, 1964).

SILVERBERG, R. F., et al., 1971, Proc. 12th Int. Conf. on Cosmic Rays (Hobart), OG-37, 1, 122.

SMITH, F. G., 1968, Nature, 218, 325.

SMITH, G. P., 1963, B.A.I.N., 17, 203.

SMITH, L. H., et al., 1972, Review Scientific Instrument, 43, 1 also Space Sciences Laboratory Series 13, Issue 69, University California, Berkeley.

SPITZER, L., 1968a, Diffuse Matter in Space, Interscience Publication, New York.

SPITZER, L., 1968b, in "Nebulae and Interstellar Matter", edited B. M. Middlehurst and L. H. Aller, Chicago, University of Chicago Press Chapter 1, page 1.

STAELIN, D. H. and REIFENSTEIN, E. C., 1969, Ap. J., 156, L121.

STRÖMGREN, B., 1948, Ap. J. 108, 242.

SUSCHENKO and FOMIN, YU. A., 1968, Preprint, University of Moscow.

SWANENBURG, B. N., et al., 1971, Proc. 12th Int. Conf. on Cosmic Rays (Hobart), OG-33, 5, 1714.

STAELIN, D. H.,and REIFENSTEIN, E. C., 1969, Ap. J., 156, L121.

TAKAKUBO, K., 1963, Sci. Rep. Tôhoku Univ. Ser. I, 47, 65.

TAKAKUBO, K.,and van WOERDEN, H., 1966, B.A.I.N., 18, 488.

TAKAKUBO, K., 1967, B.A.I.N., 19, 125.

TAYLOR, J. H., 1969, Ap. Lett., 3, L205.

TENNENT, R. M., 1967, Proc. 10th Int. Conf. on Cosmic Rays (Calgary) Can. J. Phys. 46, S1, (1968).

TERAUTI, R., 1963, Sci. Rep. Tohoku Univ., Ser. 1, 47, 114.

THEILHEIM, K. O.,and BEIERSDORF, R., 1970, J. Phys. A, 3, 79.

THEILHEIM, K. O.,and LANGHOFF, W., 1968, J. Phys. A, Gen. Phys., 1, 694.

TURTLE, A. J., et al., 1962, M.N.R.A.S., 124, 297.

TURVER, K. E., 1973, private communication

UEDA, A.,and OGITA, N., 1957, Prog. Theor. Phys, 18, 209.

VERNOV, S. N., et al., 1967, Proc. 10th Int. Conf. on Cosmic Rays (Calgary), EAS-53, Can. J. Phys., 46, S197, (1968).

VERNOV, S. N., KHRENOV, B. A., and KHRISTIANSEN, G. B., 1969, Proc. 11th Int. Conf. on Cosmic Rays (Budapest), EAS-53, Acta. Phys. Acad. Sci. Hung. 29, Suppl. 3, 627, 1970.

VERNOV, S. N., et al., 1969, Proc. 11th Int. Conf. on Cosmic Rays (Budapest), EAS-16, Acta. Phys. Acad. Sci. Hung. 29, Suppl. 3, 429, 1970.

VERONTSOV - VELYAMINOV B.A., 1955, Astron. Zh. 32(401), 1955.

VERSCHUUR, G. L., 1968, Phys. Rev. Lett., 121, 775.

VERSCHUUR, G. L., 1969 , Ap. J., 156, 861.

VERSCHUUR, G. L., 1970, I.A.U. Symposium No. 39, "Interstellar Gas Dynamics", edited H. J. Habing, Dordrecht Riedel Publication Company Dordrecht-Holland, 150.

VLADIMIRSKY, V. V., 1948, Zhur, Eksp. Teor. Fiz., 18, 392.

WADDINCTON, C. J. (and FREIER, P. S.), 1965, Proc. 9th Int. Conf. on Cosmic Rays (London), 1, 339.

WADE, C. M., 1957, A. J., 62, 148.

WALRAVEN, T., MULLER, C. A., and OORSTERHOFF, P. N., 1958, B.A.I.N., 14, 81.

WANNIER, P., et al., 1972, Astron. and Ap., 18, 224.

WEAVER, H. F., and WILLIAMS, D. R. W., 1970, private communication, Radio Astronomy Lab. University of California, Berkeley, California, U.S.A.,

WEBBER, W. R., et al., 1971, Proc. 12th Int. Conf. on Cosmic Rays, (Hobart), OG-66, 1, 229.

WEBBER, W. R., DAMLE, P., and KISH, D., 1972, Ap. and Space Science, 15, 245.

WESTERHAUT, G., 1957, B.A.I.N., 13, 201.

WESTERHAUT, G., 1958, B.A.I.N., 14, 215 and 261.

WILSON, R. W., and BURTON, J. G., 1960, Pub. Aust. Soc. Pac., 72, 331.

WOLTJER, L., 1957, B.A.I.N., 13, 301.

WOLTJER, L., 1958, B.A.I.N., 14, 39.

YANOVLEV, V. I., 1969, Thesis, Fian.

YOSHII, H., 1972, J. Phys. Soc. Japan, 32, No. 2, 295.

de YOUNG, D. S., and AXFORD, W. I., 1967, Nature, 216, 129.

ZATSEPIN, G. T., and KUZMIN, V. A., 1966, Sov. Phys. J.E.T.P. Lett., 4, 78.

ZATSEPIN, V. I., 1971, Proc. 12th Int. Conf. on Cosmic Rays, (Hobart), OG-35, 5, 1720.